

**Exchange of nitrogen dioxide (NO<sub>2</sub>)  
between plants and the atmosphere  
under laboratory and field conditions**

Dissertation

Zur Erlangung des Grades  
Doktor der Naturwissenschaften

am Fachbereich Biologie  
der Johannes Gutenberg-Universität Mainz

Claudia Breuninger  
geboren am 25. Juni 1980 in Düsseldorf

Mainz, 2011

Dekan:

1. Berichtstatter:

2. Berichtstatter:

Tag der mündlichen Prüfung: 27.10.2011

„Il semble que la perfection soit atteinte non  
quand il n’y a plus rien à ajouter,  
mais quand il n’y a plus rien à retrancher.“

„Perfektion ist nicht dann erreicht,  
wenn man nichts mehr hinzufügen,  
sondern wenn man nichts mehr weglassen kann.“

“It seems that perfection is attained not  
when there is nothing more to add,  
but when there is nothing more to remove.”

ANTOINE DE SAINT-EXUPERY



# Contents

|   |             |
|---|-------------|
| <b>Danksagung</b>   | <b>V</b>    |
| <b>Zusammenfassung</b>  | <b>VII</b>  |
| <b>Summary</b>  | <b>XI</b>   |
| <b>List of tables</b>   | <b>XIII</b> |
| <b>List of figures</b>  | <b>XV</b>   |
| <b>List of abbreviations</b>  | <b>XX</b>   |
| <br>  |             |
| <b>1 Introduction</b>   | <b>1</b>    |
| <b>1.1 Nitrogen in the atmosphere</b>   | <b>1</b>    |
| <b>1.2 Chemistry of NO, NO<sub>2</sub> and O<sub>3</sub> in the troposphere</b>               | <b>3</b>    |
| <b>1.3 NO and NO<sub>2</sub> biosphere-atmosphere exchange in ecosystem forest</b>            | <b>5</b>    |
| 1.3.1 Processes in soil   | 7           |
| 1.3.2 Interaction with plants   | 8           |
| <b>1.4 Objectives of thesis</b>   | <b>14</b>   |
| <br>  |             |
| <b>2 Material and Methods</b>   | <b>15</b>   |
| <b>2.1 Basic considerations</b>   | <b>16</b>   |
| 2.1.1 Mass balance of the NO-NO <sub>2</sub> -O <sub>3</sub> triad of a dynamic plant chamber | 16          |
| 2.1.2 Molar mass flux densities, deposition velocities and compensation point concentrations  | 19          |

## II | CONTENTS

|            |   |           |
|------------|---|-----------|
| 2.1.3      | Constraints of precision  | 23        |
| 2.1.4      | Constraints of design   | 30        |
| <b>2.2</b> | <b>Trace gas analyzers</b>  | <b>31</b> |
| <b>2.3</b> | <b>Calibrations, limits of detection, standard errors and precision of trace gas concentration measurements</b> | <b>34</b> |
| <b>2.4</b> | <b>Dynamic chamber system</b>   | <b>35</b> |
| 2.4.1      | Design and construction   | 35        |
| 2.4.2      | Implementation of concentration and flux density measurements   | 40        |
| <b>2.5</b> | <b>Experiments</b>  | <b>41</b> |
| 2.5.1      | Plant material  | 41        |
| 2.5.2      | Field site description and set-up   | 42        |
| 2.5.3      | Laboratory set-up   | 43        |
| <b>3</b>   | <b>Specification and implementation of plant dynamic chamber system</b>   | <b>45</b> |
| <b>3.1</b> | <b>Methods</b>  | <b>46</b> |
|            | Quality assurance and error analysis  |           |
| 3.1.1      | Corrections for concentration changes in long tubing  | 46        |
| 3.1.2      | Temporal response of analyzers  | 46        |
| 3.1.3      | Temperature dependence of analyzers   | 46        |
| 3.1.4      | Dynamic chamber: internal mixing, exchange rate of chamber volume, wall absorption and transmissivity           | 47        |
| 3.1.5      | Significance of concentration differences   | 48        |
| 3.1.6      | Bi-variate weighted linear least-squares fitting regression analysis  | 48        |
| 3.1.7      | Standard errors of exchange flux densities, deposition velocities and compensation point concentrations         | 50        |
| 3.1.8      | Significance of the compensation point concentrations   | 55        |
| <b>3.2</b> | <b>Results</b>  | <b>56</b> |
| 3.2.1      | Analyzers and system performance  | 56        |
| 3.2.2      | NO <sub>2</sub> blending for fumigation experiment  | 59        |
| 3.2.3      | Characterization of the dynamic plant chamber   | 59        |
| 3.2.3.1    | Radiation and NO <sub>2</sub> photolysis rate   | 59        |
| 3.2.3.2    | Sorption effects and chamber volume exchange time   | 61        |

|            |   |           |
|------------|---|-----------|
| 3.2.4      | Demonstration of exchange flux density measurements   | 62        |
| 3.2.4.1    | NO <sub>2</sub> exchange flux density: Laboratory results   | 62        |
| 3.2.4.2    | NO-NO <sub>2</sub> -O <sub>3</sub> exchange flux densities: Field results   | 66        |
| <b>3.3</b> | <b>Discussion</b>   | <b>72</b> |
| 3.3.1      | Overview of previous NO <sub>2</sub> exchange flux measurements using dynamic plant chambers  | 72        |
| 3.3.2      | Precision, data quality and photochemical reactions   | 74        |
| 3.3.2.1    | Precision and data quality  | 74        |
| 3.3.2.2    | Significance of concentration differences   | 77        |
| 3.3.2.3    | Photo-chemical reactions in the dynamic plant chamber: impact on net exchange flux densities, deposition velocities and compensation point concentrations | 78        |
| 3.3.3      | Bi-variate weighted linear regression   | 83        |
| <b>4</b>   | <b>Application of plant dynamic chamber system to field measurements</b>  | <b>85</b> |
| <b>4.1</b> | <b>Methods</b>  | <b>85</b> |
| 4.1.1      | Photosynthesis rate, transpiration rate, stomatal conductance   | 85        |
| 4.1.2      | Classification of data  | 86        |
| 4.1.3      | Monitoring of plant-physiological processes due to chambers   | 87        |
| 4.1.4      | Set-up at the ECHO project  | 88        |
| <b>4.2</b> | <b>Results</b>  | <b>89</b> |
|            | <u>EGER project</u>   |           |
| 4.2.1      | Microclimatic conditions  | 89        |
| 4.2.2      | Plant physiology  | 90        |
| 4.2.3      | Diurnal variations of gas exchange  | 92        |
| 4.2.4      | Overview of plant chamber measurements  | 96        |
| 4.2.5      | NO <sub>2</sub> exchange flux density   | 99        |
| 4.2.6      | O <sub>3</sub> exchange flux density  | 111       |
|            | <u>ECHO project</u>   |           |
| 4.2.7      | NO <sub>2</sub> exchange flux density   | 122       |

|   |            |
|---|------------|
| <b>4.3 Discussion</b>   | <b>129</b> |
| 4.3.1 Effects on enclosed plants                                  | 129        |
| 4.3.2 NO <sub>2</sub> exchange to leaves                          | 130        |
| 4.3.3 Deposition velocities of NO <sub>2</sub> and O <sub>3</sub> | 133        |
| 4.3.4 NO <sub>2</sub> compensation point concentration            | 136        |
| <br>  |            |
| <b>5 Conclusions and Perspectives</b>                             | <b>139</b> |
| <br>  |            |
| <b>6 References</b>   | <b>147</b> |
| <br>  |            |
| <b>Curriculum Vitae</b>   | <b>159</b> |



# Danksagung

An dieser Stelle möchte ich mich von ganzem Herzen bei all den Personen bedanken, die auf verschiedenster Art und Weise zum Gelingen dieser Doktorarbeit beigetragen haben.

Als erstes gilt mein Dank meinem wissenschaftlichen Betreuer für die Möglichkeit diese Arbeit unter seiner Leitung zu verwirklichen. Dank seiner Unterstützung, sein Vertrauen und das Überlassen großer Freiräume konnte diese Arbeit gelingen.

Meine tiefe Dankbarkeit möchte ich gegenüber Dr. M. ausdrücken. Seine Bürotüre war für mich stets weit geöffnet. Er stand mir bei all meinen Sorgen und Nöten immer mit Rat und Tat zur Seite. Neben seiner immerwährenden Diskussionsbereitschaft möchte ich mich für seine freundschaftliche Hilfe und für das in mich gesetzte Vertrauen bedanken.

Für die Finanzierung dieser Arbeit bedanke ich mich bei der Max-Planck-Gesellschaft (MPG) und der Deutschen Forschungsgemeinschaft (DFG).

Vielen Dank auch an das EGER-Team für all eure Hilfe und Unterstützung. Nur durch Euch konnte diese Kampagne erfolgreich sein.

Meinen Kollegen am Max-Planck-Institut möchte ich danken für ihre Diskussionsfreude, Ratschläge, Hilfe und Freundschaft.

Den fleißigen Korrekturlesern sei ebenfalls von ganzem Herzen gedankt.

Ein ganz großes Dankeschön geht an all jene, die für eine entspannende, arbeitsfreie Zeit gesorgt haben, sei es durch Quizen, Spieleabende, Rudelgucken, Rudern, Gebete, Essen oder Lachen.

Nicht zuletzt möchte ich meiner Familie danken. Danke für das Ertragen all meiner Launen und für Eure Unterstützung während dieser Zeit. Eure Liebe, Geduld und Euer Zuspruch waren stets das Wichtigste und Bedeutendste für mich und werden es auch in Zukunft immer sein.

Dank auch unserem großartigen Herrn für seine Liebe und Treue.

# Zusammenfassung

Stickstoff ist für Mensch, Tier und Pflanze ein essentieller Nährstoff, der ein wichtiges Bauelement von Proteinen und Nukleinsäuren ist. Obwohl der Großteil der Erdatmosphäre aus molekularem Stickstoff ( $N_2$ ) besteht (78 %), können nur wenige Mikroorganismen diesen direkt nutzen. Um für höhere Pflanzen oder Tiere verwertbar zu sein, muss der molekulare Stickstoff in eine reaktivere oxidierte Form überführt werden. Dies geschieht innerhalb des Stickstoffkreislaufs unter anderem durch freilebende Mikroorganismen, in Symbiose lebende Knöllchenbakterien oder durch elektrische Entladungen bei Gewittern. Dem Menschen ermöglicht das Haber-Bosch-Verfahren seit Anfang des 20. Jahrhunderts die Synthese von reaktivem Stickstoff. Damit konnte die Ernährungssicherung der Weltbevölkerung deutlich verbessert werden. Auf der anderen Seite hat der verstärkte Stickstoffeintrag die Versauerung und Eutrophierung von Ökosystemen und den Verlust an Biodiversität zu Folge. Für den Menschen ergeben sich nachteilige Auswirkungen auf die Gesundheit durch Feinstaubbildung und Sommersmog-Episoden. Reaktiver Stickstoff spielt zudem eine wichtige Rolle in der Atmosphärenchemie und deren globalen Kreisläufen von Schad- und Nährstoffen.

Stickstoffmonoxid (NO) und Stickstoffdioxid ( $NO_2$ ) gehören zu den reaktiven Spurengasen und werden unter der Bezeichnung  $NO_x$  zusammengefasst. Als wichtige Komponenten atmosphärischer oxidativer Prozesse beeinflussen sie aber auch die Lebenszeiten weniger reaktiver Treibhausgase. NO und  $NO_2$  entstehen u.a. bei Verbrennungsvorgängen durch die Oxidation von atmosphärischem Stickstoff sowie durch biologische Vorgänge in Böden. NO wird in der Atmosphäre relativ schnell zum biologisch wirksameren  $NO_2$  oxidiert.  $NO_2$  wird in der Atmosphäre langsam weiter zu Nitrat ( $NO_3^-$ ) und zu Salpetersäure ( $HNO_3$ ) aufoxidiert, lagert sich an Aerosole an und wird schließlich in der partikelgebundenen Form durch nasse und trockene Deposition aus der Atmosphäre ausgetragen. In der Atmosphärenchemie spielt  $NO_x$  zudem eine wichtige katalytische Rolle bei Bildung und Abbau von troposphärischem Ozon ( $O_3$ ).

NO, NO<sub>2</sub> und O<sub>3</sub> befinden sich in der Atmosphäre in einem photostationären Gleichgewicht, weshalb man von der NO-NO<sub>2</sub>-O<sub>3</sub> Triade spricht. In Bereichen mit erhöhtem NO-Gehalt können beispielsweise Reaktionen mit anderen Luftschadstoffen die Bildung von NO<sub>2</sub> bewirken, wodurch das Gleichgewicht zur Ozonbildung hin verschoben wird.

Für Pflanzen stellt die NO<sub>3</sub><sup>-</sup>-Aufnahme über die Wurzel die Hauptquelle des essentiellen Nährstoffs Stickstoff dar. Im Boden wird atmosphärischer Stickstoff mittels Bakterien über Stickstofffixierung oder Ammoniakbildung und Nitrifikation zu NO<sub>3</sub><sup>-</sup> oxidiert. Zusätzlich nehmen Pflanzen atmosphärisches NO<sub>2</sub> direkt über ihre Spaltöffnungen auf. NO<sub>2</sub> wird im Apoplasten durch Disproportionierung als NO<sub>3</sub><sup>-</sup> und Nitrit (NO<sub>2</sub><sup>-</sup>) der Pflanze zur Verfügung gestellt. Mittels der Enzyme Nitrat- und Nitritreduktase erfolgt daraufhin eine weitere Umwandlung in Ammonium (NH<sub>4</sub><sup>+</sup>). Beeinflusst wird der NO<sub>2</sub>-Gaswechsel vom Partialdruckgradienten in den Lufträumen der Blätter, dem Öffnungszustand der Spaltöffnungen und den im Blatt vorhandenen Widerständen. Die Regulierung der Spaltöffnungen geschieht unter anderem über klimatische Umweltbedingungen wie Lichtintensität, Temperatur und dem Wasserdampfsättigungsdefizit.

Die vorliegende Dissertation möchte dazu beitragen das Verständnis für die Rolle der Vegetation im NO<sub>2</sub>-Zyklus der Atmosphäre zu verbessern und die Frage nach einem NO<sub>2</sub>-Kompensationspunkt ( $m_{comp,NO_2}$ ) zu klären. Dazu wurde der NO<sub>2</sub>-Austausch zwischen der Atmosphäre und Fichten (*Picea abies*) auf Blattebene mittels eines dynamischen Kammersystems unter Freiland- und Laborbedingungen untersucht. Die Messungen erfolgten im Rahmen des EGER-Projekts (Juni-Juli 2008). Zusätzlich wurden zur Verfügung gestellte NO<sub>2</sub>-Messdaten ausgewertet, die während des ECHO-Projekts (Juli 2003) an Eichen (*Quercus robur*) aufgenommen wurden. Das verwendete Messsystem ermöglicht die gleichzeitige Bestimmung der Austauschraten von NO, NO<sub>2</sub>, O<sub>3</sub>, CO<sub>2</sub> und H<sub>2</sub>O. Da die Flussberechnungen von NO, NO<sub>2</sub>, und O<sub>3</sub> auf sehr kleinen Konzentrationsdifferenzen ( $\Delta m_i$ ) beruhen, die zwischen Ein- und Ausgang der Messkammer gemessen werden, ist eine hohe Genauigkeit und Spezifität der Messungen erforderlich. Um dies zu erreichen, wurde ein hoch spezifisches NO/NO<sub>2</sub> Messinstrument verwendet und das gesamte Messsystem dahingehend optimiert, dass eine hohe Messgenauigkeit dauerhaft gewährleistet werden konnte.

Die Datenanalyse ergab, dass ein signifikanter  $m_{comp,NO_2}$  nur bestimmt werden kann, wenn die statistische Signifikanz von  $\Delta m_i$  gegeben ist. In Folge dessen wurde die Signifikanz von  $\Delta m_i$  als ein Qualitätskriterium für die Daten verwendet. Bei der Bestimmung der NO-, NO<sub>2</sub>- und O<sub>3</sub>-Austauschraten müssen die photochemischen Reaktionen der NO-NO<sub>2</sub>-O<sub>3</sub> Triade innerhalb der Messkammer berücksichtigt werden, ansonsten werden Depositionsgeschwindigkeiten ( $v_{dep,NO_2}$ ) und  $m_{comp,NO_2}$  überschätzt. Für Fichten konnte unter Laborbedingungen kein signifikanter  $m_{comp,NO_2}$  bestimmt werden, unter Feldbedingungen lag  $m_{comp,NO_2}$  zwischen 0.17 und 0.65 ppb und  $v_{dep,NO_2}$  zwischen 0.07 und 0.42 mm s<sup>-1</sup>. Die Analyse der Felddaten, gemessen an Eichen, ergab ebenfalls keinen NO<sub>2</sub>-Kompensationspunkt,  $v_{dep,NO_2}$  lag zwischen 0.6 und 2.71 mm s<sup>-1</sup>. Damit verdichten sich die Hinweise, dass Wälder hauptsächlich als Senken für NO<sub>2</sub> anzusehen sind und mögliche NO<sub>2</sub>-Emissionen äußerst gering ausfallen. Nur bei hohen NO-Emissionen aus Böden, die in Reaktion mit Ozon mehr NO<sub>2</sub> liefern als von Pflanzen aufgenommen wird, könnten Wälder Quellen für NO<sub>2</sub> darstellen.



# Summary

Nitrogen is an essential nutrient. It is for human, animal and plants a constituent element of proteins and nucleic acids. Although the majority of the Earth's atmosphere consists of elemental nitrogen ( $N_2$ , 78 %) only a few microorganisms can use it directly. To be useful for higher plants and animals elemental nitrogen must be converted to a reactive oxidized form. This conversion happens within the nitrogen cycle by free-living microorganisms, symbiotic living *Rhizobium* bacteria or by lightning. Humans are able to synthesize reactive nitrogen through the Haber-Bosch process since the beginning of the 20<sup>th</sup> century. As a result food security of the world population could be improved noticeably. On the other side the increased nitrogen input results in acidification and eutrophication of ecosystems and in loss of biodiversity. Negative health effects arose for humans such as fine particulate matter and summer smog. Furthermore, reactive nitrogen plays a decisive role at atmospheric chemistry and global cycles of pollutants and nutritive substances.

Nitrogen monoxide (NO) and nitrogen dioxide ( $NO_2$ ) belong to the reactive trace gases and are grouped under the generic term  $NO_x$ . They are important components of atmospheric oxidative processes and influence the lifetime of various less reactive greenhouse gases. NO and  $NO_2$  are generated amongst others at combustion process by oxidation of atmospheric nitrogen as well as by biological processes within soil. In atmosphere NO is converted very quickly into  $NO_2$ .  $NO_2$  is then oxidized to nitrate ( $NO_3^-$ ) and to nitric acid ( $HNO_3$ ), which bounds to aerosol particles. The bounded nitrate is finally washed out from atmosphere by dry and wet deposition. Catalytic reactions of  $NO_x$  are an important part of atmospheric chemistry forming or decomposing tropospheric ozone ( $O_3$ ). In atmosphere NO,  $NO_2$  and  $O_3$  are in photostationary equilibrium, therefore it is referred as NO- $NO_2$ - $O_3$  triad. At regions with elevated NO concentrations reactions with air pollutions can form  $NO_2$ , altering equilibrium of ozone formation.

The essential nutrient nitrogen is taken up by plants mainly by dissolved  $NO_3^-$  entering the roots. Atmospheric nitrogen is oxidized to  $NO_3^-$  within soil via bacteria by

nitrogen fixation or ammonium formation and nitrification. Additionally atmospheric  $\text{NO}_2$  uptake occurs directly by stomata. Inside the apoplast  $\text{NO}_2$  is disproportionated to nitrate and nitrite ( $\text{NO}_2^-$ ), which can enter the plant metabolic processes. The enzymes nitrate and nitrite reductase convert nitrate and nitrite to ammonium ( $\text{NH}_4^+$ ).  $\text{NO}_2$  gas exchange is controlled by pressure gradients inside the leaves, the stomatal aperture and leaf resistances. Plant stomatal regulation is affected by climate factors like light intensity, temperature and water vapor pressure deficit.

This thesis wants to contribute to the comprehension of the effects of vegetation in the atmospheric  $\text{NO}_2$  cycle and to discuss the  $\text{NO}_2$  compensation point concentration ( $m_{comp,NO_2}$ ). Therefore,  $\text{NO}_2$  exchange between the atmosphere and spruce (*Picea abies*) on leaf level was detected by a dynamic plant chamber system under laboratory and field conditions. Measurements took place during the EGER project (June-July 2008). Additionally  $\text{NO}_2$  data collected during the ECHO project (July 2003) on oak (*Quercus robur*) were analyzed. The used measuring system allowed simultaneously determination of  $\text{NO}$ ,  $\text{NO}_2$ ,  $\text{O}_3$ ,  $\text{CO}_2$  and  $\text{H}_2\text{O}$  exchange rates. Calculations of  $\text{NO}$ ,  $\text{NO}_2$  and  $\text{O}_3$  fluxes based on generally small differences ( $\Delta m_i$ ) measured between inlet and outlet of the chamber. Consequently a high accuracy and specificity of the analyzer is necessary. To achieve these requirements a highly specific  $\text{NO}/\text{NO}_2$  analyzer was used and the whole measurement system was optimized to an enduring measurement precision.

Data analysis resulted in a significant  $m_{comp,NO_2}$  only if statistical significance of  $\Delta m_i$  was detected. Consequently, significance of  $\Delta m_i$  was used as a data quality criterion. Photo-chemical reactions of the  $\text{NO}-\text{NO}_2-\text{O}_3$  triad in the dynamic plant chamber's volume must be considered for the determination of  $\text{NO}$ ,  $\text{NO}_2$ ,  $\text{O}_3$  exchange rates, otherwise deposition velocity ( $v_{dep,NO_2}$ ) and  $m_{comp,NO_2}$  will be overestimated. No significant  $m_{comp,NO_2}$  for spruce could be determined under laboratory conditions, but under field conditions  $m_{comp,NO_2}$  could be identified between 0.17 and 0.65 ppb and  $v_{dep,NO_2}$  between 0.07 and 0.42  $\text{mm s}^{-1}$ . Analyzing field data of oak, no  $\text{NO}_2$  compensation point concentration could be determined,  $v_{dep,NO_2}$  ranged between 0.6 and 2.71  $\text{mm s}^{-1}$ . There is increasing indication that forests are mainly a sink for  $\text{NO}_2$  and potential  $\text{NO}_2$  emissions are low. Only when assuming high  $\text{NO}$  soil emissions, more  $\text{NO}_2$  can be formed by reaction with  $\text{O}_3$  than plants are able to take up. Under these circumstance forests can be a source for  $\text{NO}_2$ .



# List of Tables

|           |   |    |
|-----------|---|----|
| Table 1:  | Overview of global sources of nitrogen oxides   | 1  |
| Table 2:  | Typical NO <sub>x</sub> mixing ratios   | 2  |
| Table 3:  | Reported NO <sub>2</sub> compensation points obtained from the literature   | 13 |
| Table 4:  | Interferences of chemiluminescent NO-NO <sub>2</sub> -NO <sub>x</sub> analyzers used different NO <sub>2</sub> converters   | 32 |
| Table 5:  | Measured parameters and instrument specifications   | 33 |
| Table 6:  | Manufacturer details for parts of the dynamic chamber system  | 36 |
| Table 7:  | Derivatives $\partial y/\partial x_i$ of $y = F_{ex,NO_2}, F_{ex,NO}, F_{ex,O_3}$ for application of the generalized Gaussian error propagation to calculate the standard errors of $s_{Fex,NO_2}, s_{Fex,NO}$ and $s_{Fex,O_3}$                        | 52 |
| Table 8:  | Derivatives $\partial y/\partial x_i$ of $y = v_{dep,NO_2}, v_{dep,NO}, v_{dep,O_3}$ for application of the generalized Gaussian error propagation to calculate the standard errors of $s_{v,dep\_NO_2}, s_{v,dep\_NO}$ and $s_{v,dep\_O_3}$            | 53 |
| Table 9:  | Derivatives $\partial y/\partial x_i$ of $y = m_{comp,NO_2}, m_{comp,NO}$ and $m_{comp,O_3}$ for application of the generalized Gaussian error propagation to calculate the standard errors of $s_{m,comp\_NO_2}, s_{m,comp\_NO}$ and $s_{m,comp\_O_3}$ | 54 |
| Table 10: | Results of the temperature dependence tests of the used analyzers   | 56 |
| Table 11: | Parameters of sorption effects to the inner chamber walls   | 61 |
| Table 12: | Parameters for NO <sub>2</sub> laboratory measurements of simple and bi-variate weighted linear least-squares fitting regression analysis   | 65 |
| Table 13: | Percentage of data $m_i$ above $LOD(m_i)$ and significant differences $\Delta m_i = (m_{a,NO_2} - m_{s,NO_2})$ for field measurements   | 67 |
| Table 14: | Parameters of bi-variate weighted linear least-squares fitting regression analysis for field measurements   | 71 |
| Table 15: | Overview of studies that have performed dynamic chamber NO <sub>2</sub> flux measurements on different plant species  | 73 |
| Table 16: | Ambient conditions during time of field measurements (EGER)   | 89 |

#### XIV | LIST OF TABLES

|   |     |
|---|-----|
| Table 17: Results of the nutrient content analysis of the needles   | 92  |
| Table 18: Overview of chamber measurements  | 97  |
| Table 19: Percentage of significant differences ( $\Delta m_i$ ) of sample chamber 1 and 2  | 98  |
| Table 20: Conditions of the classes which were used for the classification of the measured data   | 98  |
| Table 21: Parameters of bi-variate weighted linear least-squares fitting regression analysis for data classes 1 -7 of sample chamber 1  | 108 |
| Table 22: Parameters of bi-variate weighted linear least-squares fitting regression analysis for data classes 1 -7 of sample chamber 2  | 109 |
| Table 23: Conditions of the classes which were used for the classification of the measured data within the ECHO project   | 122 |
| Table 24: Parameters of bi-variate weighted linear least-squares fitting regression analysis for data classes 1 -7 (ECHO data)  | 123 |
| Table 25: Measured and predicted leaf conductance to NO <sub>2</sub> deposition   | 132 |
| Table 26: Averages of NO <sub>2</sub> and O <sub>3</sub> deposition velocities ( $v_{dep,i}^{LAI}$ ) per ground area (LAI) and $v_{dep,NO_2}^{LAI}$ corrected ( $v_{dep,NO_2}^{LAI,cor}$ ) for NO <sub>2</sub> compensation point concentration | 135 |

# List of Figures

|            |   |    |
|------------|---|----|
| Figure 1:  | Scheme of oxidation of nitrogen oxides in the troposphere   | 4  |
| Figure 2:  | Biosphere-atmosphere interaction of the NO-NO <sub>2</sub> -O <sub>3</sub> -triad and volatile organic compounds (VOC) in a forest ecosystem  | 6  |
| Figure 3:  | Schematic representation of soil nitrogen cycle   | 8  |
| Figure 4:  | Illustrating the different pathways of trace gas uptake to a leaf   | 9  |
| Figure 5:  | Biochemical processes involved in foliar uptake and assimilation of NO <sub>x</sub> and NH <sub>3</sub>   | 11 |
| Figure 6:  | Schematic representation of the determination of bi-directional NO <sub>2</sub> exchange flux density, NO <sub>2</sub> deposition velocity and NO <sub>2</sub> compensation point concentration from measurements of NO <sub>2</sub> concentrations at the plant chamber's inlet and outlet under laboratory conditions.      | 25 |
| Figure 7:  | The dynamic plant chamber at well defined (laboratory) conditions: minimum detectable NO <sub>2</sub> compensation point concentration as function of NO <sub>2</sub> deposition velocity and the goodness of the ambient vs. sample NO <sub>2</sub> concentration measurements. Results are from data simulation.            | 28 |
| Figure 8:  | The dynamic plant chamber at well defined (laboratory) conditions: precision of NO <sub>2</sub> concentration measurements and precision of derived NO <sub>2</sub> exchange flux densities as function of the NO <sub>2</sub> concentration measured at the outlet of the dynamic chamber. Results are from data simulation. | 29 |
| Figure 9:  | Photograph and schematic drawing of a dynamic chamber   | 38 |
| Figure 10: | Schematic set-up of the system with three dynamic chambers  | 39 |
| Figure 11  | Distribution of forest species in Germany   | 41 |
| Figure 12  | Precision of the applied NO/NO <sub>2</sub> analyzer during laboratory and field experiments and the precision of the blended NO <sub>2</sub> concentration used for fumigation of the young spruce trees in the laboratory.  | 57 |
| Figure 13: | Response test for step changes between two different NO <sub>2</sub> concentrations   | 58 |

|   |    |
|---|----|
| Figure 14: Temporal course of blended NO <sub>2</sub> concentrations used for fumigation of young spruce trees during the laboratory experiments  | 60 |
| Figure 15: Simultaneous measurements of radiation in and outside a chamber.   | 60 |
| Figure 16: Results of the response time test with helium.   | 62 |
| Figure 17: Laboratory NO <sub>2</sub> fumigation of Norway Spruce under controlled conditions. NO <sub>2</sub> exchange flux density vs. NO <sub>2</sub> concentration measured at the outlet of the dynamic plant chamber for application of 2σ-LOD-definition   | 64 |
| Figure 18: Switching scheme and time series of trace gas mixing ratios over two full measurement cycles during EGER field experiment  | 68 |
| Figure 19: Field measurements: NO <sub>2</sub> concentration measured at the outlet of the dynamic plant chamber vs. NO <sub>2</sub> concentration measured at the inlet of the dynamic plant chamber and NO <sub>2</sub> exchange flux density vs. NO <sub>2</sub> concentration measured at the outlet of the dynamic plant chamber | 69 |
| Figure 20: Field measurements: O <sub>3</sub> concentration measured at the outlet of the dynamic plant chamber vs. O <sub>3</sub> concentration measured at the inlet of the dynamic plant chamber and O <sub>3</sub> exchange flux density vs. O <sub>3</sub> concentration measured at the outlet of the dynamic plant chamber     | 70 |
| Figure 21: Field measurements: NO concentration measured at the outlet of the dynamic plant chamber vs. NO concentration measured at the inlet of the dynamic plant chamber   | 71 |
| Figure 22: Percentage of gas-phase flux densities at the exchange flux densities for NO, NO <sub>2</sub> and O <sub>3</sub> .   | 80 |
| Figure 23: Photosynthetic light response curves of control and enclosed needles   | 91 |
| Figure 24: Temperature dependence of photosynthesis rate, in-situ measurements of CO <sub>2</sub> gas exchange on needle level in response to temperature   | 93 |
| Figure 25: Exchange flux densities of CO <sub>2</sub> , H <sub>2</sub> O, NO, NO <sub>2</sub> , O <sub>3</sub> with diurnal courses of PAR, leaf temperature and leaf conductance over the period from Jul 07 to Jul 08   | 94 |

|  |     |
|--|-----|
| Figure 26: Exchange flux densities of CO <sub>2</sub> , H <sub>2</sub> O, NO, NO <sub>2</sub> , O <sub>3</sub> with diurnal courses of PAR, leaf temperature and leaf conductance over the period from Jun 29 to Jun 30  | 95  |
| Figure 27: NO <sub>2</sub> measurements (EGER), data class 1 and 2 of sample chamber 1: NO <sub>2</sub> concentration measured at the outlet of the dynamic plant chamber vs. NO <sub>2</sub> concentration measured at the inlet of the dynamic plant chamber and NO <sub>2</sub> exchange flux density vs. NO <sub>2</sub> concentration measured at the outlet of the dynamic plant chamber | 100 |
| Figure 28: NO <sub>2</sub> measurements (EGER), data class 3 and 4 of sample chamber 1: NO <sub>2</sub> concentration measured at the outlet of the dynamic plant chamber vs. NO <sub>2</sub> concentration measured at the inlet of the dynamic plant chamber and NO <sub>2</sub> exchange flux density vs. NO <sub>2</sub> concentration measured at the outlet of the dynamic plant chamber | 101 |
| Figure 29: NO <sub>2</sub> measurements (EGER), data class 5 and 6 of sample chamber 1: NO <sub>2</sub> concentration measured at the outlet of the dynamic plant chamber vs. NO <sub>2</sub> concentration measured at the inlet of the dynamic plant chamber and NO <sub>2</sub> exchange flux density vs. NO <sub>2</sub> concentration measured at the outlet of the dynamic plant chamber | 102 |
| Figure 30: NO <sub>2</sub> measurements (EGER), data class 7 of sample chamber 1: NO <sub>2</sub> concentration measured at the outlet of the dynamic plant chamber vs. NO <sub>2</sub> concentration measured at the inlet of the dynamic plant chamber and NO <sub>2</sub> exchange flux density vs. NO <sub>2</sub> concentration measured at the outlet of the dynamic plant chamber       | 103 |
| Figure 31: NO <sub>2</sub> measurements (EGER), data class 1 and 2 of sample chamber 2: NO <sub>2</sub> concentration measured at the outlet of the dynamic plant chamber vs. NO <sub>2</sub> concentration measured at the inlet of the dynamic plant chamber and NO <sub>2</sub> exchange flux density vs. NO <sub>2</sub> concentration measured at the outlet of the dynamic plant chamber | 104 |
| Figure 32: NO <sub>2</sub> measurements (EGER), data class 3 and 4 of sample chamber 2: NO <sub>2</sub> concentration measured at the outlet of the dynamic plant chamber vs. NO <sub>2</sub> concentration measured at the inlet of the dynamic plant chamber and NO <sub>2</sub> exchange flux density vs. NO <sub>2</sub> concentration measured at the outlet of the dynamic plant chamber | 105 |
| Figure 33: NO <sub>2</sub> measurements (EGER), data class 5 and 6 of sample chamber 2: NO <sub>2</sub> concentration measured at the outlet of the dynamic plant chamber vs. NO <sub>2</sub> concentration measured at the inlet of the dynamic plant chamber and NO <sub>2</sub> exchange flux density vs. NO <sub>2</sub> concentration measured at the outlet of the dynamic plant chamber | 106 |
| Figure 34: NO <sub>2</sub> measurements (EGER), data class 7 of sample chamber 2: NO <sub>2</sub> concentration measured at the outlet of the dynamic plant chamber vs. NO <sub>2</sub> concentration measured at the inlet of the dynamic plant chamber and NO <sub>2</sub> exchange flux density vs. NO <sub>2</sub> concentration measured at the outlet of the dynamic plant chamber       | 107 |

|   |     |
|---|-----|
| Figure 35: Variation of NO <sub>2</sub> exchange flux density of sample chamber 1 for different leaf conductance classes  | 110 |
| Figure 36: Variation of NO <sub>2</sub> exchange flux density of sample chamber 2 for different leaf conductance classes  | 111 |
| Figure 37: O <sub>3</sub> measurements (EGER), data class 1 and 2 of sample chamber 1: O <sub>3</sub> concentration measured at the outlet of the dynamic plant chamber vs. O <sub>3</sub> concentration measured at the inlet of the dynamic plant chamber and O <sub>3</sub> exchange flux density vs. O <sub>3</sub> concentration measured at the outlet of the dynamic plant chamber | 113 |
| Figure 38: O <sub>3</sub> measurements (EGER), data class 3 and 4 of sample chamber 1: O <sub>3</sub> concentration measured at the outlet of the dynamic plant chamber vs. O <sub>3</sub> concentration measured at the inlet of the dynamic plant chamber and O <sub>3</sub> exchange flux density vs. O <sub>3</sub> concentration measured at the outlet of the dynamic plant chamber | 114 |
| Figure 39: O <sub>3</sub> measurements (EGER), data class 5 and 6 of sample chamber 1: O <sub>3</sub> concentration measured at the outlet of the dynamic plant chamber vs. O <sub>3</sub> concentration measured at the inlet of the dynamic plant chamber and O <sub>3</sub> exchange flux density vs. O <sub>3</sub> concentration measured at the outlet of the dynamic plant chamber | 115 |
| Figure 40: O <sub>3</sub> measurements (EGER), data class 7 chamber 1: O <sub>3</sub> concentration measured at the outlet of the dynamic plant chamber vs. O <sub>3</sub> concentration measured at the inlet of the dynamic plant chamber and O <sub>3</sub> exchange flux density vs. O <sub>3</sub> concentration measured at the outlet of the dynamic plant chamber                 | 116 |
| Figure 41: O <sub>3</sub> measurements (EGER), data class 1 and 2 of sample chamber 2: O <sub>3</sub> concentration measured at the outlet of the dynamic plant chamber vs. O <sub>3</sub> concentration measured at the inlet of the dynamic plant chamber and O <sub>3</sub> exchange flux density vs. O <sub>3</sub> concentration measured at the outlet of the dynamic plant chamber | 117 |
| Figure 42: O <sub>3</sub> measurements (EGER), data class 3 and 4 of sample chamber 2: O <sub>3</sub> concentration measured at the outlet of the dynamic plant chamber vs. O <sub>3</sub> concentration measured at the inlet of the dynamic plant chamber and O <sub>3</sub> exchange flux density vs. O <sub>3</sub> concentration measured at the outlet of the dynamic plant chamber | 118 |
| Figure 43: O <sub>3</sub> measurements (EGER), data class 5 and 6 of sample chamber 2: O <sub>3</sub> concentration measured at the outlet of the dynamic plant chamber vs. O <sub>3</sub> concentration measured at the inlet of the dynamic plant chamber and O <sub>3</sub> exchange flux density vs. O <sub>3</sub> concentration measured at the outlet of the dynamic plant chamber | 119 |

|   |     |
|---|-----|
| Figure 44: O <sub>3</sub> measurements (EGER), data class 7 of sample chamber 2: O <sub>3</sub> concentration measured at the outlet of the dynamic plant chamber vs. O <sub>3</sub> concentration measured at the inlet of the dynamic plant chamber and O <sub>3</sub> exchange flux density vs. O <sub>3</sub> concentration measured at the outlet of the dynamic plant chamber | 120 |
| Figure 45: Variation of O <sub>3</sub> exchange flux density of sample chamber 1 for different leaf conductance classes   | 121 |
| Figure 46: Variation of O <sub>3</sub> exchange flux density of sample chamber 2 for different leaf conductance classes   | 121 |
| Figure 47: NO <sub>2</sub> measurements (ECHO), data class 1 and 2: NO <sub>2</sub> concentration measured at the outlet of the dynamic plant chamber vs. NO <sub>2</sub> concentration measured at the inlet of the dynamic plant chamber and NO <sub>2</sub> exchange flux density vs. NO <sub>2</sub> concentration measured at the outlet of the dynamic plant chamber          | 124 |
| Figure 48: NO <sub>2</sub> measurements (ECHO), data class 3 and 4: NO <sub>2</sub> concentration measured at the outlet of the dynamic plant chamber vs. NO <sub>2</sub> concentration measured at the inlet of the dynamic plant chamber and NO <sub>2</sub> exchange flux density vs. NO <sub>2</sub> concentration measured at the outlet of the dynamic plant chamber          | 125 |
| Figure 49: NO <sub>2</sub> measurements (ECHO), data class 5 and 6: NO <sub>2</sub> concentration measured at the outlet of the dynamic plant chamber vs. NO <sub>2</sub> concentration measured at the inlet of the dynamic plant chamber and NO <sub>2</sub> exchange flux density vs. NO <sub>2</sub> concentration measured at the outlet of the dynamic plant chamber          | 126 |
| Figure 50: NO <sub>2</sub> measurements (ECHO), data class 7: NO <sub>2</sub> concentration measured at the outlet of the dynamic plant chamber vs. NO <sub>2</sub> concentration measured at the inlet of the dynamic plant chamber and NO <sub>2</sub> exchange flux density vs. NO <sub>2</sub> concentration measured at the outlet of the dynamic plant chamber                | 127 |
| Figure 51: Variation of NO <sub>2</sub> exchange flux density of measurements within ECHO for different leaf conductance classes  | 128 |

# List of Abbreviations

## General Abbreviations

|       |  |
|-------|--|
| BLC   | Blue Light Converter   |
| ECHO  | Project: Emission and CHEMical transformation of biogenic volatile Organic compounds |
| EGER  | Project: ExchanGE processes in mountainous Regions                                   |
| FEP   | Fluorinated Ethylene Propylene   |
| GOGAT | Glutamine OxoGlutarate AminoTransferase  |
| GPT   | Gas Phase Titration unit   |
| GS    | Glutamine Synthetase   |
| IOP   | Intensive Observation Period   |
| LAI   | Leaf Area Index  |
| LOD   | Limit Of Detection   |
| NiR   | Nitrite Reductase  |
| NR    | Nitrate Reductase  |
| PAR   | Photosynthetically Active Radiation  |
| PFA   | PerFluoroAlkoxy  |
| ppm   | parts per million (by volume)  |
| ppb   | parts per billion (by volume)  |
| ppt   | parts per trillion (by volume)   |
| ppth  | parts per thousand (by volume)   |
| PTFE  | PolyTetraFluoroEthylene  |
| PVC   | PolyVinyl Chloride   |



**Roman symbols**

|              |   |                                |
|--------------|---|--------------------------------|
| $A_{leaf}$   | leaf area   | $m^2$                          |
| $F_{ex,i}$   | exchange flux density of gas $i$                    | $nmol\ m^{-2}\ s^{-1}$         |
| $h\nu$       | photon's energy                                     | J                              |
| $j(NO_2)$    | photolysis rate of $NO_2$                           | $s^{-1}$                       |
| $k$          | rate constant for chemical reactions                | $cm^3\ molecule^{-1}\ s^{-1}$  |
| $m_i$        | slope of regression analysis of gas $i$             | $nmol\ m^{-3}$                 |
| $m_{a,i}$    | molar concentration in ambient air of gas $i$       | $nmol\ m^{-3}$ , ppb           |
| $m_{s,i}$    | molar concentration within plant chamber of gas $i$ | $nmol\ m^{-3}$ , ppb           |
| $m_{comp,i}$ | compensation point concentration of gas $i$         | $nmol\ m^{-3}$ or ppb          |
| $M_i$        | molar mass of gas $i$                               | $nmol\ s^{-1}$                 |
| $n_i$        | intercept of regression analysis of gas $i$         | $nmol\ m^{-3}$                 |
| N            | number of samples                                   | -                              |
| p            | air pressure  | hPa                            |
| $Q$          | purging rate  | $m^3\ s^{-1}$                  |
| R            | universal gas constant                              | $8.31441\ J\ mol^{-1}\ K^{-1}$ |
| $R^2$        | regression coefficient                              | -                              |
| $s_{m\_a,i}$ | standard error                                      |                                |
| $s_{m\_s,i}$ | standard error                                      |                                |
| t            | time  | s                              |
| T            | temperature   | $^{\circ}C$ or K               |
| $V$          | chamber volume                                      | $m^3$                          |
| $v_{dep,i}$  | deposition velocity of gas $i$                      | $m\ s^{-1}$                    |

### **Greek symbols**

|           |                           |    |
|-----------|---------------------------|----|
| $\lambda$ | wavelength of photon      | nm |
| $\sigma$  | standard deviation        |    |
| $\tau$    | characteristic time scale | s  |

# Introduction

## 1.1 Nitrogen in the atmosphere

The earth's atmosphere consists to almost 78 % of non-reactive nitrogen (N<sub>2</sub>) and 21 % of oxygen (O<sub>2</sub>). The remaining 1 % of the atmospheric gases is characterized by a high diversity of low-concentrated so-called trace gases. Although trace gases compose only a small proportion of the atmosphere they contribute significantly to atmospheric chemical processes, the Earth's radiative budget and biogeochemical cycles.

Natural sources of atmospheric nitrogen compounds are nitrogen fixation by lightning and cosmic radiation as well as biogenic emissions of nitric oxide (NO) from natural and cultivated soils (SEINFELD and PANDIS 2006). Additionally anthropogenic sources of reduced nitrogen are fossil fuel combustion in industry and traffic, land-use and biomass burning. Table 1 presented an overview of the global nitrogen oxides (NO<sub>x</sub>) sources.

**Table 1:** Overview of global sources of nitrogen oxides (NO<sub>x</sub>) (Tg-N yr<sup>-1</sup>). Values are from the IPCC Fourth Assessment Report, according to DENMAN et al., 2007.

| <b>sources</b>                                  | <b>NO<sub>x</sub> (Tg-N yr<sup>-1</sup>)</b> |
|---|--|
| <b>natural sources</b>                          |  |
| soil under natural vegetation                   | 3.3  |
| lightning                                       | 5  |
| atmospheric chemistry                           | <0.5   |
| <b>natural total</b>                            | <b>8.8</b>                                   |
| <b>anthropogenic sources</b>                    |  |
| fossil fuel combustion and industrial processes | 33   |
| aircraft  | 0.7  |
| agriculture                                     | 2.3  |
| biomass and biofuel burning                     | 7.1  |
| <b>anthropogenic total</b>                      | <b>43.1</b>                                  |
| <b>total, all sources</b>                       | <b>51.9</b>                                  |

Over the past 100 years two anthropogenic activities have greatly increased the reactive nitrogen availability, food and energy production (GALLOWAY et al. 2004). And since the discovery to synthesize  $\text{NH}_3$  from molecular  $\text{N}_2$ , known as the Haber-Bosch process, the human impact on the global nitrogen cycle raised drastically (ERISMAN et al. 2008). By now the emission of reactive nitrogen from human activities (food and energy production) increased by over a factor of 10 compared to the late 19<sup>th</sup> century (GALLOWAY et al. 2004).

Typical ambient nonurban  $\text{NO}_2$  concentrations are 0.05 to 1 ppb (LERDAU et al. 2000). In regions of little industrial activity annual means of  $\text{NO}_2$  mixing ratios are up to 5 ppb and in urban or industrialized regions about 20 ppb can be achieved. During smog events the  $\text{NO}_2$  concentration may exceed 1 ppm (STULEN et al. 1998). An overview of  $\text{NO}_x$  found in the atmosphere of urban and rural sites is presented in Table 2. It is striking that at remote sites the concentrations are a few tenth of ppb up to 1000 ppb at urban environments. The human input is clearly visible in the sharply decreasing of the  $\text{NO}_x$  mixing ratios moving from urban to rural sites.

**Table 2:** Typical  $\text{NO}_x$  mixing ratios (SEINFELD and PANDIS 2006).

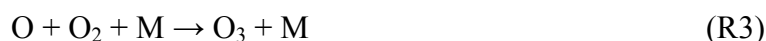
| area                    | $\text{NO}_x$ , ppb |
|-------------------------|---------------------|
| urban - suburban        | 10 - 1000           |
| rural                   | 0.2 - 10            |
| remote tropical forests | 0.02 - 0.08         |
| remote marine           | 0.02 - 0.04         |

This emission of reactive nitrogen influences biogeochemical processes in the atmosphere, in terrestrial ecosystems and in freshwater and marine aquatic ecosystems. The ecosystem productivity can be enhanced through fertilization or decreased through nutrient imbalance. The ecosystem biodiversity can be decreased through acidification and eutrophication. A higher reactive nitrogen concentration in the atmosphere can increase the incidence of human illness due to  $\text{O}_3$  and particulate matter inhalation and the greenhouse potential of the atmosphere increases through  $\text{N}_2\text{O}$  production (GALLOWAY et al. 2004).

## 1.2 Chemistry of NO, NO<sub>2</sub> and O<sub>3</sub> in the troposphere

In the troposphere nitric oxide (NO), nitrogen dioxide (NO<sub>2</sub>) and ozone (O<sub>3</sub>) are one of the most important trace species of atmospheric chemistry (CRUTZEN 1979; LOGAN et al. 1983; WARNECK 1988; SEINFELD and PANDIS 2006). These gases are strongly related to each other and known as the NO-NO<sub>2</sub>-O<sub>3</sub> triad.

Reactive nitrogen oxides are mainly emitted into troposphere as NO by natural and anthropogenic sources. In the atmosphere NO reacts with O<sub>3</sub> to form NO<sub>2</sub> (R1). Under daylight conditions NO<sub>2</sub> is photolyzed yielding NO (R2) again at wavelengths below 424 nm ( $h\nu$ ). The formed oxygen atom reacts further to reproducing O<sub>3</sub> (R3):



where O is the oxygen radical and M symbolized a molecule which absorbs the released energy, like O<sub>2</sub>, N<sub>2</sub> or H<sub>2</sub>O.

Figure 1 illustrates the processing of nitrogen oxides in the troposphere. The reactions (R1) to (R3) are the main reactions of NO and NO<sub>2</sub> in the troposphere. All other reactions involving nitrogen oxides and O<sub>3</sub> are connected to this equilibrium. Further reactions of nitrogen oxides generally forms nitrate (NO<sub>3</sub><sup>-</sup>). This oxidation path is closely connected to the photochemistry of hydroxyl radicals (OH) and hydroperoxyl radicals (HO<sub>2</sub>) with hydrocarbons, carbon monoxide (CO) (CRUTZEN 1979). Common intermediate products are nitrous acid (HNO<sub>2</sub>), nitrate radicals (NO<sub>3</sub>) and peroxyacetyl nitrate (PAN). There are two forms of nitrate present in the atmosphere, gaseous nitric acid (HNO<sub>3</sub>) and nitrate bound to aerosol particles. Dry and wet deposition of these products are an effective sink of reactive nitrogen oxides.

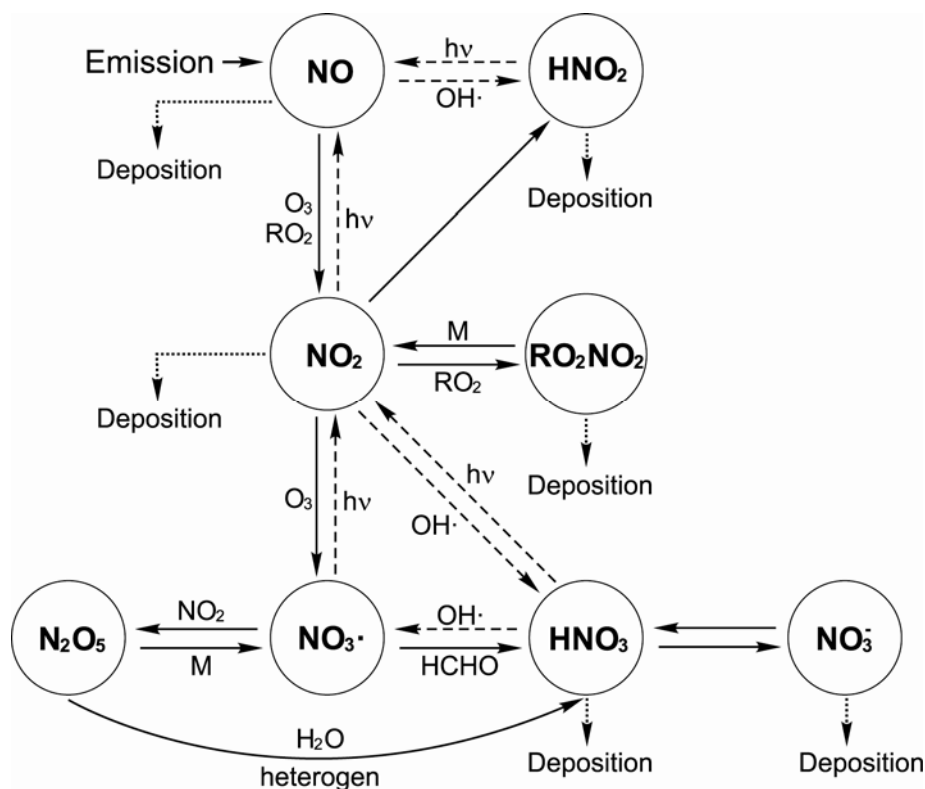


**Figure 1:** Scheme of oxidation of nitrogen oxides in the troposphere. Photochemical processes are indicated by dashed arrows (after WARNECK 1988, MEIXNER 1994).

Nitrogen oxides are of special interest due to their regulation of the  $O_3$  cycle and impact on the hydroxyl radical (OH) budget. In the absence of  $O_3$  one of the dominant reaction pathways is the oxidation of NO by  $HO_2$ :



The OH radical is the main oxidant in the atmosphere and especially in the troposphere. It is extremely reactive and able to oxidize most of the chemical compounds found in the troposphere (SEINFELD and PANDIS 2006). Though NO is oxidized to  $NO_2$  without the participation of  $O_3$  the back reaction of  $NO_2$  under daylight conditions produces  $O_3$ . This is especially important in urban and industrial areas where high emissions of both NO and CO are present (SEINFELD and PANDIS 2006). Under low NO mixing ratios, the  $HO_2$  radical reacts with  $O_3$  which leads to an overall consumption of  $O_3$ :



During night-time the NO-NO<sub>2</sub>-O<sub>3</sub> triad is influenced by the formation of nitrate radicals (NO<sub>3</sub>). These radicals are formed by the reaction of O<sub>3</sub> with NO<sub>2</sub> (R6). NO<sub>3</sub> comports with NO back to NO<sub>2</sub> (R7):



Nitrate radicals react with organic molecules in the same way as OH radicals do. They remove a hydrogen atom from alkanes to form an organic alkyl radical (R), which then reacts with O<sub>2</sub> in the air to form peroxy radicals (RO<sub>2</sub>). Formed RO<sub>2</sub> radicals are also able to oxidize NO. The availability of RO<sub>2</sub> and HO<sub>2</sub> depends on the oxidation path of CO, CH<sub>4</sub> and other hydrocarbons. Depending on the oxidation pathways RO<sub>2</sub> radicals can be formed or consumed. The used oxidation path depends on the nitrogen oxide mixing ratio in the air. Moreover, the mixing ratio of nitrogen oxides decides whether O<sub>3</sub> will be produced or consumed (CRUTZEN 1987). This is one of the main roles of nitrogen oxides in atmospheric chemistry. The lower limit of O<sub>3</sub> production is a nitrogen oxide mixing ratio of about 0.03 ppb. That means at higher values O<sub>3</sub> will be produced.

### **1.3 NO and NO<sub>2</sub> biosphere-atmosphere exchange in ecosystem forest**

The exchange of reactive nitrogen between atmosphere and the ecosystem forest depends on turbulence, uptake by vegetation, deposition to soil, emission from soil and gas phase chemistry. The surface-atmosphere exchange of most gases is coupled to biological production and consumption processes. Figure 2 displays the NO-NO<sub>2</sub>-O<sub>3</sub> triad in a forest ecosystem. NO is emitted from soil into atmosphere. If the ground is covered by vegetation a reduced wind velocity will extend the residence time of the gas inside the vegetation stand. Under these conditions parts of the emitted NO are able to react with O<sub>3</sub> to form NO<sub>2</sub> (see (R1)). Shading by plants reduces the photolysis of NO<sub>2</sub> (see (R2)) in this area. Within the vegetation stand surface exchange processes take

place and photochemical reactions continue in the atmosphere. Thus, the understanding of the separate production and destruction processes and their link with exchange processes is necessary for an understanding of the ecosystem forest.

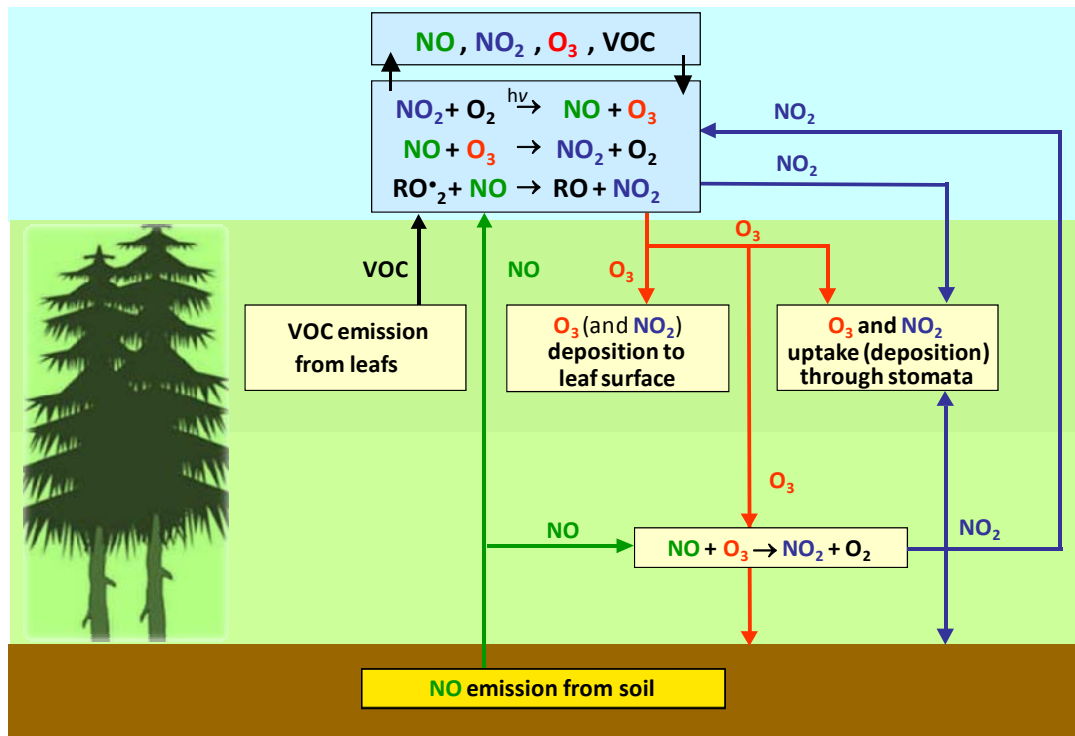


**Figure 2:** Biosphere-atmosphere interaction (surface exchange and (photo-)chemistry processes) of the  $\text{NO}$ - $\text{NO}_2$ - $\text{O}_3$ -triad and volatile organic compounds (VOC) in a forest ecosystem (after COE et al 1993).

Nitrogen is essential to the nutrition of plants and animals. It is a constituent in all proteins and in the nucleic acids of all organisms. But the atmospheric nitrogen is not available for most biological organisms because the gaseous nitrogen molecules have very strong bonds, making the gas chemically stable (SEINFELD and PANDIS 2006). Accordingly, the availability of nitrogen is often a limiting factor for the biomass production of an ecosystem. To be useful for higher plants and animals, atmospheric nitrogen has to be converted to a reduced state. Some species of bacteria possess the enzyme nitrogenase which can convert atmospheric nitrogen into ammonium ( $\text{NH}_4^+$ ) which can be metabolized by plants. These nitrogen-fixing organisms belong to the procaryotes (e.g. bacteria, cyanobacteria, actinomycetes) and may live freely in soil (e.g. *Azotobacter chroococcum*, *Clostridium pasteurianum*) or are symbionts (e.g. *Rhizobium*, *Bradyrhizobium*). Green plants can take up nitrogen directly from soil as nitrate ( $\text{NO}_3^-$ ) or as ammonium ions like mineral elements. The soil nitrate is derived



from natural mineral deposits, artificial fertilizers, animal waste or organic decay as the product of bacterial nitrification. Nitrates absorbed in this fashion are converted to nitrites ( $\text{NO}_2^-$ ) by the enzyme nitrate reductase (NR), and then converted to ammonia by another enzyme called nitrite reductase (NiR).

### 1.3.1 Processes in soil

Within the soil NO can be produced and consumed. These processes are incorporated into the metabolism of microorganisms. Hereby two main biological processes are responsible, nitrification and denitrification (WILLIAMS et al. 1992). Figure 3 displays a schematic representation of the soil nitrogen cycle and the uptake of nitrogen compounds by plants.

Nitrification is a mainly aerobic process in which ammonium ( $\text{NH}_4^+$ ) is oxidized to nitrite ( $\text{NO}_2^-$ ) and nitrate ( $\text{NO}_3^-$ ). It is a two-step process in which two different groups of microorganisms are involved, *Nitroso*-bacteria (ammonia oxidizers) and *Nitro*-bacteria (nitrite oxidizers). In the first step *Nitroso*-bacteria oxidize  $\text{NH}_4^+$  via hydroxylamine ( $\text{NH}_2\text{OH}$ ) to  $\text{NO}_2^-$  and in the second step *Nitro*-bacteria oxidize  $\text{NO}_2^-$  to  $\text{NO}_3^-$ . Within the oxidation process formation of gaseous NO and  $\text{N}_2\text{O}$  as intermediate compounds is observed (ROBERTSON and GROFFMAN 2007). But the exact pathway of this formation is still not clarified (LUDWIG et al. 2001). NO can also be produced via  $\text{NO}_2^-$  reduction by *Nitroso*-bacteria (LUDWIG et al. 2001; ROBERTSON and GROFFMAN 2007). This occurs when  $\text{O}_2$  is limited and the bacteria use  $\text{NO}_2^-$  as an electron acceptor (BOLLMANN and CONRAD 1998).

Denitrification occurs under anaerobic conditions and is the reduction of  $\text{NO}_3^-$  to  $\text{N}_2$  and the intermediate compounds  $\text{NO}_2^-$ , NO and  $\text{N}_2\text{O}$ . These microorganisms use  $\text{NO}_3^-$  rather than  $\text{O}_2$  as a terminal electron acceptor (ROBERTSON and GROFFMAN 2007). The denitrifiers are aerobic microorganisms, which can switch to anaerobic denitrification when  $\text{O}_2$  is limited. Moreover  $\text{O}_2$  is the more efficient electron acceptor, hence most denitrifiers only carry out denitrification when  $\text{O}_2$  is unavailable. This happens especially after rainfalls, when the soil pores become filled up with water and the  $\text{O}_2$  diffusion through the soil is slow.



Another source of nitrogen for plants is the uptake of atmospheric nitrogen by leaves. In general, plants are considered as a sink of atmospheric nitrogen oxides. Since the studies by HILL (1971), the deposition of atmospheric NO and NO<sub>2</sub> is demonstrated for different plants. The uptake by plants depends on the plant species. HANSON and LINDBERG (1991) provide a comprehensive overview of the deposition of NO<sub>2</sub> to leaf and canopy surfaces, respectively. The authors show that the NO<sub>2</sub> leaf conductances under daytime conditions differ by two magnitudes. Continuative studies have identified some factors, which make a contribution to the different uptake rates. JENSEN and PILEGAARD (1993) found out that the nitrate supply in the soil have an effect on the NO<sub>2</sub> uptake rate. Also the salinity of the soil plays a role (FUHRER and ERISMANN 1980). Moreover, uptake rates differ also inside one species. Apparently the plant developmental stage is an important factor as indicated by studies of GRENNFELT et al. (1983) who investigated different ages of Scots pine needles. They identified NO<sub>2</sub> uptake variability of about 100 %.

The uptake of NO<sub>2</sub> proceeds mainly by diffusion through the stoma (SKÄRBY et al. 1981; SAXE 1986; HANSON et al. 1989; THOENE et al. 1991). A smaller fraction of NO<sub>2</sub> is absorbed by the cuticula of the leaves or the surface water film if present (KISSER-PRIESACK et al. 1987, 1990; BURKHARD and EIDEN 1994) (Figure 4).

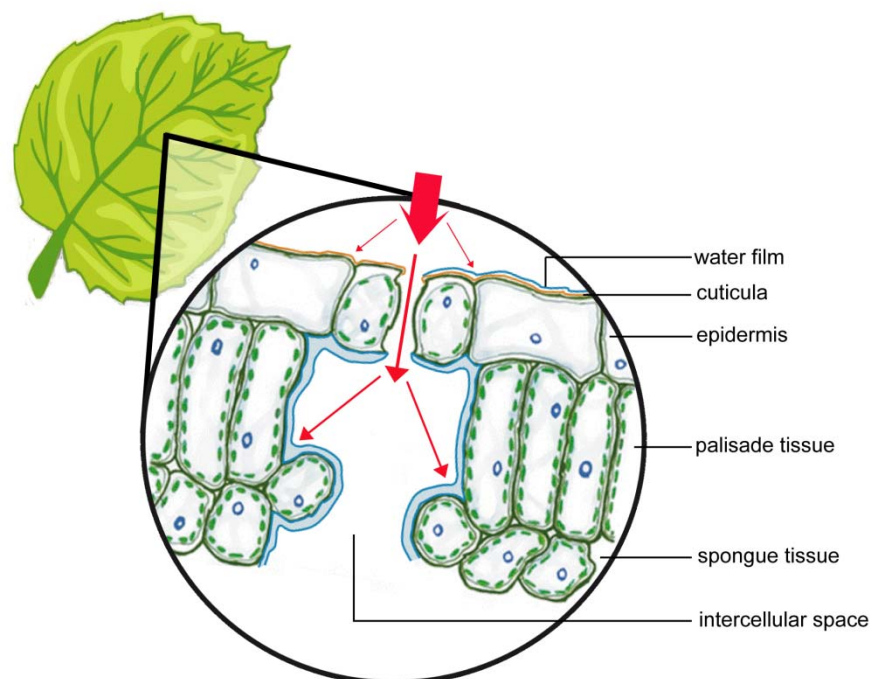


**Figure 4:** Illustrating the different pathways of trace gas uptake to a leaf.

The deposition on a dry or wet cuticle is at least one or two orders of magnitude lower than the stomatal uptake (WELLBURN 1990). The  $\text{NO}_2$  molecule can undergo irreversible as well as reversible reactions with phenolic components of the cuticle (LENDZIAN and KERSTIENS 1988; KISSER-PRIESACK et al. 1990) Hence,  $\text{NO}_2$  can also be re-emitted into atmosphere. However, these processes seem to be negligible in comparison to the total  $\text{NO}_2$  flux.

The gas uptake through the stomata is driven by the concentration gradient between the gas phase inside and outside the leaf. Several studies have demonstrated a linear increase of  $\text{NO}_2$  uptake with rising atmospheric  $\text{NO}_2$  concentration (JOHANSSON 1987; THOENE et al. 1991, 1996).

A plant can control the entry of gases into the leaf by varying the stomatal aperture. Number, distribution, size, shape and activity of the stoma are species specific. Additional they vary with adaptation to the place of growth and one individual to another as well. The stomatal movement is regulated mainly by two controlling cycles, carbon dioxide and water. The degree of opening is adjusted continuously to changes in the environment, such as light intensity, temperature, air humidity and carbon dioxide concentration.

In the substomatal cavity  $\text{NO}_2$  dissolves rapidly in the aqueous phase of the apoplastic space where it disproportionates to  $\text{NO}_2^-$  and  $\text{NO}_3^-$  (LEE and SCHWARTZ 1981; RAMGE et al. 1993). Due to the better solubility in aqueous solutions  $\text{NO}_2$  will be dissolved easier than  $\text{NO}$ . However, the observed uptake rate of  $\text{NO}_2$  cannot be explained by the liquid solubility only. The disproportionation reaction appears too slow to explain the measured leaf fluxes of  $\text{NO}_2$  (PARK and LEE 1988; RAMGE et al. 1993). Hence, the reduction of  $\text{NO}_2$  by apoplastic antioxidants, particularly ascorbate, has been proposed (RAMGE et al. 1993). The theoretical calculations of RAMGE et al. (1993) demonstrated sufficient rates to explain observed  $\text{NO}_2$  leaf fluxes if the reactions between water and  $\text{NO}_2$  and between  $\text{NO}_2$  and ascorbate are taken into account. The role of ascorbate in the foliar uptake of  $\text{NO}_2$  has been experimentally demonstrated by TEKLEMARIAM and SPARKS (2006). They observed a significant correlation between leaf ascorbate concentrations and the leaf fluxes of  $\text{NO}_2$ . However, apoplastic ascorbate concentrations differ between species but also between individuals of the same species depending on environmental factors (POLLE et al. 1995; LUWE 1996).

Apoplastic  $\text{NO}_2$  and  $\text{NO}_3^-$  can be incorporated into the general nitrogen metabolism of the leaves. Taking all these steps into account Figure 5 gives an overview about the different assimilation pathways for atmospheric  $\text{NO}$ ,  $\text{NO}_2$  and  $\text{NH}_3$ . After taken up into the apoplast the formed  $\text{NO}_2^-$  and  $\text{NO}_3^-$  are transported into the cytoplasm of mesophyll cells (AMMANN et al. 1995) where  $\text{NO}_3^-$  is reduced to  $\text{NO}_2^-$  by nitrate reductase (NR) (THOENE et al. 1991, TISCHNER 2000).  $\text{NO}_2^-$  is then transported into the chloroplast, where it is reduced to  $\text{NH}_4^+$  by nitrite reductase (NiR). Moreover,  $\text{NH}_4^+$  can be formed by assimilation of gaseous ammonia ( $\text{NH}_3$ ). The  $\text{NH}_4^+$  is then incorporated into the amino acid glutamine by the enzyme glutamine synthetase (GS) inside the cytoplasm. Alternatively,  $\text{NH}_4^+$  can be incorporated by chloroplastic glutamate synthetase, a step also known as GOGAT cycle (LEA and MIFLIN 1974). Different studies revealed that GS is located in the cytoplasm ( $\text{GS}_1$ ) and in the chloroplast ( $\text{GS}_2$ ) of plant cells (MAECK 1995; SAKAKIBARA et al. 1996).

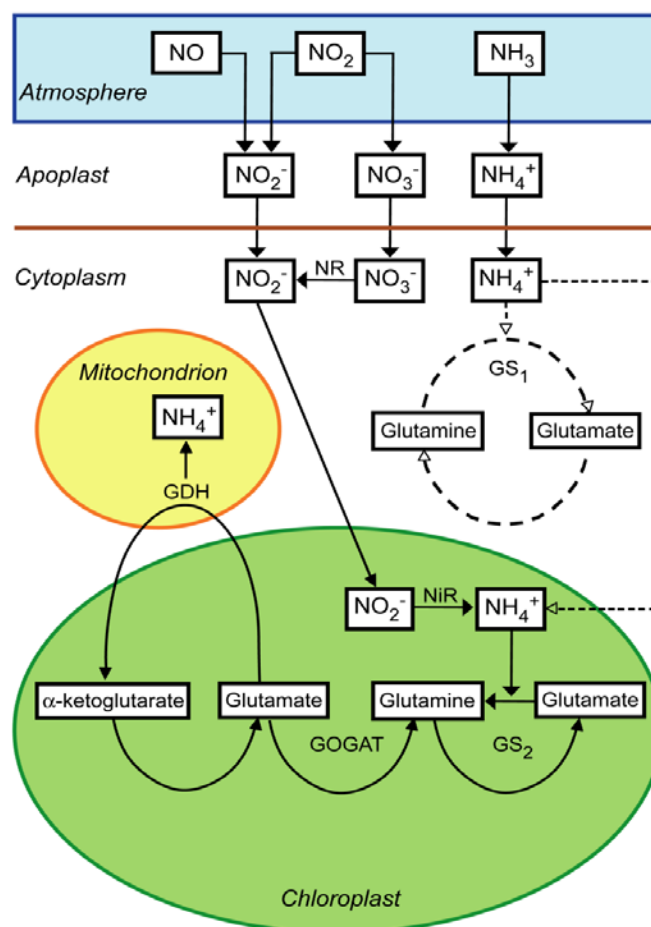


**Figure 5:** Biochemical processes involved in foliar uptake and assimilation of  $\text{NO}_x$  and  $\text{NH}_3$ . Dashed lines indicate the possible role of cytosolic glutamine synthetase ( $\text{GS}_1$ ) or chloroplastic glutamate synthetase ( $\text{GS}_2$ ) in the assimilation of  $\text{NH}_4^+$  derived from gaseous  $\text{NH}_3$  (after LEA et al. 1994; STULEN et al. 1998)

The ability of plants to incorporate atmospheric  $\text{NO}_2$  into free amino acids was demonstrated by numerous studies using  $^{15}\text{N}$  as a tracer (NUSSBAUM et al. 1993; WEBER et al. 1995; YONEYAMA et al. 2003). The studies have demonstrated that the primary assimilation of inorganic nitrogen into amino acids is largely through the GS/GOGAT pathway (YONEYAMA et al. 2003).

The question whether atmospheric nitrogen uptake by leaves affects the nitrogen uptake by roots is still under discussion. According to SCHULZE (1989) additional leaf uptake of atmospheric nitrogen causes a nutrient imbalance due to nitrogen to cation discrepancies, which result in decline symptoms like needle yellowing and loss. RENNENBERG and GEBLER (1999) reported on a down-regulation of the nitrogen uptake by roots to an extent that equals nitrogen uptake by leaves. We understand that the foliar uptake is significant enough (10 - 25 %) to influence plant metabolism but the complex regulation between root uptake, nitrogen availability and foliar uptake is a complex interaction of metabolic processes and physiological regulations and need further research (VALLANO and SPARKS 2008).

Moreover, plants can also act as a source of gaseous nitrogen compounds. The emission of ammonia ( $\text{NH}_3$ ) by plants has been reported (KESSELMEIER et al. 1993; FANGMEIER et al. 1994; SCHJOERRING et al. 1998, 2000). Contrasting the emission of  $\text{NO}$  and  $\text{NO}_2$  by plants is not accepted finally.  $\text{NO}$  emission is demonstrated only by a few studies (KLEPPER 1997; DEAN and HARPER 1986; WILDT et al. 1997). However, WILDT et al. (1997) estimated that plants emitted only 1 - 5 %  $\text{NO}$  compared to the global emission rate of  $\text{NO}$  from soils. Because  $\text{NO}$  has a lower water solubility than  $\text{NO}_2$ , the  $\text{NO}$  uptake by plants is lower than for  $\text{NO}_2$  (MEIXNER 1994).

Similarly the potential emission of  $\text{NO}_2$  by plants is still under discussion. A release may be expected when atmospheric  $\text{NO}_2$  mixing ratios are below a certain compensation point concentration. LERDAU et al. (2000) reported that depending on the leaf area indices of the relevant sites only 25 to max. 80 % of the  $\text{NO}_x$  mainly derived from  $\text{NO}$  emission is escaping the forest (see JACOB and WOFSY 1990; YIENGER and LEVY 1995; WANG et al. 1998). However, such results do not agree with leaf-level measurements reporting about  $\text{NO}_2$  emission from plants (besides plant uptake of  $\text{NO}_2$ ). Corresponding compensation point concentrations of  $\text{NO}_2$  between 0.3 and 3 ppb have been reported (RONDÓN et al. 1993; THOENE et al. 1996; WEBER and RENNENBERG 1996a;

SPARKS et al. 2001; GEBLER et al. 2000, 2002; HEREID and MONSON 2001), suggesting plants to act as a sink for atmospheric NO<sub>2</sub> when ambient NO<sub>2</sub> concentrations are exceeding, or as a source of NO<sub>2</sub> when ambient NO<sub>2</sub> concentrations are below the NO<sub>2</sub> compensation point concentration. Table 3 gives an overview of reported NO<sub>2</sub> compensation points. According to LERDAU et al. (2000), these results and discussions contradict the reports of JACOB and WOFYSY (1990), who demonstrated that even at ambient NO<sub>2</sub> concentrations of 0.2 to 0.4 ppb a strong uptake of NO<sub>2</sub> by plants (primary rainforest) is still required to align measured NO<sub>2</sub> concentrations in the canopy with the measured NO soil emission rates. LERDAU et al. (2000) emphasized the urgent need to find an explanation for this discrepancy, particularly in remote regions far away from anthropogenic NO<sub>x</sub> sources (e.g. primary rain and boreal forests under low NO<sub>x</sub> regimes). Thus it is required to investigate the contribution of the NO<sub>2</sub> uptake by plants and to ensure NO<sub>2</sub> compensation point concentrations at (sub-) ppb levels.

**Table 3:** Reported NO<sub>2</sub> (or NO<sub>y</sub>) compensation point concentrations obtained from literature.

| NO <sub>2</sub><br>compensation<br>point, ppb | plant species   | author                        |
|---|---|-------------------------------|
| 0.03 - 17*                                    | Scots pine  | Raivonen et al. (2009)        |
| 1 - 3   | Scots pine ( <i>Pinus sylvestris</i> )  | Johansson (1987)              |
| 1.8 - 1.9                                     | Beech ( <i>Fagus sylvatica</i> )  | Geßler et al. (2000)          |
| 1.7   | Norway spruce ( <i>Picea abies</i> )  | Geßler et al. (2002)          |
| 1.64 ± 0.3                                    | Norway spruce ( <i>Picea abies</i> )  | Thoene et al. (1996)          |
| 0.53 - 1.6                                    | tropical trees  | Sparks et al. (2001)          |
| 1.0 - 1.2                                     | Wheat ( <i>Triticum aestivum</i> )<br>Corn ( <i>Zea mays</i> )<br>Sunflower ( <i>Helianthus annuus</i> )<br>Catharanthus ( <i>Madagascar periwinkle</i> ) | Teklemariam & Sparks (2006)   |
| 1.15  | Wheat ( <i>Triticum aestivum</i> )  | Weber and Rennenberg (1996)   |
| 0.02 - 1.1                                    | European tree species<br>( <i>Fagus sylvatica</i> , <i>Quercus robur</i> , <i>Quercus ilex</i> , <i>Betula pendula</i> , <i>Pinus sylvestris</i> )        | Chaparro-Suarez et al. (2011) |
| 0.9   | Corn ( <i>Zea mays</i> )  | Hereid & Monson (2001)        |
| 0.1 - 0.7                                     | Scots pine ( <i>Pinus sylvestris</i> )<br>Norway spruce ( <i>Picea abies</i> )  | Rondón et al. (1993)          |
| <0.1 - 0.6                                    | Norway spruce ( <i>Picea abies</i> )  | Rondón & Granat (1994)        |
| <0.1 - 0.3                                    | Scots pine ( <i>Pinus sylvestris</i> )  | Rondón & Granat (1994)        |

\* (NO<sub>y</sub>)

## 1.4 Objectives of thesis

In this study measurements with a dynamic chamber system were performed to determine plant surface-atmosphere exchange fluxes of  $\text{NO}_2$  ( $\text{NO}$  and  $\text{O}_3$ ) under typical field conditions (uncontrolled) for a relatively remote, managed Norway spruce forest site as well as under controlled conditions including (laboratory) fumigation experiments. Because  $\text{NO}_2$  compensation point concentrations were reported at (sub-)ppb levels, our laboratory  $\text{NO}_2$  fumigation experiments were performed with 3- to 4-yr old Norway Spruce trees at 0.3 - 3.4 ppb. Also under field conditions, such low ambient  $\text{NO}_2$  concentrations can be expected.

Moreover, exchange fluxes derived from dynamic chamber measurements are based on generally (very) small differences of  $\text{NO}_2$  ( $\text{NO}$ ,  $\text{O}_3$ ) concentrations between inlet and outlet of the chamber. Consequently, detection limits of corresponding analyzers, statistical significance of the concentration differences, as well as the statistical goodness of measurements definitely have a substantial impact on the identification and quantification of statistically significant deposition velocities and compensation point concentrations, and have been considered correspondingly. Furthermore, as the exchange of  $\text{NO}_2$  is a complex interaction of transport, chemistry and plant physiology, in our field experiments we determined fluxes of  $\text{NO}$ ,  $\text{NO}_2$ ,  $\text{O}_3$ ,  $\text{CO}_2$  and  $\text{H}_2\text{O}$ .

This thesis presents basic considerations of dynamic plant chamber system measurements and the constraints of precision and design for chamber measurements as well as results of laboratory and field measurements. In chapter 3 specification and implementation of the performed dynamic plant chamber system are presented. The performance of data analysis is demonstrated on values from laboratory experiments and selected results from field measurements. The application of the chamber system to field measurements and the results for the trace gas exchange between plants and the atmosphere under field conditions are described in chapter 4.



# Material and Methods

The commonly used technique for leaf-level exchange measurements of NO<sub>2</sub> is the dynamic chamber technique (a technique also used for many non-reactive (e.g. CO<sub>2</sub>, H<sub>2</sub>O, COS) and reactive trace gases (e.g. NO, O<sub>3</sub>, VOCs, DMS, CS<sub>2</sub>, HONO, HNO<sub>3</sub>, CH<sub>2</sub>O, HCOOH, CH<sub>3</sub>COOH)). Here, an entire plant (or parts of a plant) is enclosed in a (transparent) chamber which is purged by (preferably ambient) air. Two measurements of NO<sub>2</sub> concentration are usually performed, namely (1) at the entrance of the chamber (= ambient NO<sub>2</sub> concentration) and (2) within the chamber. If the chamber is well mixed, the latter measurement can be replaced by that of the outlet NO<sub>2</sub> concentration. Alternatively, a set of two chambers, one enclosing the plant the other being empty, can be used. To relate these two concentration measurements to the exchange (i.e. the uni- or bi-directional flux) of NO<sub>2</sub> between the (chamber) atmosphere and the enclosed plant (or parts of plant), the full mass balance of the dynamic chamber must be considered, i.e. NO<sub>2</sub> fluxes entering and leaving the chamber, as well as all other fluxes due to NO<sub>2</sub> sinks and sources within the chamber's volume. Under typical field conditions (i.e. ambient air enters the dynamic chamber), not only NO<sub>2</sub> is purged through the chamber, but also ambient NO and O<sub>3</sub>. Fast reaction between NO and O<sub>3</sub> forms a "chemical" source of NO<sub>2</sub>, while (under daylight conditions) photolysis of NO<sub>2</sub> ( $\lambda = 420$  nm) is a "chemical" sink. Depending on actual ambient NO<sub>2</sub>, NO and O<sub>3</sub> concentrations as well on UV irradiation intensity, corresponding "gas phase fluxes" may reach the magnitude of the NO<sub>2</sub> flux from/to the enclosed plant(s) (MEIXNER et al. 1997; PAPE et al. 2009). Consequently, simultaneous measurements of NO<sub>2</sub>, NO and O<sub>3</sub> concentrations at the outlet of the chamber are required. However, since there is substantial uptake of O<sub>3</sub> by the plants (to a much lesser extent also of NO), NO<sub>2</sub>, NO and O<sub>3</sub> concentrations at the inlet of the chamber have to be measured, too. As a positive "by-product" of these additional concentration measurements, deposition velocities of O<sub>3</sub> (and NO) may be inferred considering the dynamic chamber's mass balances of O<sub>3</sub> and NO.

## 2.1 Basic considerations

A small branch of a tree (leaf area  $A_{leaf}$ ), which is enclosed in a transparent plant chamber of volume  $V$  was considered. The air within the plant chamber is well mixed by action of one (or more) fan(s). Ambient air (containing  $\text{NO}_2$ ,  $\text{NO}$  and  $\text{O}_3$ ) is entering the plant chamber at the inlet, flushing the chamber with the purging rate  $Q$  ( $\text{m}^3 \text{s}^{-1}$ ) and leaving the chamber at the outlet. Within plant chamber trace gases of the  $\text{NO}$ - $\text{NO}_2$ - $\text{O}_3$  triad may be (a) emitted and/or taken up from/by leaves, (b) deposited to the inner walls of the plant chamber and (c) destroyed and/or generated by (fast) photo-chemical reactions.

### 2.1.1 Mass balance of the $\text{NO}$ - $\text{NO}_2$ - $\text{O}_3$ triad of a dynamic plant chamber

Considering the molar mass flux of the trace gas  $i$  ( $i = \text{NO}_2, \text{NO}, \text{O}_3$ ), i.e. the derivative of molar mass  $M_i$  with respect to time ( $\partial M_i / \partial t$  in  $\text{nmol s}^{-1}$ ), the individual flux components of the dynamic plant chamber system are defined as follows:

$\partial M_{in,i} / \partial t :=$  molar mass flux of trace gas  $i$  entering the plant chamber

$\partial M_{out,i} / \partial t :=$  molar mass flux of trace gas  $i$  leaving the plant chamber

$\partial M_{wall,i} / \partial t :=$  molar mass flux of trace gas  $i$  to the inner wall of the plant chamber (due to ad-/absorption of trace gas  $i$ )

$\partial M_{em,i} / \partial t :=$  molar mass flux of trace gas  $i$  caused by (biogenic) emission from the leaves

$\partial M_{dep,i} / \partial t :=$  molar mass flux of trace gas  $i$  caused by uptake to the leaves (e.g. cuticular, stomatal and/or mesophyllic uptake)

$\partial M_{prod,i} / \partial t :=$  molar mass flux of trace gas  $i$  into the plant chamber's volume caused by gas phase production, i.e. from photochemical decay or fast chemical reaction of other trace gas(es)

$\partial M_{dest,i} / \partial t :=$  molar mass flux of trace gas  $i$  out of the plant chamber's volume caused by gas-phase destruction, i.e. by photochemical decay of trace gas  $i$  or by fast chemical reaction with other trace gas(es).

Under steady-state conditions (i.e. concentrations of trace gas  $i$  are constant (have reached equilibrium)) and considering the convention, that mass fluxes into (out) of the plant chamber's volume are counted positive (negative), the molar mass flux balance of the trace gas  $i$  is given by

$$+\frac{\partial M_{in,i}}{\partial t} - \frac{\partial M_{out,i}}{\partial t} - \frac{\partial M_{wall,i}}{\partial t} + \frac{\partial M_{em,i}}{\partial t} - \frac{\partial M_{dep,i}}{\partial t} + \frac{\partial M_{prod,i}}{\partial t} - \frac{\partial M_{dest,i}}{\partial t} = 0 \quad (1)$$

While the first three and the last two left-hand terms of Eq. (1) may be known and/or are determined by laboratory or *in-situ* measurements,  $\partial M_{em,i}/\partial t$  and  $\partial M_{dep,i}/\partial t$  are the unknown fluxes of trace gas  $i$ . We combine these two fluxes to the bi-directional “exchange flux”  $\partial M_{ex,i}/\partial t$

$$\frac{\partial M_{ex,i}}{\partial t} = +\frac{\partial M_{em,i}}{\partial t} - \frac{\partial M_{dep,i}}{\partial t} \quad i = NO_2, NO, O_3 \quad (2)$$

Considering the purging rate  $Q$  ( $m^3 s^{-1}$ ) and the molar concentration  $m_{a,i}$  ( $nmol m^{-3}$ ) of trace gas  $i$  in ambient air, the ingoing flux is

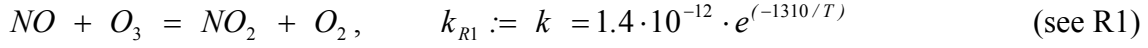
$$\frac{\partial M_{in,i}}{\partial t} = Q \cdot m_{a,i} \quad i = NO_2, NO, O_3 \quad (3)$$

The molar concentration at the outlet of the plant chamber is equivalent to the molar concentration within the plant chamber ( $m_{s,i}$  in  $nmol m^{-3}$ ), provided the plant chamber's volume is well mixed by one (or more) appropriate fan(s) (see MEIXNER et al. 1997; PAPE et al. 2009). Then, the flux leaving the chamber is defined by

$$\frac{\partial M_{out,i}}{\partial t} = Q \cdot m_{s,i} \quad i = NO_2, NO, O_3 \quad (4)$$

The flux to the inner walls can be easily determined by corresponding laboratory experiments (e.g. LUDWIG 1994; MEIXNER et al. 1997). If the material of the plant chamber is consisting of chemically inert material, the flux  $\partial M_{wall,i}/\partial t$  can usually be

neglected. In case of the NO-NO<sub>2</sub>-O<sub>3</sub> triad, the relevant photochemical reactions controlling the gas-phase production and destruction of the respective trace gas are



Applying simple reaction kinetics, the corresponding fluxes  $\partial M_{prod,i}/\partial t$  and  $\partial M_{dest,i}/\partial t$  are given by

$$\frac{\partial M_{prod,NO_2}}{\partial t} = \frac{\partial M_{dest,NO}}{\partial t} = \frac{\partial M_{dest,O_3}}{\partial t} = V \cdot k \cdot m_{s,NO} \cdot m_{s,O_3} \quad (5)$$

and

$$\frac{\partial M_{dest,NO_2}}{\partial t} = \frac{\partial M_{prod,NO}}{\partial t} = \frac{\partial M_{prod,O_3}}{\partial t} = V \cdot j(NO_2) \cdot m_{s,NO_2} \quad (6)$$

where  $V$  is the plant chamber's volume (m<sup>3</sup>),  $k$  is the (temperature-dependent) reaction coefficient of the NO + O<sub>3</sub> reaction (m<sup>3</sup> nmol<sup>-1</sup> s<sup>-1</sup>) (ATKINSON et al. 2004) and  $j(NO_2)$  (s<sup>-1</sup>) is the photolysis rate of reaction (R2), which can be measured *in-situ* (or parameterized from data of global radiation; see TREBS et al. 2009).

Considering Eqs. (1) - (6), the molar mass flux balances of the trace gas triad NO-NO<sub>2</sub>-O<sub>3</sub> (under steady state conditions) can be formulated as follows:

$$\frac{\partial M_{ex,NO_2}}{\partial t} = Q \cdot m_{s,NO_2} - Q \cdot m_{a,NO_2} - V \cdot k \cdot m_{s,NO} \cdot m_{s,O_3} + V \cdot j(NO_2) \cdot m_{s,NO_2} \quad (7.1)$$

$$\frac{\partial M_{ex,NO}}{\partial t} = Q \cdot m_{s,NO} - Q \cdot m_{a,NO} + V \cdot k \cdot m_{s,NO} \cdot m_{s,O_3} - V \cdot j(NO_2) \cdot m_{s,NO_2} \quad (7.2)$$

$$\frac{\partial M_{ex,O_3}}{\partial t} = Q \cdot m_{s,O_3} - Q \cdot m_{a,O_3} + V \cdot k \cdot m_{s,NO} \cdot m_{s,O_3} - V \cdot j(NO_2) \cdot m_{s,NO_2} \quad (7.3)$$

Equations (7.1) - (7.3) explicitly define the molar mass fluxes (in nmol s<sup>-1</sup>) of the NO<sub>2</sub>, NO and O<sub>3</sub> surface exchange between the plant chamber's atmosphere and the enclosed leaves in terms of measured and/or *a priori* known quantities only.

### 2.1.2 Molar mass flux densities, deposition velocities and compensation point concentrations

Equations (7.1) - (7.3) are formulated in terms of molar mass fluxes (in  $\text{nmol s}^{-1}$ ). However, considering the exchange of reactive trace gases between the plant chamber's atmosphere and the enclosed leaves, the exchange flux density ( $F_{ex,i}$ ) of the molar mass (in  $\text{nmol m}^{-2} \text{s}^{-1}$ ) is commonly used rather than the molar mass flux itself. In case of plant chamber studies, the appropriate reference surface (reference area) is the surface area ( $A_{leaf}$ , in  $\text{m}^2$ ) of the leaves. Therefore, the exchange flux density  $F_{ex,i}$  is defined as  $F_{ex,i} := (\partial M_i / \partial t) / A_{leaf}$ , and the corresponding balance equations will read as follows:

$$F_{ex,NO_2} = -\frac{Q}{A_{leaf}} \left( m_{a,NO_2} - m_{s,NO_2} + \frac{V}{Q} k m_{s,NO} m_{s,O_3} - \frac{V}{Q} j(NO_2) m_{s,NO_2} \right) \quad (8.1)$$

$$F_{ex,NO} = -\frac{Q}{A_{leaf}} \left( m_{a,NO} - m_{s,NO} - \frac{V}{Q} k m_{s,NO} m_{s,O_3} + \frac{V}{Q} j(NO_2) m_{s,NO_2} \right) \quad (8.2)$$

$$F_{ex,O_3} = -\frac{Q}{A_{leaf}} \left( m_{a,O_3} - m_{s,O_3} - \frac{V}{Q} k m_{s,NO} m_{s,O_3} + \frac{V}{Q} j(NO_2) m_{s,NO_2} \right) \quad (8.3)$$

In case of defined laboratory experiments, where plants may be fumigated with only one of the three trace gases (i.e., gas-phase production and/or destruction of the trace gas can be ruled out), Eqs. (8.1) - (8.3) will reduce to the well-known form of

$$F_{ex,i}^* = -\frac{Q}{A_{leaf}} (m_{a,i} - m_{s,i}) \quad i = NO_2, NO, O_3 \quad (8.4)$$

In case of bi-directional exchange (see Eq. (2)), the exchange between the plant chamber's atmosphere and the leaves can be directed to or away from the leaves. This exchange process can be subject to the so-called "compensation point concentration" ( $m_{comp,i}$ , in  $\text{nmol m}^{-3}$ ). According to CONRAD (1994),  $m_{comp,i}$  is "that concentration at which the consumption rate reaches the same value as the production rate, so that the result of both processes is zero flux". The exchange flux density  $F_{ex,i}$  is commonly parameterized (e.g. HICKS et al. 1987) by the so-called "deposition velocity"  $v_{dep,i}$  (in  $\text{m s}^{-1}$  or  $\text{mm s}^{-1}$ ) of trace gas  $i$  and its compensation point concentration,  $m_{comp,i}$ :

$$F_{ex,NO_2} = -v_{dep,NO_2} (m_{s,NO_2} - m_{comp,NO_2}) \quad (9.1)$$

$$F_{ex,NO} = -v_{dep,NO} (m_{s,NO} - m_{comp,NO}) \quad (9.2)$$

$$F_{ex,O_3} = -v_{dep,O_3} (m_{s,O_3} - m_{comp,O_3}) \quad (9.3)$$

Note, that (by convention)  $F_{ex,i}$  is directed “downward” to the leaves, if  $m_{s,i} > m_{comp,i}$ ,  $F_{ex,i}$  is zero, if  $m_{s,i} = m_{comp,i}$  and  $F_{ex,i}$  is directed “upward” from the leaves, if  $m_{s,i} < m_{comp,i}$ .

Given, that the quantities  $Q$ ,  $A_{leaf}$ ,  $k$  and  $j(NO_2)$  are *a priori* known and/or simultaneously measured with  $m_{s,i}$  and  $m_{a,i}$ . Then, the desired quantities,  $v_{dep,i}$  and  $m_{comp,i}$ , are commonly determined from the linear relationship between  $F_{ex,i}$  and  $m_{s,i}$ , where  $v_{dep,i}$  is the slope and  $m_{comp,i}$  is the intersect of  $F_{ex,i}$  with the  $m_{s,i}$ -axis (see RONDÓN and GRANAT 1994; THOENE et al. 1996; WEBER and RENNENBERG 1996a; SPARKS et al. 2001; HEREID and MONSON 2001; GEBLER et al. 2002).

However, due to the fact, that  $F_{ex,i}$  (see Eqs. (8.1) - (8.3)) contains the term  $Q/A_{leaf} \cdot (m_{a,i} - m_{s,i})$ , the calculation of any form of linear regression between  $F_{ex}$  and  $m_{s,i}$  is mathematically not correct, because the dependent variable  $F_{ex,i}$  contains the independent variable ( $m_{s,i}$ ).

This problem can be resolved by returning to the originally measured quantities,  $m_{a,i}$  and  $m_{s,i}$ . If we combine Eqs. (8.1) - (8.3) and Eqs. (9.1) - (9.3) and resolve these equations for  $m_{s,NO_2}$ ,  $m_{s,NO}$  and  $m_{s,O_3}$ , we yield three linear relationships between the measured variables  $m_{s,NO_2}$  and  $m_{a,NO_2}$ ,  $m_{s,NO}$  and  $m_{a,NO}$  and  $m_{s,O_3}$  and  $m_{a,O_3}$ :

$$m_{s,NO_2} = n_1 + m_1 \cdot m_{a,NO_2} \quad (10.1)$$

$$m_{s,NO} = n_2 + m_2 \cdot m_{a,NO} \quad (10.2)$$

$$m_{s,O_3} = n_3 + m_3 \cdot m_{a,O_3} \quad (10.3)$$

using the definitions:

$$n_1 := \frac{\bar{A}_{leaf} v_{dep,NO_2} m_{comp,NO_2} + V \bar{k} \bar{m}_{s,NO} \bar{m}_{s,O_3}}{\bar{Q} + \bar{A}_{leaf} v_{dep,NO_2} + V \bar{j}(NO_2)} ; \quad m_1 := \frac{\bar{Q}}{\bar{Q} + \bar{A}_{leaf} v_{dep,NO_2} + V \bar{j}(NO_2)} \quad (11.1)$$

$$n_2 := \frac{\bar{A}_{leaf} v_{dep,O3} m_{comp,O3} + V \bar{j}(NO_2) \bar{m}_{s,NO2}}{\bar{Q} + \bar{A}_{leaf} v_{dep,O3} + V \bar{k} \bar{m}_{s,O3}} ; \quad m_2 := \frac{\bar{Q}}{\bar{Q} + \bar{A}_{leaf} v_{dep,NO} + V \bar{k} \bar{m}_{s,O3}} \quad (11.2)$$

$$n_3 := \frac{\bar{A}_{leaf} v_{dep,O3} m_{comp,O3} + V \bar{j}(NO_2) \bar{m}_{s,NO2}}{\bar{Q} + \bar{A}_{leaf} v_{dep,O3} + V \bar{k} \bar{m}_{s,NO}} ; \quad m_3 := \frac{\bar{Q}}{\bar{Q} + \bar{A}_{leaf} v_{dep,O3} + V \bar{k} \bar{m}_{s,NO}} \quad (11.3)$$

The quantities  $n_i$  and  $m_i$  may be evaluated (graphically) as the intercept and the slope of the plot of measured  $m_{s,i}$  versus measured  $m_{a,i}$ . Application of different forms of linear regression analysis delivers  $n_i$  and  $m_i$  and bi-variate weighted linear least-squares fitting (which considers uncertainties of both,  $m_{s,i}$  and  $m_{a,i}$ ) provides also their standard errors  $s_{n,i}$  and  $s_{m,i}$  (see Sect. 3.1.6).

The linear relationships between  $F_{ex,i}$  and  $m_{s,i}$  are still maintained. This can be shown by resolving Eqs. (10.1) - (10.3) for  $m_{a,i}$  and making use of Eqs. (8.1) - (8.3):

$$F_{ex,NO2} = \frac{\bar{Q}}{\bar{A}_{leaf}} \left( \frac{n_1}{m_1} - \frac{V}{\bar{Q}} \bar{k} \bar{m}_{s,NO} \bar{m}_{s,O3} \right) + \frac{\bar{Q}}{\bar{A}_{leaf}} \left( 1 - \frac{1}{m_1} + \frac{V}{\bar{Q}} \bar{j}(NO_2) \right) \cdot m_{s,NO2} \quad (12.1)$$

$$F_{ex,NO} = \frac{\bar{Q}}{\bar{A}_{leaf}} \left( \frac{n_2}{m_2} - \frac{V}{\bar{Q}} \bar{j}(NO_2) \bar{m}_{s,NO2} \right) + \frac{\bar{Q}}{\bar{A}_{leaf}} \left( 1 - \frac{1}{m_2} + \frac{V}{\bar{Q}} \bar{k} \bar{m}_{s,O3} \right) \cdot m_{s,NO} \quad (12.2)$$

$$F_{ex,O3} = \frac{\bar{Q}}{\bar{A}_{leaf}} \left( \frac{n_3}{m_3} - \frac{V}{\bar{Q}} \bar{j}(NO_2) \bar{m}_{s,NO2} \right) + \frac{\bar{Q}}{\bar{A}_{leaf}} \left( 1 - \frac{1}{m_3} + \frac{V}{\bar{Q}} \bar{k} \bar{m}_{s,NO} \right) \cdot m_{s,O3} \quad (12.3)$$

Finally, the desired deposition velocities ( $v_{dep,i}$ ) of the NO-NO<sub>2</sub>-O<sub>3</sub> triad result from Eqs. (11.1) - (11.3), resolving for  $v_{dep,i}$ ,

$$v_{dep,NO2} = \frac{\bar{Q}}{\bar{A}_{leaf}} \left( \frac{1}{m_1} - 1 - \frac{V}{\bar{Q}} \bar{j}(NO_2) \right) \quad (13.1)$$

$$v_{dep,NO} = \frac{\bar{Q}}{\bar{A}_{leaf}} \left( \frac{1}{m_2} - 1 - \frac{V}{\bar{Q}} \bar{k} \bar{m}_{s,O3} \right) \quad (13.2)$$

$$v_{dep,O3} = \frac{\bar{Q}}{\bar{A}_{leaf}} \left( \frac{1}{m_3} - 1 - \frac{V}{\bar{Q}} \bar{k} \bar{m}_{s,NO} \right) \quad (13.3)$$

and the desired compensation point concentrations ( $m_{comp,i}$ ) of the NO-NO<sub>2</sub>-O<sub>3</sub> triad result from combining Eqs. (11.1) - (11.3) and Eqs. (13.1) - (13.3):

$$m_{comp,NO_2} = \frac{n_1 - m_1 \frac{V}{Q} \bar{k} \bar{m}_{s,NO} \bar{m}_{s,O_3}}{1 - m_1 - m_1 \frac{V}{Q} \bar{j}(NO_2)} \quad (14.1)$$

$$m_{comp,NO} = \frac{n_2 - m_2 \frac{V}{Q} \bar{j}(NO_2) \bar{m}_{s,NO_2}}{1 - m_2 - m_2 \frac{V}{Q} \bar{k} \bar{m}_{s,O_3}} \quad (14.2)$$

$$m_{comp,O_3} = \frac{n_3 - m_3 \frac{V}{Q} \bar{j}(NO_2) \bar{m}_{s,NO_2}}{1 - m_3 - m_3 \frac{V}{Q} \bar{k} \bar{m}_{s,NO}} \quad (14.3)$$

The quantities  $n_1, n_2, n_3$  and  $m_1, m_2, m_3$  cannot be determined (graphically or numerically) from single pairs of  $m_{a,i}$  and  $m_{s,i}$ , but from a (statistically sufficient) set of measured  $m_{a,i}$  and  $m_{s,i}$  (i.e. data sets classified for defined conditions of irradiation, temperature, humidity, concentrations, respectively). Therefore,  $n_1, n_2, n_3$  and  $m_1, m_2, m_3$  represent mean values for these data sets. Consequently, the quantities  $Q, A_{leaf}, j(NO_2), k, m_{s,NO_2}, m_{s,NO}$  and  $m_{s,O_3}$  in Eqs. (12.1) - (12.3), (13.1) - (13.3) and (14.1) - (14.3) must be averaged over the same (time) period (the same data set) of  $m_{a,i}$  and  $m_{s,i}$  measurements from which the quantities  $n_i$  and  $m_i$  have been derived.

$F_{ex,i}, v_{dep,i}$  and  $m_{comp,i}$  of the NO-NO<sub>2</sub>-O<sub>3</sub> triad were calculated from trace gas concentrations which were normalized for temperature and barometric pressure (0 °C, 1013.25 hPa).



### 2.1.3 Constraints of precision

Exchange flux densities  $F_{ex,i}$  are determined from molar concentrations of the NO-NO<sub>2</sub>-O<sub>3</sub> triad, ambient ones ( $m_{a,i}$ ) as well as those in the plant chamber ( $m_{s,i}$ ) (see Eqs. (8.1) - (8.3)). They are all measured with one set of analyzers only. The calculation procedure of exchange flux densities, deposition velocities as well as compensation point concentrations is based on linear regression analysis of  $m_{a,i}$  and  $m_{s,i}$ , which are (a) both error-prone and (b) not very different of each other, i.e. their difference is usually (very) small. The uncertainties of these differences depend mainly on the precision of the analyzers; the uncertainties might be large and consequently those of the derived quantities  $F_{ex,i}$ ,  $v_{dep,i}$  and  $m_{comp,i}$ .

For the sake of simplicity we assume well defined laboratory conditions. Then, the trace gas exchange flux densities  $F_{ex,i}$  are described by Eq. (8.4), which is equivalent to (a) only pre-scribed concentrations of trace gas  $i$  ( $= m_{a,i}$ ) will enter the dynamic plant chamber, (b) the enclosed leaves are only exposed to corresponding  $m_{s,i}$ , (c) purging rate  $Q$  and leaf area  $A_{leaf}$  are known and constant and (d) sample concentrations of the other trace gases ( $m_{s,j \neq i}$ ), photolysis rate  $j(NO_2)$  as well as wall-sorptions of trace gas  $i$  are negligible. After evaluation of the linear relationship between  $m_{a,i}$  and  $m_{s,i}$ , corresponding exchange flux densities  $F^*_{ex,i}$ , deposition velocities  $v^*_{dep,i}$  and compensation point concentrations  $m^*_{comp,i}$  are given by

$$F^*_{ex,NO_2} = \frac{\bar{Q}}{A_{leaf} m_1} (n_1 + (m_1 - 1) \cdot m_{s,NO_2}) \quad (15.1.1)$$

$$F^*_{ex,NO} = \frac{\bar{Q}}{A_{leaf} m_2} (n_2 + (m_2 - 1) \cdot m_{s,NO}) \quad (15.1.2)$$

$$F^*_{ex,O_3} = \frac{\bar{Q}}{A_{leaf} m_3} (n_3 + (m_3 - 1) \cdot m_{s,O_3}) \quad (15.1.3)$$

$$v^*_{dep,NO_2} = \frac{\bar{Q}}{A_{leaf}} \frac{1 - m_1}{m_1} \quad (15.2.1)$$

$$v^*_{dep,NO} = \frac{\bar{Q}}{A_{leaf}} \frac{1 - m_2}{m_2} \quad (15.2.2)$$

$$v^*_{dep,O3} = \frac{\bar{Q}}{A_{leaf}} \frac{1-m_3}{m_3} \quad (15.2.3)$$

$$m^*_{comp,NO2} = \frac{n_1}{1-m_1} \quad (15.3.1)$$

$$m^*_{comp,NO} = \frac{n_2}{1-m_2} \quad (15.3.2)$$

$$m^*_{comp,O3} = \frac{n_3}{1-m_3} \quad (15.3.3)$$

Confining to  $NO_2$ , a schematic representation (using simulated data) of how the quantities defined by Eqs. (15.1.1), (15.2.1) and (15.3.1) are determined from genuine measurements of  $m_{a,NO2}$  and  $m_{s,NO2}$  is given in Figure 6a. Since the “1:1”-line is equivalent to  $m_{a,NO2} = m_{s,NO2}$  (i.e.  $F_{ex,NO2} = 0$ , see Eq. (8.4)), the intersect of the linear regression line and the “1:1”-line is the  $NO_2$  compensation point concentration,  $m_{comp,NO2}$ . Here, the dilemma of the experimental proof of a (highly) significant  $m_{comp,NO2}$  becomes obvious. The lower  $m_{comp,NO2}$  will be, the more the intersect shifts down the “1:1”-line, closer and closer to the limit of detection of the  $NO_2$  concentration measurements ( $LOD(m_{a,NO2})$ ,  $LOD(m_{s,NO2})$ ;  $3\sigma$ -definition). This dilemma becomes even more obvious, if we consider the schematic representation of Eq. (8.4) in Figure 6b, where  $LOD(F_{ex,NO2})$  has been calculated from corresponding  $s_{m_s,NO2}$  and  $s_{m_a,NO2}$  by Gaussian error propagation. Here,  $m_{comp,NO2}$  ( $F_{ex,NO2} = 0$ ) is the intersect of the  $m_{s,NO2}$ -axis with the best-fit line of  $F_{ex,NO2}$  vs.  $m_{s,NO2}$  (which is mathematically not correct, see above). For high  $NO_2$  compensation point concentrations (as in Figure 6),  $m_{comp,NO2}$  can still be evaluated by interpolation from significant data pairs (i.e. data pairs, where  $> LOD(m_{NO2})$ ,  $\geq +LOD(F_{ex,NO2})$  or  $\leq -LOD(F_{ex,NO2})$ , respectively). If  $m_{comp,NO2}$  falls below  $LOD(m_{s,NO2})$  and  $F_0$  is consequently below  $+LOD(F_{ex,NO2})$ ,  $m_{comp,NO2}$  could only be determined by extrapolation from significant data pairs.

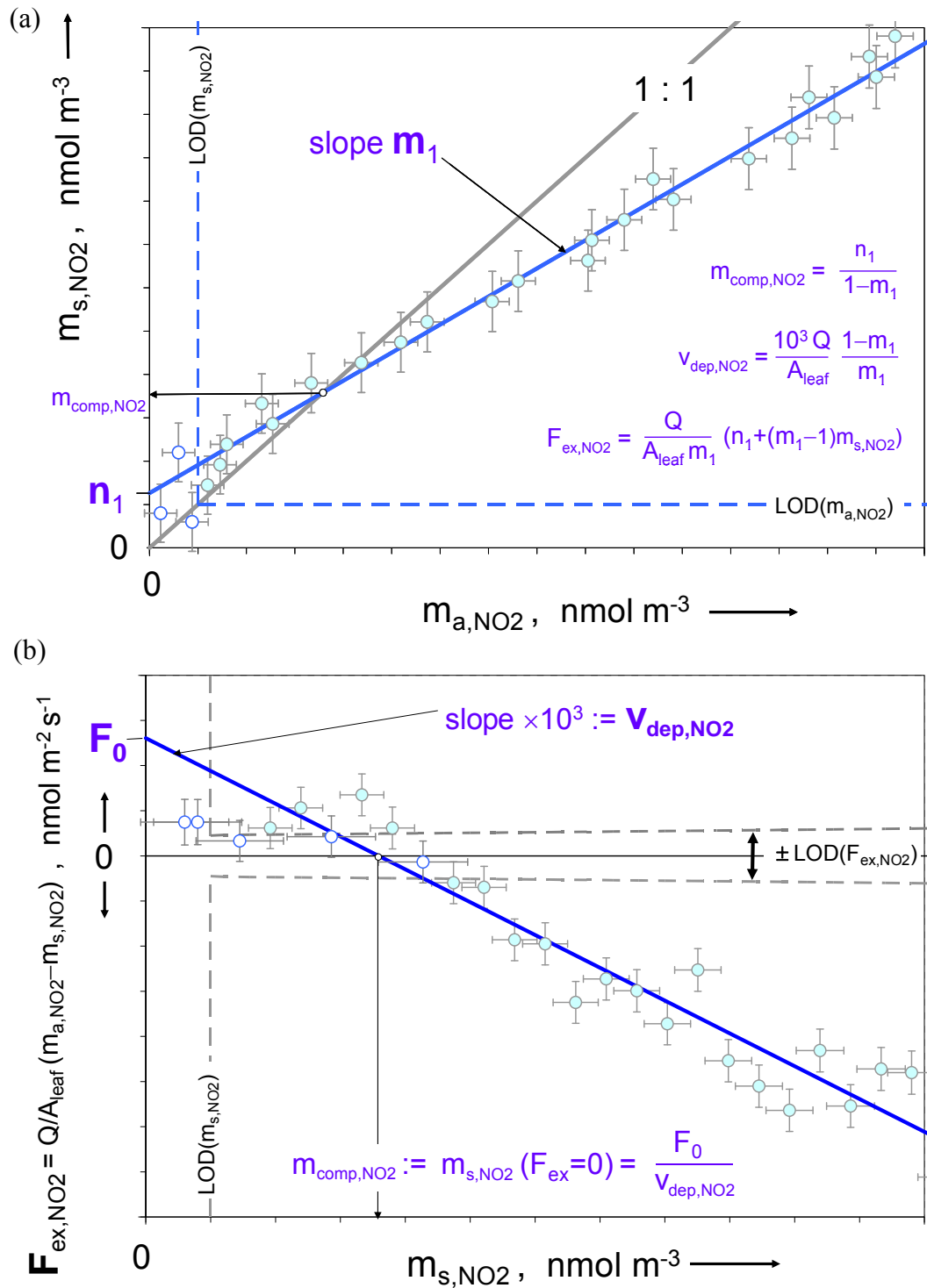


**Figure 6:** Schematic representation of the determination of bi-directional  $\text{NO}_2$  exchange flux density ( $F_{ex,NO_2}$ ),  $\text{NO}_2$  deposition velocity ( $v_{dep,NO_2}$ ) and  $\text{NO}_2$  compensation point concentration ( $m_{comp,NO_2}$ ) from measurements of  $\text{NO}_2$  concentrations at the plant chamber's inlet ( $m_{a,NO_2}$ ) and outlet ( $m_{s,NO_2}$ ) under laboratory conditions ( $m_{a,NO} = m_{a,O_3} = j(\text{NO}_2) \approx 0$ ). **(a)** by linear regression of  $m_{s,NO_2}$  with  $m_{a,NO_2}$ . **(b)** by plotting  $F_{ex,NO_2}$  vs.  $m_{s,NO_2}$ . Dashed lines represent the limits of detection ( $3\sigma$ -definition) for  $\text{NO}_2$  concentration measurements ((a) and (b) panel) and the determination of the  $\text{NO}_2$  exchange flux density ((b) panel), which are both defined by the sensitivity of the applied  $\text{NO}_2$  analyzer (note:  $LOD(m_{a,NO_2}) = LOD(m_{s,NO_2})$ ). Data points and error bars of  $\text{NO}_2$  concentrations have been simulated to match  $R^2(m_{a,NO_2}, m_{s,NO_2}) = 0.9925$ , error bars of  $\text{NO}_2$  exchange flux have been calculated by Gaussian error propagation (c.f. Eq. (8.4)). Filled circles identify data points  $> LODs$ , hollow circles those  $\leq LODs$ .

According to Eqs. (15.1.1), (15.2.1) and (15.3.1), the errors of  $F_{ex,NO_2}$ ,  $v_{depNO_2}$  and  $m_{comp,NO_2}$  are entirely due to the errors of  $n_l$  and  $m_l$ , which are in turn entirely due to the goodness of the linear relationship between  $m_{a,NO_2}$  and  $m_{s,NO_2}$  as well as to the errors of  $m_{a,NO_2}$  and  $m_{s,NO_2}$  ( $s_{m_a,NO_2}$  and  $s_{m_s,NO_2}$  see Sect. 3.1.7). This leads to the simple conclusion, that the determination of  $F_{ex,NO_2}$ ,  $v_{depNO_2}$  and  $m_{comp,NO_2}$  is as more precise, as higher the regression coefficient  $R^2(m_{s,NO_2}, m_{a,NO_2})$  and as lower the standard errors  $s_{m_s,NO_2}$  and  $s_{m_a,NO_2}$  are.

Only one  $NO_2$  analyzer is used for the measurements of both concentrations,  $m_{a,NO_2}$  and  $m_{s,NO_2}$ . As shown below (Sect. 2.3), the standard error  $s_{m_a,NO_2}$  ( $s_{m_s,NO_2}$ ) was found to be a weak exponential function of  $m_{a,NO_2}$  ( $m_{s,NO_2}$ ), starting with a fixed value  $s_{m,LOD(NO_2)}$  at  $m_{a,NO_2} = m_{s,NO_2} = 0$ . To demonstrate, how the goodness ( $R^2(m_{s,NO_2}, m_{a,NO_2})$ ) of the linear relationship between  $m_{a,NO_2}$  and  $m_{s,NO_2}$  and how the magnitude of  $s_{m_a,NO_2}$  and  $s_{m_s,NO_2}$  impact the  $NO_2$  exchange measurements, we consider (a) the determination of the minimum possible, but still highly significant  $NO_2$  compensation point concentration ( $m_{comp,NO_2}$ ) and (b) the precision of the  $NO_2$  exchange flux density ( $F_{ex,NO_2}$ ).

For that we simulated data sets of  $m_{a,NO_2}$  and  $m_{s,NO_2}$  within the range  $LOD(m_{s,NO_2}) \leq m_{s,NO_2} \leq 615 \text{ nmol m}^{-3}$  (15 ppb) for prescribed  $NO_2$  deposition velocities ( $0.1 \leq v_{dep,NO_2} \leq 0.8 \text{ mm s}^{-1}$ , per leaf area) and for pre-scribed  $R^2(m_{s,NO_2}, m_{a,NO_2})$  between 0.999 and 0.6. The latter was achieved by random number application to the  $m_{a,NO_2}$  data. Standard errors  $s_{m_s,NO_2}$  and  $s_{m_a,NO_2}$  were calculated from  $m_{a,NO_2}$  and  $m_{s,NO_2}$  (see Eq. (16.1), Sect. 2.3), while the standard error of  $F_{ex,NO_2}$  ( $s_{F_{ex,NO_2}}$ ) was calculated from  $s_{m_s,NO_2}$ ,  $s_{m_a,NO_2}$  and  $r(m_{s,NO_2}, m_{a,NO_2}) = [R^2(m_{s,NO_2}, m_{a,NO_2})]^{1/2}$  by application of the general form of Gaussian error propagation (see Sect. 3.1.7).

Application of bi-variate linear regression analysis to this simulated data set delivers the quantities  $n_l$  and  $m_l$  as well their standard errors  $s_{n,l}$  and  $s_{m,l}$  (which depend on  $s_{m_s,NO_2}$ ,  $s_{m_a,NO_2}$  and  $R^2(m_{s,NO_2}, m_{a,NO_2})$ ). Application of the general form of Gaussian error propagation (see Sect. 3.1.7) to Eq. (15.3.1) delivers the standard error of the  $NO_2$  compensation point concentration ( $s_{m_{comp,NO_2}}$ ). The “detectable existence” of  $m_{comp,NO_2}$  (i.e. testing the hypothesis  $m_{comp,NO_2} \neq 0$ ) has been statistically secured by application of the t-test to the values of  $m_{comp,NO_2}$ ,  $s_{m_{comp,NO_2}}$  and N (number of ( $m_{s,NO_2}$ ,  $m_{a,NO_2}$ ) data pairs). In Figure 7, the minimum detectable  $NO_2$  compensation point concentration, i.e. the lowest, but still highly significant  $m_{comp,NO_2}$  ( $P \geq 0.999$ ) is shown for a pre-scribed

range of  $\text{NO}_2$  deposition velocities as function of the regression coefficient  $R^2(m_{s,\text{NO}_2}, m_{a,\text{NO}_2})$  and for three different values of  $\text{LOD}(m_{s,\text{NO}_2})$ , namely 0.4, 4.5 and  $44.6 \text{ nmol m}^{-3}$  (0.01, 0.1, 1.0 ppb). These three values represent a certain “history” of  $\text{NO}/\text{NO}_2$  chemiluminescence analyzers:  $\text{LOD}(m_{s,\text{NO}_2}) = 44.6 \text{ nmol m}^{-3}$  (1 ppb) represents the state-of-art of commercial  $\text{NO}_2$  analyzers of 1985-1995,  $\text{LOD}(m_{s,\text{NO}_2}) = 4.5 \text{ nmol m}^{-3}$  (0.1 ppb) the best performance between 1995-2005’s, while  $\text{LOD}(m_{s,\text{NO}_2}) = 0.4 \text{ nmol m}^{-3}$  (0.01 ppb) is characteristic for the most advanced  $\text{NO}/\text{NO}_2$  analyzers which have been recently applied over the remote Southern Atlantic Ocean (HOSAYNALI BEYGI et al. 2011). For typical ranges of laboratory measurements, i.e.  $0.9 \leq R^2 \leq 0.99$ , minimum detectable  $\text{NO}_2$  compensation point concentrations range between  $17.5 - 99.4 \text{ nmol m}^{-3}$  (0.39 - 2.23 ppb), if  $\text{NO}_2$  analyzers with  $\text{LOD}(m_{s,\text{NO}_2}) = 44.6 \text{ nmol m}^{-3}$  (1.0 ppb) have been used. Best performance of present-day  $\text{NO}_2$  analyzers allow minimum detectable  $m_{\text{comp},\text{NO}_2}$  between  $3.6$  and  $21.3 \text{ nmol m}^{-3}$  (0.08 - 0.48 ppb). Very low minimum detectable  $m_{\text{comp},\text{NO}_2}$  ( $0.8 - 4.0 \text{ nmol m}^{-3}$  or  $0.02 - 0.09$  ppb) may be reached if the most advanced state of  $\text{NO}_2$  analyzers is considered. It should be noted that, due to the potential goodness of the measurements, the minimum detectable  $m_{\text{comp},\text{NO}_2}$  could be lower than the actual  $\text{LOD}(m_{s,\text{NO}_2})$ , but statistically still highly significant.

The impact of  $s_{m_s,\text{NO}_2}$ ,  $s_{m_a,\text{NO}_2}$  and  $R^2(m_{s,\text{NO}_2}, m_{a,\text{NO}_2})$  on the precision of the  $\text{NO}_2$  exchange flux density ( $= s_{F_{\text{ex},\text{NO}_2}}/F_{\text{ex},\text{NO}_2}$ ) is demonstrated in Figure 8. For the sake of clarity, another data set has been simulated (random number application), namely for pre-scribed  $\text{NO}_2$  deposition velocities ( $0.3 \leq v_{\text{dep},\text{NO}_2} \leq 0.6 \text{ mm s}^{-1}$ , per leaf area), a pre-scribed  $\text{NO}_2$  compensation point concentration ( $m_{\text{comp},\text{NO}_2} = 67 \text{ nmol m}^{-3}$  (1.5 ppb)) and for  $0.99 \leq R^2 \leq 0.9$ . Also shown in Figure 8 is the precision of  $m_{s,\text{NO}_2}$  ( $= s_{m_s,\text{NO}_2}/m_{s,\text{NO}_2}$ ; right axis) for the “history” of  $\text{LOD}(m_{s,\text{NO}_2})$  values, namely  $\text{LOD}(m_{s,\text{NO}_2}) = 44.6, 4.5$  and  $0.4 \text{ nmol m}^{-3}$  (1.0, 0.1, 0.01 ppb). Before 1995 ( $\text{LOD}(m_{\text{NO}_2}) = 1$  ppb), a precision of  $m_{s,\text{NO}_2}$  better than 10 % could hardly be achieved in the lower ppb-range. Best performing present-day  $\text{NO}_2$  chemiluminescence analyzers ( $\text{LOD}(m_{\text{NO}_2}) = 0.1$  ppb) exceed the 10 % level of  $m_{s,\text{NO}_2}$  precision not before  $m_{s,\text{NO}_2}$  falls below  $14.8 \text{ nmol m}^{-3}$  (0.33 ppb), while another step of magnitude can be reached with most advanced  $\text{NO}_2$  analyzers ( $s_{m_s,\text{NO}_2}/m_{s,\text{NO}_2} > 10\%$  not before  $m_{s,\text{NO}_2} < 1.5 \text{ nmol m}^{-3}$  (0.03 ppb)). The “history” of  $\text{NO}_2$  analyzers is also mirrored in the precision of  $F_{\text{ex},\text{NO}_2}$  (reddish, bluish and greenish areas in Figure 8). In any case, the precision of

$F_{ex,NO_2} (= s_{F_{ex,NO_2}}/F_{ex,NO_2})$  reaches infinity at  $m_{s,NO_2} = m_{comp,NO_2}$ , since there the  $NO_2$  exchange flux density equals zero. Otherwise, the precision of  $F_{ex,NO_2}$  rapidly falls (very) well below the 10 % level. This is a consequence of the fact, that  $m_{a,NO_2}$  and  $m_{s,NO_2}$  are the decisive quantities for the determination of  $F_{ex,NO_2}$ . Since  $m_{a,NO_2}$  and  $m_{s,NO_2}$  are highly correlated, the standard error of  $F_{ex,NO_2}$  is proportional to  $[s_{m_{a,NO_2}}^2 + s_{m_{s,NO_2}}^2]^{1/2} - 2 s_{m_{a,NO_2}} s_{m_{s,NO_2}} [R^2(m_{s,NO_2}, m_{a,NO_2})]^{1/2}$ , rather than proportional to  $[s_{m_{a,NO_2}}^2 + s_{m_{s,NO_2}}^2]^{1/2}$  alone (see Sect. 3.1.7). In other words, the error of  $F_{ex,NO_2}$  benefits from the compensation of the errors of  $m_{a,NO_2}$  and  $m_{s,NO_2}$ .

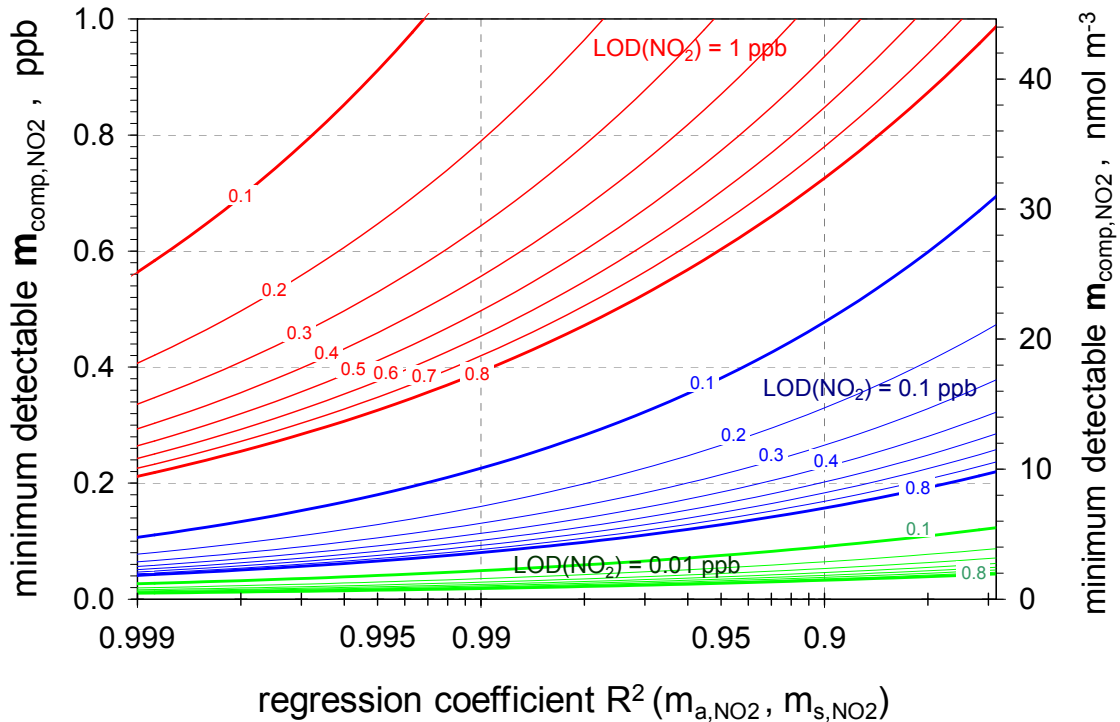


**Figure 7:** The dynamic plant chamber at well defined (laboratory) conditions: minimum detectable  $NO_2$  compensation point concentrations ( $m_{comp,NO_2}$  at  $P \geq 0.999$ , i.e. “highly significant”) as function of  $NO_2$  deposition velocity ( $v_{dep,NO_2}$ ; per leaf area) and the goodness ( $R^2$ ) of the ambient vs. sample  $NO_2$  concentration measurements (standard errors of  $NO_2$  concentration measurements considered). Results are from data simulation (random number application) matching pre-scribed  $R^2(m_{a,NO_2}, m_{s,NO_2})$  and prescribed  $v_{dep,NO_2}$  ( $0.999 \leq R^2 \leq 0.6$  and  $v_{dep,NO_2} = 0.1, 0.2, \dots, 0.8 \text{ mm s}^{-1}$ ). The greenish range represents simulated data of a  $NO_2$  analyzer with  $LOD(m_{NO_2}) = 0.4 \text{ nmol m}^{-3}$  (0.01 ppb), the bluish range for  $LOD(m_{NO_2}) = 4.5 \text{ nmol m}^{-3}$  (0.1 ppb), the reddish range for  $LOD(m_{NO_2}) = 44.6 \text{ nmol m}^{-3}$  (1.0 ppb).

Finally, it should be emphasized, that the estimates of this sub-section are made on the basis of Eqs. (15.1.1), (15.2.1) and (15.3.1) for (best) defined laboratory conditions. Under field conditions, however, the equations for the determination of  $F_{ex,NO_2}$ ,  $v_{dep,NO_2}$  and  $m_{comp,NO_2}$  will contain also average quantities of  $m_{s,NO}$ ,  $m_{s,O_3}$ ,  $j(NO_2)$  and  $k$  (see Eqs. (12.1), (13.1), (14.1)). It is obvious, that their variability (standard errors) will enlarge standard errors of  $n_I$  and  $m_I$  and diminish  $R^2(m_{s,NO_2}, m_{a,NO_2})$ . Consequently, corresponding minimum detectable  $NO_2$  compensation point concentrations will certainly be higher and precisions of  $F_{ex,NO_2}$  will be lower than those given in Figure 7 and Figure 8.

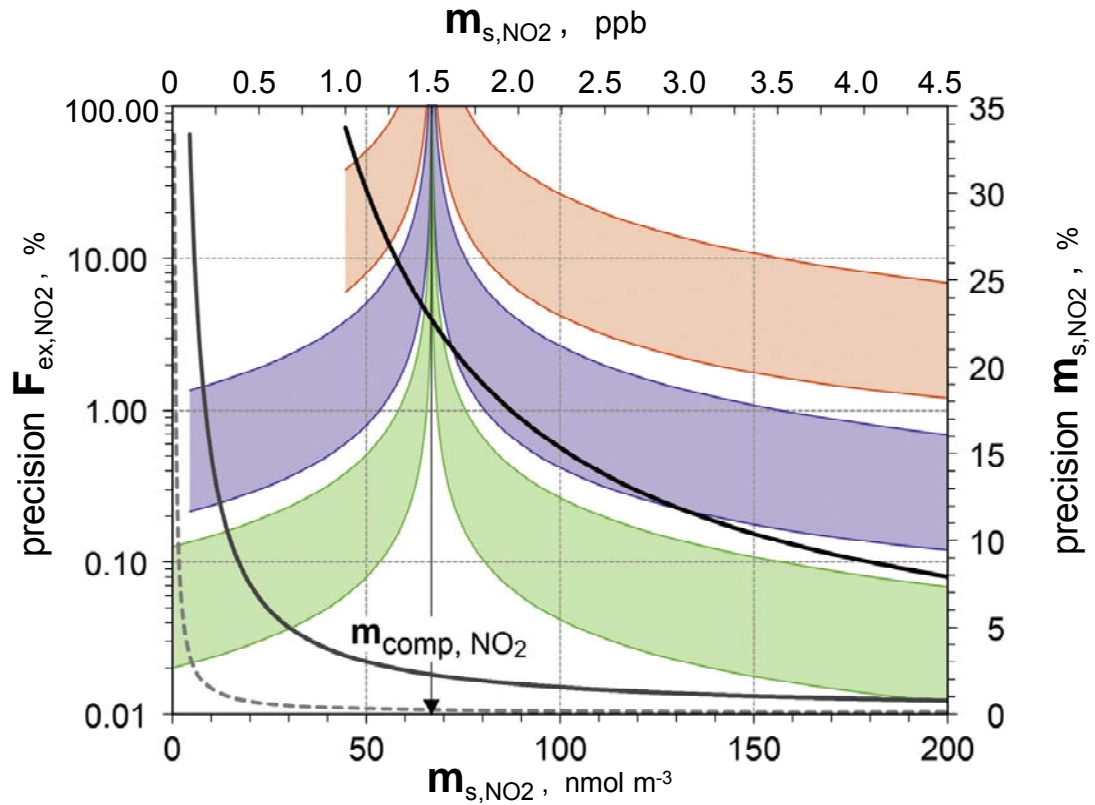


**Figure 8:** The dynamic plant chamber at well defined (laboratory) conditions: precision of  $NO_2$  concentration measurements ( $= s_{m,s,NO_2}/m_{s,NO_2}$ ; right axis) and precision of derived  $NO_2$  exchange flux densities ( $= s_{F_{ex,NO_2}}/F_{ex,NO_2}$ ; left axis) as function of the  $NO_2$  concentration measured at the outlet of the dynamic chamber (precision  $m_{s,NO_2}$ , right axis). Results are from data simulation (random number application), which considers standard errors of  $NO_2$  concentration measurements, and which matches pre-scribed  $R^2(m_{a,NO_2}, m_{s,NO_2})$  and pre-scribed  $m_{comp,NO_2} = 67 \text{ nmol m}^{-3}$  (1.5 ppb). Dark purple, purple and pink lines (= precision of  $m_{s,NO_2}$ ) represent data for a  $NO_2$  analyzer characterized by  $LOD(m_{s,NO_2}) = 44.6 \text{ nmol m}^{-3}$  (1.0 ppb),  $LOD(m_{s,NO_2}) = 4.5 \text{ nmol m}^{-3}$  (0.1 ppb) and  $LOD(m_{s,NO_2}) = 0.4 \text{ nmol m}^{-3}$  (0.01 ppb), respectively. Ranges of the precision of derived  $NO_2$  exchange flux densities are identified by reddish, bluish and greenish areas for  $LOD(m_{s,NO_2}) = 44.6 \text{ nmol m}^{-3}$  (1.0 ppb),  $LOD(m_{s,NO_2}) = 4.5 \text{ nmol m}^{-3}$  (0.1 ppb) and  $LOD(m_{s,NO_2}) = 0.4 \text{ nmol m}^{-3}$  (0.01 ppb). The width of the colored areas stands for all considered combinations of  $R^2$  and  $v_{dep,NO_2}$  ( $0.99 \leq R^2 \leq 0.9$  and  $0.3 \leq v_{dep,NO_2} \leq 0.6 \text{ mm s}^{-1}$ ). The respective upper boundary of each colored area represents the combination  $v_{dep,NO_2} = 0.3 \text{ mm s}^{-1}$  and  $R^2 = 0.9$ , while the lower boundary represents  $v_{dep,NO_2} = 0.6 \text{ mm s}^{-1}$  and  $R^2 = 0.99$ .

#### 2.1.4 Constraints of design

Aside the strong demand for precise and highly sensitive measurements of NO<sub>2</sub> concentration, there are more requirements to the dynamic leaf chamber system and the measurements of the surface exchange fluxes of NO<sub>2</sub> (NO, O<sub>3</sub>):

- (1) The environment in the chamber should as closely as possible represent the surrounding (ambient) environment.
- (2) Enclosing the plant (part of plants) by the chamber should not affect the plant itself, neither through mechanical stress nor due to changed environmental conditions. Changes in concentrations of relevant trace gases should be small in order to prevent affecting plant metabolism and stomata regulation.
- (3) Primary plant-physiological processes, such as CO<sub>2</sub> surface exchange fluxes (assimilation) and H<sub>2</sub>O surface exchange fluxes (transpiration) should be closely followed, measured and finally related to the NO<sub>2</sub> (NO, O<sub>3</sub>) surface exchange.
- (4) Losses of NO<sub>2</sub> (NO, O<sub>3</sub>) on chamber materials must be negligible (if not: must be quantified).
- (5) The chamber system should be applicable for laboratory and field measurements without substantial modifications.
- (6) Simultaneous measurements of surface exchange fluxes of NO<sub>2</sub>, O<sub>3</sub>, NO, CO<sub>2</sub> and H<sub>2</sub>O should be feasible.
- (7) Differences of NO<sub>2</sub> (NO, O<sub>3</sub>) concentrations between inlet and outlet of the dynamic chamber, which are expected to be (very) small, must be resolved with statistical significance.

Furthermore, fumigation experiments to study the NO<sub>2</sub> surface exchange in the laboratory (NO<sub>2</sub> exchange under controlled conditions) demand the generation of very low (ppb- and sub-ppb levels) and temporally stable NO<sub>2</sub> concentrations in order to identify statistically significant NO<sub>2</sub> compensation point concentrations. These low NO<sub>2</sub> concentrations have to be reproducible and verifiable.



## 2.2 Trace gas analyzers

NO and NO<sub>2</sub> concentrations were measured by a gas-phase chemiluminescence NO analyzer (Model 42C, Thermo Electron Corporation, USA). In a low pressure reaction chamber, the NO of the air sample reacts with ozone (provided by the analyzer) forming electronically excited NO<sub>2</sub> molecules. Decaying to the ground state, the excited NO<sub>2</sub> molecule emits a photon (chemiluminescence) and the total light intensity in the reaction chamber, detected by a photomultiplier, is proportional to the NO concentration. NO<sub>2</sub> in the air sample is also measured by the NO analyzer after conversion of NO<sub>2</sub> to NO. In most commercial NO/NO<sub>2</sub> analyzers a molybdenum converter is applied (heated to 300 - 400 °C), where NO<sub>2</sub> is catalytically reduced to NO at the converter's surface. However, previous studies demonstrated that molybdenum converters are non-specific for NO<sub>2</sub> because other oxidized nitrogen compounds of ambient air, like gaseous nitrous acid (HONO), nitric acid (HNO<sub>3</sub>), the nitrate radical (NO<sub>3</sub>), dinitrogen pentoxide (N<sub>2</sub>O<sub>5</sub>), peroxyacetyl nitrate (PAN) and other organic nitrates were found to be also converted to NO, which leads to systematic and considerable overestimation of the measured NO<sub>2</sub> values (WINER et al. 1974; MATTHEWS et al. 1977; GROSJEAN and HARRISON 1985; GEHRIG and BAUMANN 1993; STEINBACHER et al. 2007). During some studies hydrated, crystalline ferrous sulfate (FeSO<sub>4</sub>) for the surface reduction of NO<sub>2</sub> to NO were used. However, FeSO<sub>4</sub> converter also overestimates the mixing ratio of NO and NO<sub>2</sub> (RIDLEY et al. 1988). Significant interferences of *n*-propyl nitrate, nitrous acid (HNO<sub>2</sub>) and PAN were reported (KELLY et al. 1980; COX et al. 1983; FEHSENFELD et al. 1987). As a consequence FEHSENFELD et al. (1987) did not recommend FeSO<sub>4</sub> converter for measuring NO<sub>2</sub>. Another frequently used analyzer to measure NO<sub>2</sub> is the Luminol detector (LMA-3, Scintrex/Unisearch Inc.). Its measurement principle is based on the chemiluminescent reaction of NO<sub>2</sub> with luminol in aqueous solution (MAEDA et al. 1980; WENDEL et al. 1983; SCHIFF et al. 1986). The luminol technique is noted for interferences by ambient O<sub>3</sub> and PAN, and exhibits non-linear response at low NO<sub>2</sub> concentrations. The interferences due to O<sub>3</sub> and PAN are significant especially at low NO<sub>2</sub> concentrations (KELLY et al. 1990). Table 4 shows an overview about commonly used NO<sub>2</sub> converters and their reported interferences. No interferences or any artifacts were reported for photolytic converters, where NO<sub>2</sub> is photolyzed by ultraviolet light < 420 nm (FEHSENFELD et al. 1990) or were negligible, respectively (RYERSON et al. 2000). Consequently, we used a highly NO<sub>2</sub> specific blue light converter which

photodissociates NO<sub>2</sub> into NO at a wavelength of approximately 395 nm (manufactured by Droplet Measurement Technologies Inc., Colorado, USA). To obtain a better accuracy and precision of the NO<sub>2</sub> (and NO) measurements at sub-ppb concentrations, the NO/NO<sub>2</sub> analyzer has always been operated with pure oxygen (instead with the oxygen of ambient air) for the internal generation of ozone, necessary for the reaction with NO in the low pressure reaction chamber.

**Table 4:** Interferences of chemiluminescent NO-NO<sub>2</sub>-NO<sub>x</sub> analyzers used different NO<sub>2</sub> converters.

| NO <sub>2</sub> converter                 | conversion principle                         | compound                        | Response % of concn                                  | author                    |
|---|--|---------------------------------|--|---------------------------|
| <b>luminol</b>                            | NO <sub>2</sub> reacts with luminol solution | PAN                             | 25 %   | Drummond et al., 1989     |
|   |  | O <sub>3</sub>                  | 0.0033 ppb NO <sub>2</sub> (per ppb O <sub>3</sub> ) | Kelly et al., 1990        |
| <b>molybdenum (Mo)</b>                    | heated ~ 400 °C surface oxidation            | PAN                             | 92 %   | Winer et al., 1974        |
|   |  | ethyl nitrate                   | 103 %  |                           |
|   |  | ethyl nitrite                   | 92 %   |                           |
|   |  | HNO <sub>3</sub>                | not quantified                                       |                           |
|   |  | HNO <sub>3</sub>                | ≥ 98 %   | Grosjean & Harrison, 1985 |
|   |  | PAN                             | ≥ 98 %   |                           |
|   |  | methyl nitrate                  | ≥ 98 %   |                           |
|   |  | n-propyl nitrate                | ≥ 98 %   |                           |
| n-butyl nitrate                           | ≥ 98 %                                       |                                 |  |                           |
| hydrocarbons                              | negative interferences                       | Kurtenbach et al., 2001         |  |                           |
| <b>ferrous sulfate (FeSO<sub>4</sub>)</b> | surface oxidation                            | PAN                             | 20 %   | Kelly et al., 1980        |
|   |  | HONO                            | 100 %  | Cox et al., 1983          |
|   |  | n-propyl nitrate                | 32 %   | Fehsenfeld et al., 1987   |
|   |  | PAN                             | 35 - 45 %  |                           |
| <b>photolytic</b>                         | ultraviolet light (320 - 500 nm)             | none                            |  | Fehsenfeld et al., 1990   |
| <b>photolytic</b>                         | ultraviolet light (> 350 nm)                 | HONO                            | 37 %   | Ryerson et al., 2000      |
|   |  | BrONO <sub>2</sub>              | 5 %  |                           |
|   |  | NO <sub>3</sub>                 | 10 %   |                           |
|   |  | N <sub>2</sub> O <sub>5</sub>   | 3 %  |                           |
|   |  | HO <sub>2</sub> NO <sub>2</sub> | 12 %   |                           |

Measurements of CO<sub>2</sub> and H<sub>2</sub>O concentrations were performed by infrared dual channel gas analyzer for difference measurements between the outlet of an empty reference chamber and the sample gas (LI-7000, LiCor, Lincoln, NE, USA). An additional gas analyzer (LI-6262, LiCor, Lincoln, NE, USA) monitored the absolute CO<sub>2</sub> and H<sub>2</sub>O concentrations to deliver a base signal for the LI-7000 operating in differential mode. O<sub>3</sub> concentration was detected using an UV-absorption analyzer (Model 49C, Thermo Electron Corporation, USA). All measured parameters are listed in Table 5.

**Table 5:** Measured parameters and instrument specifications. Limit of detection ( $LOD(m_i)$ ,  $3\sigma$ -definition) for the gas concentrations were determined under field and laboratory conditions.

| parameter                       | symbol           | unit                                 | LOD( $m_i$ ) |          | instrument (model)       |
|---------------------------------|------------------|--------------------------------------|--------------|----------|--------------------------|
|                                 |                  |                                      | lab          | field    |                          |
| nitric oxide                    | NO               | ppb                                  | 0.23 ppb     | 0.10 ppb | ThermoElectron, 42C      |
| nitrogen dioxide                | NO <sub>2</sub>  | ppb                                  | 1.01 ppb     | 0.31 ppb | ThermoElectron, 42C      |
| ozone                           | O <sub>3</sub>   | ppb                                  | 0.8 ppb      | 0.98 ppb | ThermoElectron, 49C      |
| carbon dioxide                  | CO <sub>2</sub>  | ppm                                  | 1.2 ppm      | 1.5 ppm  | LiCor, LI-6262 / LI-7000 |
| water vapor                     | H <sub>2</sub> O | ppth                                 | 0.3 ppth     | 0.2 ppth | LiCor, LI-6262 / LI-7000 |
| air temperature                 | T                | °C                                   |              |          | thermocouple             |
| relative humidity               | rH               | %                                    |              |          | Rotronic, MP100A         |
| photosynthetic active radiation | PAR              | $\mu\text{mol m}^{-2} \text{s}^{-1}$ |              |          | LiCor, LI-190SA          |
| photolysis rate                 | $j(NO_2)$        | $\text{s}^{-1}$                      |              |          | filter radiometer        |
| air pressure                    | P                | hPa                                  |              |          | Ammonit                  |

### 2.3 Calibrations, limits of detection, standard errors and precision of trace gas concentration measurements

For the calibration of the NO/NO<sub>2</sub> analyzer (field conditions), a NO standard (5.09 ± 0.1 ppm, Air Liquide, Germany) was applied. The standard was diluted by synthetic air, which has been additionally cleaned with activated charcoal and Purafil<sup>®</sup> (Purafil, Inc., USA) to remove any potential NO and NO<sub>2</sub> contaminations. For the dilution of the NO standard a gas phase titration unit was applied (GPT, 146C Dynamic Gas Calibrator, Thermo Electron Corporation, USA). In the GPT, NO<sub>2</sub> calibration gas is produced by titration (see Reaction (R1)) of the diluted NO standard with O<sub>3</sub> (generated by a UV lamp in the GPT). The BLC's efficiency was determined by the ratio of measured NO<sub>2</sub> and the known value of NO<sub>2</sub> obtained by titration of NO. The O<sub>3</sub> analyzer was calibrated by the GPT-generated O<sub>3</sub>, where the exact O<sub>3</sub> concentration is known from the gas phase titration of the NO standard. For the calibration of the CO<sub>2</sub>/H<sub>2</sub>O analyzers three gaseous CO<sub>2</sub> standards were used (355.4 ppm, 401.1 ppm, 453.8 ppm, Air Liquid, Germany); the H<sub>2</sub>O signal has been calibrated by a dew point generator (LI-610, LiCor, Lincoln, NE, USA). To maintain high quality concentration measurements even under long-term field conditions, it was necessary to control and to service the system frequently. In the field, calibrations were performed once a week to ensure stability of the analyzers (quantifying potential drifts), while in the laboratory calibrations were performed just before the start of the experiment.

The determination of the limit of detection (LOD) is particularly important for the exchange measurements of NO and NO<sub>2</sub>, as (very) low concentrations have been encountered under both, laboratory and field conditions. According to MACDOUGALL and CRUMMETT (1980) the "limit of detection" is the lowest concentration level that can be determined to be statistically different from a measurement of "zero" concentration. Here we define  $LOD(m_{NO_2})$ ,  $LOD(m_{NO})$  and  $LOD(m_{O_3})$  as three times that standard deviation ( $s_{m\_NO_2,0}$ ,  $s_{m\_NO,0}$ ,  $s_{m\_O_3,0}$ ), which has been obtained through a statistically significant number (laboratory: 360, field: 160 - 360) of zero-air measurements. In Table 5 the  $LOD(m_i)$  of the instruments are summarized. The conversion efficiency of the BLC for NO<sub>2</sub> was around 25 % during laboratory measurements and 32 - 36.5 % under field conditions.

Besides the determination and rigorous control of the LOD's, the quantification of the analyzers' reproducibility (precision) is as more necessary, as exchange fluxes of the NO-NO<sub>2</sub>-O<sub>3</sub> triad are evaluated from very small differences of concentrations measured at the inlet and the outlet of the dynamic plant chamber. We define the precision of the analyzers as the ratio of the standard errors  $s_{m,i}$  and the corresponding concentrations  $m_i$  ( $i = \text{NO}, \text{NO}_2, \text{O}_3$ ). The standard errors of NO and NO<sub>2</sub> measurements have been found to be a (weak) function of the NO and NO<sub>2</sub> concentrations themselves:

$$s_{m,\text{NO}_2} = s_{m_{\text{NO}_2,0}} \cdot \exp(b_{\text{NO}_2} \cdot m_{\text{NO}_2}) \quad (16.1)$$

$$s_{m,\text{NO}} = s_{m_{\text{NO},0}} \cdot \exp(b_{\text{NO}} \cdot m_{\text{NO}}) \quad (16.2)$$

where  $s_{m_{\text{NO}_2,0}}$  and  $s_{m_{\text{NO},0}}$  are the standard errors at  $m_{\text{NO}_2} = 0$  and  $m_{\text{NO}} = 0$ ,  $b_{\text{NO}_2}$  and  $b_{\text{NO}}$  (in  $\text{nmol}^{-1} \text{m}^3$ ) have been derived from calibration exercises.

## 2.4 Dynamic chamber system

### 2.4.1 Design and construction

The open (flow through), dynamic chamber system was a further development of the systems operated in previous studies (SCHÄFER et al. 1992; KESSELMEIER et al. 1996; KUHN et al. 2002). The system was designed for measurements of trace gas exchange in the field with minimal effects on the gases. The system has been demonstrated to be easily handled under field conditions. The design of the chambers is illustrated in Figure 9 and details of the used materials and parts are listed in **Table 6**. The chambers had an inner diameter of 40 cm. The height of the chambers could be varied by extending the frame and could be adjusted to the plant specimen. Our initial height was 45 cm and we used extensions of 15 cm at field measurements. The chamber frame and the lid were made of PVC and acrylic glass.

**Table 6:** Manufacturer details for parts of the dynamic chamber system.

| part                            | manufacturer                            | specifications   |
|---------------------------------|---|--|
| (1) + (2) chamber frame and lid | MPI workshop, Germany                   | PVC, acrylic glass   |
| (3) inner chamber wall          | Saint Gobain, Germany                   | FEP (fluorinated ethylene propylene) film, thickness 0.05 mm, chemically inert, transparent for visible and UV light |
| (4) clamps                      | Horex, Germany                          | parallel clamp, typ 25   |
| (5) silicon straps              | Dichtungstechnik Bensheim GmbH, Germany | transparent MVQ-silicone cord, diameter 5 mm   |
| (6) inlet fan                   | Micronel, Switzerland                   | axial fan, model D344T012GK-2  |
| (7) air mass flow sensor        | Honeywell International Inc., USA       | model AWM 700  |
| (8) propeller                   | APC Propellers, USA                     | Sport Prop, 10x7, Teflon® coating by MPI workshop  |
| (9) mixing fan                  | Micronel, Switzerland                   | ultra slim fan, model F62MM012GK-9, Teflon® coating by MPI workshop  |
| (10) tubing                     | diverse                                 | 1/4" PFA tubing  |
| (11) in-line filter case        | Entegris Inc., USA                      | Galtek® Integral Ferrule in-line filters   |
| particulate membrane filter     | Pall Corporation, USA                   | Zefluor™ membrane disc filters, model P5PJ047, pore size 2 µm, diameter 47 mm  |
| solenoid valves                 | Entegris Inc., USA                      | Galtek® diaphragm valves, 3-way, 1/4" orifice  |
| sample pump                     | Vakuubrand, Germany                     | diaphragm pump, model MZ4C, chemical resistant   |
| heating tape                    | EHT Haustechnik AEG, Germany            | typ HT SLH 15/L300, self limiting, max. holding temperature 60°C, heat output 15 W/m                                 |

The inner walls consisted of a thin transparent Teflon film (FEP). Previous investigations of the spectral transmissivity of the FEP film have shown that photosynthetically active radiation (PAR) nearly completely transmits this film: in the spectral range of PAR (400 - 700 nm) transmissivity is about 95 %. In the range of  $\lambda \leq 400$  nm, the transmissivity of the FEP film is about 90 % (SCHÄFER et al. 1992; PAPE et al. 2009). A consequence of the horizontal installation of the chamber during field measurement is that transmissivities of the acrylic glass parts of the chamber play only a very minor role. Furthermore, the Teflon film was reported to show no interferences with trace gases tested such as organic acids (SCHÄFER et al. 1992; KESSELMEIER et al. 1997), monoterpenes and isoprene (KESSELMEIER et al. 1996, 1997; KUHN et al. 2000) and reduced sulfur compounds (KESSELMEIER et al. 1993).

The FEP film was fixed with elastic silicone straps around the outer side of the frame. The inner side of the lid was covered by the Teflon film as well. The lid was

fixed to the chamber with four clamps. Several holes in the lid allowed the installation of tubes, mixing fans and the intake system of purging air. The purging air flow through the chamber was established in the field by a blowing axial inlet fan which was controlled by an air mass flow sensor installed outside the chamber frame. At laboratory we used pressurized air for flushing the chamber. For a continuous turbulent mixing of the air inside the chamber a Teflon propeller driven by a magnetically coupled motor attached outside as well as two Teflon coated mixing fans were used. This design ensured that the air pumped through the chamber only came into contact with parts made of Teflon (PFA or PTFE). For the measurements several chambers were combined (Figure 10). As in former studies on the  $\text{NO}_2$  exchange with different plants, an extra empty (“reference”) chamber was also applied. The empty chamber was used to detect basic contamination in the system, adsorption/desorption, as well as to investigate gas-phase chemical reactions within the chamber volume and at the wall surface. A central V25 microprocessor unit (PASCAL based code) controlled the power supply for the mass flow sensors, purging and mixing fans, and signal recording by a PC card. Each chamber could be controlled independently. Furthermore, the V25 operated a number of environmental sensors for air and needle temperature, photosynthetically active radiation (PAR) and relative humidity, and recorded their signals.

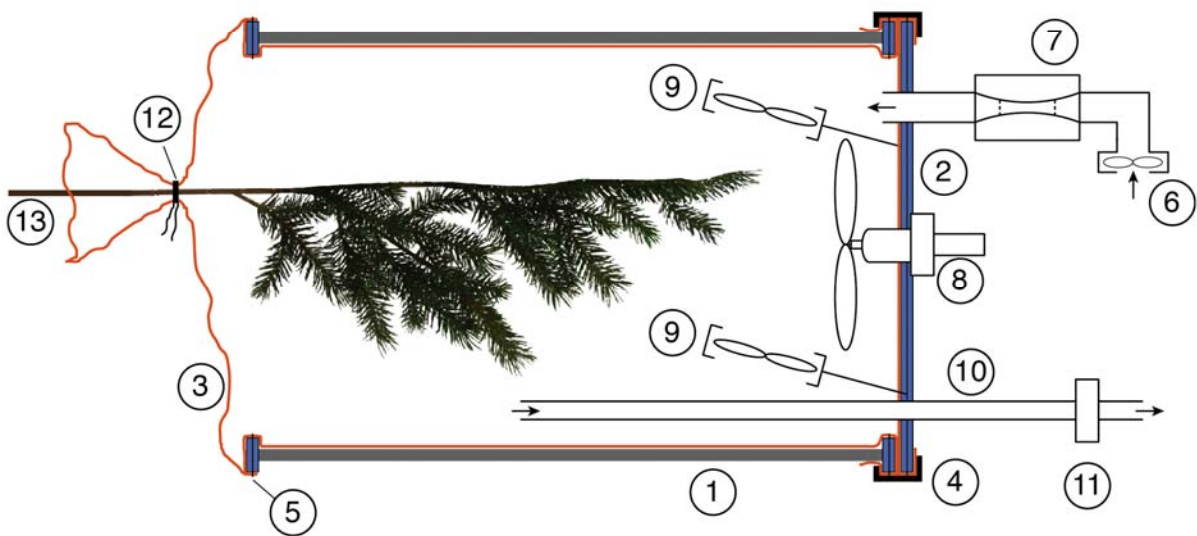
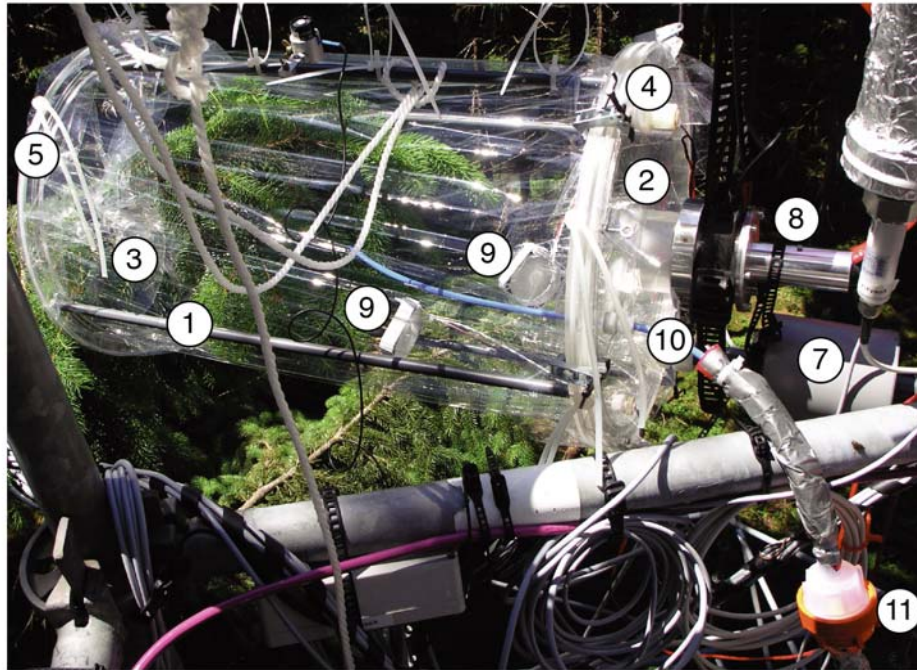


**Figure 9:** Photograph and schematic drawing of a dynamic chamber consisting of: (1) PVC (grey parts) frame, (2) acrylic glass (blue parts) lid, (3) FEP film (red parts in the scheme), (4) clamp to attach lid to frame, (5) silicon straps, (6) inlet fan, (7) air mass flow sensor, (8) Teflon propeller, (9) mixing fan, (10) sample tube for chamber air, (11) filter, (12) closure, (13) plant material.



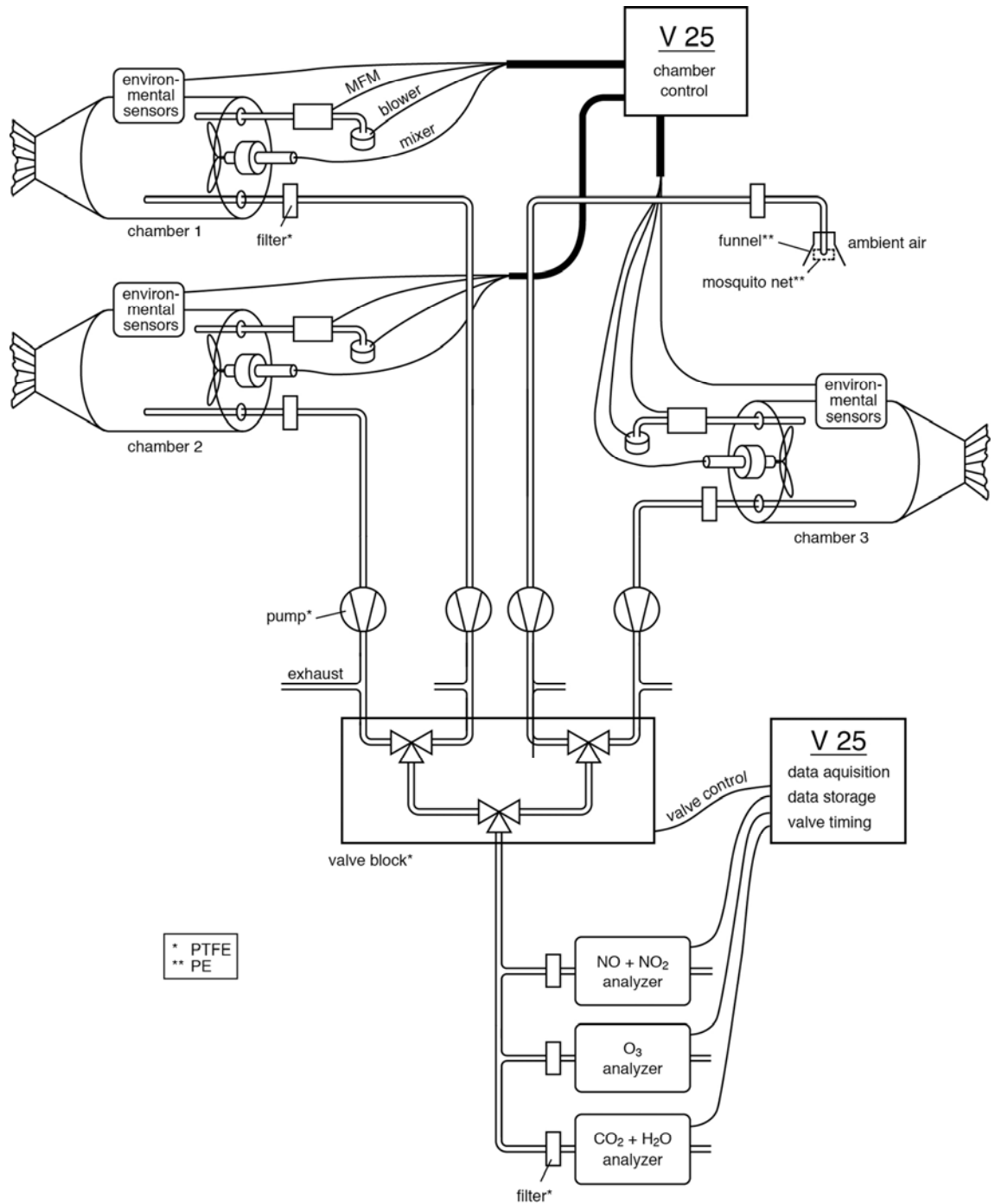


**Figure 10:** Schematic set-up of the system with three dynamic chambers. Open lines are PFA sampling tubes, black lines are cables for data acquisition and control.

### 2.4.2 Implementation of concentration and flux density measurements

Exchange flux densities of the NO-NO<sub>2</sub>-O<sub>3</sub> triad as well as of CO<sub>2</sub> and H<sub>2</sub>O are determined from the difference of molar concentrations measured at the inlet and outlet of the dynamic chambers. Ideally, a total of 10 analyzers per dynamic chamber would guarantee simultaneous concentration measurements at all these positions. However, full simultaneity is usually prohibited not only for cost arguments; operation of two trace gas analyzers with an agreement (in their absolute accuracy) much less of the expected difference between inlet and outlet concentration is currently not feasible. Therefore, only one set of analyzers was used operating in a mode of continuous switching between the inlet and outlet position(s) of the (different) dynamic chamber(s). For gas piping the tubes from the different positions at the chambers were combined to one insulated and heated (above ambient temperature) bundle to prevent water vapor condensation. To ensure similar conditions for all lines, all tubes were set to the same length (in this field study 37 m). The sampling air flow was maintained by Teflon membrane pumps with an air flow of 8 - 10 L min<sup>-1</sup>. To avoid contamination of tubes and analyzers a PTFE particulate filter (pore size 2 μm) was installed in front of the intake line. Switching between the different intake lines was maintained by several 3-way PFA solenoid valves. The necessary quantity of valves depends on the number of dynamic chambers in operation. The sample line connected the valve block to the analyzers. Even when an individual intake line was not switched to the analyzers, the air flow through it was kept constant. A second V25 unit was used to control the solenoid valves and the cycle times and recorded the data of the trace gas analyzers. Measurement cycle times and switching (during field experiments) is shown in Figure 18a. The shown cycling time of 4 minutes is a result of optimization between fast switching and the analyzers' and system's capabilities: the most important issues in this respect are the analyzers' (moving) averaging times of 30 s and the temporal response of the analyzers to switching concentrations.

Air temperature and needle surface temperatures inside the chambers were continuously recorded by Teflon covered thermocouples (0.005", Chromega<sup>TM</sup>-Constantan, Omega, UK). PAR was detected outside the chamber with a LiCor quantum sensor (model LI-190SA, LiCor, Lincoln, NE, USA). Relative humidity was measured with a combined temperature and relative humidity probe (Model MP100A, Rotronic, Switzerland).

## 2.5 Experiments

The results of this study are based on datasets obtained during the second intensive observation period (IOP II) of the project EGER (ExchanGE processes in mountainous Regions) and laboratory measurements.

### 2.5.1 Plant material

Measurements of NO-NO<sub>2</sub>-O<sub>3</sub> trace gas exchange fluxes were done at Norway spruce (*Picea abies* L.) also commonly known as the European spruce. Spruce is a coniferous evergreen tree of the genus *Picea* in the family *Pinaceae*. The Norway spruce grows throughout Europe from Norway in the northwest to Poland eastward, and also in the mountains of central Europe, southwest to the western end of the Alps, and southeast in the Carpathians and Balkans to the extreme north of Greece. It prefers a damp and cool climate, therefore it is a mountains tree in the south part of the distribution area. The primary habitat requirement is the water supply and a sufficient ventilation of the soil.

The Norway spruce is one of the most economically important coniferous species in Europe. The distribution of forest species in Germany is displayed in Figure 11. Spruce is the widespread species with 28.2 % of the total population followed by pine and beech. 58.1 % of the German forests consist of conifer due to economical reasons.

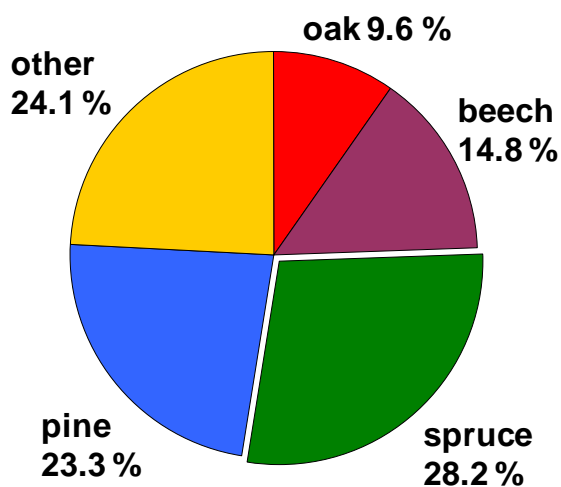


**Figure 11:** Distribution of forest species in Germany (National Forest Inventory, second survey 2001 - 2002). (<http://www.bundeswaldinventur.de/enid/a79fe9863d10b628447a8f74a2f2ee12,0/a9.html>)

Laboratory experiments were performed with 3- to 4-yr old Norway spruce trees (*Picea abies* L.) grown in pots in a commercial soil mixture. All specimens originated from the EGER field site and were dug out half a year before the measurements started. For the laboratory studies the above-ground parts of the whole tree were enclosed in the chamber. A typical young tree had a leaf area ( $A_{leaf}$ ) of 0.16 m<sup>2</sup> in total (projected leaf area). For the field experiments branches of adult Norway spruces were investigated. The front part of an intact branch with older needles and new shoots, still attached to the tree, was enclosed to around 40 cm length in the chamber. Two plant chambers on different trees were used for the field studies. At the end of the studies the enclosed leaf area was measured to be 0.36 m<sup>2</sup> (tree 1, projected leaf area) and 0.37 m<sup>2</sup> (tree 2, projected leaf area) with a dry weight of 66 g (tree 1) and 78 g (tree 2). All exchange measurements started one day after enclosure in order to allow an acclimatization of the branch or plant.

At the end of the experiments leaves of the enclosed branches were harvested for determination of leaf area and dry weight. Leaves were scanned by a calibrated scanner system (DeskSCAN II, Hewlett-Packard, USA; area determining software SIZE, Müller, Germany). Dry leaf weight was obtained after drying for 2 days at 70 °C in an oven (Heraeus, Germany). The needles of spruce have stomata on the entire needle surface, therefore the area of the whole surface was used. For needle surface area calculation the single surface area was multiplied by factor 2.74 according to RIEDERER et al. (1988). Leaf area during the field measurements varied with the leaf flushing, therefore we interpolated the leaf area retroactively.

### **2.5.2 Field site description and set-up**

The field experiment was conducted within the project EGER. The project was focused on the role of process interactions among the different scales of soil, in-canopy and atmospheric exchange processes of mass, energy, and non-reactive as well as reactive trace substances. It took place in summer 2008 (01 June - 15 July) in northeast Bavaria, Germany (Fichtelgebirge), a mountainous area, covered mainly with forest, agricultural area and including meadows and lakes. The research site "Weidenbrunnen" (50°08'31" N, 11°52'01" E; 774 m a.s.l.) was part of a spruce forest ecosystem, which resulted from intensive reforestation in the last century. The plant cover was dominated

by Norway spruce (*Picea abies*). The main understory types were moss, grass (*Deschampsia flexuosa* and *Calamagrostis villosa*), blueberries (*Vaccinium myrtillus*) and young spruce. The stand-age was 56 years (according to ALSHEIMER 1997) and the mean canopy height was 23 m (SERAFIMOVICH et al. 2008). The tree density of the stand was 1007/ha (ALSHEIMER 1997), with a leaf area index (LAI) of 5.2 (THOMAS and FOKEN 2007). The Fichtelgebirge is located in the transition zone from maritime to continental climates with maritime impact (FOKEN 2003). The annual average temperatures are 5.0 °C (1971-2000; FOKEN 2003) with extreme values of -20 °C during wintertime and 30° C during summer. In the summer period, Atlantic air masses account for the temperate climate, whereas during winter continental influence due to easterly winds can result in short but extreme cold periods. The annual precipitation is 1162 mm (1971-2000; FOKEN 2003). The main wind direction is a west or south west wind (GERSTBERGER et al. 2004). This field site is maintained for more than 10 years by the University of Bayreuth and a lot of studies have been conducted there.

### 2.5.3 Laboratory set-up

For laboratory experiments the plant chambers were installed inside a thermostatted cabinet (Heraeus, Germany), which was kept under controlled temperature and humidity conditions (day: 25 °C, 60 %; night: 20 °C, 50 %) with a light/dark regime of 12/12 hours. In addition to the cabinet irradiation (Osram Powerstar HQI-BT 400 W/D) we used a set of light emitting diodes with a spectral bandwidth of 400 - 700 nm. The total measured PAR in the middle of the chamber was about 450  $\mu\text{mol photons m}^{-2} \text{s}^{-1}$ . The plant chambers were continuously flushed with purified air, obtained by passing compressed air through a gas purification system consisting of several columns in series, filled with silica gel (2 - 5 mm, Merck, Germany), molecular sieve (0.3 nm perlform, Merck, Germany), charcoal (0.3 mm LS-Labor Service, Germany) and glass wool (Merk, Germany). The purified air was then led through a glass tank filled with demineralized water to humidify the air. Different NO<sub>2</sub> concentrations (between 0.3 and 4 ppb) were generated by mixing NO<sub>2</sub> from a pressurized standard cylinder ( $m_{std,NO_2} = 41151 \pm 2049 \text{ nmol m}^{-3}$  (1.004  $\pm$  0.050 ppm) NO<sub>2</sub> in N<sub>2</sub>; Air Liquide, Germany) into the purified air stream. Mixing was performed by adjustment of two mass flow controllers (MKS Instruments, USA), one to keep the flow of NO<sub>2</sub> standard

gas ( $Q_{std,NO_2}$ ), the other the flow of the purified air stream ( $Q_{dil}$ ) constant. The blended  $NO_2$  concentration ( $m_{blend,NO_2}$ ) and its standard error ( $s_{m\_blend,NO_2}$ ) are given by

$$m_{blend,NO_2} = \frac{(m_{std,NO_2} Q_{std,NO_2} + m_{dil,NO_2} Q_{dil})}{(Q_{std,NO_2} + Q_{dil})} \quad (17.1)$$

$$s_{m\_blend,NO_2} = \pm \frac{(m_{blend,NO_2})^2}{m_{std,NO_2} Q_{std,NO_2}} \sqrt{\left(\frac{s_{Q\_std,NO_2} Q_{dil}}{Q_{std,NO_2}}\right)^2 + (s_{Q,dil})^2} \quad (17.2)$$

where  $s_{m\_blend,NO_2}$  results of Gaussian error propagation applied to Eq. (17.1); concentrations (and standard errors) of  $m_{std,NO_2}$ ,  $m_{blend,NO_2}$  and  $m_{dil,NO_2}$  are in  $\text{nmol m}^{-3}$ , flow rates (and standard errors) of in  $Q_{std,NO_2}$  and  $Q_{dil}$  are in  $\text{m}^3 \text{s}^{-1}$ . For calculation of  $s_{m\_blend,NO_2}$  it is assumed, that  $m_{std,NO_2}$  is constant (during the time of the laboratory experiment) and  $m_{dil}$  is zero.

The  $NO_2$  mixture was directed into the dynamic plant chambers (without using the blowing axial inlet fan as for our field studies). For the laboratory measurements one plant chamber and one empty chamber with a volume ( $V$ ) of 57 L were used. Each chamber was flushed at a constant flow ( $Q$ ) of  $14 \text{ L min}^{-1}$ , controlled by mass flow controllers (MKS Instruments, USA), resulting in an exchange of the entire chamber's volume every 4 minutes. For two minutes each, air samples were directed to the analyzers from three different intake lines (purging  $NO_2$  mixture (upstream of the chambers), outlet of empty and plant chambers). All analyzers were placed inside a cabinet (GKPV 6522, Liebherr, Germany) thermostatted at  $25 \text{ }^\circ\text{C}$  to minimize variations of the analyzers' signals caused by temperature fluctuations.

# Specification and implementation of dynamic plant chamber system

In this chapter a dynamic chamber system based on previous measurements of volatile organic compounds, formaldehyde, formic and acetic acid and sulfur compounds (e.g. KESSELMEIER et al. 1993, 1996, 1998; KUHN et al. 2000) is presented. The dynamic chamber system allows exchange measurements of  $\text{NO}_2$  ( $\text{O}_3$  and  $\text{NO}$ ) under field conditions (uncontrolled) as well as studies under controlled conditions including (laboratory) fumigation experiments.

Because  $\text{NO}_2$  compensation point concentrations were reported at (sub-)ppb levels, our laboratory  $\text{NO}_2$  fumigation experiments were performed with 3- to 4-yr old Norway Spruce trees at 0.3 - 3.4 ppb. Also under field conditions, such low ambient  $\text{NO}_2$  concentrations can be expected. Moreover, exchange fluxes derived from dynamic chamber measurements are based on generally (very) small differences of  $\text{NO}_2$  ( $\text{NO}$ ,  $\text{O}_3$ ) concentrations between inlet and outlet of the chamber. Consequently, detection limits of corresponding analyzers, statistical significance of the concentration differences, as well as the statistical goodness of measurements definitely have a substantial impact on the identification and quantification of statistically significant deposition velocities and compensation point concentrations, and have been considered correspondingly. Furthermore, as the exchange of  $\text{NO}_2$  is a complex interaction of transport, chemistry and plant physiology, fluxes of  $\text{NO}$ ,  $\text{NO}_2$ ,  $\text{O}_3$ ,  $\text{CO}_2$  and  $\text{H}_2\text{O}$  were determined in the field experiments.

## 3.1 Methods

### Quality assurance and error analysis

#### 3.1.1 Corrections for concentration changes in long tubing

Long intake lines (mostly necessary for field experiments) may impact the trace gas concentrations (BEIER and SCHNEEWIND 1991). Trace gases may adsorb on the inner walls of the tubing and/or react with each other according to reactions (R1) and (R2). Therefore, we used opaque tubing to completely prevent photolysis of NO<sub>2</sub>. Hence, reaction (R1) (NO + O<sub>3</sub>) was the most important reaction to consider. For a known residence time, temperature and pressure in the tubes, the mixing ratios of NO, NO<sub>2</sub> and O<sub>3</sub> can be corrected according to BEIER and SCHNEEWIND (1991). To proceed, the residence time of the individual trace gas in the tubing as well as the characteristic chemical reaction time ( $\tau_i$ ;  $i = \text{NO}, \text{O}_3$ ) must be known. The latter is calculated by  $\tau_{\text{NO}} = (k N_{\text{O}_3})^{-1}$  and  $\tau_{\text{O}_3} = (k N_{\text{NO}})^{-1}$ , respectively ( $N_{\text{O}_3}$  and  $N_{\text{NO}}$  in molecules cm<sup>-3</sup>,  $k_{\text{R1}} = k = 1.4 \times 10^{-12} \exp(-1310/T)$  in cm<sup>3</sup> molecules<sup>-1</sup> s<sup>-1</sup>; see ATKINSON et al. 2004).

#### 3.1.2 Temporal response of analyzers

Response tests were carried out to check the response of analyzers to changes of concentrations when switching between intake lines with low concentration of the respective trace gas (NO, NO<sub>2</sub>, O<sub>3</sub>) to another intake line with high trace gas concentration (after stabilization) and back to the intake line of low concentration.

#### 3.1.3 Temperature dependence of analyzers

The signals of analyzers are sensitive to the surrounding temperature. These effects are of special importance for field studies where it is more difficult to keep temperatures constant. Thus a series of tests were performed to determine the temperature dependence of all trace gas analyzers. The tests were done inside the conditioning cabinet (Heraeus, Germany) under different temperature conditions (temperature range: 18 - 46 °C). For each analyzer a calibration was carried out at each temperature level. We considered the correction of the analyzers' signals necessary if the observed drift



with temperature exceeded the maximum signal noise measured with zero air. We did not perform a correction when the drift was below 1 % for the entire temperature range or the analyzer's noise was greater than the temperature drift.

### 3.1.4 Dynamic chamber: internal mixing, exchange rate of chamber volume, wall absorption and transmissivity

The effective turbulent mixing as well as the fast exchange of the plant chamber's volume is essential for the determination of exchange flux densities of reactive as well as non-reactive trace gases (see MEIXNER 1994; MEIXNER et al. 1997). Particularly, the derivation of accurate NO<sub>2</sub> and O<sub>3</sub> leaf conductances from NO<sub>2</sub> and O<sub>3</sub> deposition velocities obtained by dynamic chamber measurements critically depends from the effectiveness of internal mixing and the chamber volume's exchange rate (see PAPE et al. 2009). Fast internal mixing of the chamber's volume has been assured by operation of three fans (see Figure 9) inside the chamber. A similar procedure was chosen by PAPE et al. (2009), who quantified complete mixing of the chamber volume in less than 2 s. The exchange rate of the chamber's volume is primarily determined by the volume  $V$  and the purging rate  $Q$ . However, due to delay effects of the sampling lines and due to the limited response times of the analyzers after switching between the different intakes, it is not possible to directly observe the trace gas' mixing in the plant chamber. Therefore, the time needed for temporal equilibrium of trace gas concentrations in an empty plant chamber was determined by measurements of a fast-response helium detector (Pico leak detector, MKS Instrument Inc., USA). A helium pulse was released into the purging stream of the chamber and the needed time for equilibration was determined.

Sorption effects (ad-, ab-, desorption) to and from the inner wall materials of the dynamic chamber should not modify the concentrations of (reactive) trace gases. Using the laboratory set-up, we investigated potential sorption effects to the inner walls of an empty chamber by fumigating it consecutively with different NO, NO<sub>2</sub> and O<sub>3</sub> concentrations. There were no desorption effects observed. Wall absorption was quantified in form of "blank" deposition velocities, where  $v_{dep\_wall,i} = Q(m_{a,i} - m_{s,i}) / (A_{wall} m_{s,i})$  ( $i = \text{NO}_2, \text{NO}, \text{O}_3$ ).

In the field, the transmissivity of the FEP film (the dynamic chamber's wall) for PAR and the  $\text{NO}_2$  photolysis rate  $j(\text{NO}_2)$  has been monitored by continuous and simultaneous measurements of corresponding radiation fluxes inside and outside the chamber. PAR was measured with a LiCor quantum sensor (model LI-190SA, LiCor, Lincoln, NE, USA) and  $j(\text{NO}_2)$  was determined as an omni-directional actinic UV radiation flux using a  $j(\text{NO}_2)$ -sensor (filter radiometer, Meteorologie Consult GmbH, Königstein, Germany).

### 3.1.5 Significance of concentration differences

Particularly in the laboratory, the exchange flux density is directly proportional to  $\Delta m_i = (m_{a,i} - m_{s,i})$ , the difference of trace gas concentrations at the inlet and the outlet of the dynamic chamber (see Eq. (8.4)). Even under field conditions, the major component of the exchange flux density  $F_{ex,i}$  is  $Q/A_{leaf} \Delta m_i$ . Keeping in mind, that (a) the sign of  $\Delta m_i$  determines direction of the exchange flux density and (b) the errors of  $m_{a,i}$  and  $m_{s,i}$  are decisively controlling the error of  $\Delta m_i$  (and consequently that of  $F_{ex,i}$ ), it is more than obvious to control the significance of  $\Delta m_i$ . The corresponding statistical test requires the number of individual measurements, the averages and standard errors of  $m_{s,i}$  and  $m_{a,i}$ . These were provided and calculated from the individual concentration measurements during one measurement cycle (laboratory: 30 min, field: 4 min). Prior to this, we identified outliers in the data sets by application of the Nalimov-test, a variant of Grubbs' test. Then, the significance of differentiation between the two averages of  $m_{s,i}$  and  $m_{a,i}$  was statistically secured by application of the t-test.  $\Delta m$  with statistical significance below 99 % ( $\alpha < 0.99$ ) were correspondingly flagged and not included in subsequent calculations.

### 3.1.6 Bi-variate weighted linear least-squares fitting regression analysis

Since the concentrations  $m_{a,i}$  and  $m_{s,i}$  are measured with identical analyzers (see above), corresponding standard errors  $s_{ms,i}$  and  $s_{ma,i}$  are of the same order of magnitude. Therefore, bi-variate weighted linear least-squares fitting (which considers uncertainties of both,  $m_{s,i}$  and  $m_{a,i}$ ) is preferred to any standard forms of linear regression analysis (which consider, at best, uncertainties in the  $y$ -values, but no uncertainties in the

$x$ -values). The preferred algorithm delivers corresponding values of intersect ( $n_i$ ) and slope ( $m_i$ ) and other statistical quantities, like the standard errors of  $n_i$  and  $m_i$  ( $s_{n,i}$ ,  $s_{m,i}$ ), as well as correlation and regression coefficients,  $r(m_{s,i}, m_{a,i})$  and  $R^2(m_{s,i}, m_{a,i})$ . YORK et al. (2004) presented the original set of equations for bi-variate weighted linear least-squares fitting regression analysis, where the slope  $m_i$  has to be solved iteratively (see below). For the iterative calculation a Microsoft Excel<sup>®</sup> spreadsheet was used, which has been provided by CANTRELL (2008) as a supplement of his paper (<http://www.atmos-chem-phys.net/8/5477/2008/acp-8-5477-2008-supplement.zip>).

Field data of concentrations in particular, have usually not all the same uncertainty. All kinds of linear least square fitting methods (considering errors in  $y$  and  $x$ ) account for the fact, that data with the least uncertainty should have the greatest influence on the intercept  $n$  and the slope  $m$  of the fitted line. This is achieved by weighting each of the data points ( $m_{a,i}$ ,  $m_{s,i}$ ) with a factor  $\omega_i$ , which is usually set to the inverse of the square of standard errors (standard deviations) of  $x$  and  $y$ -values (here:  $s_{ma,i}^{-2}$  and  $s_{ms,i}^{-2}$ ).

YORK et al. (2004) have provided a very detailed description of the bi-variate weighted linear least-squares fitting method. Here, only those equations are presented which are necessary to calculate the intersect  $n$  and the slope  $m$  of the best straight line (and related standard errors,  $s_n$  and  $s_m$ ). For the sake of comparability with YORK et al. (2004),  $m_{a,i} := X_i$  and  $m_{s,i} := Y_i$ ,  $s_{ma,i}^{-2} := \omega X_i$  and  $s_{ms,i}^{-2} = \omega Y_i$  were set. The method of YORK et al. (2004) to calculate the intercept  $n$  ( $s_n$ ) and the slope  $m$  ( $s_m$ ) comprises the following set of four equations:

$$n = \bar{Y} - m \bar{X} ; \quad i = 1, 2, \dots, N \quad (18.1)$$

$$m = \frac{\sum W_i \beta_i (Y_i - \bar{Y})}{\sum W_i (X_i - \bar{X})} \quad (18.2)$$

$$s_n^2 = \frac{1}{\sum W_i} + \bar{x}^2 s_m^2 \quad (18.3)$$

$$s_m^2 = \frac{1}{\sum W_i (x_i - \bar{x})^2} \quad (18.4)$$

where,

$$\begin{aligned}
 x_i &= \bar{X} + \beta_i; & y_i &= \bar{Y} + \beta_i; \\
 \bar{X} &= \frac{\sum W_i X_i}{W_i}; & \bar{Y} &= \frac{\sum W_i Y_i}{W_i}; & \bar{x} &= \frac{\sum W_i x_i}{W_i}; & \bar{y} &= \frac{\sum W_i y_i}{W_i} \\
 W_i &= \frac{\omega(X_i)\omega(Y_i)}{\omega(X_i) + m^2\omega(Y_i)}; & \omega(X_i) &= s_{X,i}^{-2}; & \omega(Y_i) &= s_{Y,i}^{-2} \\
 \beta_i &= W_i \left( \frac{X_i - \bar{X}}{\omega(Y_i)} + \frac{m(Y_i - \bar{Y})}{\omega(X_i)} \right);
 \end{aligned} \tag{18.5}$$

The original set of equations presented by YORK et al. (2004) contain additional terms in the equations for  $W_i$  and  $\beta_i$  for consideration of potential correlations between  $s_{X,i}$  and  $s_{Y,i}$ , which are set to zero here (i.e.  $s_{ma,i}$  and  $s_{ms,i}$  are assumed to be uncorrelated). Since the equation for the slope  $m$  (Eq. 18.2) contains the variables  $W_i$  and  $\beta_i$ , which are in turn functions of  $m$  (see Eq. (18.5)), Eq. (18.2) has to be solved iteratively.

### 3.1.7 Standard errors of exchange flux densities, deposition velocities and compensation point concentrations

Standard errors of exchange flux densities  $F_{ex,i}$ , deposition velocities  $v_{dep,i}$  and compensation point concentrations  $m_{comp,i}$  of the NO-NO<sub>2</sub>-O<sub>3</sub> triad may be derived by applying standard Gaussian error propagation. For that the standard errors of all variables on the right hand side of Eqs. (8.1) - (8.3), (13.1) - (13.3) and (14.1) - (14.3) must be known, and all variables of each individual equation should be independent of each other. However, the latter is not the case for (at least)  $m_{s,i}$  and  $m_{a,i}$  (see Eqs. (8.1) - (8.3)). Therefore, application of the generalized form of the Gaussian error propagation is preferred, which considers the mutual dependence of each pair variables (TAYLOR 1982; PHILLIPS et al. 2002). The general formulation of the standard error  $s_y$  of a quantity  $y = f(x_1, x_2, x_3, \dots, x_n)$  reads as follows:

$$s_y^2 = \sum_{i=1}^n \left( \frac{\partial y}{\partial x_i} \cdot s_{x,i} \right)^2 + 2 \cdot \sum_{i=1}^{n-1} \sum_{j=i+1}^n \frac{\partial y}{\partial x_i} \cdot \frac{\partial y}{\partial x_j} \cdot s_{x,i} \cdot s_{x,j} \cdot r(x_i, x_j) \tag{19}$$

where  $r(x_i, x_j)$  are the correlation coefficients between each pairs of all  $x_i$  and  $x_j$ .

The individual variables  $x_i$  for the quantities  $y = F_{exNO_2}, F_{exNO}, F_{exO_3}, v_{dep,NO_2}, v_{dep,NO}, v_{dep,O_3}, m_{comp,NO_2}, m_{comp,NO}$  and  $m_{comp,O_3}$  are defined by Eqs. (8.1) - (8.3), (13.1) - (13.3) and (14.1) - (14.3).

During field experiments, all  $m_{a,i}$  and  $m_{s,i}$  of the NO-NO<sub>2</sub>-O<sub>3</sub> triad have been measured in cycles of 4 minutes. During this time period, it has been shown, that the error of the purging rate  $Q$  is negligible. The volume  $V$  of the chambers is *a priori* known, its error is considered to be zero. Standard errors of  $m_{a,i}$  and  $m_{s,i}$  are known for each data pair of measurements. Averages and standard errors of  $A_{leaf}, j(NO_2), k$  and conjugated concentrations  $m_{s,j}$  ( $j \neq i$ ) have to be calculated individually from each data set which is used for the determination of  $F_{ex,i}, v_{dep,i}$  and  $m_{comp,i}$ .

Therefore, according to Eq. (8.1), the mass exchange flux density  $F_{exNO_2}$  is a function of 7 error-prone variables, namely  $x_1 = m_{a,NO_2}, x_2 = m_{s,NO_2}, x_3 = j(NO_2), x_4 = k, x_5 = m_{s,NO}, x_6 = m_{s,O_3}$  and  $x_7 = A_{leaf}$ . Analogously to  $F_{exNO_2}$ , the 7 variables for  $F_{ex,NO}$  ( $F_{ex,O_3}$ ) in Eq. (8.2) (Eq. 8.3) are  $x_1 = m_{a,NO} (m_{a,O_3}), x_2 = m_{s,NO} (m_{s,O_3}), x_3 = j(NO_2), x_4 = k, x_5 = m_{s,NO_2}, x_6 = m_{s,O_3} (m_{s,NO})$  and  $x_7 = A_{leaf}$ . Considering Eq. (13.1), the deposition velocity  $v_{dep,NO_2}$  is a function of 3 error-prone variables,  $x_1 = m_1, x_2 = j(NO_2)$  and  $x_3 = A_{leaf}$ , while the deposition velocity  $v_{dep,NO}$  ( $v_{dep,O_3}$ ) depends on 4 error-prone variables, namely  $x_1 = m_2 (m_3), x_2 = k, x_3 = m_{s,O_3} (m_{s,NO})$  and  $x_4 = A_{leaf}$ . The compensation point concentrations  $m_{comp,NO_2}$  ( $m_{comp,NO}, m_{comp,O_3}$ ) are each functions of 6 error-prone variables (see Eqs. (14.1) - (14.3)). These are  $x_1 = n_1 (n_2, n_3), x_2 = m_1 (m_2, m_3), x_3 = j(NO_2), x_4 = k, x_5 = m_{s,NO} (m_{s,NO_2}, m_{s,NO_2})$  and  $x_6 = m_{s,O_3} (m_{s,O_3}, m_{s,NO})$ . Bi-variate weighted linear least-squares fitting regression analysis of measured  $m_{s,i}$  versus  $m_{a,i}$  (which considers both,  $S_{m,a,i}$  and  $S_{m,s,i}$ ) delivers the quantities  $n_1, n_2, n_3$  and  $m_1, m_2, m_3$  as well as their standard errors  $S_{n1}, S_{n2}, S_{n3}$  and  $S_{m1}, S_{m2}, S_{m3}$ . To calculate the standard errors  $S_{Fex,NO_2}, S_{Fex,NO}, S_{Fex,O_3}, S_{v,dep\_NO_2}, S_{v,dep\_NO}, S_{v,dep\_O_3}, S_{m,comp\_NO_2}, S_{m,comp\_NO}$  and  $S_{m,comp\_O_3}$  by application of the general Gaussian error propagation (Eq. (19)), one have to calculate all the derivatives of  $y_i = F_{ex,i}, y_i = v_{dep,i}$  and  $y_i = m_{comp,i}$ , ( $i = NO_2, NO, O_3$ ) with respect to the corresponding variables  $x_1, x_2, \dots, x_n$  mentioned above. The derivatives of  $\partial y/\partial x_i$  are given in Table 7, Table 8 and Table 9.

**Table 7:** Derivatives  $\partial y/\partial x_i$  of  $y = F_{ex,NO_2}, F_{ex,NO}, F_{ex,O_3}$  with respect to the variables  $x_i$  in Eqs. (8.1) – (8.3) for application of the generalized Gaussian error propagation to calculate the standard errors of  $s_{F_{ex,NO_2}}, s_{F_{ex,NO}}$  and  $s_{F_{ex,O_3}}$  according to Eq. (19).

| variable<br>$x$ | dependent variable $y$                                 |  |   |
|-----------------|--|--|---|
|                 | $F_{ex,NO_2}$  | $F_{ex,NO}$  | $F_{ex,O_3}$  |
| $m_{a,NO_2}$    | $-\frac{Q}{A_{leaf}}$                                  |  |   |
| $m_{s,NO_2}$    | $+\frac{Q}{A_{leaf}}\left(1+\frac{V}{Q}j(NO_2)\right)$ | $-\frac{V}{A_{leaf}}j(NO_2)$                               | $-\frac{V}{A_{leaf}}j(NO_2)$                              |
| $m_{a,NO}$      |  | $-\frac{Q}{A_{leaf}}$                                      |   |
| $m_{s,NO}$      | $-\frac{V}{A_{leaf}}k m_{s,O_3}$                       | $+\frac{Q}{A_{leaf}}\left(1+\frac{V}{Q}k m_{s,O_3}\right)$ | $+\frac{V}{A_{leaf}}k m_{s,O_3}$                          |
| $m_{a,O_3}$     |  |  | $-\frac{Q}{A_{leaf}}$                                     |
| $m_{s,O_3}$     | $-\frac{V}{A_{leaf}}k m_{s,NO}$                        | $+\frac{V}{A_{leaf}}k m_{s,NO}$                            | $+\frac{Q}{A_{leaf}}\left(1+\frac{V}{Q}k m_{s,NO}\right)$ |
| $j(NO_2)$       | $+\frac{V}{A_{leaf}}m_{s,NO_2}$                        | $-\frac{V}{A_{leaf}}m_{s,NO_2}$                            | $-\frac{V}{A_{leaf}}m_{s,NO_2}$                           |
| $k$             | $-\frac{V}{A_{leaf}}m_{s,NO} m_{s,O_3}$                | $+\frac{V}{A_{leaf}}m_{s,NO} m_{s,O_3}$                    | $+\frac{V}{A_{leaf}}m_{s,NO} m_{s,O_3}$                   |
| $A_{leaf}$      | $-\frac{F_{ex,NO_2}}{A_{leaf}}$                        | $-\frac{F_{ex,NO}}{A_{leaf}}$                              | $-\frac{F_{ex,O_3}}{A_{leaf}}$                            |

**Table 8:** Derivatives  $\partial y/\partial x_i$  of  $y = v_{dep,NO_2}, v_{dep,NO}, v_{dep,O_3}$  with respect to the variables  $x_i$  in Eqs. (13.1) – (13.3) for application of the generalized Gaussian error propagation to calculate the standard errors of  $s_{v,dep\_NO_2}, s_{v,dep\_NO}$  and  $s_{v,dep\_O_3}$  according to Eq. (19).

| variable<br>$x$   | dependent variable $y$                  |   |   |
|-------------------|---|---|---|
|                   | $v_{dep,NO_2}$                          | $v_{dep,NO}$                            | $v_{dep,O_3}$                           |
| $\bar{m}_{s,NO}$  |   |   | $-\frac{V}{A_{leaf}} \bar{k}$           |
| $\bar{m}_{s,O_3}$ |   | $-\frac{V}{A_{leaf}} \bar{k}$           |   |
| $\bar{j}(NO_2)$   | $-\frac{V}{A_{leaf}}$                   |   |   |
| $\bar{k}$         |   | $-\frac{V}{A_{leaf}} \bar{m}_{s,O_3}$   | $-\frac{V}{A_{leaf}} \bar{m}_{s,NO}$    |
| $\bar{A}_{leaf}$  | $-\frac{v_{dep,NO_2}}{\bar{A}_{leaf}}$  | $-\frac{v_{dep,NO}}{\bar{A}_{leaf}}$    | $-\frac{v_{dep,O_3}}{\bar{A}_{leaf}}$   |
| $m_1$             | $-\frac{\bar{Q}}{\bar{A}_{leaf} m_1^2}$ |   |   |
| $m_2$             |   | $-\frac{\bar{Q}}{\bar{A}_{leaf} m_2^2}$ |   |
| $m_3$             |   |   | $-\frac{\bar{Q}}{\bar{A}_{leaf} m_3^2}$ |

**Table 9:** Derivatives  $\partial y/\partial x_i$  of  $y = m_{comp,NO_2}$ ,  $m_{comp,NO}$  and  $m_{comp,O_3}$  with respect to the variables  $x_i$  in Eqs. (14.1) – (14.3) for application of the generalized Gaussian error propagation to calculate the standard errors of  $s_{m,comp\_NO_2}$ ,  $s_{m,comp\_NO}$  and  $s_{m,comp\_O_3}$  according to Eq. (19).

| variable<br>$x$    | dependent variable $y$  |  |  |
|--------------------|---|--|--|
|                    | $m_{comp,NO_2}$   | $m_{comp,NO}$  | $m_{comp,O_3}$   |
| $\bar{m}_{s,NO_2}$ |   | $-\frac{m_2 V}{Q} \bar{j}(NO_2) \cdot D_2^{-1}$  | $-\frac{m_3 V}{Q} \bar{j}(NO_2) \cdot D_3^{-1}$  |
| $\bar{m}_{s,NO}$   | $-\frac{V}{Q} m_1 \bar{k} \bar{m}_{s,O_3} \cdot D_1^{-1}$   |  | $\left( n_3 - m_3 \frac{V}{Q} \bar{j}(NO_2) \bar{m}_{s,NO_2} \right) \frac{m_3 V \bar{k}}{Q} \cdot D_3^{-2}$                       |
| $\bar{m}_{s,O_3}$  | $-\frac{V}{Q} m_1 \bar{k} \bar{m}_{s,NO} \cdot D_1^{-1}$  | $\left( n_2 - m_2 \frac{V}{Q} \bar{j}(NO_2) \bar{m}_{s,NO_2} \right) \frac{m_2 V \bar{k}}{Q} \cdot D_2^{-2}$                         |  |
| $\bar{j}(NO_2)$    | $\left( n_1 - m_1 \frac{V}{Q} \bar{k} \bar{m}_{s,NO} \bar{m}_{s,O_3} \right) \frac{m_1 V}{Q} \cdot D_1^{-2}$                            | $-\frac{m_2 V}{Q} \bar{m}_{s,NO_2} \cdot D_2^{-1}$   | $-\frac{m_3 V}{Q} \bar{m}_{s,NO_2} \cdot D_3^{-1}$   |
| $\bar{k}$          | $-\frac{V}{Q} m_1 \bar{m}_{s,NO} \bar{m}_{s,O_3} \cdot D_1^{-1}$  | $\left( n_2 \bar{m}_{s,O_3} - m_2 \frac{V}{Q} \bar{j}(NO_2) \bar{m}_{s,NO_2} \bar{m}_{s,O_3} \right) \frac{m_2 V}{Q} \cdot D_2^{-2}$ | $\left( n_3 \bar{m}_{s,NO} - m_3 \frac{V}{Q} \bar{j}(NO_2) \bar{m}_{s,NO_2} \bar{m}_{s,NO} \right) \frac{m_3 V}{Q} \cdot D_3^{-2}$ |
| $n_1$              | $\left( 1 - m_1 - m_1 \frac{V}{Q} \bar{j}(NO_2) \right)^{-1} := D_1^{-1}$   |  |  |
| $n_2$              | $\left( 1 - m_2 - m_2 \frac{V}{Q} \bar{k} \bar{m}_{s,O_3} \right)^{-1} := D_2^{-1}$   |  |  |
| $n_3$              | $\left( 1 - m_3 - m_3 \frac{V}{Q} \bar{k} \bar{m}_{s,NO} \right)^{-1} := D_3^{-1}$  |  |  |
| $m_1$              | $\left[ n_1 \left( 1 + \frac{V}{Q} \bar{j}(NO_2) \right) - \frac{V}{Q} \bar{k} \bar{m}_{s,NO} m_{s,O_3} \right] \cdot D_1^{-2}$         |  |  |
| $m_2$              | $\left[ n_2 \left( 1 + \frac{V}{Q} \bar{k} \bar{m}_{s,O_3} \right) - \frac{V}{Q} \bar{j}(NO_2) \bar{m}_{s,NO_2} \right] \cdot D_2^{-2}$ |  |  |
| $m_3$              | $\left[ n_3 \left( 1 + \frac{V}{Q} \bar{k} \bar{m}_{s,NO} \right) - \frac{V}{Q} \bar{j}(NO_2) \bar{m}_{s,NO_2} \right] \cdot D_3^{-2}$  |  |  |



### 3.1.8 Significance of the compensation point concentrations

The bi-variate weighted linear least-squares regression analysis of  $m_{a,i}$  and  $m_{s,i}$  delivers the intercept  $n_i$ , the slope  $m_i$  and their standard errors  $s_{n,i}$  and  $s_{m,i}$ . According to Eqs. (14.1) - (14.3), each of the compensation point concentrations  $m_{comp,i}$  of the NO-NO<sub>2</sub>-O<sub>3</sub> triad can be considered as a random variable, represented by the average of  $m_{comp,i}$  and the standard error  $s_{m,comp,i}$ . The decision whether or not a compensation point concentration exists is equivalent to the test of the hypothesis whether or not the average of  $m_{comp,i}$  is highly significantly ( $\alpha = 0.999$ ), significantly ( $\alpha = 0.99$ ) or likely ( $\alpha = 0.95$ ) different from  $m^*_{comp,i} = 0$ .

For that, it is assumed that each of the test quantities  $T_i$

$$T_i = \left( \overline{m}_{comp,i} - m^*_{comp,i} \right) \cdot \frac{\sqrt{N}}{s_{m,comp,i}} \quad i = NO_2, NO, O_3 \quad (20)$$

matches the  $t$ -distribution with  $N-1$  degrees of freedom. Depending on  $\alpha$ , the hypothesis  $m_{comp,i} = m^*_{comp,i}$  must be rejected, if

$$\left| \overline{m}_{comp,i} - m^*_{comp,i} \right| \geq \frac{s_{m,comp,i}}{\sqrt{N}} \cdot t_{\alpha;N-1}; \quad \left( i.e. \frac{t_{\alpha;N-1}}{T_i} \leq 1 \right) \quad (21)$$

where  $t_{\alpha;N-1}$  are the values of the  $t$ -distribution ( $N-1$ ) for  $\alpha = 0.999, 0.99, 0.95$ , respectively.

## 3.2 Results

### 3.2.1 Analyzers and system performance

The results for the test of temperature dependence of all analyzers (see Sect. 3.1.3) are listed in Table 10. Between 18 and 46 °C the efficiency of the BLC drifted at from 37.0 % to 47.4 % over the whole temperature range. This means that for an initial concentration of 10 ppb NO<sub>2</sub> a drift of 2.2 ppb over the whole temperature range would be observed, which is equivalent to 3.6 nmol m<sup>-3</sup>/K (0.08 ppb/K). For NO the signal drift was 2.8 nmol m<sup>-3</sup>/K (0.07 ppb/K). The data of the CO<sub>2</sub> and O<sub>3</sub> analyzers did not need to be corrected because the signal drift was below 1 % for the entire temperature range, in contrast to the NO and NO<sub>2</sub> values. For the mathematical correction the slope of the regression line of the temperature tests (trace gas concentration versus temperature) was used.

**Table 10:** Results of the temperature dependence tests of the used analyzers. The temperatures are internal temperatures of the analyzers. The drift specifies the signal change during the whole temperature range. The signal noise is the maximum noise ( $3\sigma$ ) detected with zero air during the test.

| analyzer    | trace gas       | temperature range | drift      | signal noise ( $3\sigma$ ) |
|-------------|-----------------|-------------------|------------|----------------------------|
| LI-7000     | CO <sub>2</sub> | 22 – 44 °C        | + 0.97 ppm | 0.25 ppm                   |
| LI-6262     | CO <sub>2</sub> | 22 – 44 °C        | - 3.5 ppm  | 0.23 ppm                   |
| TEI 49C     | O <sub>3</sub>  | 21 – 46 °C        | + 0.4 ppb  | 0.7 ppb                    |
| TEI 42C     | NO              | 18 – 46 °C        | - 1.9 ppb  | 0.2 ppb                    |
| TEI 42C/BLC | NO <sub>2</sub> | 18 – 46 °C        | - 10.4 %   | 0.5 ppb                    |

On the basis of the results of calibration procedures it was found, that the standard error of the O<sub>3</sub> concentration measurements could be considered as constant ( $\pm 13.3$  nmol m<sup>-3</sup> or  $\pm 0.32$  ppb) for the observed range of O<sub>3</sub> concentrations (719 - 2866 nmol m<sup>-3</sup> or 19 - 77 ppb). The standard errors of NO<sub>2</sub> and NO concentration measurements are described by Eqs. (16.1) and (16.2); the parameters  $s_{m\_NO_2,0}$  and  $s_{m\_NO,0}$  are given in Table 5 ( $3\sigma$ -definition:  $LOD(m_i) = 3 s_{m,i,0}$ ),  $b_{NO_2} = 3.42 \times 10^{-4}$  nmol<sup>-1</sup> m<sup>3</sup> ( $1.40 \times 10^{-2}$  ppb<sup>-1</sup>) and  $b_{NO} = 7.88 \times 10^{-4}$  nmol<sup>-1</sup> m<sup>3</sup> ( $3.23 \times 10^{-2}$  ppb<sup>-1</sup>).

In Figure 12, the precision ( $s_{m,i}/m_i$ ) of the concentration measurements is exemplified for  $\text{NO}_2$  during laboratory (red curve) and field experiments (green curve). The precision of  $m_{\text{NO}_2}$  was only approx. 35 % during laboratory experiments at  $\text{LOD}(m_{\text{NO}_2}) = 1.04$  ppb ( $46.4 \text{ nmol m}^{-3}$ ). After considerable improvement of the NO/ $\text{NO}_2$  analyzer precision at 1 ppb improved to nearly 10 % in the field (however, precision was still 35 % at  $\text{LOD}(m_{\text{NO}_2}) = 0.31$  ppb ( $13.8 \text{ nmol m}^{-3}$ )). For further comparison, we consider that concentration  $m_i$ , where corresponding precision curves fall short of the 10 %-precision lines. These concentrations were  $161.9 \text{ nmol m}^{-3}$  (3.63 ppb; laboratory conditions),  $45.9 \text{ nmol m}^{-3}$  (1.03 ppb; field conditions), and they would be  $14.7 \text{ nmol m}^{-3}$  (0.33 ppb) and  $1.3 \text{ nmol m}^{-3}$  (0.03 ppb), if analyzers could be applied with  $\text{LOD}(m_{\text{NO}_2}) = 0.1$  and 0.01 ppb, respectively. For the NO and  $\text{O}_3$  analyzers applied under field conditions, corresponding NO and  $\text{O}_3$  concentrations ( $< 10$  % precision) were  $15.2 \text{ nmol m}^{-3}$  (0.34 ppb;  $\text{LOD}(m_{\text{NO}}) = 0.10$  ppb) and  $144.5 \text{ nmol m}^{-3}$  (3.24 ppb;  $\text{LOD}(m_{\text{O}_3}) = 0.98$  ppb), respectively.

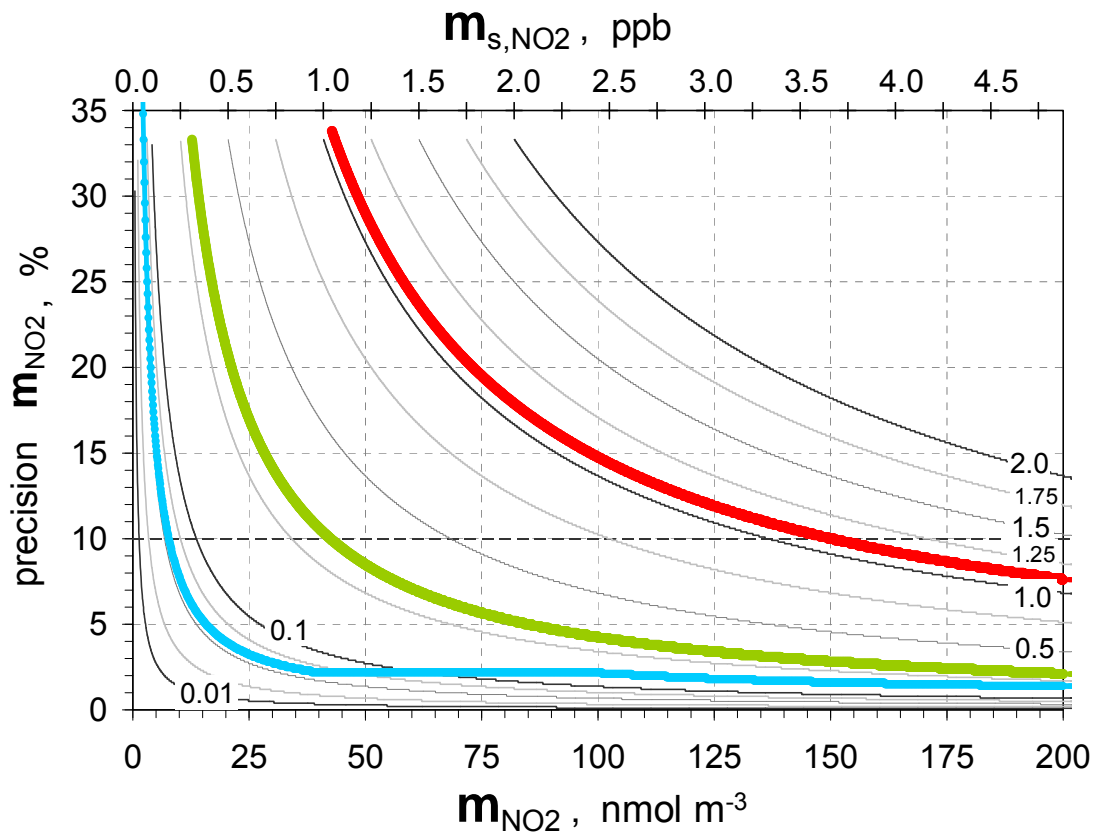


**Figure 12:** Precision ( $s_{m,\text{NO}_2}/m_{\text{NO}_2}$ ) of the applied NO/ $\text{NO}_2$  analyzer during laboratory (red curve) and field experiments (green curve). For comparison, curves for precisions of hypothetical analyzers with  $0.01 \leq \text{LOD}(m_{\text{NO}_2}) \leq 2$  ppb are also shown (numbers on black and grey curves). The blue curve is the precision of the blended  $\text{NO}_2$  concentration used for fumigation of the young spruce trees in the laboratory.

The performance of the dynamic chamber system depends critically on the temporal delay of concentrations (measured by only one set of analyzers) which are caused by switching between different intake lines of considerable length and by chemical reactions inside corresponding tubing (see Sect. 3.1.1). The tubing residence time for the 36.5 m long tubes of the field experiment was  $\leq 4.1$  s under ambient temperature and pressure conditions, calculated from sample flow ( $1.42 - 1.67 \text{ m}^3 \text{ s}^{-1}$  or  $8.5 - 10 \text{ L min}^{-1}$ ), the length of the tubes and the tubes' inner diameter (0.00435 m). Since a considerable high flow through the intake filters and the long, thin tubes caused a distinct pressure drop (approx. 490 hPa), the actual residence time was consequently shorter (1.9 s). The characteristic chemical time scale ( $\tau_{chem}$ ; e-fold time) for the  $\text{NO} + \text{O}_3$  reaction (see (R1)) was within  $20 < \tau_{chem} < 120$  s during the entire field experiment. Since  $\tau_{chem}$  was always much longer than the tubing's residence time, any effects of the  $\text{NO} + \text{O}_3$  reaction on measured concentrations could be neglected (as well as for the  $\text{NO}_2 + h\nu$  reaction (R2), since opaque tubes have been used). However, the flow rate between the valve block (see Figure 10) and the analyzers is about 1/10 of the tubing purge flow; therefore, the “response time” of the entire system for a sudden change of concentrations was tested. Results are shown in Figure 13 for  $\text{NO}_2$  (step change from 41 to  $861 \text{ nmol m}^{-3}$ ). Immediately after switching some typical pressure effects (valves) could be observed, but a temporally stable concentration was reached after 90 s. For the return switch a quite similar effect were observed and “response times” of  $\text{NO}$ ,  $\text{O}_3$ ,  $\text{CO}_2$  and  $\text{H}_2\text{O}$  were comparable (data not shown). Based on these tests, the first 90 s of each concentration measurement were skipped from further data processing.

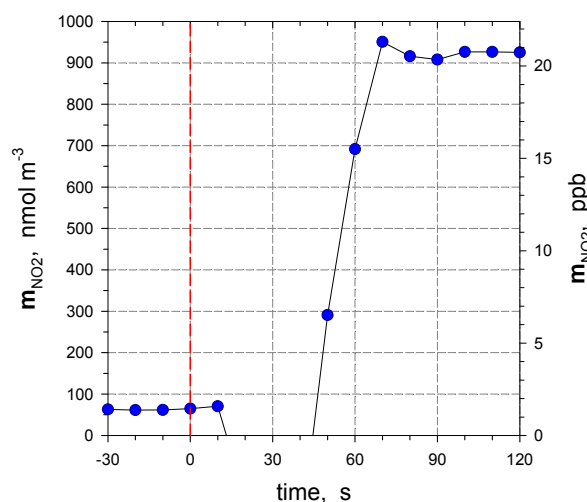


**Figure 13:** Response test for step changes between two different  $\text{NO}_2$  concentrations ( $m_{\text{NO}_2}$ ). The red dashed line marks the switching point.

### 3.2.2 NO<sub>2</sub> blending for fumigation experiment

For laboratory NO<sub>2</sub> fumigation experiments very low (ppb- and sub-ppb levels) and temporally stable NO<sub>2</sub> concentrations have to be made available. That is essentially necessary to significantly identify any NO<sub>2</sub> compensation point whose concentrations are expected at these low concentration levels. Blended NO<sub>2</sub> concentrations ( $m_{blend,NO_2}$ ) of 13.4, 26.8, 44.6, 80.3 and 151.7 nmol m<sup>-3</sup> (0.3, 0.6, 1.0, 1.8, 3.4 ppb) were provided by diluting an NO<sub>2</sub> standard into purified air (see Sect. 2.5.3). A typical course of these concentrations are shown in Figure 14, where the vertical dashed lines indicate times where blending was changed to obtain the next NO<sub>2</sub> concentration. A stable course of the new NO<sub>2</sub> concentration level was reached after max. 60 min. Fluctuation of the blended NO<sub>2</sub> concentration was between 8.0 and 16.1 nmol m<sup>-3</sup> (0.18 - 0.36 ppb). These fluctuations do not depend on the analyzers' temperature (see Sect. 3.2.1). During laboratory measurements, the temperature variation of the instrument was only ±0.5 °C, which would be equivalent to a change of  $m_{blend,NO_2} = 44.6$  nmol m<sup>-3</sup> (1 ppb) of less than 1 %. The measured fluctuations could be also due to the precision of  $m_{blend,NO_2}$  which depends on the precision of the applied mass flow controllers. According to the manufacturer, the precision of the mass flow controllers is ±0.8 % of full scale. Using this information, the precision of  $m_{blend,NO_2}$  has been calculated through Eqs. (17.1) and (17.2) and is also shown in Figure 12. Uncertainty of the mass flow controllers may have added < 20 % to the observed variation of measured the blended NO<sub>2</sub> concentration.

### 3.2.3 Characterization of the dynamic plant chamber

#### 3.2.3.1 Radiation and NO<sub>2</sub> photolysis rate

Transmissivity of PAR through the chamber walls (FEP film) is one of the fundamental requirements that the plant will be not affected by the chamber itself. Moreover, the calculation of the exchange flux density  $F_{ex,i}$  (see Eqs. (8.1) - (8.3)) has to consider the NO<sub>2</sub> +  $h\nu$  reaction. For this, the photolysis rate  $j(NO_2)$  inside the chamber volume has to be known. Therefore the transmissivity was controlled by simultaneous measurements inside and outside the chamber. While PAR was 10 % lower inside the chamber than outside,  $j(NO_2)$  was 30 % lower inside the chamber (Figure 15).

Therefore, 70 % of ambient  $j(NO_2)$  was used for the calculations of  $F_{ex,i}$ ,  $v_{dep,i}$ ,  $m_{comp,i}$  and their standard errors.

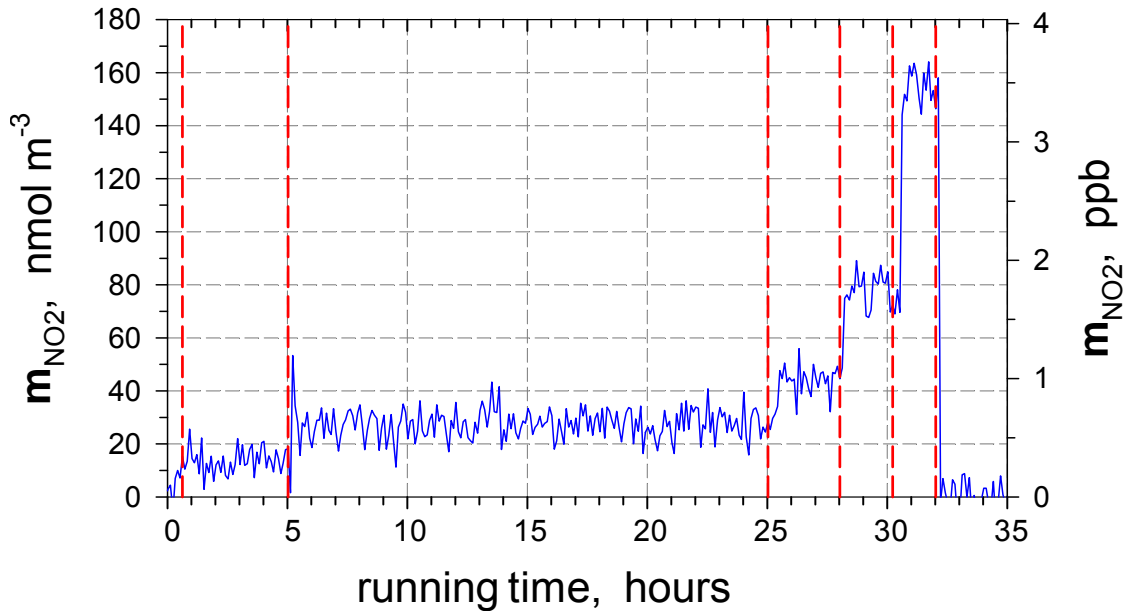


**Figure 14:** Temporal course of blended  $NO_2$  concentrations (12.3, 24.6, 41.0, 73.8 and 139.4  $nmol\ m^{-3}$  (0.3, 0.6, 1.0, 1.8, 3.4 ppb)) used for fumigation of young spruce trees during the laboratory experiments.  $NO_2$  concentrations were provided by diluting a  $NO_2$  standard into purified air. Red dashed lines indicate times where blending was changed to obtain the next  $NO_2$  concentration.

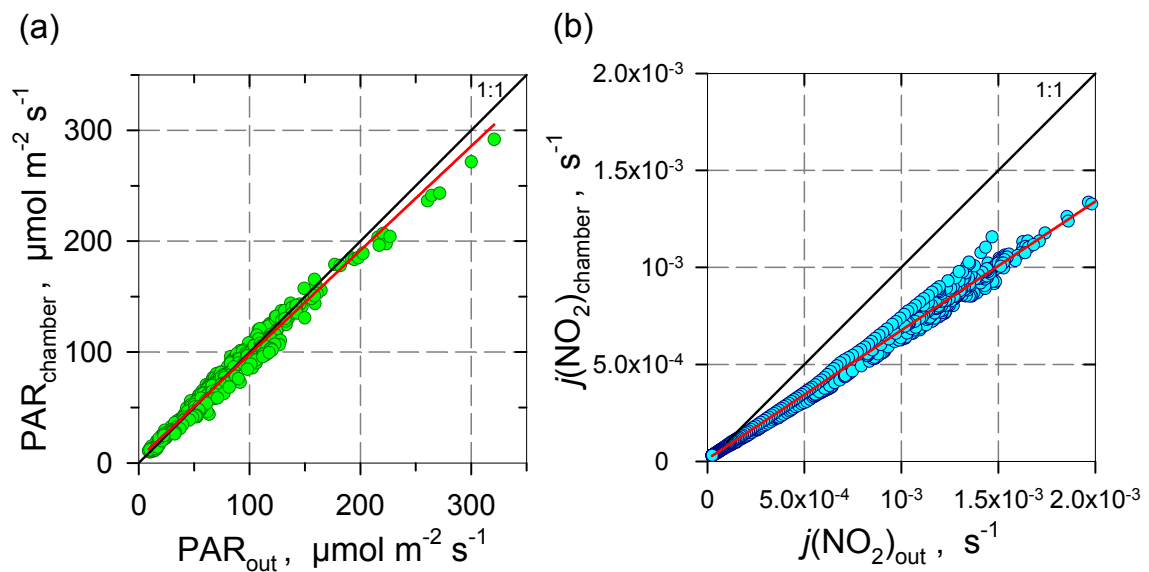


**Figure 15:** Simultaneous measurements of radiation in and outside a chamber. **(a)** Photosynthetically active radiation  $PAR$  (slope = 0.94,  $R^2 = 0.98$ ,  $n = 456$ ), **(b)** photolysis rate  $j_{NO_2}$  (slope = 0.66,  $R^2 = 0.99$ ,  $n = 1440$ ). The black line indicates the 1:1 line and the red line represents the linear fit on the data points.

### 3.2.3.2 Sorption effects and chamber volume exchange time

An empty dynamic chamber has been exposed to various concentrations of NO<sub>2</sub>, NO and O<sub>3</sub> concentrations and “blank flux densities” have determined according to Eq. (8.4). “Blank flux densities” for NO, NO<sub>2</sub> and O<sub>3</sub> are listed in Table 11. They were always negative (i.e. no desorption from the chamber’s inner surfaces) and revealed very low values. Expressed in corresponding “wall deposition velocities”  $-2.12 \times 10^{-3}$  (NO),  $-2.92 \times 10^{-3}$  (NO<sub>2</sub>) and  $-1.94 \times 10^{-3}$  mm s<sup>-1</sup> (O<sub>3</sub>) were found. These values were two orders of magnitude lower than  $v_{dep,i}$  observed under laboratory as well as under field conditions. Comparing incoming and outgoing concentrations of the NO-NO<sub>2</sub>-O<sub>3</sub> triad, a maximum of 2 % of the trace gases might have been absorbed by the inner surfaces of the plant chamber. Therefore, with regard to the mass balance of the dynamic plant chamber, neglecting of any mass fluxes to the walls of the chamber ( $\partial M_{wall,i}/\partial t$  see Sect. 2.1.1) is certainly justified.

**Table 11:** Parameters of sorption effects to the inner chamber walls determined by laboratory experiments.  $q_{10}$  and  $q_{90}$  denote the 10 % and 90 % quantiles of the entire blank flux density  $F_{wall,i}$  data, concentration ranges represent applied fumigation concentrations during the experiment,  $\Delta c_{mean}$  denotes the mean concentration difference of incoming and outgoing chamber air in % (range of differences in %).

| gas             | $F_{wall,i}$ , pmol m <sup>-2</sup> s <sup>-1</sup> |                      | $v_{dep\_wall,i}$ , m s <sup>-1</sup> | concentrations |                   |
|-----------------|---|----------------------|---------------------------------------|----------------|-------------------|
|                 | mean ( $\pm\sigma$ )                                | $q_{10}\dots q_{90}$ |                                       | range, ppb     | $\Delta c_{mean}$ |
| NO              | -4.47 ( $\pm 3.52$ )                                | -7.95...-1.13        | $-2.12 \times 10^{-6}$                | 10 - 62        | 0.8 % (0.3 - 1.6) |
| NO <sub>2</sub> | -4.43 ( $\pm 3.11$ )                                | -9.11...-1.51        | $-2.92 \times 10^{-6}$                | 6 - 47         | 1.8 % (0.4 - 3.4) |
| O <sub>3</sub>  | -4.88 ( $\pm 2.47$ )                                | -7.05...-2.05        | $-1.94 \times 10^{-6}$                | 7 - 45         | 1.6 % (0.5 - 3.7) |

The chamber volume exchange time was determined from an experiment, where a short pulse of (chemically inert) helium (He) has been added to the purging flow of the dynamic chamber (see Sect. 3.1.4). Results are shown in Figure 16. For the time of complete exchange (i.e., a constant level of He is observed), we used the time interval to reach 98 % of the final He concentration ( $t_{98}$ ). Due to the limited temporal resolution of the He detector (5 s),  $t_{98}$  might have been between 80 and 85 s. This result was nearly identical to the time calculated from chamber volume ( $V = 79$  L) and purging rate ( $Q = 60$  L min<sup>-1</sup>), which equals 79 s.

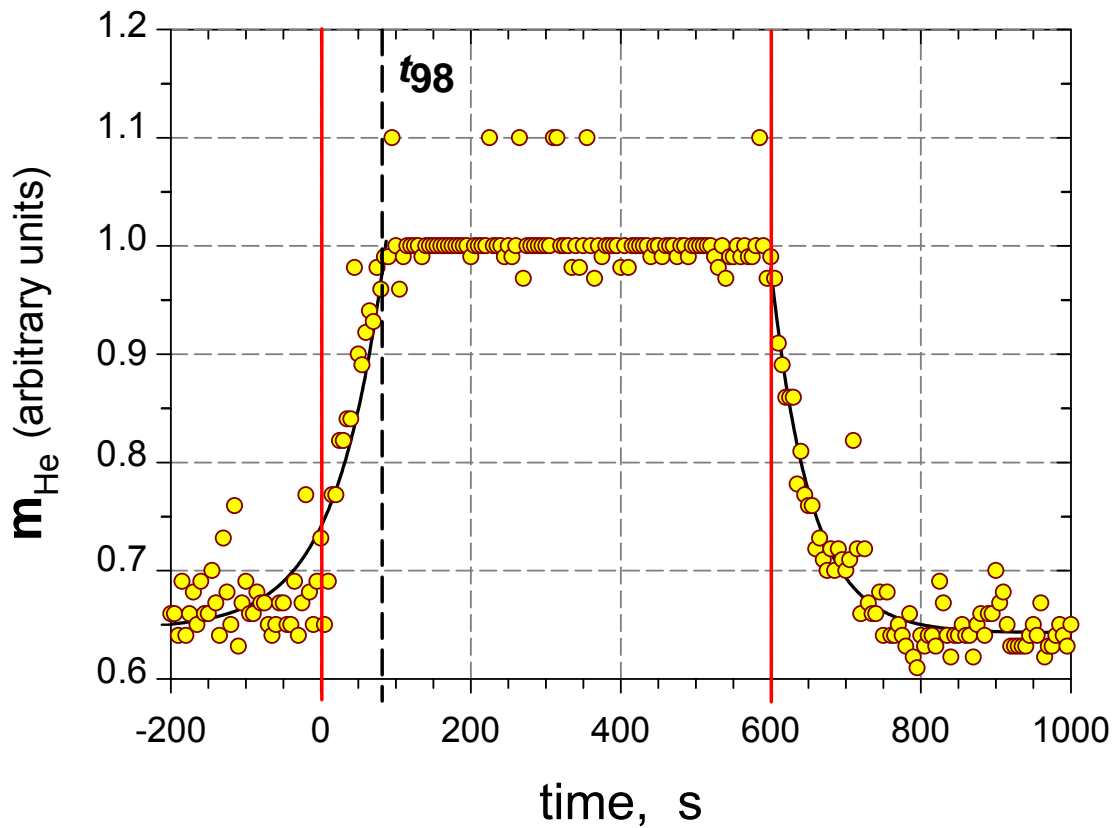


**Figure 16:** Results of the response time test with helium. The chamber ( $V = 0.079 \text{ m}^3$ ) was operated with purging air flow rate  $Q = 60 \text{ L min}^{-1}$ . The red lines represent start and end of the helium addition, the black dashed line marks the end of equilibration. For the approximation of a complete exchange we used the time interval for 98 % approximation ( $t_{98}$ ).

### 3.2.4 Demonstration of exchange flux density measurements

#### 3.2.4.1 $\text{NO}_2$ exchange flux density: Laboratory results

Here, we confine ourselves to the results of “daytime” experiments, i.e. fumigation of the 3- to 4-yr old Norway Spruce trees with  $13 < m_{a,\text{NO}_2} < 152 \text{ nmol m}^{-3}$  (0.3 - 3.4 ppb), controlled temperature (25 °C), relative humidity (60 %) and PAR ( $450 \text{ } \mu\text{mol photons m}^{-2} \text{ s}^{-1}$ , for 12 h) conditions. During experiment no significant difference of  $m_{\text{O}_3}$  or  $m_{\text{NO}}$  between reference and plant chamber could be detected, also the amount of  $j(\text{NO}_2)$  inside the chamber was negligible with respect to any measurable effects due to reaction (R2). As shown in Sect. 3.2.1, the performance of the  $\text{NO}_2$  analyzer was definitely sub-optimal ( $\text{LOD}(m_{\text{NO}_2}) = 1.04 \text{ ppb}$ ;  $3\sigma$ -definition). Therefore,



we based our evaluations of  $F_{ex,NO_2}$ ,  $v_{dep,NO_2}$  and  $m_{comp,NO_2}$  on a  $2\sigma$   $NO_2$  detection limit ( $28.5 \text{ nmol m}^{-3}$  or  $0.6 \text{ ppb}$ ) for the observed concentrations ( $m_{a,NO_2}$ ,  $m_{s,NO_2}$ ). A total of 51 pairs of  $m_{a,NO_2}$  and  $m_{s,NO_2}$  have been obtained during the fumigation experiments. 17 data pairs passed the  $LOD(m_{NO_2})$  criterion, where another three of them had to be rejected due to the significance criterion for  $\Delta m_{NO_2} = (m_{a,NO_2} - m_{s,NO_2})$ . Fourteen data pairs of  $m_{a,NO_2}$  and  $m_{s,NO_2}$  have been subjected to a bi-variate weighted regression analysis (see Sect. 3.1.6), which resulted in  $R^2 = 0.9706$ ,  $n_I = 1.7 \pm 2.63 \text{ nmol m}^{-3}$ ,  $m_I = 0.71 \pm 0.035$ ,  $v_{dep,NO_2} = 0.22 \pm 0.013 \text{ mm s}^{-1}$  and  $m_{comp,NO_2} = 5.9 \pm 9.13 \text{ nmol m}^{-3}$ . The significance probability of  $m_{comp,NO_2} \neq 0$  is 96.87 % (“likely”).  $NO_2$  exchange flux densities ( $F_{ex,NO_2}$ ) and their standard errors have been calculated according to Eq. (11) and are shown in Figure 17. Figure 17a displays results of  $F_{ex,NO_2}$  where the  $2\sigma$ - $LOD(m_{NO_2})$ -definition, Figure 17b where the  $1\sigma$ - $LOD(m_{NO_2})$ -definition has been applied. Furthermore, in both panels  $F_{ex,NO_2}$  data were separated for the significance of  $\Delta m_{NO_2}$  (significant: blue circles, non-significant: reddish diamonds); the  $(F_{ex,NO_2}; m_{s,NO_2})$ -regression lines have been calculated according to Eq. (8.1.1) for all  $F_{ex,NO_2}$  data (pink line) and for those  $F_{ex,NO_2}$  data, where  $\Delta m_{NO_2}$  is significant (blue line). Corresponding  $NO_2$  compensation point concentrations  $m_{comp,NO_2}$  were calculated according Eq.(8.3.1) and are represented by red filled circles (significant  $\Delta m_{NO_2}$ ) and pink hollow circles (all data). Details of statistical evaluation are listed in Table 12. The most striking result is, that (regardless of which linear least-square fitting algorithm and which  $LOD(m_{NO_2})$ -definition is applied) the values of  $m_{comp,NO_2}$  are always highly significant, if all  $F_{ex,NO_2}$  data were used. Applying the simple linear least-square fitting algorithm (without considering  $s_{m_a,NO_2}$  nor  $s_{m_s,NO_2}$ )  $m_{comp,NO_2}$  remains highly significant, even if only those  $F_{ex,NO_2}$  data are considered where  $\Delta m_{NO_2}$  is significant. However, applying linear least-square fitting algorithms which consider either  $s_{m_s,NO_2}$  or  $s_{m_a,NO_2}$  and  $s_{m_s,NO_2}$ , the existence of  $m_{comp,NO_2}$  becomes “unlikely” (“likely”). With the exception of applying the  $2\sigma$   $NO_2$  detection limit to all  $F_{ex,NO_2}$  data, the impact of different statistical treatments on the evaluation of  $NO_2$  deposition velocities is small ( $0.19 \leq v_{dep,NO_2} \leq 0.22 \text{ mm s}^{-1}$ ).

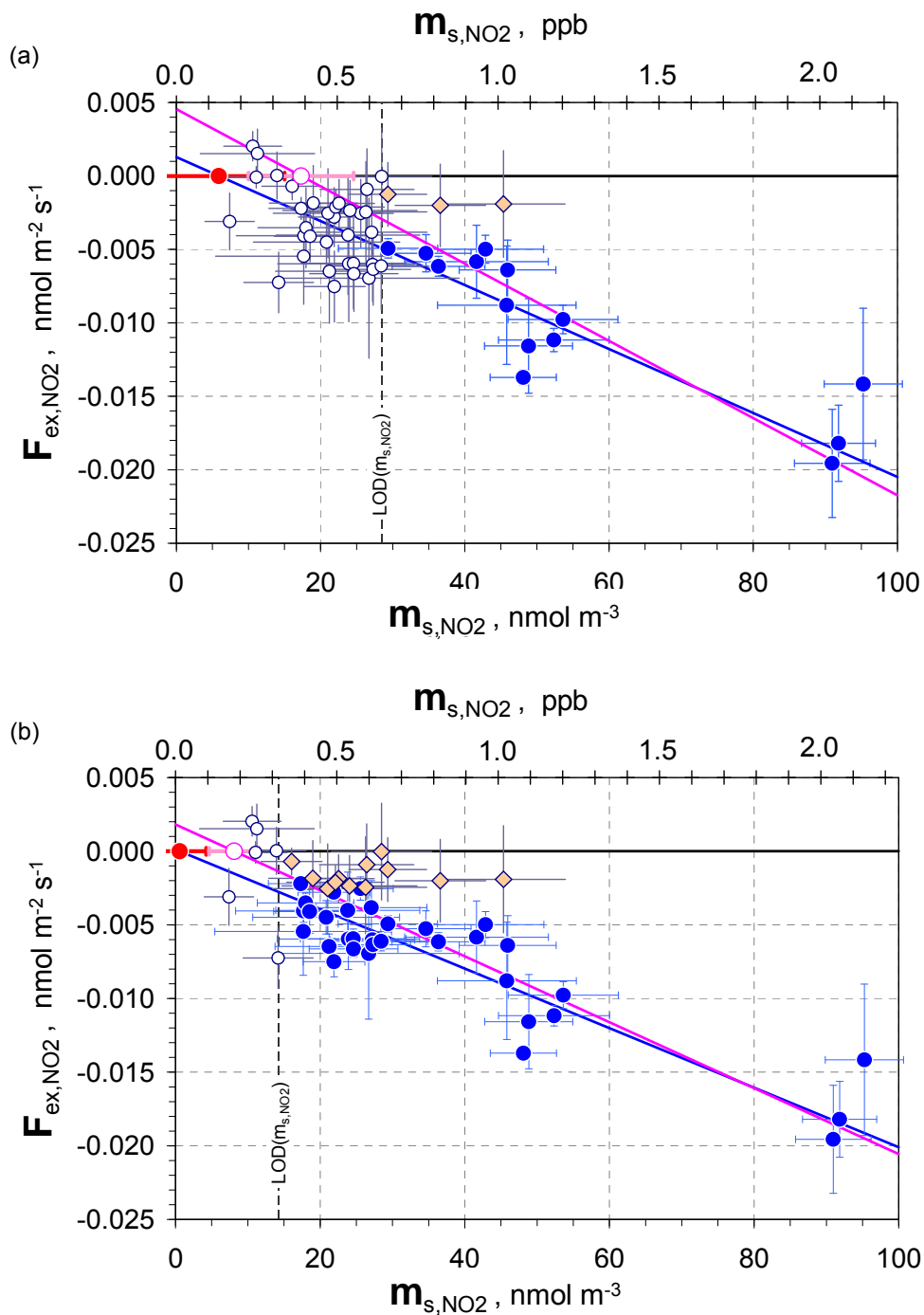


**Figure 17:** Laboratory NO<sub>2</sub> fumigation of 3 - 4yr old Norway Spruce trees (*Picea abies* L.) under controlled conditions (25 °C, 60 %, 450  $\mu\text{mol photons m}^{-2} \text{s}^{-1}$ ): NO<sub>2</sub> exchange flux density ( $F_{ex,NO_2}$ ) vs. NO<sub>2</sub> concentration measured at the outlet of the dynamic plant chamber ( $m_{s,NO_2}$ ) for application of  $2\sigma$ -LOD( $m_{s,NO_2}$ )-definition ((a) panel) and  $1\sigma$ -LOD( $m_{s,NO_2}$ )-definition ((b) panel).  $F_{ex,NO_2}$  data were calculated according Eq. (8.4), their standard errors according to Eq. (19). Blue circles identify  $F_{ex,NO_2}$  where  $m_{s,NO_2} > LOD(m_{s,NO_2})$ , white circles stand for  $F_{ex,NO_2}$  where  $m_{s,NO_2} \leq LOD(m_{s,NO_2})$  and reddish diamonds for those  $F_{ex,NO_2}$  data, which have to be rejected for non-significance of  $\Delta m_{NO_2} = (m_{a,NO_2} - m_{s,NO_2})$ . Blue line (considering blue circle data) and pink line (considering blue circle and reddish diamond data) are calculated according to Eq. (15.1.1). NO<sub>2</sub> compensation point concentration  $m_{comp,NO_2}$  is calculated according to Eq. (15.3.1) and is represented by red filled circles (considering blue circle data) and pink hollow circles (considering blue circle and reddish diamond data). More details of statistical evaluation are listed in Table 12.

**Table 12:** Parameters for NO<sub>2</sub> laboratory measurements of simple (no errors considered), simple (standard error of  $m_{s,NO_2}$  considered) and bi-variate weighted (standard error of  $m_{s,NO_2}$  and  $m_{a,NO_2}$  considered) linear least-squares fitting regression analysis. Data were separated for all data of  $\Delta m_{NO_2}$  ( $m_{a,NO_2} - m_{s,NO_2}$ ) and the significance of  $\Delta m_{NO_2}$ .  $2\sigma$ ,  $1\sigma$  and no NO<sub>2</sub> detection limit was applied to the data.

| $LOD(m_{NO_2})$<br>definition                                   | statistical<br>quantity       | unit                 | all ( $m_{a,NO_2} - m_{s,NO_2}$ ) data<br>linear least-squares fitting algorithm |  |  | only significant ( $m_{a,NO_2} - m_{s,NO_2}$ ) data<br>linear least-squares fitting algorithm |  |  |
|---|-------------------------------|----------------------|--|--|--|---|--|--|
|   |                               |                      | simple,<br>no errors<br>considered   | simple,<br>only $S_{m,s,NO_2}$<br>considered | bi-variate &<br>weighted,<br>$S_{m,a,NO_2}$ & $S_{m,s,NO_2}$<br>considered | simple,<br>no errors<br>considered  | simple,<br>only $S_{m,s,NO_2}$<br>considered | bi-variate &<br>weighted,<br>$S_{m,a,NO_2}$ & $S_{m,s,NO_2}$<br>considered |
| $LOD(m_{NO_2})$<br>$2 \times \sigma_{m_{NO_2},0}$<br>definition | $N$                           | [1]                  | 17   | 17   | 17   | 14  | 14   | 14   |
|   | $R^2(m_{a,NO_2}, m_{s,NO_2})$ | [1]                  | 0.9692   | 0.9716                                       | 0.9610   | 0.9794  | 0.9778                                       | 0.9706   |
|   | $m_{comp,NO_2}$               | nmol m <sup>-3</sup> | 16.5 ± 1.81  | 14.2 ± 12.15                                 | 17.3 ± 7.29  | 6.8 ± 2.22  | 2.2 ± 16.76                                  | 5.9 ± 9.13   |
|   | $m_{comp,NO_2} \neq 0?$       | %                    | 99.99 (HS)   | 99.99 (HS)                                   | 99.99 (HS)   | 99.99 (HS)  | 37.1 (UL)                                    | 96.6 (L)   |
|   | $v_{dep,NO_2}$                | mm s <sup>-1</sup>   | 0.27 ± 0.007   | 0.24 ± 0.016                                 | 0.26 ± 0.014   | 0.21 ± 0.006  | 0.20 ± 0.015                                 | 0.22 ± 0.013   |
| $LOD(m_{NO_2})$<br>$1 \times \sigma_{m_{NO_2},0}$<br>definition | $N$                           | [1]                  | 45   | 45   | 45   | 33  | 33   | 33   |
|   | $R^2(m_{a,NO_2}, m_{s,NO_2})$ | [1]                  | 0.9695   | 0.9754                                       | 0.9605   | 0.9847  | 0.9851                                       | 0.9782   |
|   | $m_{comp,NO_2}$               | nmol m <sup>-3</sup> | 6.8 ± 0.52   | 7.3 ± 5.95                                   | 8.1 ± 3.46   | -1.8 ± 0.63   | -0.7 ± 7.82                                  | 0.6 ± 3.67   |
|   | $m_{comp,NO_2} \neq 0?$       | %                    | 99.99 (HS)   | 99.99 (HS)                                   | 99.99 (HS)   | 99.99 (HS)  | 39.5 (UL)                                    | 61.8 (UL)  |
|   | $v_{dep,NO_2}$                | mm s <sup>-1</sup>   | 0.21 ± 0.004   | 0.22 ± 0.012                                 | 0.22 ± 0.010   | 0.19 ± 0.003  | 0.20 ± 0.012                                 | 0.20 ± 0.009   |
| $LOD(m_{NO_2})$<br>not<br>considered                            | $N$                           | [1]                  | 51   | 51   | 51   | 36  | 36   | 36   |
|   | $R^2(m_{a,NO_2}, m_{s,NO_2})$ | [1]                  | 0.9682   | 0.9728                                       | 0.9575   | 0.9819  | 0.9815                                       | 0.9719   |
|   | $m_{comp,NO_2}$               | nmol m <sup>-3</sup> | 7.1 ± 0.44   | 6.8 ± 4.72                                   | 7.6 ± 3.07   | -1.6 ± 0.60   | -0.4 ± 6.22                                  | 0.5 ± 3.67   |
|   | $m_{comp,NO_2} \neq 0?$       | %                    | 99.99 (HS)   | 99.99 (HS)                                   | 99.99 (HS)   | 99.99 (HS)  | 27.6 (UL)                                    | 60.4 (UL)  |
|   | $v_{dep,NO_2}$                | mm s <sup>-1</sup>   | 0.22 ± 0.004   | 0.22 ± 0.012                                 | 0.22 ± 0.010   | 0.19 ± 0.003  | 0.20 ± 0.011                                 | 0.20 ± 0.010   |

### 3.2.4.2 NO-NO<sub>2</sub>-O<sub>3</sub> exchange flux densities: Field results

In Figure 18, typical time series of trace gas mixing ratios are shown, measured at two different spruce branches during the EGER field campaign. The observed mixing ratio changes were due to switching between the different intakes. After switching, concentration changes showed the delay effects mentioned above (see Sect. 3.2.1). Due to this, the first 90 s after valve switching were skipped from subsequent data processing (these first 90 s interval indicated as grey shaded vertical bars in Figure 18). Values for CO<sub>2</sub> and H<sub>2</sub>O were measured as the difference between empty chamber and each switched intake. The temporal variation of CO<sub>2</sub> and H<sub>2</sub>O concentrations of the plant chambers versus ambient air or empty chamber represented the physiological activity of the plants, since the CO<sub>2</sub> exchange flux density represents the photosynthetic CO<sub>2</sub> assimilation and the H<sub>2</sub>O flux density the transpiration of the enclosed plant parts.

During the field experiment nearly 3000 pairs of  $m_{a,i}$  and  $m_{s,i}$  have been obtained. Applying the  $LOD(m_i)$  ( $3\sigma$ -definition) and the significance criterion for  $\Delta m_i = (m_{a,i} - m_{s,i})$ , around 60 % of the NO<sub>2</sub> data pairs remained. In Table 13 the details of the data pairs selection for both trees are listed for NO, NO<sub>2</sub> and O<sub>3</sub>. Classification according to measurements during day and night demonstrated, that during night less data pairs were distinguishable from each other, especially those of NO. Between the spruce branches in both sampling chambers no differences were noticeable.

After classification of all individual concentration data into different classes of leaf conductance (approx. identical to different classes of radiation conditions), bi-variate weighted regression analysis between classified pairs of  $m_{a,i}$  and  $m_{s,i}$  was performed (see Sect. 3.1.6). The data pairs were additionally screened for singular concentration peaks of NO, NO<sub>2</sub> and O<sub>3</sub>, which mainly occurred due to advection of automobile exhaust gases from a busy country road (2000 cars/h) in a distance of about 1-2 km from the site. The problem of advection at this field site is well known and has been documented through profile measurements of in- and above canopy concentrations, as well as through eddy covariance flux measurements of NO-NO<sub>2</sub>-O<sub>3</sub> performed simultaneously to our dynamic chamber measurements (PLAKE et al. 2009). For the analysis of dynamic chamber derived O<sub>3</sub> flux densities, we assumed  $m_{comp,O3} = 0$  ( $n_3 = 0$ ), since emissions of O<sub>3</sub> from plants are not known so far.

For the present study, we restrict our results to one spruce branch (chamber 1) and one class with high PAR radiation (mean PAR = 355  $\mu\text{mol photons m}^{-2} \text{s}^{-1}$ ). The analysis for  $\text{NO}_2$  resulted in  $R^2(m_{a,\text{NO}_2}, m_{s,\text{NO}_2}) = 0.9480$ ,  $n_1 = 6.5 \pm 1.59 \text{ nmol m}^{-3}$ ,  $m_1 = 0.79 \pm 0.016$ ,  $v_{\text{dep},\text{NO}_2} = 0.18 \pm 0.034 \text{ mm s}^{-1}$  and  $m_{\text{comp},\text{NO}_2} = -9.5 \pm 14.75 \text{ nmol m}^{-3}$ . The probability of  $m_{\text{comp},\text{NO}_2} \neq 0$  is 99.99 % (“highly significant”); however, a negative  $\text{NO}_2$  compensation point concentration is physically meaningless. For  $\text{O}_3$  the analysis resulted in  $R^2(m_{a,\text{O}_3}, m_{s,\text{O}_3}) = 0.9847$ ,  $m_3 = 0.80 \pm 0.005$  and  $v_{\text{dep},\text{O}_3} = 0.32 \pm 0.018 \text{ mm s}^{-1}$ . In Figure 19a (Figure 20a), results of bi-variate weighted regression analysis between  $m_{a,\text{NO}_2}$  and  $m_{s,\text{NO}_2}$  ( $m_{a,\text{O}_3}$  and  $m_{s,\text{O}_3}$ ) are shown, while in Figure 19b (Figure 20b) those of  $F_{\text{ex},\text{NO}_2}$  ( $F_{\text{ex},\text{O}_3}$ ) versus  $m_{s,\text{NO}_2}$  ( $m_{s,\text{O}_3}$ ). In Figure 19a and b, data can be individually identified for their significance of  $\Delta m_{\text{NO}_2}$  by corresponding color coding. For  $\text{O}_3$ , there is no corresponding color coding, since all  $\Delta m_{\text{O}_3}$  were significant (see Table 13). Linear relationships between  $F_{\text{ex},\text{NO}_2}$  and  $m_{s,\text{NO}_2}$  were calculated by Eq. 12.1 for data pairs owing significant  $\Delta m_{\text{NO}_2}$  and for all data pairs. In Table 14 all results of statistical analysis of  $F_{\text{ex},\text{NO}_2}$  and  $F_{\text{ex},\text{O}_3}$  data are listed. Results of bi-variate weighted regression analysis for NO are shown in Figure 21. A large part of  $m_{\text{NO}}$  was lower than  $\text{LOD}(m_{\text{NO}})$  (grey diamonds) or corresponding data pairs were non-significant with respect to  $\Delta m_{\text{NO}} = (m_{a,\text{NO}} - m_{s,\text{NO}})$  (reddish diamonds). The regression coefficient  $R^2(m_{a,\text{NO}}, m_{s,\text{NO}})$  was only 0.5355. Therefore, consecutive analyses are biased: probabilities of significant  $m_{\text{comp},\text{NO}}$  and  $v_{\text{dep},\text{NO}}$  becomes unlikely (51.7 and 22.4 %, respectively). Hence, there were no further evaluations for  $F_{\text{ex},\text{NO}}$ ,  $v_{\text{dep},\text{NO}}$  and  $m_{\text{comp},\text{NO}}$ .

**Table 13:** Percentage of data  $m_i$  above  $\text{LOD}(m_i)$  ( $3\sigma$ -definition) and significant differences  $\Delta m_i = (m_{a,\text{NO}_2} - m_{s,\text{NO}_2})$  of tree 1 and 2 for field measurements.

|                       | tree 1   |            |              | tree 2   |            |              |
|-----------------------|--|------------|--------------|--|------------|--------------|
|                       | $m_i > \text{LOD} + \text{significant } \Delta m_i \text{ \% of total}$<br>(number of total) |            |              | $m_i > \text{LOD} + \text{significant } \Delta m_i \text{ \% of total}$<br>(number of total) |            |              |
|                       | all (2988)   | day (1885) | night (1103) | all (2993)   | day (1887) | night (1106) |
| <b>NO</b>             | 24   | 33         | 7            | 24   | 33         | 8            |
| <b>NO<sub>2</sub></b> | 57   | 62         | 48           | 67   | 69         | 63           |
| <b>O<sub>3</sub></b>  | 96   | 98         | 93           | 98   | 99         | 97           |

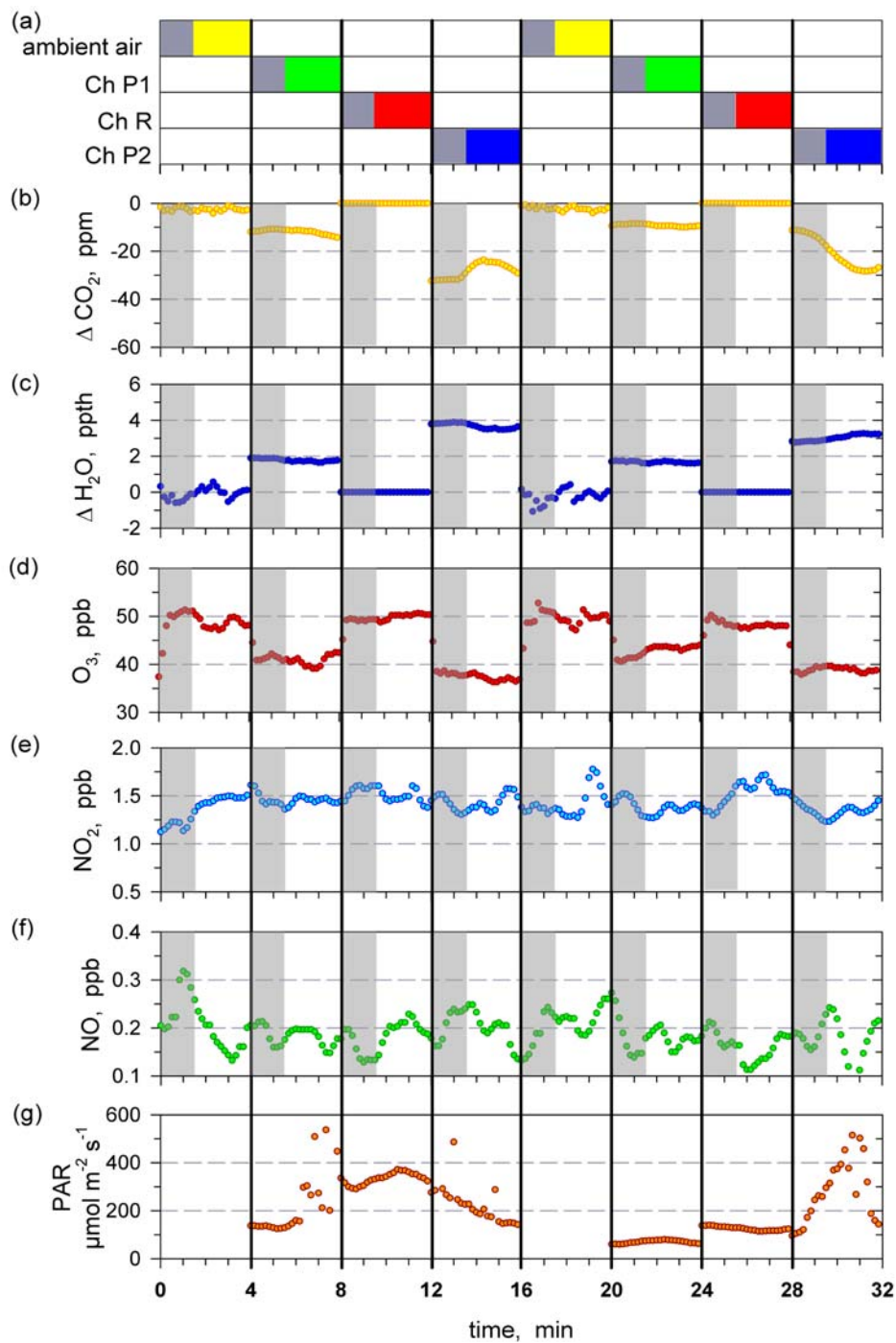


**Figure 18:** Switching scheme and time series of trace gas mixing ratios over two full measurement cycles during EGER field experiment. Data were corrected for calibration factors, temperature dependency and offset of analyzers. **(a)** Control scheme indicating periods of skipped data (first 90 s) for data processing (grey bars), sampling/analysis of ambient air (yellow bars), sampling/analysis of plant chamber 1 (green bars), sampling/analysis of reference chamber (red bars) and sampling/analysis of plant chamber 2 (blue bars). **(b-c)** Time series of  $\text{CO}_2$  and  $\text{H}_2\text{O}$  mixing ratios measured as difference between reference chamber and respectively switched intake. **(d-f)** Time series of  $\text{O}_3$ ,  $\text{NO}_2$  and  $\text{NO}$  mixing ratios. **(g)** Photosynthetic active radiation (PAR).

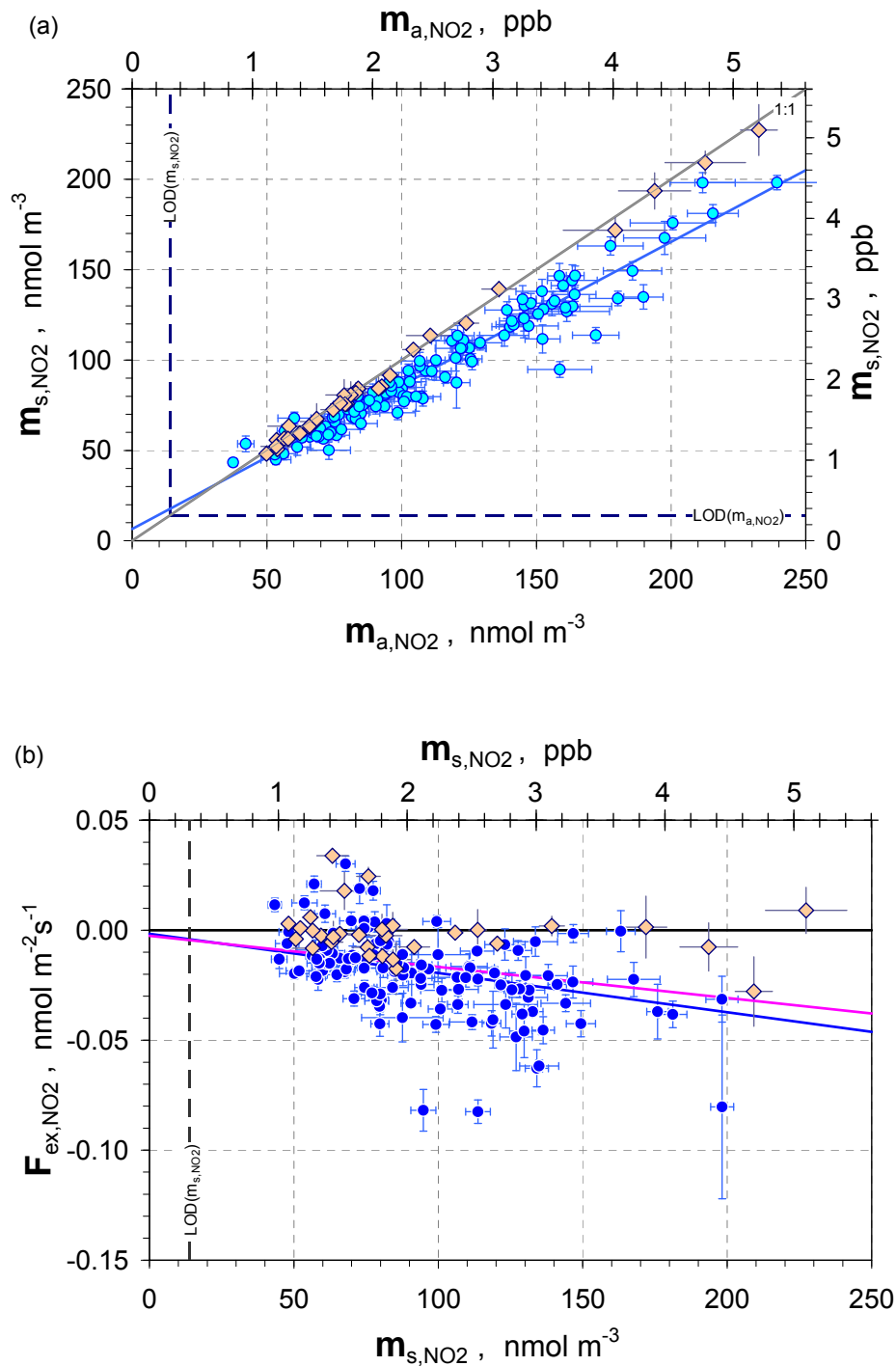


**Figure 19:** Field measurements: **(a)**  $NO_2$  concentration measured at the outlet of the dynamic plant chamber ( $m_{s,NO_2}$ ) vs.  $NO_2$  concentration measured at the inlet of the dynamic plant chamber ( $m_{a,NO_2}$ ). Light blue circles identify data pairs for significance of  $\Delta m_{NO_2} = (m_{a,NO_2} - m_{s,NO_2})$  and reddish diamonds for those data pairs, which have to be rejected for non-significance of  $\Delta m_{NO_2} = (m_{a,NO_2} - m_{s,NO_2})$ . Blue line (considering blue circle data) is calculated according to bi-variate weighted linear least-squares fitting regression analysis (see Sect. 3.1.6). **(b)**  $NO_2$  exchange flux density ( $F_{ex,NO_2}$ ) vs.  $NO_2$  concentration measured at the outlet of the dynamic plant chamber ( $m_{s,NO_2}$ ).  $F_{ex,NO_2}$  data were calculated according Eq. (8.4), their standard errors according to Eq.(19). Reddish diamonds stand for those  $F_{ex,NO_2}$  data, which have to be rejected for non-significance of  $\Delta m_{NO_2} = (m_{a,NO_2} - m_{s,NO_2})$ . Blue line (considering blue circle data) and pink line (considering blue circle and reddish diamond data) are calculated according to Eq. (15.1.1).

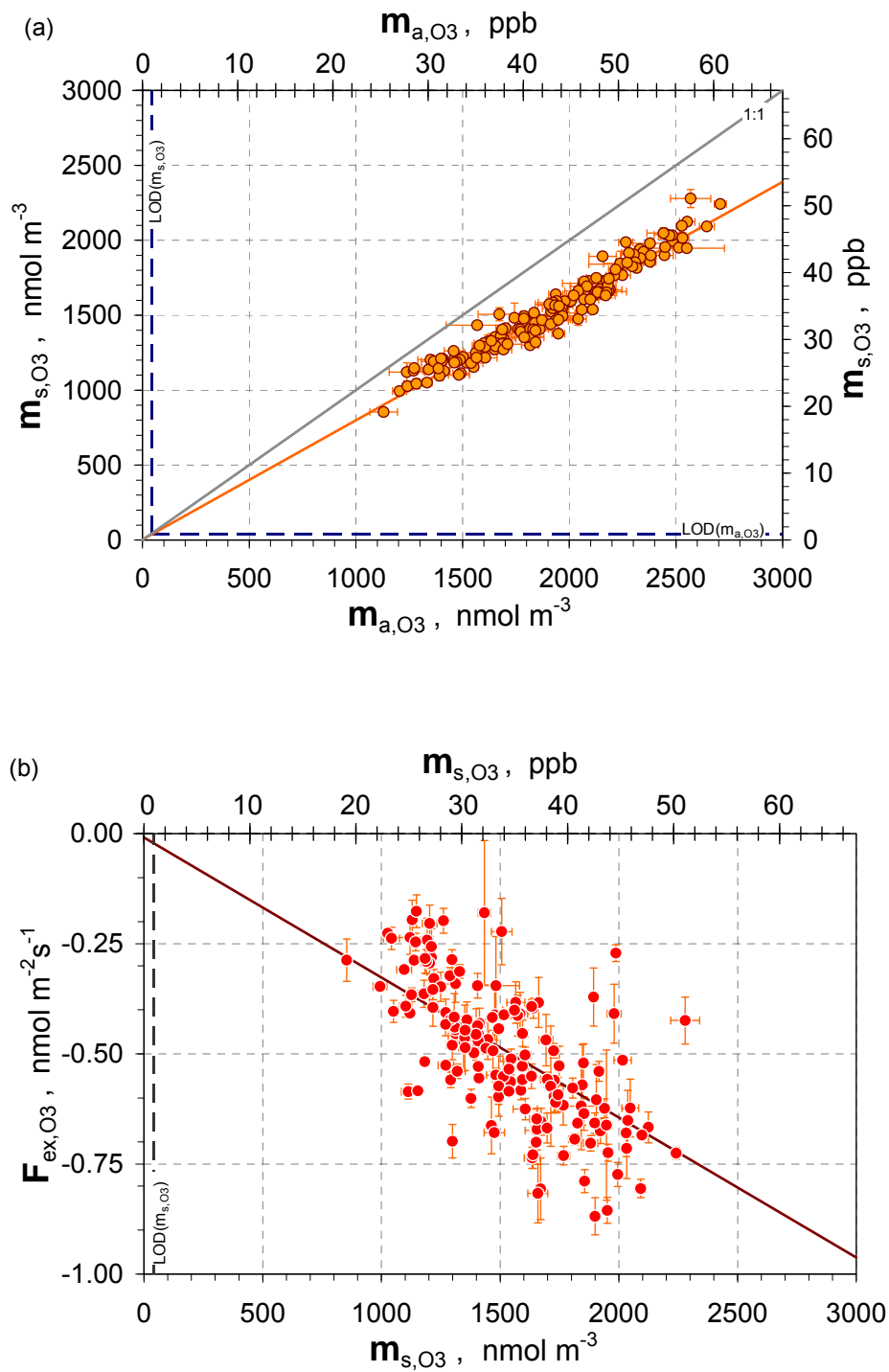


**Figure 20:** Field measurements: **(a)** O<sub>3</sub> concentration measured at the outlet of the dynamic plant chamber ( $m_{s,O_3}$ ) vs. O<sub>3</sub> concentration measured at the inlet of the dynamic plant chamber ( $m_{a,O_3}$ ). Orange circles identify data pairs for significance of  $\Delta m_{O_3} = (m_{a,O_3} - m_{s,O_3})$ . Orange line is calculated according to bi-variate weighted linear least-squares fitting regression analysis (see Sect. 3.1.6). **(b)** O<sub>3</sub> exchange flux density ( $F_{ex,O_3}$ ) vs. O<sub>3</sub> concentration measured at the outlet of the dynamic plant chamber ( $m_{s,O_3}$ ).  $F_{ex,O_3}$  data were calculated according Eq. (8.4), their standard errors according to Eq. (19). Dark red line is calculated according to Eq. (15.1.1).



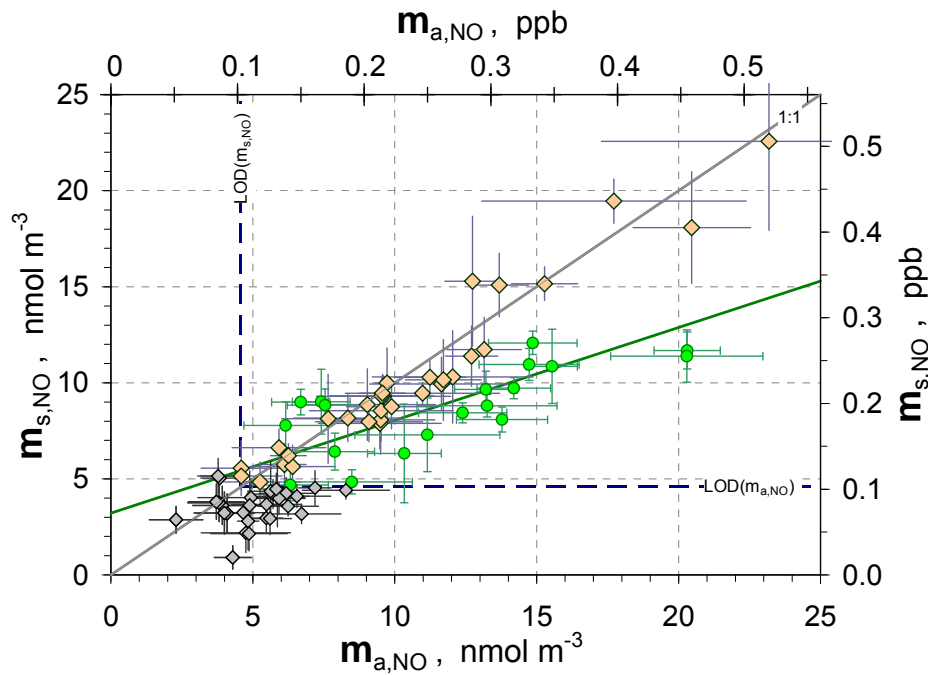


**Figure 21:** Field measurements: NO concentration measured at the outlet of the dynamic plant chamber ( $m_{s,NO}$ ) vs. NO concentration measured at the inlet of the dynamic plant chamber ( $m_{a,NO}$ ). Light green circles identify data pairs for significance of  $\Delta m_{NO} = (m_{a,NO} - m_{s,NO})$ , reddish diamonds stand for those data pairs, which have to be rejected for non-significance of  $\Delta m_{O_3}$  and grey diamonds for data pairs where  $m_{NO} \leq LOD(m_{NO})$ . Green line (considering green circle data) is calculated according to bi-variate weighted linear least-squares fitting regression analysis (see Sect. 3.1.6).

**Table 14:** Parameters of bi-variate weighted linear least-squares fitting regression analysis for field measurements.  $NO_2$  data were separated for all data of  $\Delta m_{NO_2} (m_{a,NO_2} - m_{s,NO_2})$  and the significance of  $\Delta m_{NO_2}$ . Data of  $O_3$  were almost significant for  $\Delta m_{O_3} (m_{a,O_3} - m_{s,O_3})$ .  $3\sigma$  detection limit was applied to the data.

| statistical quantity    | unit           | all                                 | only significant                    | only significant                  |
|-------------------------|----------------|-------------------------------------|-------------------------------------|-----------------------------------|
|                         |                | $(m_{a,NO_2} - m_{s,NO_2})$<br>data | $(m_{a,NO_2} - m_{s,NO_2})$<br>data | $(m_{a,O_3} - m_{s,O_3})$<br>data |
|                         |                | $NO_2$                              | $NO_2$                              | $O_3$                             |
| $N$                     | [1]            | 154                                 | 123                                 | 155                               |
| $R^2(m_{a,i}; m_{s,i})$ | [1]            | 0.9404                              | 0.9480                              | 0.9847                            |
| $m_{comp,i}$            | $nmol\ m^{-3}$ | $-18.2 \pm 17.57$                   | $-9.5 \pm 14.75$                    | 0*                                |
| $m_{comp,i} \neq 0?$    | %              | 99.99 (HS)                          | 99.99 (HS)                          | -                                 |
| $v_{dep,i}$             | $mm\ s^{-1}$   | $0.14 \pm 0.031$                    | $0.18 \pm 0.034$                    | $0.32 \pm 0.018$                  |

\* assumption for  $O_3$ :  $m_{comp,O_3} = 0$ .

### 3.3 Discussion

#### 3.3.1 Overview of previous NO<sub>2</sub> exchange flux measurements using dynamic plant chambers

Table 15 shows a list of past dynamic chamber studies that have focused on NO<sub>2</sub> exchange between different plant species and the atmosphere. Most of these measurements were made with NO<sub>2</sub> converters which were not specific for NO<sub>2</sub> detection. Some authors used heated molybdenum converters (THOENE et al. 1991, 1996; TEKLEMARIAM and SPARKS 2006; RAIVONEN et al. 2009), heated ferrous sulphate converters (RONDÓN et al. 1993, RONDÓN and GRANAT 1994), or a detector based on chemiluminescence on liquid surfaces (HANSON et al. 1989; HEREID and MONSON 2001; SPARKS et al. 2001). All these converters overestimate NO<sub>2</sub> concentrations because of interferences with other (oxidized) nitrogen compounds (see Sect. 2.2). Only the application of photolytic converter guarantees the interference-free determination of particularly (very) low NO<sub>2</sub> concentrations.

During most of the field studies filtered air was used for purging the dynamic chambers. In most cases, this air was free of O<sub>3</sub> and NO<sub>x</sub>, and known NO<sub>2</sub> concentrations were delivered to the dynamic chamber by diluting standard mixtures of NO<sub>2</sub> from a cylinder (GEBLER et al. 2000, 2002; SPARKS et al. 2001; HEREID and MONSON 2001). Some studies additionally controlled the CO<sub>2</sub> and water vapor concentrations of the purging air, the irradiance and temperature conditions inside the chamber (HEREID and MONSON 2001; SPARKS et al. 2001). Filtered and/or synthetic air (i.e. home-made H<sub>2</sub>O and CO<sub>2</sub> concentrations, free of non target reactive trace gases) hardly represents ambient air. Therefore, a potential influence on the physiological behavior of the plant cannot entirely be excluded.

**Table 15:** Overview of studies that have performed dynamic chamber NO<sub>2</sub> flux measurements on different plant species.

| author                     | plant species          | measured gases                       | location     | wall material <sup>1</sup> | purging air <sup>2</sup>  | NO <sub>2</sub> concentration in purging air, ppb | chamber volume, L | NO <sub>2</sub> converter <sup>3</sup> | analyzer                           | LOD <sup>4</sup> , ppb<br>3σ-definition                         |
|----------------------------|------------------------|--------------------------------------|--------------|----------------------------|---|---|-------------------|--|------------------------------------|---|
| Hanson et al. 1989         | deciduous, coniferous  | NO <sub>2</sub>                      | lab          | glass                      | pure air <sup>w</sup> + CO <sub>2</sub> + NO <sub>2</sub>                           | 60 - 70   | 22.7              | Luminol                                | LMA-3, Luminox                     | n.s.  |
| Thoene et al. 1991,1996    | spruce                 | NO <sub>2</sub>                      | lab          | glass                      | zero air <sup>w</sup> + NO <sub>2</sub>   | 1.6 - 125   | 3                 | Mo                                     | Thermo Electron, 14B/E             | NO <sub>2</sub> : 1.0*  |
| Neubert et al. 1993        | sunflower, tobacco     | NO, NO <sub>2</sub> , O <sub>3</sub> | lab          | PTFE                       | zero air <sup>w</sup> + NO/NO <sub>2</sub> /O <sub>3</sub>                          | < 100   | 160               | PLC                                    | Tecan, CLD 770 AL ppt              | NO: 0.02; NO <sub>2</sub> : 0.1*                                |
| Rondón et al. 1993         | pine, spruce           | NO, NO <sub>2</sub> , O <sub>3</sub> | field        | FEP                        | ambient air, O <sub>3</sub> free + NO <sub>2</sub><br>ambient air + NO <sub>2</sub> | 0.25 - 120  | 10                | FeSO <sub>4</sub><br>Mo                | Teco, 14D<br>Tecan, CLD 770 AL ppt | NO: 0.3*<br>NO: 0.06*   |
| Rondón & Granat 1994       | pine, spruce           | NO, NO <sub>2</sub> , O <sub>3</sub> | lab          | FEP                        | zero air <sup>w</sup> + CO <sub>2</sub> + NO <sub>2</sub> +O <sub>3</sub>           | 0.2 - 25  | 12.6              | FeSO <sub>4</sub> /PLC                 | Tecan, CLD 770 AL ppt              | NO: 0.075; NO <sub>2</sub> : 0.3                                |
| Weber & Rennenberg 1996a,b | wheat                  | NO, NO <sub>2</sub>                  | lab          | PMMA                       | zero air <sup>w</sup> + NO <sub>2</sub>   | 0 - 90  | 18-124            | PLC                                    | Tecan, CLD 770 AL ppt              | NO: 0.075**   |
| Geßler et al. 2000, 2002   | beech, spruce          | NO <sub>2</sub> , NH <sub>3</sub>    | field, lab   | BG                         | zero air <sup>w</sup> + NO <sub>2</sub> /NH <sub>3</sub>                            | 0.2 - 37  | 3                 | PLC                                    | Tecan, CLD 770 AL ppt              | NO <sub>2</sub> : < 0.1*  |
| Sparks et al. 2001         | tropical trees         | NO <sub>2</sub>                      | field        | n.s. (L)                   | pure air <sup>w</sup> + CO <sub>2</sub> + NO <sub>2</sub>                           | 0.1 - 13  | n.s.              | Luminol                                | LMA-3, Luminox                     | NO <sub>2</sub> : 0.005*  |
| Hereid & Monson 2001       | corn                   | NO, NO <sub>2</sub>                  | field        | n.s. (L)                   | pure air <sup>w</sup> + CO <sub>2</sub> +NO/NO <sub>2</sub>                         | 0.1- >10  | n.s.              | Luminol                                | LMA-3, Luminox                     | NO <sub>2</sub> : 0.005*  |
| Gut et al. 2002            | tropical trees         | NO, NO <sub>2</sub> , O <sub>3</sub> | lab          | FEP                        | ambient air   | 5 - 18  | 75                | PLC                                    | Eco-Physics, CLD 780 TR            | NO: 0.052*  |
| Teklemariam & Sparks 2006  | corn, sunflower, wheat | NO, NO <sub>2</sub>                  | lab          | n.s. (L)                   | pure air <sup>w</sup> + CO <sub>2</sub> +NO/NO <sub>2</sub>                         | 1 - 5   | n.s.              | Mo                                     | TEI 42                             | NO <sub>2</sub> : 0.5*  |
| Raivonen et al. 2009       | Scots pine             | NO, NO <sub>2</sub>                  | field        | FEP, QG                    | ambient air   | < 1   | 1                 | Mo                                     | TEI 42S                            | n.s.  |
| Chaparro-Suarez 2008       | deciduous, coniferous  | NO, NO <sub>2</sub> , O <sub>3</sub> | lab          | FEP                        | zero air <sup>w</sup> + NO <sub>2</sub>   | 0 - 5   | 7.3               | PLC                                    | Eco-Physics, CLD 780 TR            | NO: 0.06  |
| this study                 | spruce                 | NO, NO <sub>2</sub> , O <sub>3</sub> | field<br>lab | FEP                        | ambient air<br>zero air <sup>w</sup> + NO <sub>2</sub>                              | 0.4 - 21<br>0.3 - 4                               | 75<br>60          | BLC                                    | TEI 42C                            | NO: 0.1; NO <sub>2</sub> :0.31<br>NO: 0.2; NO <sub>2</sub> :1.0 |

n.s. = not specified

<sup>1</sup> QG = quartz glass; BG = borosilicate glass; FEP, PFA, PTFE = Teflon materials; PMMA = polymethylmethacrylate (Plexiglas); L = dynamic leaf chamber of gas exchange system Model LI-6400, LiCor, Lincoln, Nebraska, USA

<sup>2</sup> <sup>w</sup> air humidified; pure air = air from a pure air generator; zero air = reactive trace gases removed with filters (NO<sub>x</sub>, NH<sub>3</sub>, H<sub>2</sub>S, SO<sub>2</sub>, O<sub>3</sub>)

<sup>3</sup> Mo = molybdenum converter; PLC = photolytic converter; FeSO<sub>4</sub> = ferrous sulphate converter; BLC = blue light converter

<sup>4</sup> \* LOD definition unknown; \*\* manufacturer's data

For field measurements of the NO-NO<sub>2</sub>-O<sub>3</sub> triad under ambient conditions, fast gas phase reactions inside the chambers have to be considered. Therefore, NO, NO<sub>2</sub> and O<sub>3</sub> concentrations have to be measured simultaneously, even if only one of the trace gases is of interest (PAPE et al. 2009). All previous field studies described corrections of the calculated exchange flux densities not in detail. RONDÓN et al. (1993) specified some corrections for measured NO concentrations only, although O<sub>3</sub> and UV radiation were present in their dynamic chamber. In those cases where measurements of exchange flux densities were performed applying a simultaneously operated empty chamber (as “reference” chamber), corresponding flux densities were calculated from the concentration differences  $\Delta m_{NO_2}$  between the outlet of the plant and empty chambers, respectively. This allowed a certain correction for chamber specific wall absorption and/or desorption processes (GEBLER et al. 2000, 2002; RAIVONEN et al. 2009). However, this procedure may not rule out adverse effects of fast gas-phase reactions on the evaluated flux densities, deposition velocities and compensation point concentrations (see below).

### 3.3.2 Precision, data quality and photochemical reactions

#### 3.3.2.1 Precision and data quality

As shown in Sect. 3.2.1, the precision of NO<sub>2</sub> concentration measurements of our NO<sub>2</sub> analyzer improves from 35 % (at its limits of detection) rapidly to < 10 % at 162 nmol m<sup>-3</sup> (3.63 ppb; laboratory) and 46 nmol m<sup>-3</sup> (1.03 ppb; field). In Sect. 2.1.2 we presented the expected precision of the NO<sub>2</sub> exchange flux density for NO<sub>2</sub> concentrations up to 200 nmol m<sup>-3</sup>, for pre-scribed  $m_{comp,NO_2} = 67$  nmol m<sup>-3</sup> (1.5 ppb), pre-scribed NO<sub>2</sub> deposition velocities (0.3 - 0.6 mm s<sup>-1</sup>) and typical  $R^2(m_{a,NO_2}; m_{s,NO_2})$  ranging from 0.99 to 0.9 (see Figure 8). Since  $F_{ex,NO_2}$  approaches zero at  $m_{s,NO_2} = m_{comp,NO_2}$ , the exchange flux density's precision ( $\sigma_{F_{ex,NO_2}} / F_{ex,NO_2}$ ) will become indefinite there. Consequently, the uncertainty of  $F_{ex,NO_2}$  will become as higher as closer  $m_{s,NO_2}$  approaches  $m_{comp,NO_2}$  (from either side). Analogously to the results shown in Figure 8, we determined which NO<sub>2</sub> concentration difference,  $\pm |m_{s,NO_2} - m_{comp,NO_2}|$ , will be necessary to keep the NO<sub>2</sub> exchange flux density's precision for our NO<sub>2</sub> analyzer under 10 %. For laboratory conditions ( $LOD(m_{NO_2}) = 45$  nmol m<sup>-3</sup> or 1.01 ppb), this difference was  $\pm 13.8$  nmol m<sup>-3</sup> or  $\pm 0.31$  ppb ( $v_{dep,NO_2} = 0.6$  mm s<sup>-1</sup>;  $R^2(m_{a,NO_2}; m_{s,NO_2}) = 0.99$ ) and

$\pm 91 \text{ nmol m}^{-3}$  or  $\pm 2.05 \text{ ppb}$  ( $v_{dep,NO_2} = 0.3 \text{ mm s}^{-1}$ ;  $R^2(m_{a,NO_2}; m_{s,NO_2}) = 0.9$ ). During the EGER field experiment ( $LOD(m_{NO_2}) = 13.8 \text{ nmol m}^{-3}$  or  $0.31 \text{ ppb}$ ) corresponding values were  $\pm 4.5$  and  $\pm 8.5 \text{ nmol m}^{-3}$  ( $0.1$  and  $\pm 0.19 \text{ ppb}$ ), respectively. It is a serious consequence of these calculations, that, for a given detection limit, there is a well defined limit of  $m_{comp,NO_2}$  where the  $NO_2$  compensation point concentration can be inferred from flux density data ( $\sigma_{F_{ex,NO_2}} / F_{ex,NO_2} \leq 10\%$ ) by interpolation of data measured on both sides of  $m_{comp,NO_2}$ . Below that limit, due to the obvious conflict of the requested  $|m_{s,NO_2} - m_{comp,NO_2}|$  and  $LOD(m_{NO_2})$ ,  $m_{comp,NO_2}$  can only be inferred from flux density data at  $m_{s,NO_2} > m_{comp,NO_2}$  by extrapolation, owing the risk of (much) higher uncertainties. These limits were for our  $NO_2$  analyzer  $33.5$  and  $133.8 \text{ nmol m}^{-3}$  ( $0.75$  and  $3.0 \text{ ppb}$ ; laboratory) and  $13.4$  and  $44.6 \text{ nmol m}^{-3}$  ( $0.3$  and  $1.0 \text{ ppb}$ ; field) for the above mentioned combinations of  $v_{dep,NO_2}$  and  $R^2(m_{a,NO_2}; m_{s,NO_2})$ .

In previous studies the  $NO_2$  sensitivity (a proxy for precision) of corresponding  $NO_x$  or  $NO_2$  analyzers has been specified through their detection limit only (see Table 15). NEUBERT et al. (1993) and GEBLER et al. (2000), who used analyzers equipped with photolytic  $NO_2$  converters mentioned a  $LOD(m_{NO_2})$  of  $4.5 \text{ nmol m}^{-3}$  ( $0.1 \text{ ppb}$ ); however, the corresponding definition of LOD ( $1\sigma$ ,  $2\sigma$  or  $3\sigma$  of  $\sigma_{NO_2,0}$ ) is not reported. Based on the manufacturer's data of the analyzers and on our experience, we assume that the reported values correspond to the  $1\sigma$ -definition ( $P = 0.68$ ). This assumption is in agreement with the values of RONDÓN and GRANAT (1994), who have used the same  $NO_2$  analyzer model, namely with  $LOD(m_{NO_2}) = 8.9 \text{ nmol m}^{-3}$  ( $0.2 \text{ ppb}$ ;  $2\sigma$  definition). Using the same LOD-definition ( $2\sigma$ ), RONDÓN and GRANAT (1994) reported a four times lower LOD for  $NO$  of  $2.2 \text{ nmol m}^{-3}$  ( $0.05 \text{ ppb}$ ). WEBER and RENNEBERG (1996a; 1996b) using also a photolytic  $NO_2$  converter, have not reported any specifications about their instrument's sensitivity; therefore, we assumed that, based on the manufacturer's information about the applied  $NO/NO_2$  analyzer, the LOD for  $NO$  was  $33.5 \text{ nmol m}^{-3}$  ( $0.075 \text{ ppb}$ ;  $3\sigma$ -definition). According to RONDÓN and GRANAT (1994), and based on our experience the corresponding LOD for  $NO_2$  can be assumed to have not been better than  $10 \text{ nmol m}^{-3}$  ( $0.225 \text{ ppb}$ ;  $3 \times LOD(m_{NO})$ ). Using the results of our simulation of the minimum detectable  $NO_2$  compensation point concentration (see Sect. 2.1.3), we can state that  $NO_2$  compensation point concentrations  $\geq 44.6 \text{ nmol m}^{-3}$  ( $\geq 1 \text{ ppb}$ ) can be detected with high significance, if  $NO_2$  analyzers with

$LOD(m_{NO_2}) \approx 13.4 \text{ nmol m}^{-3}$  (0.3 ppb) were used (as WEBER and RENNENBERG 1996a and GEBLER et al. 2002) and  $R^2(m_{a,NO_2}, m_{s,NO_2})$  was in a typical range (0.9 - 0.99) of laboratory measurements. Using  $NO_2$  analyzers with  $LOD(m_{NO_2}) \approx 44.6 \text{ nmol m}^{-3}$  ( $\approx 1$  ppb; e.g. analyzers with molybdenum converters) the significant detection of  $m_{comp,NO_2} > 44.6 \text{ nmol m}^{-3}$  (1 ppb) would already be difficult, if the  $v_{dep,NO_2}$  is very small ( $< 0.3 \text{ mm s}^{-1}$ ). For example, THOENE et al. (1996) reported  $m_{comp,NO_2} = 73.1 \text{ nmol m}^{-3}$  (1.64 ppb) which has most likely be detected with high significance, because they reported  $v_{dep,NO_2} = 0.8 \text{ mm s}^{-1}$ . On the other hand, the detection of  $m_{comp,NO_2} = 13.4 - 31.2 \text{ nmol m}^{-3}$  (0.3 - 0.7 ppb; RONDÓN et al. 1993) at  $v_{dep,NO_2} = 0.8 \text{ mm s}^{-1}$  seems now, from a statistical point of view, to be unlikely.

The data quality of exchange flux densities requires the control of quantifiable parameters of the measurement technique. To these belong the results of regular calibrations of the applied analyzers, their detection limits and those parameters which quantify the dependence of the analyzers' signals from other external factors like the ambient temperature. Our studies showed that the temperature dependency of the applied chemiluminescence  $NO/NO_2$  analyzer can not be neglected (0.08 ppb/K). Hence, constant ambient temperature is definitely necessary to operate the analyzers at the requested level of precision. For our laboratory experiments we solved this problem with a commercial thermostat housing the analyzers. During field experiments this may be not always feasible. There, we used an air conditioning system for the entire instruments' shelter (container). Since the still remaining fluctuations of temperature were large enough to affect the precision of the  $NO/NO_2$  analyzer, we corrected the analyzer's signals (see Sect. 3.2.1) It should be stated, that all mentioned previous studies on  $NO_2$  exchange flux densities have even not mentioned this problem.

Laboratory measurements at very low concentrations demand low and stable blended  $NO_2$  concentrations for fumigation of the plants. During our experiments we observed substantial fluctuations of the blended  $NO_2$  concentration which entered the dynamic plant chamber. These fluctuations were due to the blending procedure (and the limited sensitivity of the  $NO/NO_2$  analyzer). As shown in Figure 12 (blue line), the noise of  $NO_2$  concentrations caused by the blending procedure itself will substantially affect the precision of the  $NO_2$  concentration measurements (and consequently those of  $NO_2$  flux density), particularly if the detection limit of future  $NO_2$  analyzers will be improved to be better than  $10 \text{ nmol m}^{-3}$  (0.25 ppb). Then, the improved precision of the

NO<sub>2</sub> concentration measurements will fall short of the noise of the blended NO<sub>2</sub> concentration at the inlet of the dynamic chamber (see Figure 12) and the improvement of the blending procedure (e.g. by application of more precise flow controllers) will become necessary.

### 3.3.2.2 Significance of concentration differences

The error of NO<sub>2</sub> exchange flux density measurements by the dynamic chamber method mainly depends on the error of trace gas concentration differences,  $\Delta m_i$  between the inlet and the outlet of the dynamic plant chamber. In contrast to laboratory conditions, NO<sub>2</sub> concentrations in the field were relative high and rarely conflicted  $LOD(m_{NO_2})$ . However, during field measurements about 30 to 40 % of daytime  $\Delta m_{NO_2}$  data were found to be not significantly different from each other (Table 13) and had to be rejected from further analysis. This rather high percentage of rejected data was mostly due to the temporal variation of ambient NO<sub>2</sub> concentration ( $m_{a,NO_2}$ ) during the 4 min measurement interval, rather than due to the precision or to  $LOD(m_{NO_2})$ . Ambient NO<sub>2</sub> mixing ratio can rapidly change due to the spatially and temporally varying sources within area surrounding the site of measurements (nearby country roads). In our laboratory studies the percentage of non-significant  $\Delta m_{NO_2}$  “daytime” data was 37 % for  $m_{a,NO_2} < 44.6 \text{ nmol m}^{-3}$  (1 ppb) and vanished for  $m_{a,NO_2} \geq 71.4 \text{ nmol m}^{-3}$  (1.6 ppb).

In some of the previous studies means or data sets were compared for significant differences by analysis of variance (e.g. WEBER and RENNENBERG 1996a, 1996b; HEREID and MONSON 2001; SPARKS et al. 2001). However, actual numbers on significant  $\Delta m_{NO_2}$  were not reported. We like to emphasize, that (1) our approach to apply a significance test on the measured concentrations directly is rather novel, and (2) the control of the significance of  $\Delta m_{NO_2}$  is one of the fundamental quality control criteria for highly significant NO<sub>2</sub> exchange flux densities, NO<sub>2</sub> deposition velocities and above all the detection of highly significant NO<sub>2</sub> compensation point concentrations. When using data without significance control of  $\Delta m_{NO_2}$ , NO<sub>2</sub> compensation point concentrations will be overestimated (see below) and therefore be (highly) significant but not true.

### 3.3.2.3 Photo-chemical reactions in the dynamic plant chamber: impact on net exchange flux densities, deposition velocities and compensation point concentrations

In the mentioned previous studies, the impact of photo-chemical reactions was mostly not considered, neither for the calculation of  $v_{dep,NO_2}$  nor for that of  $m_{comp,NO_2}$ . Partly, not all components of the NO-NO<sub>2</sub>-O<sub>3</sub> triad were always measured. Furthermore, most field studies have not used ambient air as purging air. Instead, ambient air was filtered to remove reactive trace gases, particularly O<sub>3</sub> and NO<sub>x</sub>. Afterwards, the desired NO<sub>2</sub> concentration was blended (e.g. GEBLER et al. 2000). Using filtered air, free of NO and O<sub>3</sub>, allows to neglect reaction (R1), but photolysis of NO<sub>2</sub> (R2) will still occur, as soon as appreciable amounts of  $j(NO_2)$  are present in the plant chamber. Consideration of photo-chemical reactions, like the NO<sub>2</sub> loss by reaction (R2) and the formation of NO<sub>2</sub> by reaction (R1) were mentioned by NEUBERT et al. (1993), the production and destruction of NO by RONDÓN et al. (1993).

With the framework of equations developed in Sects. 2.1.2 and 2.1.3, we provide a straightforward tool to examine the impact of photo-chemical reactions on the determination of exchange flux densities, deposition velocities and compensation point concentrations. While actual  $F_{ex,i}$ ,  $v_{dep,i}$  and  $m_{comp,i}$  are described by Eqs. (12.1) - (12.3), (13.1) - (13.3) and (14.1) - (14.3), the quantities  $F_{ex,i}^*$ ,  $v_{dep,i}^*$  and  $m_{comp,i}^*$  are given by Eqs. (15.1.1) - (15.1.3), (15.2.1) - (15.2.3) and (15.3.1) - (15.3.3). The latter are those quantities, which would have been observed if no photo-chemical reactions had taken place (e.g. for NO<sub>2</sub> during our laboratory experiments, see Sect. 3.2.1). According to Eqs. (8.4), (15.1.1), (15.2.1) and (15.3.1), the exchange flux densities  $F_{ex,i}^*$  are identical to the so-called “chamber flux densities”,  $F_{cham,I} = -Q/A_{leaf}(m_{a,i} - m_{s,i})$ .

In previous experiments, where photo-chemical reactions have not been considered, the actual exchange flux densities  $F_{ex,i}$  have just been substituted by  $F_{cham,i}$  alone. During some of the more recent experiments photo-chemical reactions have been either (partially) excluded by corresponding set-ups or were “considered” by application of an empty chamber (“reference chamber”) (RONDÓN et al. 1993; GEBLER et al. 2000, 2001; HEREID and MONSON 2001; Sparks et al. 2001; RAIVONEN et al. 2009). However, photo-chemical reactions within the latter chamber will be definitely different from those in the dynamic plant chamber, simply for the fact, that neither  $j(NO_2)$ , nor  $m_{s,NO_2}$ ,  $m_{s,NO}$  or



$m_{s,O_3}$  are identical in both chambers. In order to examine potential under/overestimation of simple “chamber flux densities”  $F_{cham,i}$ , by neglecting NO-NO<sub>2</sub>-O<sub>3</sub> gas-phase production and destruction fluxes, we combine the mentioned equations to obtain:

$$F_{ex,NO_2} = F_{cham,NO_2} - \frac{V}{A_{leaf}} \left( \bar{k} \bar{m}_{s,NO} \bar{m}_{s,O_3} - \bar{j}(NO_2) \bar{m}_{s,NO_2} \right) \quad (22.1)$$

$$F_{ex,NO} = F_{cham,NO} - \frac{V}{A_{leaf}} \left( \bar{j}(NO_2) \bar{m}_{s,NO_2} - \bar{k} \bar{m}_{s,NO} \bar{m}_{s,O_3} \right) \quad (22.2)$$

$$F_{ex,O_3} = F_{cham,O_3} - \frac{V}{A_{leaf}} \left( \bar{j}(NO_2) \bar{m}_{s,NO_2} - \bar{k} \bar{m}_{s,NO} \bar{m}_{s,O_3} \right) \quad (22.3)$$

Whether actual exchange flux densities  $F_{ex,i}$  are higher, equal or lower than corresponding  $F_{cham,i}$  depends whether the difference of the corresponding gas-phase destruction and production fluxes (second term, right hand side of Eqs. (22.1) - (22.3)) is positive, negative and different from zero.

If we differentiate our calculated exchange flux densities  $F_{ex,i}$  of the field experiment into the chamber flux densities  $F_{cham,i}$  and the gas-phase flux densities  $F_{gas,i}$ , which comprised the gas-phase production and destruction of NO-NO<sub>2</sub>-O<sub>3</sub>, we can identify the fraction of  $F_{gas,i}$  of each  $F_{ex,i}$ . For the selected leaf conductance class (see Sect. 3.2.4.2), the percentage of  $F_{gas,i}$  is displayed in Figure 22 for NO, NO<sub>2</sub> and O<sub>3</sub>. The fraction of  $F_{gas,O_3}$  at the exchange flux density of O<sub>3</sub> is very small ( $\pm 1\%$ ); therefore, it can be neglected. For the NO<sub>2</sub> exchange flux density the fraction of  $F_{gas,NO_2}$  becomes much more important. The median contribution of  $F_{gas,NO_2}$  to  $F_{ex,NO_2}$  was just +8 %, but in particular cases it could be +22 % or -12 %, respectively. Quite clear becomes the impact of the gas-phase reactions for the NO exchange flux density. Here,  $F_{gas,NO}$  amounted +42 % (median value), but ranging from +85 % to -170 %. That means, that under certain conditions  $F_{ex,NO}$  can change its sign, if  $F_{gas,NO}$  will not be considered: the estimated NO emission will convert to a NO deposition (or vice versa).

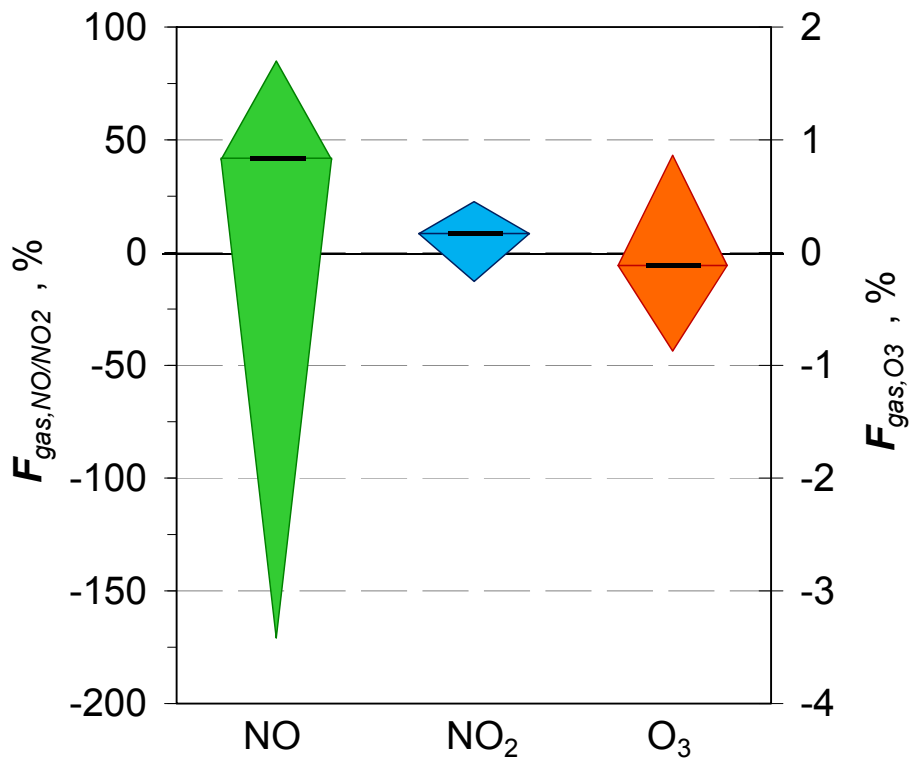


**Figure 22:** Percentage of gas-phase flux densities  $F_{gas,i}$  at the exchange flux densities  $F_{ex,i}$  for NO (green diamond),  $NO_2$  (blue diamond) and  $O_3$  (orange diamond). Results are from the field experiment, restricted to one selected data class (see Sect. 3.2.4.2). The apexes of the diamonds represented the upper (75 %) and the lower (25 %) quantile and the black dash in the middle of the diamonds the median.  $F_{gas,NO}$  and  $F_{gas,NO_2}$  were applied to the left y-axis and  $F_{gas,O_3}$  to the right y-axis.

Similar relations can be developed for deposition velocities  $v_{dep,i}$  by combining Eqs. (13.1) - (13.3) with Eqs. (15.2.1) - (15.2.3):

$$v_{dep,NO_2} = v_{dep,NO_2}^{cham} - \frac{V}{A_{leaf}} \bar{j}(NO_2) \quad (23.1)$$

$$v_{dep,NO} = v_{dep,NO}^{cham} - \frac{V}{A_{leaf}} \bar{k} \bar{m}_{s,O_3} \quad (23.2)$$

$$v_{dep,O_3} = v_{dep,O_3}^{cham} - \frac{V}{A_{leaf}} \bar{k} \bar{m}_{s,NO} \quad (23.3)$$

where the quantities with the superscript “*cham*” are those which be derived from using “chamber flux densities”  $F_{cham,i}$  instead of actual exchange flux densities  $F_{ex,i}$ . The actual deposition velocities  $v_{dep,i}$  are in any case lower than  $v_{dep,i}^{cham}$  with the exception  $m_{s,O_3} = 0$ ,  $m_{s,NO} = 0$  and  $j(NO_2) = 0$  (i.e. during nighttime). To examine how much the

gas-phase reactions will affect  $v_{dep,i}$ , we split our calculated deposition velocity  $v_{dep,i}$  for the field data into  $v_{dep,i}^{cham}$  and the complementary part caused by gas-phase reactions. The contribution of photolysis (see Eq. 23.1) to  $v_{dep,NO_2}$  was 80 %, that of reaction (R1) on  $v_{dep,O_3}$  only 3 %. Corresponding estimates on  $v_{dep,NO}$  were not performed, since NO deposition velocities were not significant during the EGER field experiment. For their experimental conditions, NEUBERT et al. (1993) identified an error of about 20 % for their  $v_{dep,NO_2}$  determination, if they would neglect photolysis of  $NO_2$ . However, our results should be compared to those of previous studies with caution: in most of the previous studies it is not clear whether the photolysis of  $NO_2$  was correctly taken into account. Nevertheless, we tried to estimate the potential impact of  $NO_2$  photolysis on these, previously reported  $v_{dep,NO_2}$ . For that, the quantities  $A_{leaf}$ ,  $V$ ,  $j(NO_2)$  and  $v_{dep,NO_2}$  have to be *a priori* known or they must be derived from other (accompanying) data. Most of the authors have not reported any data of  $A_{leaf}$ . So, we estimated the unknown  $A_{leaf}$  on the basis of available information about chamber design and our experience concerning the ratio between length of branch and needle area. Moreover, most authors did not specify the used chamber wall material nor its transmissivity for the wavelength range of  $j(NO_2)$ . Therefore, we estimated the transmissivity on basis of available material information. THOENE et al. (1991, 1996) and GEBLER et al. (2002) used borosilicate glass (Schott Glaswerke, Mainz, Germany). Combining the manufacturer's specification (<http://www.schott.com/tubing>) and our experience with different wall materials (including glass) we estimated the  $j(NO_2)$  transmissivity of borosilicate glass to 60 %. For FEP-Teflon film, used by RONDÓN et al. (1993), we estimated 70 % transmissivity (related to our Teflon film). If  $NO_2$  photolysis would not have been considered at all, THOENE et al. (1991,1996) and RONDÓN et al. (1993) would have potentially overestimated their  $v_{dep,NO_2}$  values by 17 – 81 % and GEBLER et al. (2002) by up to 100 % (according to Eq. (23.1), depending on prevailing radiation conditions). However, since these authors have applied an empty (“reference”) chamber (see Sect. 3.3.1), the impact on  $NO_2$  photolysis on their reported  $v_{dep,NO_2}$  values might be smaller if the underlying assumption is correct that the effect of  $NO_2$  photolysis is identical in the plant and in the empty chamber. The results of field measurements by SPARKS et al. (2001) and HEREID and MONSON (2001) most likely have not been affected by  $NO_2$  photolysis because they used a leaf chamber system with red light-emitting diodes which produce no appreciable radiation in the wavelength range of  $j(NO_2)$ .

The corresponding relations for the compensation point concentrations  $m_{comp,i}$  are obtained by combining Eqs. (14.1) - (14.3) with Eqs. (15.3.1) - (15.3.3):

$$m_{comp,NO_2} = m_{comp,NO_2}^{cham} \cdot \frac{1 - m_1 \left[ 1 + \frac{V}{n_1 \bar{Q}} \bar{k} \bar{m}_{s,NO} \bar{m}_{s,O_3} (1 - m_1) \right]}{1 - m_1 \left( 1 + \frac{V}{\bar{Q}} \bar{j}(NO_2) \right)} \quad (24.1)$$

$$m_{comp,NO} = m_{comp,NO}^{cham} \cdot \frac{1 - m_2 \left[ 1 + \frac{V}{n_2 \bar{Q}} \bar{j}(NO_2) \bar{m}_{s,NO_2} (1 - m_2) \right]}{1 - m_2 \left( 1 + \frac{V}{\bar{Q}} \bar{k} \bar{m}_{s,O_3} \right)} \quad (24.2)$$

$$m_{comp,O_3} = m_{comp,O_3}^{cham} \cdot \frac{1 - m_3 \left[ 1 + \frac{V}{n_3 \bar{Q}} \bar{j}(NO_2) \bar{m}_{s,NO_2} (1 - m_3) \right]}{1 - m_3 \left( 1 + \frac{V}{\bar{Q}} \bar{k} \bar{m}_{s,NO} \right)} \quad (24.3)$$

Here, the value of the fraction (right hand side of Eqs. (24.1) - (24.3)) determines whether the actual compensation point concentrations  $m_{comp,i}$  are higher, equal, or lower than  $m_{comp,i}^{cham}$ .

For our experimental conditions,  $m_{comp,NO_2}$  would be overestimated by 10 %, if the gas-phase reactions would not have been considered (i.e. assuming  $m_{comp,NO_2} = m_{comp,NO_2}^{cham}$ ). For the compensation point concentration of  $O_3$  the overestimation would be only 1 %. The  $m_{comp,NO_2}$  values reported in previous studies (THOENE et al. 1991, 1996; RONDÓN et al. 1993, GEßLER et al. 2002) would be overestimated between 3 and 17 %, if the photolysis of  $NO_2$  was not considered.

When the value of the fractions on the right hand side of Eqs. (24.1) - (24.3) are examined for being greater, equal, or lower than unity, the following relations are obtained:

$$m_{comp,NO_2} > (=, <) m_{comp,NO_2}^{cham}, \quad \text{if} \quad m_{comp,NO_2}^{cham} > (=, <) \frac{\bar{k} \bar{m}_{s,NO} \bar{m}_{s,O_3}}{\bar{j}(NO_2)} \quad (25.1)$$

$$m_{comp,NO} > (=, <) m_{comp,NO}^{cham}, \quad \text{if} \quad m_{comp,NO}^{cham} > (=, <) \frac{\bar{j}(NO_2) \bar{m}_{s,NO_2}}{\bar{k} \bar{m}_{s,O_3}} \quad (25.2)$$

$$m_{comp,O3} > (=, <) m_{comp,O3}^{cham}, \quad \text{if} \quad m_{comp,O3}^{cham} > (=, <) \frac{\bar{j}(NO_2)\bar{m}_{s,NO2}}{\bar{k}\bar{m}_{s,NO}} \quad (25.3)$$

The relevance of these relations consists in their potential for the easy check, whether or not the correct evaluation of compensation point concentrations has to consider photo-chemical reactions. Having evaluated measured concentrations  $m_{a,i}$  and  $m_{s,i}$  by bi-variate weighted linear regression (which delivers  $n_i$  and  $m_i$ ), the quantities  $m_{comp,i}^{cham}$  are determined. Using the simultaneously measured averages of  $k$ ,  $j(NO_2)$ ,  $m_{s,NO2}$ ,  $m_{s,NO}$  and  $m_{s,O3}$ , the right hand fractions of relations (25.1) - (25.3) can be calculated, which provide the necessary quantities to test whether or not  $m_{comp,i}^{cham}$  have to be corrected for photo-chemical reactions in the dynamic plant chamber (by Eqs. (24.1) - (24.3)).

### 3.3.3 Bi-variate weighted linear regression

The determination of deposition velocities  $v_{dep,i}$ , as well as compensation point concentrations  $m_{comp,i}$  is based on linear regression of the measured concentration of trace gas  $i$  in ambient air and within the dynamic plant chamber. Therefore, it is indispensable that errors of both variables were considered in the determination of  $v_{dep,i}$  and  $m_{comp,i}$ . For our laboratory results (see Sect. 3.2.4.1) we have shown the effect of applying simple linear regression (no errors considered at all), linear regression (y-errors considered) and bi-variate weighted linear regression (y- and x-errors considered) on the significance of derived  $v_{dep,NO2}$  and  $m_{comp,NO2}$  data (see Table 12). Generally speaking, applying a simple linear least-square fitting algorithm, the probability of  $m_{comp,i} \neq 0$  can be highly significant, while applying the bi-variate weighted linear least-square fitting algorithm the probability for the existence of  $m_{comp,i}$  could easily become “likely” or even “unlikely”. In the fewest cases previous authors have applied the bi-variate algorithm (e.g. GEBLER et al. 2000, 2002). Finally, it should be stated that in all previous studies values of  $v_{dep,NO2}$  and  $m_{comp,NO2}$  have been derived from linear relationships between  $F_{ex,NO2}$  and  $m_{s,NO2}$  which is mathematically not correct, since the dependent variable  $F_{ex,NO2}$  contains the independent variable  $m_{s,NO2}$  (see Sect. 2.1.2).



# Application of dynamic plant chamber system to field measurements

In this chapter the application of the dynamic plant chamber system to field measurements is presented. The chamber system was used during the second intensive observation period of the EGER project from 01 June to 15 July 2008. It took place in northeast Bavaria, Germany (see Sect. 2.5.2). Additionally, data measured during the project ECHO (Emission and CHEmical Transformation of Biogenic Volatile Organic Compounds) within the German Atmospheric Research Program (AFO 2000) were provided to me for analysis. For this study the exchange rates of NO, NO<sub>2</sub>, O<sub>3</sub>, CO<sub>2</sub> and H<sub>2</sub>O on oak (*Quercus robur*) under environmental conditions were measured.

## 4.1 Methods

### 4.1.1 Photosynthesis rate, transpiration rate, stomatal conductance

Considering the exchange of the non-reactive trace gases CO<sub>2</sub> and H<sub>2</sub>O between the plant chamber's atmosphere and the enclosed leaves, the exchange flux densities of the net rate of photosynthesis (photosynthesis rate minus the simultaneously proceeding photorespiration)  $F_{ex,CO_2}$  (in  $\mu\text{mol m}^{-2} \text{s}^{-1}$ ) and the transpiration rate  $F_{ex,H_2O}$  (in  $\text{mmol m}^{-2} \text{s}^{-1}$ ) were calculated after VON CAEMMERER and FARQUHAR (1981):

$$F_{ex,n} = -\frac{Q}{A_{leaf}}(m_{r,n} - m_{s,n}) \quad n = CO_2, H_2O \quad (26)$$

The calculation is based on the difference between the molar concentration  $m_{r,n}$  and  $m_{s,n}$  ( $\mu\text{mol m}^{-3}$  or  $\text{mmol m}^{-3}$ ) of trace gas  $n$  within the empty reference chamber and the plant

chamber, respectively, the enclosed leaf area ( $A_{leaf}$ ) and the chamber purging rate ( $Q$ ). Equation (26) is comparable with Eq. (8.4), which describes the exchange flux density  $F_{ex,i}$  of the reactive trace gas  $i$  ( $i = \text{NO}_2, \text{NO}, \text{O}_3$ ) if gas-phase production and/or destruction of the reactive trace gas can be ruled out.

The stomatal conductance for  $\text{H}_2\text{O}$  ( $g_{\text{H}_2\text{O}}$  in  $\text{m s}^{-1}$ ) was calculated from the transpiration rate (in  $\text{kg m}^{-2} \text{s}^{-1}$ ) and the humidity gradient, which is the difference between the absolute humidity inside the leaf ( $ah_{leaf}$  in  $\text{kg m}^{-3}$ ) and the absolute humidity of ambient air ( $ah_a$  in  $\text{kg m}^{-3}$ ). The humidity inside the leaf was calculated as saturated vapor concentration at leaf temperature:

$$g_{\text{H}_2\text{O}} = \frac{F_{\text{H}_2\text{O}}}{ah_{leaf} - ah_a} \quad (27)$$

The predicted leaf conductance of the gas  $i$  ( $g_{i,p}$ ) ( $i = \text{NO}_2, \text{O}_3$ ) was estimated from stomatal conductance to water vapor ( $g_{\text{H}_2\text{O}}$ ) by scaling it

$$g_{i,p} = g_{\text{H}_2\text{O}} \cdot R_D \quad (28)$$

where  $R_D$  is the ratio of diffusivities ( $\text{cm}^2 \text{s}^{-1}$ ) of  $\text{NO}_2$  or  $\text{O}_3$  and water vapor in air. According to MASSMAN (1998) values of  $R_D$  were amounted to 0.62 for  $\text{NO}_2$  and 0.66 for  $\text{O}_3$  at conditions near standard temperature and pressure ( $T = 0 \text{ }^\circ\text{C}$ ,  $p = 101.325 \text{ kPa}$ ).

#### 4.1.2 Classification of data

Consideration of a possible compensation point concentration and determination of the deposition velocity require a certain amount of measuring points. During data selection it is necessary to find comparable conditions for the plant. This avoids comparison of, for example, trace gas exchange rates measured during a physiologically active phase of the plant with wide opened stoma and exchange rates measured at a phase of closed stoma. A suitable parameter with which to select data points is the stomatal conductance for  $\text{H}_2\text{O}$  ( $g_{\text{H}_2\text{O}}$ ) because this parameter gives information about the condition of the plant and indirect information about air temperature, radiation and water vapor deficit (VPD). Furthermore, it is known that the  $\text{NO}_2$  exchange is strongly



regulated by stomatal conductance (THOENE et al. 1991; GEßLER et al. 2000; TEKLEMARIAM and SPARKS 2006; CHAPARRO-SUAREZ 2008). Hence, the data were classified into seven classes of  $g_{H_2O}$ . The interval between the several classes is based on a logarithmical scale.

#### 4.1.3 Monitoring of plant-physiological processes due to chambers

Working with chambers and enclosed plants (parts of plants) necessitates control of the plant living conditions. The design and operation of the chambers needs to guarantee an undisturbed metabolism. For example, if the purging air flow is too low, it would disturb the gas exchange of the plant because  $CO_2$  and  $H_2O$  concentrations would be reduced or accumulate inside the chamber. Plants will react with some regulation mechanisms on the modified conditions. Adequate experiments are needed to show that the plant is unaffected. This must be done for each plant and site. Simultaneous measurements of  $CO_2$  surface exchange fluxes (assimilation),  $H_2O$  surface exchange fluxes (transpiration) and determination of stomatal conductance can provide an indication of the plant condition. For long-term field measurements further control experiments including unenclosed plants (part of the plants) would be advantageous to ensure the same behavior of control and enclosed plants even after long enclosure periods. For example, measurements of the photosynthetic capacity in response to temperature, radiation,  $CO_2$  mixing ratio and relative humidity or analysis of the nutrient composition of enclosed and control plants could be tested.

We proved the photosynthetic capacity of the enclosed needles in comparison to control needles. Measurements of *in-situ*  $CO_2$  and  $H_2O$  needle gas exchange in response to temperature, radiation,  $CO_2$  mixing ratio and relative humidity were made using a portable gas exchange system (WALZ GFS3000, Walz, Effeltrich/Germany). From these light-response curves the light compensation point ( $I_c$ ) and the light-saturated point ( $I_s$ ) could be identified. The  $I_c$  marked the irradiance level where  $CO_2$  uptake and respiratory  $CO_2$  release were in equilibrium. By definition the  $I_s$  was reached at 90 % of maximal yield of photosynthesis. Additionally we have analyzed the nutrient composition (calcium, potassium, magnesium, manganese, phosphorus, sulfur, carbon and nitrogen) of control and enclosed needles according to validated analytical methods by the Bayreuth Center of Ecology and Environmental Research (BayCEER).

#### 4.1.4 Set-up at the ECHO project

For the measurements within the ECHO project a comparable dynamic chamber system was used. The measurement site was located in an urban area (Jülich, Germany) in a deciduous forest stand and took place from 12 to 19 July 2003. For a detailed description of the field site and the measurement system see DINDORF et al. (2006).

During the measurements, a branch of the oak tree (*Quercus robur*) was enclosed in a dynamic plant chamber with a height of 60 cm and a diameter of 40 cm, equivalent to ~75 L. The total enclosed leaf area was 0.26 m<sup>2</sup> and the total dry-leaf weight 24.0 g. The sample chamber and an empty reference chamber of identical volume were continuously flushed with 35 L min<sup>-1</sup> of ambient air, which results in a residence time of 129 s. The chambers were installed close to each other at a height of 18 m. Air was sampled alternately from the reference and the plant chamber outlets for 90 s.

NO and NO<sub>2</sub> concentrations were measured with a chemiluminescence NO analyzer (Eco Physics CLD 780 TR). The  $LOD(m_{NO})$  of the instrument amounts to 30 ppt for a 3 s integration time. O<sub>3</sub> concentrations were measured with an UV-absorption analyzer (Model 49C, Thermo Environment). CO<sub>2</sub> and H<sub>2</sub>O concentrations were measured with an infrared gas analyzer (LI-6262, LiCor, Lincoln, NE, USA).

## 4.2 Results

### EGER project

#### 4.2.1 Microclimatic conditions

The ambient concentrations of NO, NO<sub>2</sub>, O<sub>3</sub>, CO<sub>2</sub> and H<sub>2</sub>O and the relative humidity and air temperature were recorded in addition to the chamber measurements. Global radiation was detected on the top of the tower. A summary of the ambient measurements is given in Table 16. NO concentrations were mostly close to the detection limit. Sporadic NO peaks occurred due to advection of automobile exhaust gases from a busy country road (2000 cars/h) at a distance of about 1 - 2 km from the site. The NO<sub>2</sub> concentration varied between 0.4 and 21.5 ppb including concentration peaks from the road. A diurnal distribution was seen with higher NO<sub>2</sub> concentrations at night. O<sub>3</sub> mixing ratios ranged between 3 and 78 ppb. In the morning hours a gradual decline of O<sub>3</sub> concentration was observed. Weather conditions during measurements were characteristic of the region. Air temperature ranged from 4 to 28 °C with a mean temperature of 14 °C.

**Table 16:** Ambient conditions during time of field measurements. Given are mean values and minimum and maximum data over the measuring period (1 June to 15 July 2008).

|                                     | average       | range        |
|-------------------------------------|---------------|--------------|
| NO, ppb                             | 0.19 ± 0.17   | 0.07 - 2.89  |
| NO <sub>2</sub> , ppb               | 2.46 ± 1.42   | 0.42 - 21.49 |
| O <sub>3</sub> , ppb                | 47.12 ± 11.67 | 19.0 - 77.1  |
| CO <sub>2</sub> , ppm               | 380 ± 8       | 293 - 409    |
| H <sub>2</sub> O, ppth              | 13 ± 2.6      | 7 - 25       |
| relative humidity, %                | 68.3 ± 17.4   | 32.3 - 99.9  |
| temperature, °C                     | 14.4 ± 4.5    | 3.8 - 27.7   |
| global radiation, W m <sup>-2</sup> | 232 ± 276     | 0 - 1005     |

### 4.2.2 Plant physiology

The photosynthetic capacity control measurements of enclosed and control needles as performed to detect effects caused by the chambers on the enclosed plant parts are presented in Figure 23 for one example tree. We distinguished between control and enclosed needles and between young and old needles. The control needles were outside the chambers during the whole field campaign. The photosynthesis rate was measured under different light conditions at ambient CO<sub>2</sub> concentrations (370 - 390 ppm). It is obvious that enclosed and control needles have the same photosynthesis rates. Young and old needles behaved similarly.  $I_c$  was in a range of 40 to 70  $\mu\text{mol photons m}^{-2} \text{s}^{-1}$  and  $I_s$  between 500 and 1100  $\mu\text{mol photons m}^{-2} \text{s}^{-1}$ .

The results of the nutrient composition analysis (see Table 17) of the needles exhibited no obvious differences between control and enclosed needles for total carbon and total nitrate concentration as well for magnesium, manganese, phosphate and sulfur. Only for potassium and calcium were major differences recognizable between young control and enclosed needles. As the low concentration of potassium in the young needles does not go below the limit of potassium (PFLÜGER and MENGEL 1972; SIEGHARDT 1988; LARCHER 2003), these differences were not a sign of a harmful effect of the chamber. Furthermore, young plants have higher potassium concentrations than older plants because potassium is needed during leaf development. Potassium ions are responsible for the maintenance of the status of plasma swelling. Potassium deficit can be identified by fading of leaves and later leaf die off (LARCHER 2003). These symptoms were not observed.

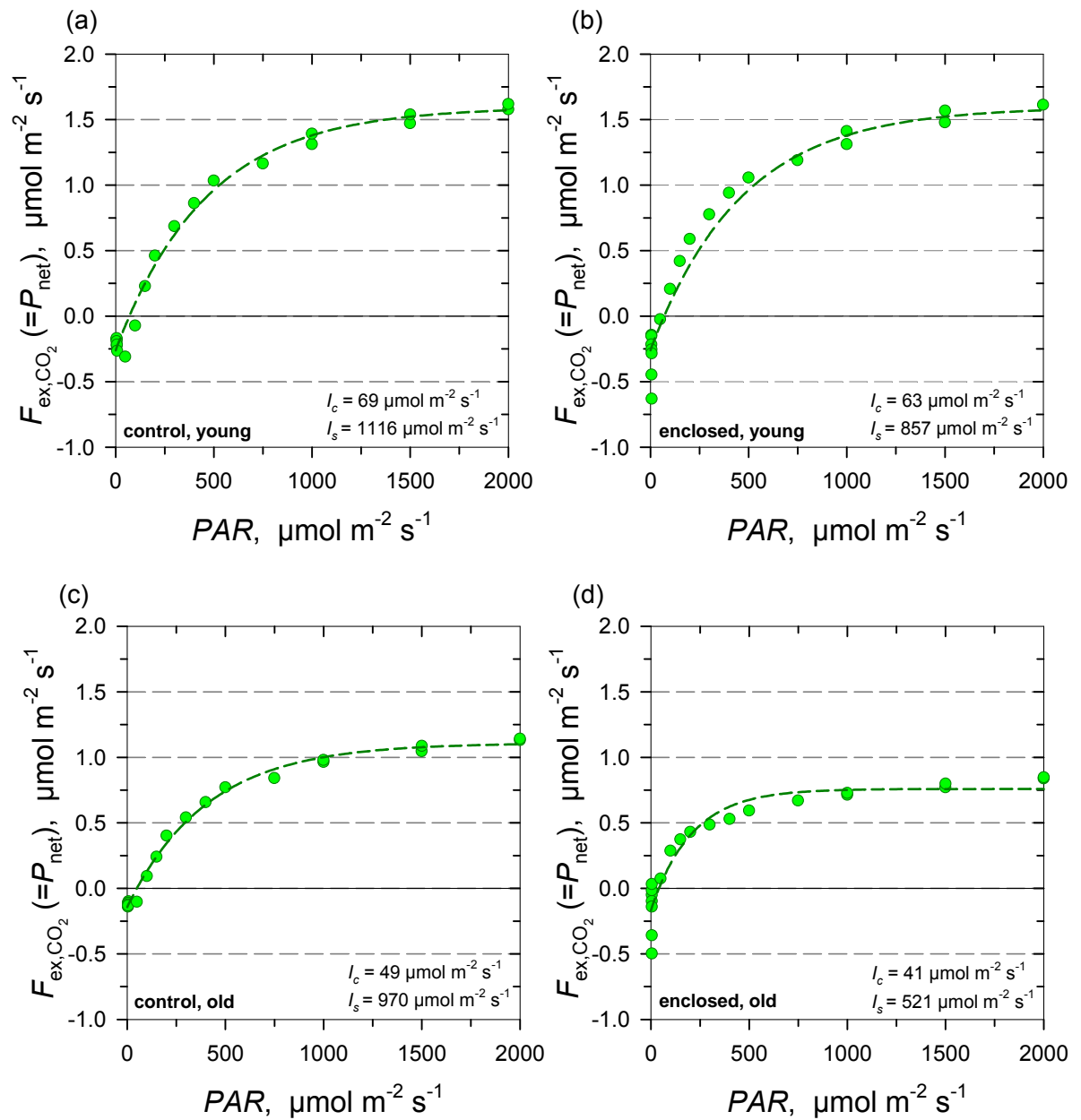


**Figure 23:** Photosynthetic light response curves at ambient CO<sub>2</sub> concentration (370 - 390 ppm) of control and enclosed needles. **(a)** young control needles, **(b)** young enclosed needles, **(c)** older control needles, **(d)** older enclosed needles.

**Table 17:** Results of the nutrient content analysis of the needles.

|                             | Tree 1  |          |         |          | Tree 2  |          |         |          |
|-----------------------------|---------|----------|---------|----------|---------|----------|---------|----------|
|                             | young   |          | old     |          | young   |          | old     |          |
|                             | control | enclosed | control | enclosed | control | enclosed | control | enclosed |
| <b>mg g<sup>-1</sup> dw</b> |         |          |         |          |         |          |         |          |
| <b>Ca</b>                   | 2.05    | 2.11     | 3.07    | 2.83     | 2.99    | 2.20     | 6.85    | 6.70     |
| <b>K</b>                    | 6.91    | 8.66     | 4.65    | 5.06     | 4.58    | 5.87     | 2.61    | 2.53     |
| <b>Mg</b>                   | 0.67    | 0.78     | 0.54    | 0.64     | 0.63    | 0.58     | 0.66    | 0.69     |
| <b>Mn</b>                   | 0.17    | 0.17     | 0.28    | 0.24     | 0.12    | 0.09     | 0.27    | 0.26     |
| <b>P</b>                    | 1.40    | 1.61     | 1.15    | 1.15     | 1.21    | 1.34     | 0.88    | 0.89     |
| <b>S</b>                    | 0.67    | 0.74     | 0.83    | 0.83     | 0.62    | 0.64     | 0.76    | 0.74     |
| <b>%</b>                    |         |          |         |          |         |          |         |          |
| <b>N</b>                    | 1.13    | 1.35     | 1.40    | 1.49     | 1.09    | 1.10     | 1.27    | 1.26     |
| <b>C</b>                    | 47.48   | 47.63    | 48.75   | 48.87    | 47.94   | 48.72    | 49.51   | 49.53    |

### 4.2.3 Diurnal variations of gas exchange

The diurnal variation of exchange flux densities of CO<sub>2</sub>, H<sub>2</sub>O, NO, NO<sub>2</sub> and O<sub>3</sub> for Tree 1 for the period from 7 to 8 July are presented in Figure 25. At these two days maximal PAR reached 575 μmol photons m<sup>-2</sup> s<sup>-1</sup> and leaf temperature ( $T_{leaf}$ ) was always below 18 °C. The O<sub>3</sub> exchange flux density ( $F_{ex,O_3}$ ) ranged between -0.02 and -0.61 nmol m<sup>-2</sup> s<sup>-1</sup>. On both days a gradual increase of  $F_{ex,O_3}$  was observed, started rising at sunrise at 06:00 and reaching maximum values at 14:00. Then the  $F_{ex,O_3}$  declined to minimum values, as did the leaf conductance, before it began to increase again the next morning. Compared to O<sub>3</sub> the diurnal course of NO<sub>2</sub> exchange flux density ( $F_{ex,NO_2}$ ) was not so pronounced. Moreover, for NO<sub>2</sub> more  $F_{ex,NO_2}$  data had to be rejected for non-significance of  $\Delta m_{NO_2} = (m_{a,NO_2} - m_{s,NO_2})$  than for O<sub>3</sub>. The range of  $F_{ex,NO_2}$  was between -0.04 and 0.01 nmol m<sup>-2</sup> s<sup>-1</sup>. The diurnal NO distribution was not identifiable. Most of the  $F_{ex,NO}$  measurements had to be rejected as  $\Delta m_{NO} = (m_{a,NO} - m_{s,NO})$  was not significant or the concentrations were under the  $LOD(m_{NO})$ . The positive values of  $F_{ex,NO}$  occurred by corrections for the chemical gas phase reactions and not by higher NO concentrations inside the sample chamber compared to concentrations in ambient air.

Exchange flux densities of NO and NO<sub>2</sub> between 06:00 and 12:00 have to be interpreted with caution because in this time interval advection of automobile exhaust

gases from a country road cannot be excluded. As mentioned above this problem of advection is well known. It has been identified in simultaneously-performed profile measurements of in- and above canopy concentrations and eddy covariance flux measurements of NO-NO<sub>2</sub>-O<sub>3</sub> (PLAKE et al. 2009).

Figure 26 presents the diurnal variations of the period from 29 to 30 June. During these two days PAR reached maximal values of 1800  $\mu\text{mol photons m}^{-2} \text{s}^{-1}$  with an average of 400  $\mu\text{mol photons m}^{-2} \text{s}^{-1}$  under daylight conditions. Compared to the two days presented before, these days were much sunnier and therefore  $T_{leaf}$  reached values above 20 °C around noon. The distribution of the leaf conductance (Figure 26c) is strongly connected to the leaf temperature. If  $T_{leaf}$  exceeds values of around 23 °C stomata began to close. This temperature effect has been documented through independent measurements of temperature dependence of photosynthesis on leaf level (see Figure 24, data provided by E. Falge, personal communication, 2009). To that effect the diurnal course of  $F_{ex,O_3}$  only reached maximum values of  $-0.51 \text{ nmol m}^{-2} \text{s}^{-1}$  and began to decrease earlier. During such days diurnal distributions of  $F_{ex,NO_2}$  could hardly be seen, because when stomata closed around noon only very small NO<sub>2</sub> exchange fluxes could be detected. In most cases  $F_{ex,NO_2}$  data had to be rejected for non-significance of  $\Delta m_{NO_2} = (m_{a,NO_2} - m_{s,NO_2})$ . There was an additional problem with the measurements of NO for these two days: Most of the measured NO concentrations were below the detection limit of the NO analyzer or the concentration differences  $\Delta m_{NO}$  were not significant, therefore we can not calculate any exchange fluxes.

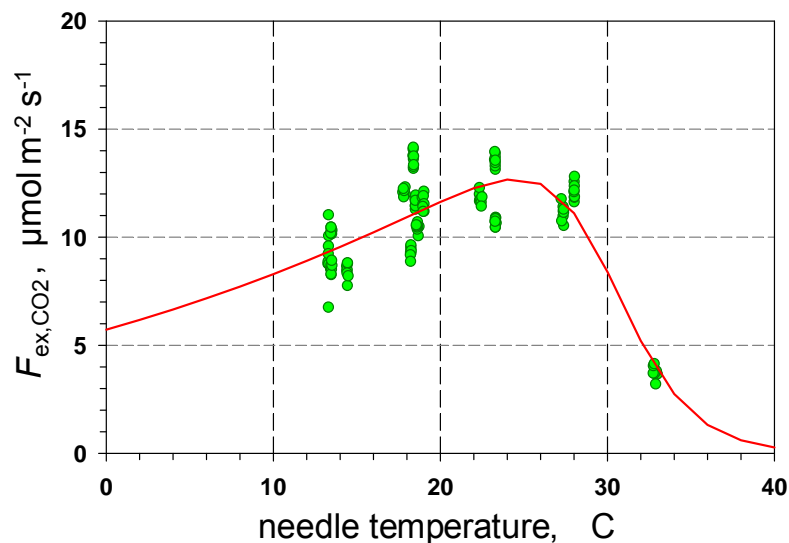


**Figure 24:** Temperature dependence of photosynthesis rate ( $F_{ex,CO_2}$ ). *In-situ* measurements of CO<sub>2</sub> gas exchange on needle level in response to temperature, using a portable gas exchange system (WALZ GFS3000, Walz, Effeltrich/Germany). Here photosynthesis rates were represented with positive sign. Data provided by E. Falge, (personal communication, 2009).

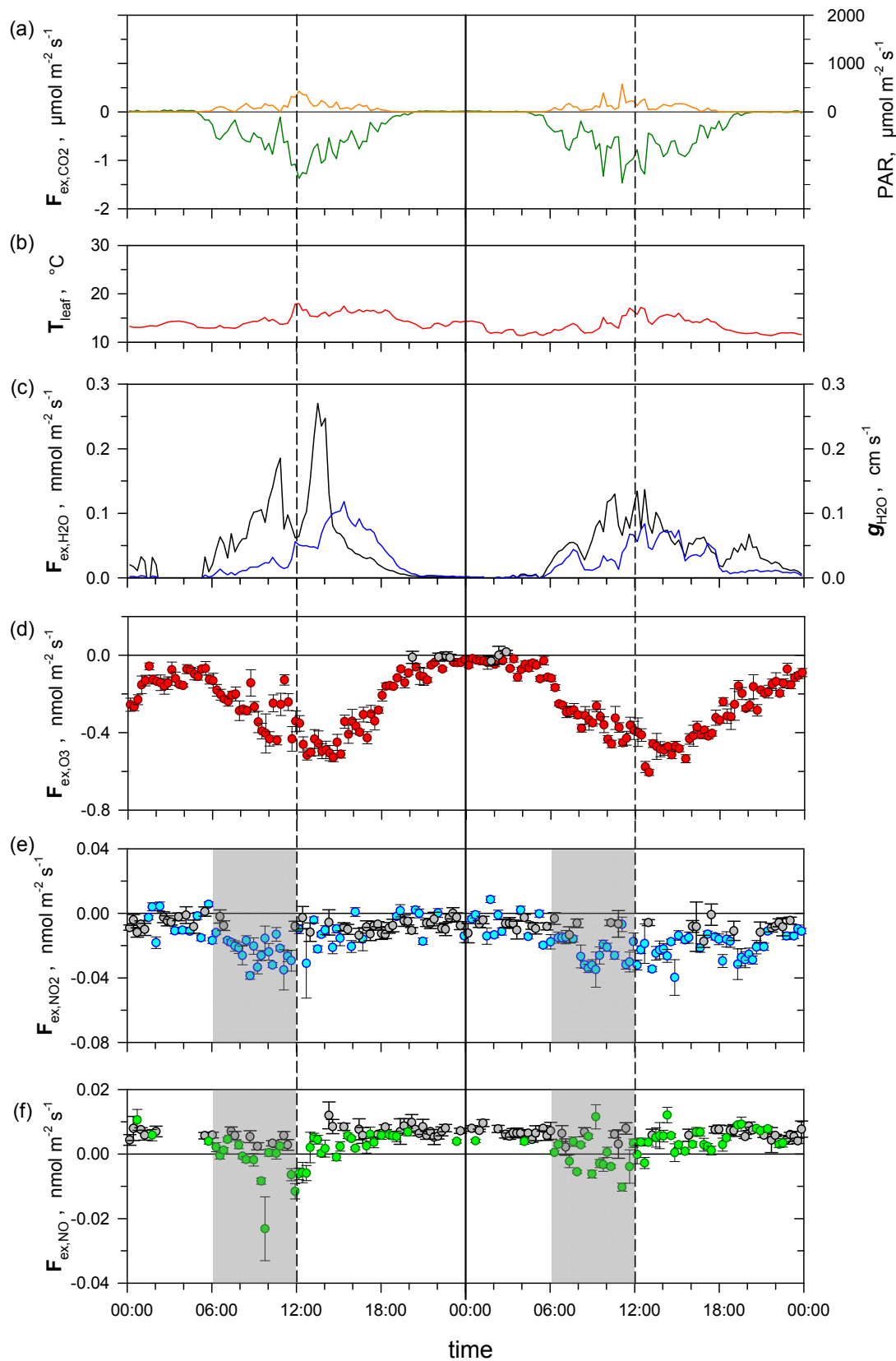


**Figure 25:** Exchange flux densities ( $F_{\text{ex}}$ ) of  $\text{CO}_2$  (panel (a), green line),  $\text{H}_2\text{O}$  (panel (c), blue line),  $\text{NO}$ ,  $\text{NO}_2$ ,  $\text{O}_3$  (panel (d-f)) with diurnal courses of PAR (panel (a), orange line), leaf temperature ( $T_{\text{leaf}}$ ) (panel (b)) and leaf conductance ( $g_{\text{H}_2\text{O}}$ ) (panel (c)) black line) over the period from Jul 07 to Jul 08. The flux data are 16 min averages. Grey circles identify  $F_{\text{ex},i}$  data, which have to be rejected for non-significance of  $\Delta m_i = (m_{a,i} - m_{s,i})$ . Grey bars indicate time interval of possible advection of automobile exhaust gases from a country road.



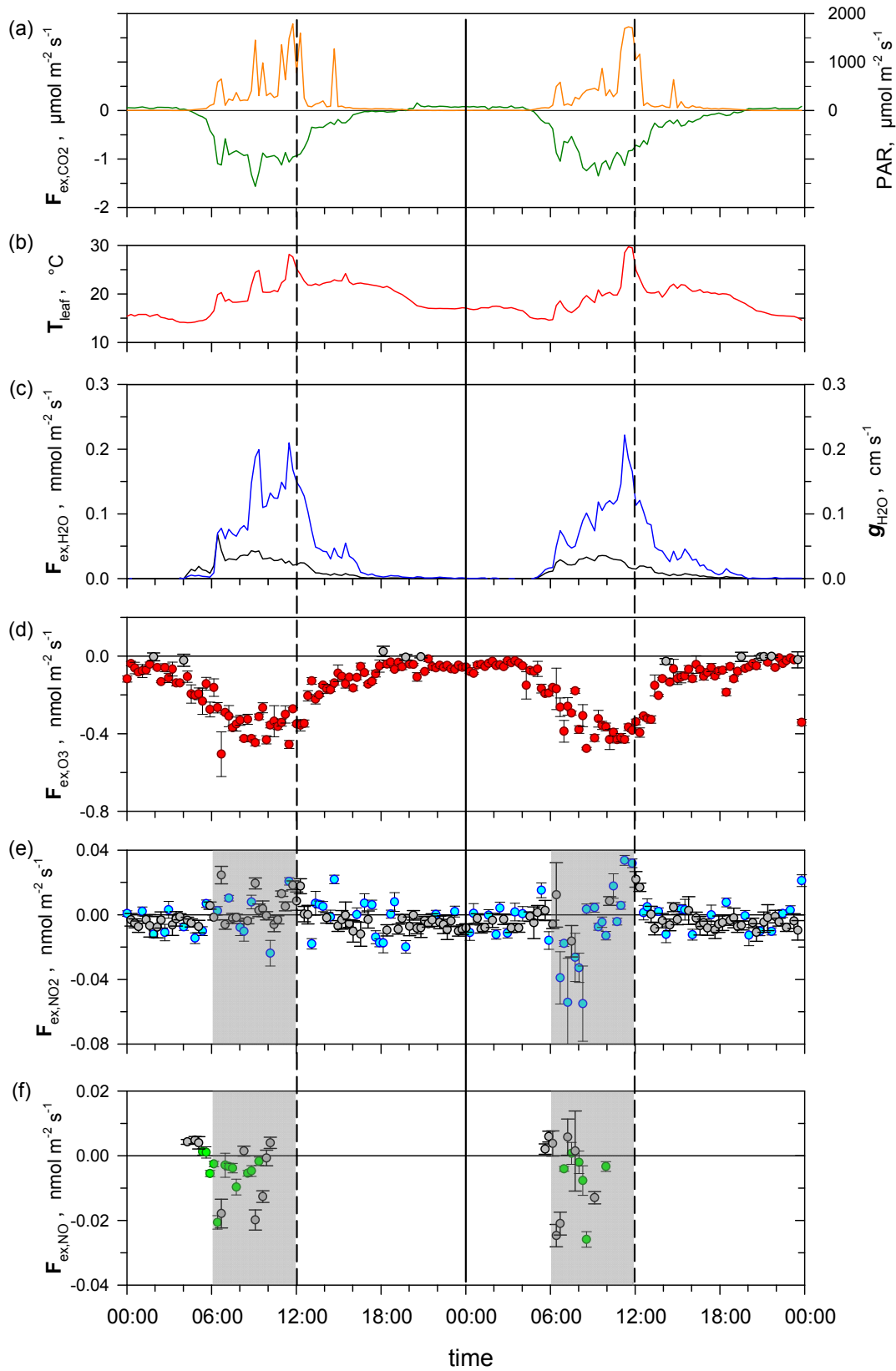


**Figure 26:** Exchange flux densities ( $F_{\text{ex}}$ ) of  $\text{CO}_2$  (panel (a), green line),  $\text{H}_2\text{O}$  (panel (c), blue line),  $\text{NO}$ ,  $\text{NO}_2$ ,  $\text{O}_3$  (panel (d-f)) with diurnal courses of PAR (panel (a), orange line), leaf temperature ( $T_{\text{leaf}}$ ) (panel (b)) and leaf conductance ( $g_{\text{H}_2\text{O}}$ ) (panel (c)) over the period from Jun 29 to Jun 30. The flux data are 16 min averages. Grey circles identify  $F_{\text{ex},i}$  data, which have to be rejected for non-significance of  $\Delta m_i = (m_{a,i} - m_{s,i})$ . Grey bars indicate time interval of possible advection of automobile exhaust gases from a country road.

#### 4.2.4 Overview of plant chamber measurements

The field measurements took place over a period of six weeks. Table 18 presents the results of both dynamic sample chambers (trace gas concentration measurements of NO, NO<sub>2</sub>, O<sub>3</sub>, photosynthesis, transpiration, exchange flux densities of NO, NO<sub>2</sub>, O<sub>3</sub>, leaf conductance, light and temperature conditions). The NO concentration ( $m_{s,NO}$ ) inside the two sample chambers was on average 0.16 ppb at day and 0.1 ppb at night which approached limit of detection of the analyzer ( $LOD(m_{NO}) = 0.1 \text{ ppb} = 4.46 \text{ nmol m}^{-3}$ ). The NO<sub>2</sub> concentration  $m_{s,NO_2}$  were in contrast always above the limit of detection ( $LOD(m_{NO_2}) = 0.31 \text{ ppb} = 13.8 \text{ nmol m}^{-3}$ ). At day and night the mean NO<sub>2</sub> values were around 2 ppb. Some high concentration peaks were observable, especially for NO<sub>2</sub>, up to a maximum of 17 ppb. This temporary concentration rise resulted from the traffic road near by the site, frequently during the rush-hour traffic in the morning between 06:00 and 12:00. The O<sub>3</sub> concentrations  $m_{s,O_3}$  reached averages of 40 ppb. Both branches demonstrated similar photosynthesis, respiration and transpiration activities. Leaf conductances of H<sub>2</sub>O ( $g_{H_2O}$ ) were also comparable. Consequently there was no evidence for different behavior of the two trees or enclosed parts of the plants.

The data selection of statistically-significant differences of trace gas concentrations at the inlet and the outlet of the dynamic chamber (see Sect. 3.1.5) resulted in different numbers for NO, NO<sub>2</sub> and O<sub>3</sub>, which were used to calculate the exchange flux densities. Table 19 presents the percentage of significant concentration differences  $\Delta m_i = (m_{a,i} - m_{s,i})$  measured at the inlet and outlet of the dynamic sample chamber 1 and 2. It becomes apparent that for O<sub>3</sub> most of the concentration differences were significant. Most statistically insignificant concentration differences were found for NO, especially at night. Overall, only one fourth of the NO data pairs passed the significance criterion. For NO<sub>2</sub> measurements the percentage of significant data pairs was 60 - 70 %.

The bi-variate weighted regression analysis for NO resulted in very small  $R^2(m_{a,NO}, m_{s,NO})$  between 0.0173 and 0.9031. Moreover, the probabilities of significant NO compensation point concentrations  $m_{comp,NO}$  and NO deposition velocities  $v_{dep,NO}$  are generally unlikely. Continulative evaluations for  $m_{comp,NO}$  and  $v_{dep,NO}$  were not practical.

**Table 18:** Overview of chamber measurements. Given are mean data from 4 minute average values of day and night measurements.

|  | sample chamber 1                  |                                   | sample chamber 2                  |                                   |
|--|-----------------------------------|-----------------------------------|-----------------------------------|-----------------------------------|
|  | day <sup>a</sup>                  | night                             | day <sup>a</sup>                  | night                             |
| $m_{s,NO}$ , ppb                                     | 0.16 ±0.12<br>(0.10* - 1.53)      | 0.10 ±0.04<br>(0.10* - 0.35)      | 0.16 ±0.13<br>(0.10* - 1.75)      | 0.09 ±0.04<br>(0.10* - 0.35)      |
| $F_{ex,NO}$ , nmol m <sup>-2</sup> s <sup>-1</sup>   | -0.006 ±0.015<br>(-0.110 - 0.044) | 0.009 ±0.005<br>(0.002 - 0.019)   | -0.005 ±0.007<br>(-0.026 - 0.090) | 0.010 ±0.004<br>(0.002 - 0.023)   |
| $m_{s,NO_2}$ , ppb                                   | 2.19 ±1.35<br>(0.73 - 17.19)      | 2.28 ±1.31<br>(0.76 - 12.28)      | 2.13 ±1.27<br>(0.77 - 11.91)      | 2.30 ±0.91<br>(0.66 - 7.63)       |
| $F_{ex,NO_2}$ , nmol m <sup>-2</sup> s <sup>-1</sup> | -0.011 ±0.015<br>(-0.079 - 0.058) | -0.014 ±0.025<br>(-0.414 - 0.085) | -0.019 ±0.020<br>(-0.341 - 0.045) | -0.013 ±0.022<br>(-0.205 - 0.155) |
| $v_{dep,NO_2}$ , mm s <sup>-1</sup>                  | 0.19 ±0.11<br>(0.07 - 0.35)       |                                   | 0.24 ±0.11<br>(0.14 - 0.42)       |                                   |
| $m_{s,O_3}$ , ppb                                    | 40.80 ±11.88<br>(17.76 - 72.41)   | 37.41 ±8.23<br>(21.31 - 63.41)    | 40.16 ±11.88<br>(15.58 - 72.95)   | 40.42 ±10.80<br>(19.41 - 70.27)   |
| $F_{ex,O_3}$ , nmol m <sup>-2</sup> s <sup>-1</sup>  | -0.367 ±0.174<br>(-1.153 - 0.086) | -0.019 ±0.316<br>(-0.889 - 0.293) | -0.386 ±0.156<br>(-1.167 - 0.152) | -0.180 ±0.123<br>(-1.141 - 0.255) |
| $v_{dep,O_3}$ , mm s <sup>-1</sup>                   | 0.22 ±0.11<br>(0.07 - 0.38)       |                                   | 0.20 ±0.09<br>(0.06 - 0.32)       |                                   |
| $F_{ex,CO_2}$ , μmol m <sup>-2</sup> s <sup>-1</sup> | -0.57 ±0.47<br>(-2.66 - 0.20)     | 0.09 ±0.07<br>(-0.05 - 0.34)      | -0.59 ±0.45<br>(-2.01 - 0.24)     | 0.13 ±0.07<br>(-0.77 - 0.52)      |
| $F_{ex,H_2O}$ , mmol m <sup>-2</sup> s <sup>-1</sup> | 0.07 ±0.06<br>(0 - 0.39)          | 0.01 ±0.01<br>(0 - 0.03)          | 0.09 ±0.06<br>(0 - 0.28)          | 0.01 ±0.01<br>(0 - 0.03)          |
| $g_{H_2O}$ , cm s <sup>-1</sup>                      | 0.03 ±0.04<br>(0 - 0.54)          | 0.01 ±0.03<br>(0 - 0.07)          | 0.05 ±0.06<br>(0 - 0.83)          | 0.01 ±0.014<br>(0 - 0.17)         |
| $g_{NO_2,p}$ , cm s <sup>-1</sup>                    | 0.020 ±0.022<br>(0 - 0.34)        | 0.007 ±0.006<br>(0 - 0.042)       | 0.031 ±0.040<br>(0 - 0.513)       | 0.006 ±0.005<br>(0 - 0.107)       |
| $T_{leaf}$ , °C                                      | 17.9 ±4.7<br>(6.5 - 38.7)         | 11.3 ±2.8<br>(6.3 - 16.7)         | 18.3 ±4.9<br>(6.3 - 33.1)         | 13.3 ±3.3<br>(6.3 - 22.4)         |
| $rH_{out}$ , %                                       | 66.7 ±17.5<br>(32.3 - 99.9)       | 85.4 ±11.1<br>(62.5 - 99.9)       | 66.0 ±17.8<br>(32.6 - 99.9)       | 79.0 ±14.2<br>(40.3 - 99.9)       |
| PAR, μmol m <sup>-2</sup> s <sup>-1</sup>            | 231 ±273<br>(0 - 1875)            | -<br>-                            | 255 ±280<br>(0 - 1848)            | -<br>-                            |

<sup>a</sup> daytime values were used when global radiation > 5 W m<sup>-2</sup>

\* limit of detection (LOD)

**Table 19:** Percentage of significant differences ( $\Delta m_i$ ) of sample chamber 1 and 2. Only concentrations above LOD were considered.

|                       | sample chamber 1<br>significant $\Delta m_i$ % of total<br>(number of total) |               |                 | sample chamber 2<br>significant $\Delta m_i$ % of total<br>(number of total) |               |                 |
|-----------------------|--|---------------|-----------------|--|---------------|-----------------|
|                       | all<br>(2988)  | day<br>(1885) | night<br>(1103) | all<br>(2993)  | day<br>(1887) | night<br>(1106) |
|                       | <b>NO</b>  | 24            | 33              | 7  | 24            | 33              |
| <b>NO<sub>2</sub></b> | 57   | 62            | 48              | 67   | 69            | 63              |
| <b>O<sub>3</sub></b>  | 96   | 98            | 93              | 98   | 99            | 97              |

**Table 20:** Definition of the classes, which were used for the classification of measured data. All displayed data are mean values. Leaf conductance ( $g_{H_2O}$ ) were calculated on basis of projected leaf area and total leaf surface area.

| class                   |                           | 1                         | 2                   | 3                   | 4                   | 5                   | 6                   | 7                   |                     |
|-------------------------|---------------------------|---------------------------|---------------------|---------------------|---------------------|---------------------|---------------------|---------------------|---------------------|
| $g_{H_2O}$<br>projected | $cm\ s^{-1}$              | 0.01                      | 0.025               | 0.06                | 0.08                | 0.1                 | 0.13                | 0.16                |                     |
|                         | $A_{leaf}$                | -                         | -                   | -                   | -                   | -                   | -                   | -                   |                     |
| $g_{H_2O}$<br>total     | $cm\ s^{-1}$              | 0.025                     | 0.06                | 0.08                | 0.1                 | 0.13                | 0.16                | 1.0                 |                     |
|                         | $A_{leaf}$                | -                         | -                   | -                   | -                   | -                   | -                   | -                   |                     |
| chamber 1               | <b>PAR</b>                | $\mu mol\ m^{-2}\ s^{-1}$ | 130 $\pm$ 261       | 200 $\pm$ 334       | 253 $\pm$ 311       | 279 $\pm$ 300       | 297 $\pm$ 312       | 355 $\pm$ 335       | 319 $\pm$ 365       |
|                         | <b>T<sub>air</sub></b>    | $^{\circ}C$               | 18.8 $\pm$ 4.9      | 16.8 $\pm$ 4.9      | 16.5 $\pm$ 4.2      | 15.7 $\pm$ 3.7      | 14.3 $\pm$ 3.8      | 13.9 $\pm$ 3.6      | 12.0 $\pm$ 3.4      |
|                         | <b>r.H.</b>               | %                         | 54 $\pm$ 17         | 64 $\pm$ 18         | 64 $\pm$ 16         | 67 $\pm$ 14         | 69 $\pm$ 14         | 70 $\pm$ 13         | 80 $\pm$ 14         |
|                         | <b>F<sub>ex,CO2</sub></b> | $\mu mol\ m^{-2}\ s^{-1}$ | -0.15<br>$\pm$ 0.12 | -0.37<br>$\pm$ 0.22 | -0.62<br>$\pm$ 0.26 | -0.74<br>$\pm$ 0.31 | -0.86<br>$\pm$ 0.37 | -1.02<br>$\pm$ 0.42 | -1.05<br>$\pm$ 0.46 |
|                         | <b>F<sub>ex,H2O</sub></b> | $mmol\ m^{-2}\ s^{-1}$    | 0.03<br>$\pm$ 0.02  | 0.05<br>$\pm$ 0.04  | 0.08<br>$\pm$ 0.05  | 0.09<br>$\pm$ 0.05  | 0.10<br>$\pm$ 0.06  | 0.11<br>$\pm$ 0.07  | 0.09<br>$\pm$ 0.08  |
|                         | <b>PAR</b>                | $\mu mol\ m^{-2}\ s^{-1}$ | 51 $\pm$ 158        | 157 $\pm$ 251       | 279 $\pm$ 353       | 336 $\pm$ 387       | 278 $\pm$ 290       | 320 $\pm$ 307       | 322 $\pm$ 329       |
|                         | <b>T<sub>air</sub></b>    | $^{\circ}C$               | 16.9 $\pm$ 4.7      | 17.4 $\pm$ 5.1      | 17.4 $\pm$ 4.7      | 16.8 $\pm$ 4.2      | 15.8 $\pm$ 3.9      | 14.6 $\pm$ 3.7      | 12.6 $\pm$ 3.5      |
| chamber 2               | <b>r.H.</b>               | %                         | 63 $\pm$ 19         | 61 $\pm$ 19         | 59 $\pm$ 17         | 61 $\pm$ 16         | 66 $\pm$ 14         | 69 $\pm$ 14         | 77 $\pm$ 16         |
|                         | <b>F<sub>ex,CO2</sub></b> | $\mu mol\ m^{-2}\ s^{-1}$ | -0.03<br>$\pm$ 0.11 | -0.25<br>$\pm$ 0.22 | -0.53<br>$\pm$ 0.26 | -0.67<br>$\pm$ 0.31 | -0.77<br>$\pm$ 0.31 | -0.88<br>$\pm$ 0.36 | -0.98<br>$\pm$ 0.42 |
|                         | <b>F<sub>ex,H2O</sub></b> | $mmol\ m^{-2}\ s^{-1}$    | 0.02<br>$\pm$ 0.02  | 0.06<br>$\pm$ 0.05  | 0.10<br>$\pm$ 0.06  | 0.11<br>$\pm$ 0.07  | 0.11<br>$\pm$ 0.06  | 0.11<br>$\pm$ 0.06  | 0.09<br>$\pm$ 0.06  |

Before calculating exchange flux densities, compensation point concentrations and deposition velocities, all data were not only controlled for significant concentration differences but also classified (see Sect. 4.1.2). Table 20 displays the ambient and plant conditions of the single classes for each chamber. Depending on the placement of chamber installation the ambient conditions might differ between the two chambers, especially for PAR. Using leaf conductance of  $0.01 \text{ cm s}^{-1}$  ( $0.004 \text{ cm s}^{-1}$  per total  $A_{leaf}$ ) as lower limit excluded situations of condensation inside the chamber from further considerations.

#### 4.2.5 NO<sub>2</sub> exchange flux density

The exchange flux densities of NO<sub>2</sub> ( $F_{ex,NO_2}$ ) were calculated according to Eq. (8.4) and their standard errors according to Eq. (19). NO<sub>2</sub> deposition velocities ( $v_{dep,NO_2}$ ) and NO<sub>2</sub> compensation point concentrations ( $m_{comp,NO_2}$ ) were determined using the bi-variate regression analysis (see Sect. 2.1.2). The results of the single classes 1 -7 are displayed in Figure 27 to Figure 30 for data from sample chamber 1 and in Figure 31 to Figure 34 for data from sample chamber 2 (refer to the schematic representation in Figure 6). Panels 1a -7a represent the results of bi-variate weighted linear regression analysis between NO<sub>2</sub> concentrations at the plant chamber's inlet ( $m_{a,NO_2}$ ) and outlet ( $m_{s,NO_2}$ ), while at panels 1b -7b show these data for  $F_{ex,NO_2}$  versus  $m_{s,NO_2}$ . The blue line represents  $v_{dep,NO_2}$  and the red filled circle marks  $m_{comp,NO_2}$ . The blue circles identify  $F_{ex,NO_2}$  data which were significant for  $\Delta m_{NO_2} = (m_{a,NO_2} - m_{s,NO_2})$ . The bi-variate regression analysis (see Sect. 3.1.6) of the data from sample chamber 1 resulted in  $R^2(m_{a,NO_2}, m_{s,NO_2})$  between 0.8709 and 0.9401 and  $v_{dep,NO_2}$  between 0.07 and  $0.35 \text{ mm s}^{-1}$ . The  $v_{dep,NO_2}$  increased with the number of the classes, that is, as the class number and  $g_{H_2O}$  gets higher the deposition velocity increases. The determined  $m_{comp,NO_2}$  ranged between  $2.4 \pm 9.63$  and  $29.0 \pm 16.30 \text{ nmol m}^{-3}$  (0.05 - 0.65 ppb). The significance probabilities of  $m_{comp,NO_2} \neq 0$  vary from 96.90 % ("likely") to 99.99 % ("highly significant"). The results of sample chamber 2 were mostly comparable.  $R^2(m_{a,NO_2}, m_{s,NO_2})$  reached values between 0.8106 and 0.9702.  $v_{dep,NO_2}$  reached values mainly in the same range but the determination of  $m_{comp,NO_2}$  became complicated at this point. For classes 2, 3 and 6,  $m_{comp,NO_2}$  results in negative values with a probability of 99.99 % ("highly significant"). However a negative NO<sub>2</sub> compensation point concentration is physically meaningless.

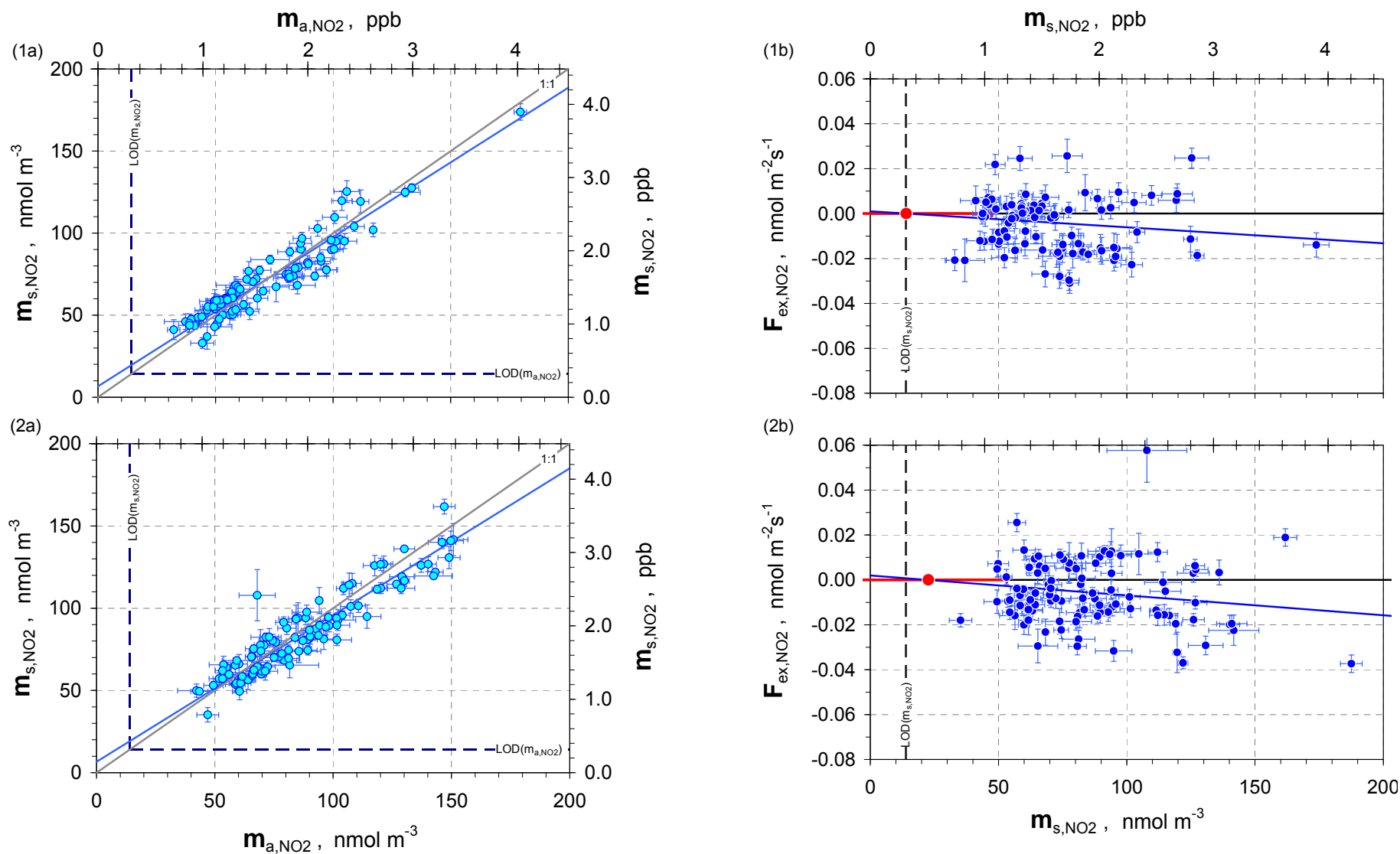


**Figure 27: NO<sub>2</sub> measurements, data class 1 and 2 of sample chamber 1**

(1a), (2a) NO<sub>2</sub> concentration measured at the outlet of the dynamic plant chamber ( $m_{s,NO_2}$ ) vs. NO<sub>2</sub> concentration measured at the inlet of the dynamic plant chamber ( $m_{a,NO_2}$ ). Blue circles identify data pairs for significance of  $\Delta m_{NO_2} = (m_{a,NO_2} - m_{s,NO_2})$ . Blue line is calculated according to bi-variate weighted linear least-squares fitting regression analysis. (1b), (2b) NO<sub>2</sub> exchange flux density ( $F_{ex,NO_2}$ ) vs. NO<sub>2</sub> concentration measured at the outlet of the dynamic plant chamber ( $m_{s,NO_2}$ ). NO<sub>2</sub> compensation point concentration  $m_{comp,NO_2}$  is represented by red filled circle.

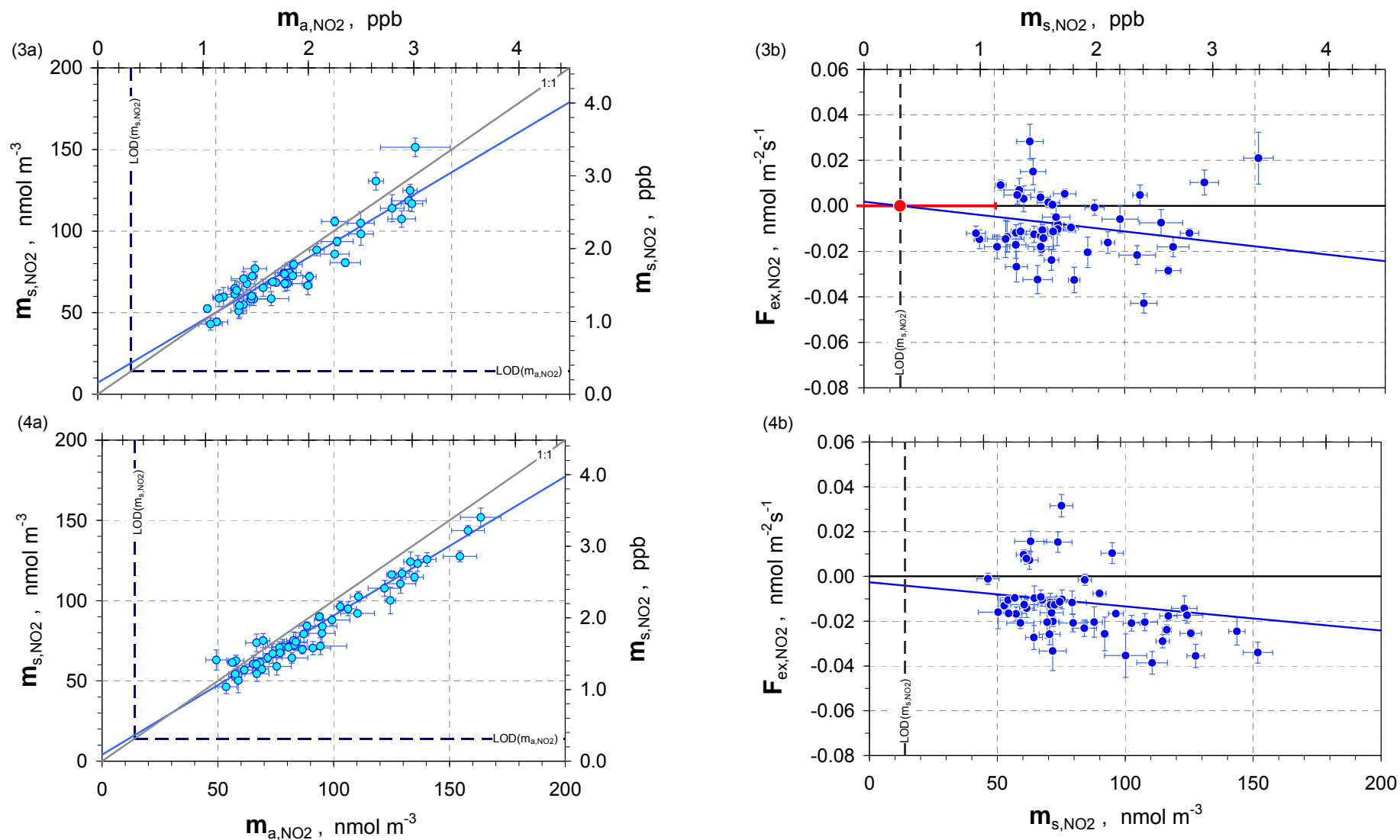


**Figure 28: NO<sub>2</sub> measurements, data class 3 and 4 of sample chamber 1**

**(3a), (4a)** NO<sub>2</sub> concentration measured at the outlet of the dynamic plant chamber ( $m_{s,NO_2}$ ) vs. NO<sub>2</sub> concentration measured at the inlet of the dynamic plant chamber ( $m_{a,NO_2}$ ). Blue circles identify data pairs for significance of  $\Delta m_{NO_2} = (m_{a,NO_2} - m_{s,NO_2})$ . Blue line is calculated according to bi-variate weighted linear least-squares fitting regression analysis. **(3b), (4b)** NO<sub>2</sub> exchange flux density ( $F_{ex,NO_2}$ ) vs. NO<sub>2</sub> concentration measured at the outlet of the dynamic plant chamber ( $m_{s,NO_2}$ ). NO<sub>2</sub> compensation point concentration  $m_{comp,NO_2}$  is represented by red filled circle.

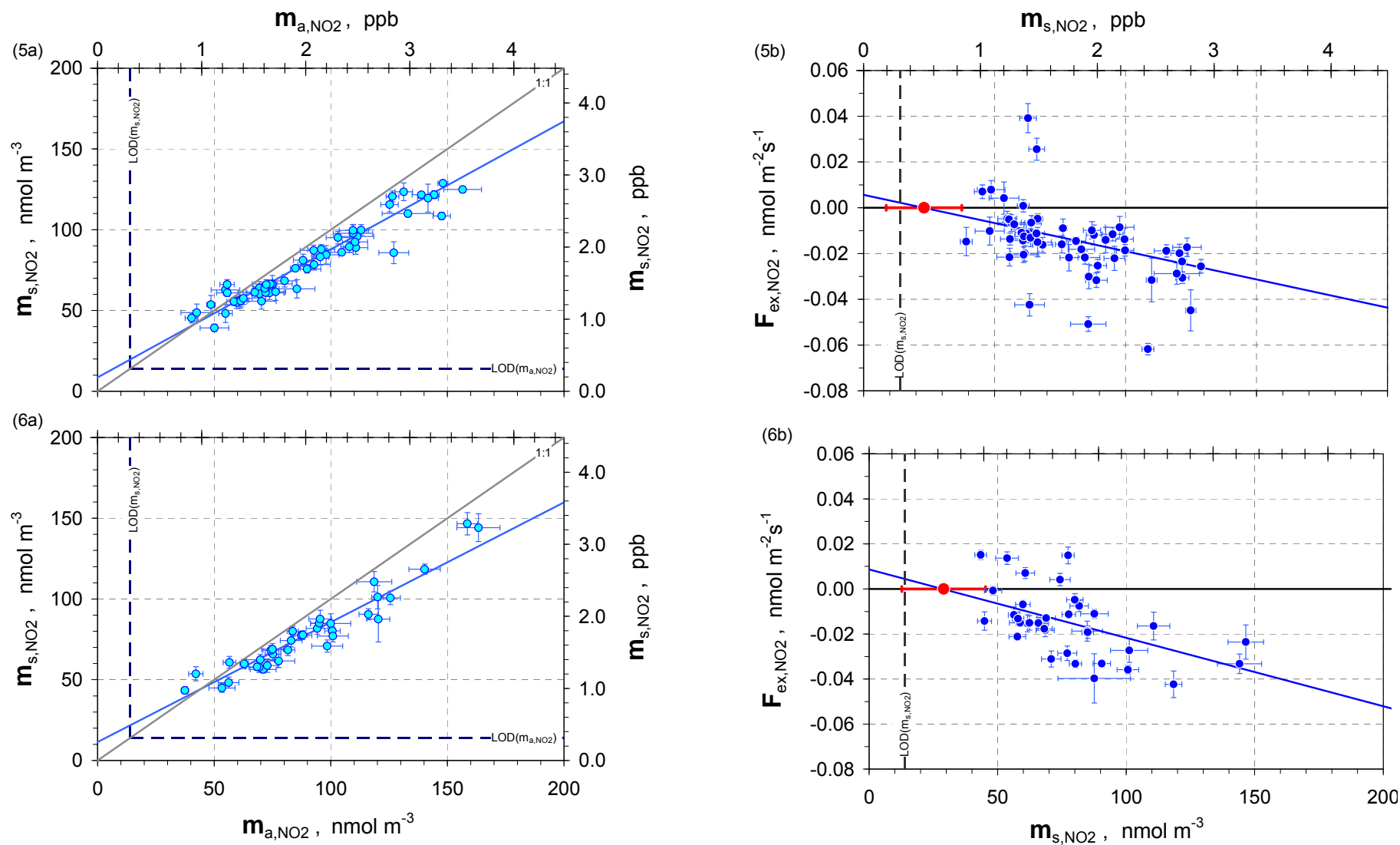


**Figure 29: NO<sub>2</sub> measurements, data class 5 and 6 of sample chamber 1**

(5a), (6a) NO<sub>2</sub> concentration measured at the outlet of the dynamic plant chamber ( $m_{s,NO_2}$ ) vs. NO<sub>2</sub> concentration measured at the inlet of the dynamic plant chamber ( $m_{a,NO_2}$ ). Blue circles identify data pairs for significance of  $\Delta m_{NO_2} = (m_{a,NO_2} - m_{s,NO_2})$ . Blue line is calculated according to bi-variate weighted linear least-squares fitting regression analysis. (5b), (6b) NO<sub>2</sub> exchange flux density ( $F_{ex,NO_2}$ ) vs. NO<sub>2</sub> concentration measured at the outlet of the dynamic plant chamber ( $m_{s,NO_2}$ ). NO<sub>2</sub> compensation point concentration  $m_{comp,NO_2}$  is represented by red filled circle.



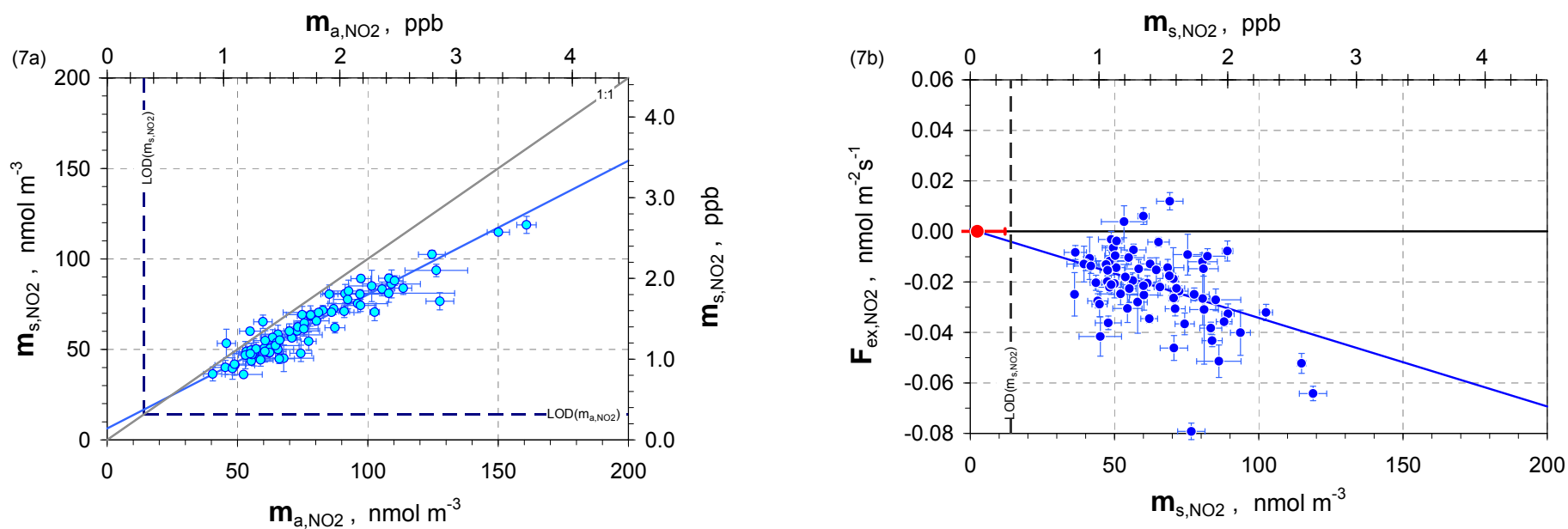


**Figure 30: NO<sub>2</sub> measurements, data class 7 of sample chamber 1**

**(7a)** NO<sub>2</sub> concentration measured at the outlet of the dynamic plant chamber ( $m_{s,NO_2}$ ) vs. NO<sub>2</sub> concentration measured at the inlet of the dynamic plant chamber ( $m_{a,NO_2}$ ). Blue circles identify data pairs for significance of  $\Delta m_{NO_2} = (m_{a,NO_2} - m_{s,NO_2})$ . Blue line is calculated according to bi-variate weighted linear least-squares fitting regression analysis. **(7b)** NO<sub>2</sub> exchange flux density ( $F_{ex,NO_2}$ ) vs. NO<sub>2</sub> concentration measured at the outlet of the dynamic plant chamber ( $m_{s,NO_2}$ ). NO<sub>2</sub> compensation point concentration  $m_{comp,NO_2}$  is represented by red filled circle.

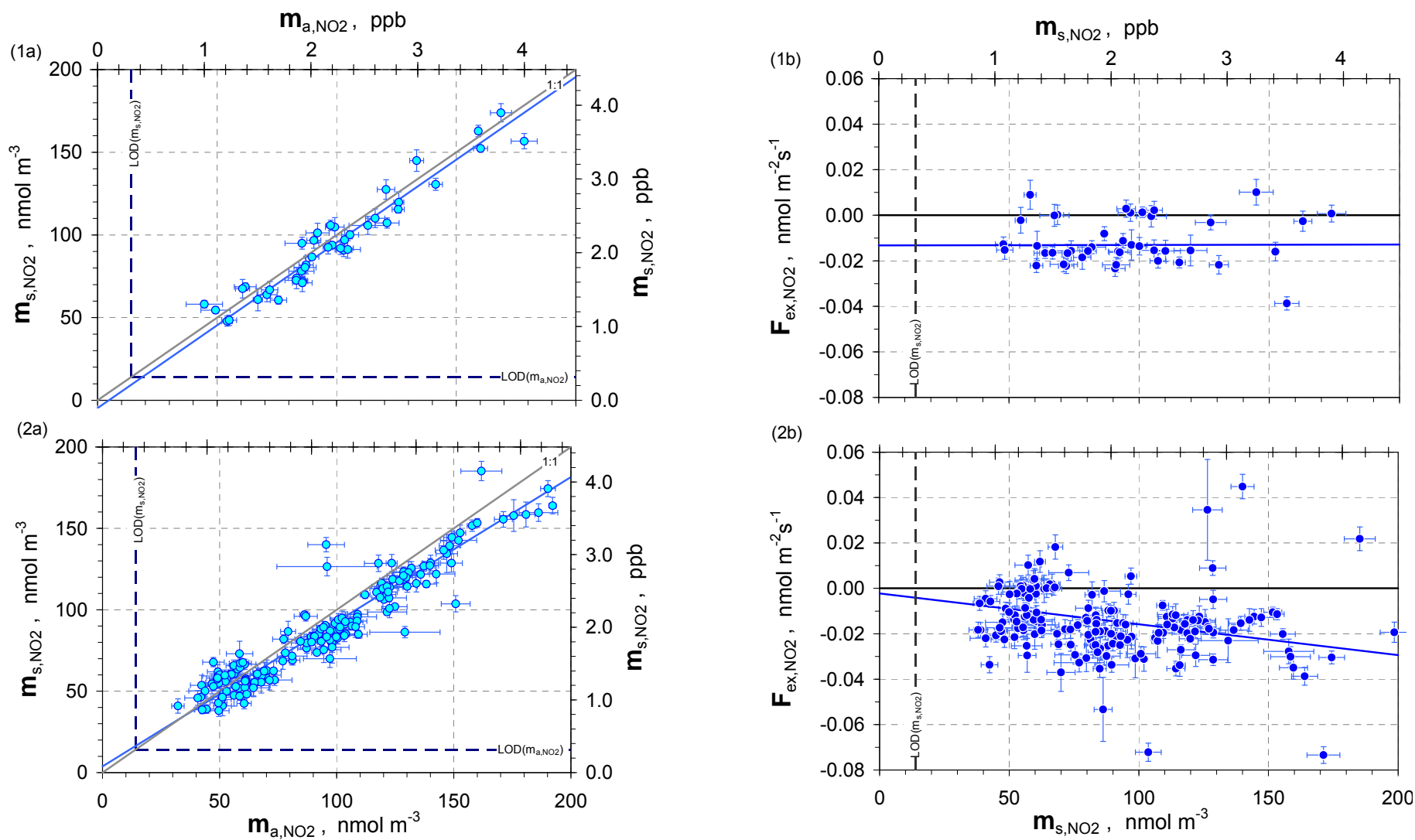


**Figure 31: NO<sub>2</sub> measurements, data class 1 and 2 of sample chamber 2**

**(1a), (2a)** NO<sub>2</sub> concentration measured at the outlet of the dynamic plant chamber ( $m_{s,NO_2}$ ) vs. NO<sub>2</sub> concentration measured at the inlet of the dynamic plant chamber ( $m_{a,NO_2}$ ). Blue circles identify data pairs for significance of  $\Delta m_{NO_2} = (m_{a,NO_2} - m_{s,NO_2})$ . Blue line is calculated according to bi-variate weighted linear least-squares fitting regression analysis. **(1b), (2b)** NO<sub>2</sub> exchange flux density ( $F_{ex,NO_2}$ ) vs. NO<sub>2</sub> concentration measured at the outlet of the dynamic plant chamber ( $m_{s,NO_2}$ ). NO<sub>2</sub> compensation point concentration  $m_{comp,NO_2}$  is represented by red filled circle.

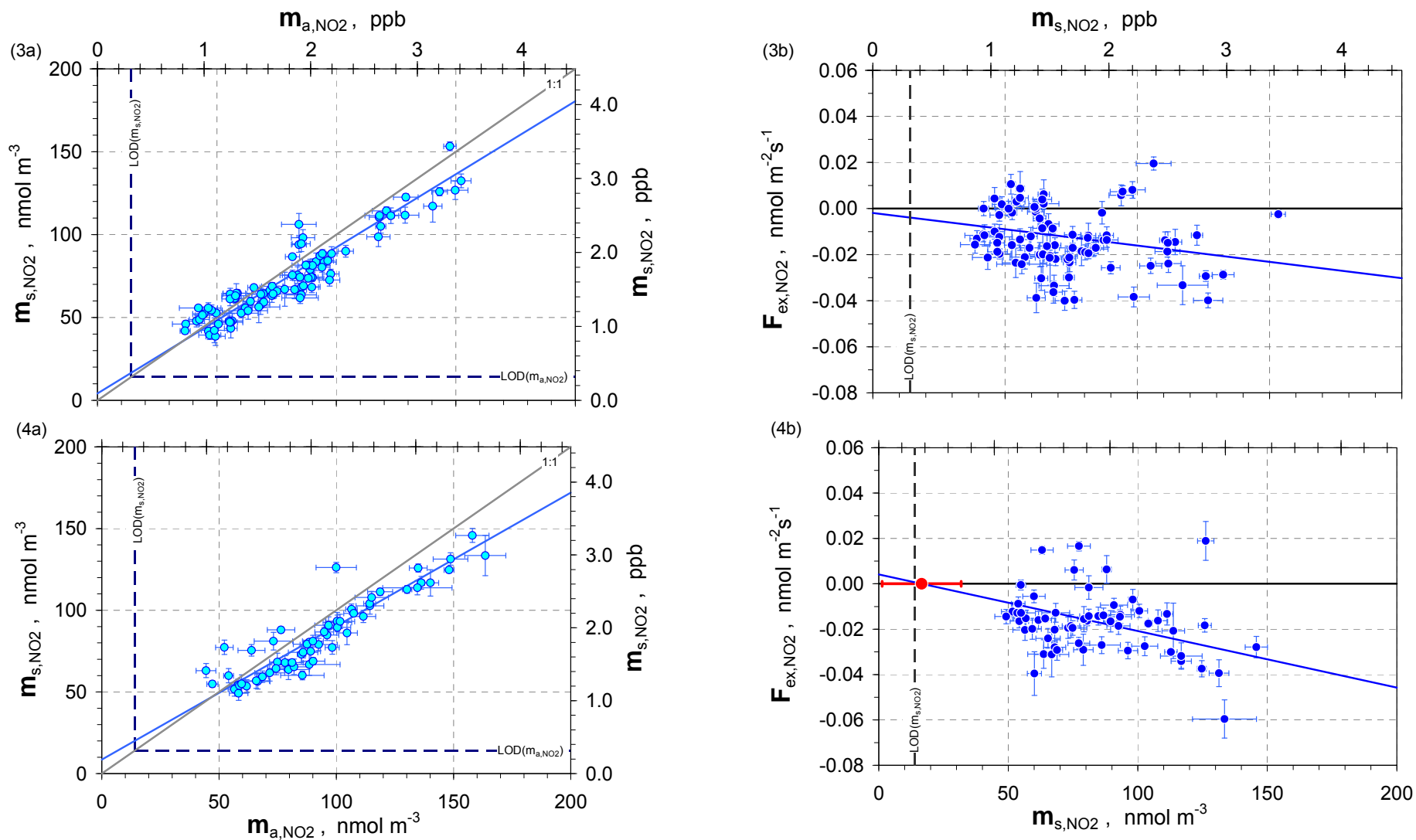


**Figure 32: NO<sub>2</sub> measurements, data class 3 and 4 of sample chamber 2**

**(3a), (4a)** NO<sub>2</sub> concentration measured at the outlet of the dynamic plant chamber ( $m_{s,NO_2}$ ) vs. NO<sub>2</sub> concentration measured at the inlet of the dynamic plant chamber ( $m_{a,NO_2}$ ). Blue circles identify data pairs for significance of  $\Delta m_{NO_2} = (m_{a,NO_2} - m_{s,NO_2})$ . Blue line is calculated according to bi-variate weighted linear least-squares fitting regression analysis. **(3b), (4b)** NO<sub>2</sub> exchange flux density ( $F_{ex,NO_2}$ ) vs. NO<sub>2</sub> concentration measured at the outlet of the dynamic plant chamber ( $m_{s,NO_2}$ ). NO<sub>2</sub> compensation point concentration  $m_{comp,NO_2}$  is represented by red filled circle.

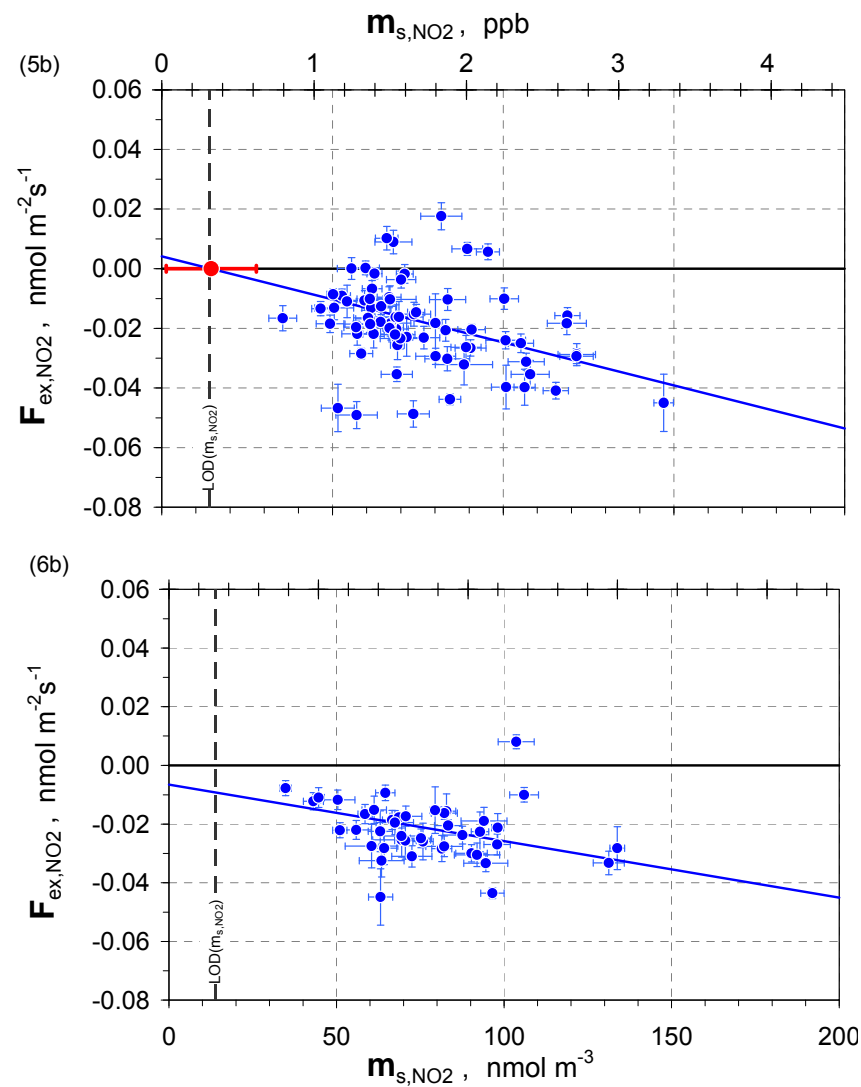
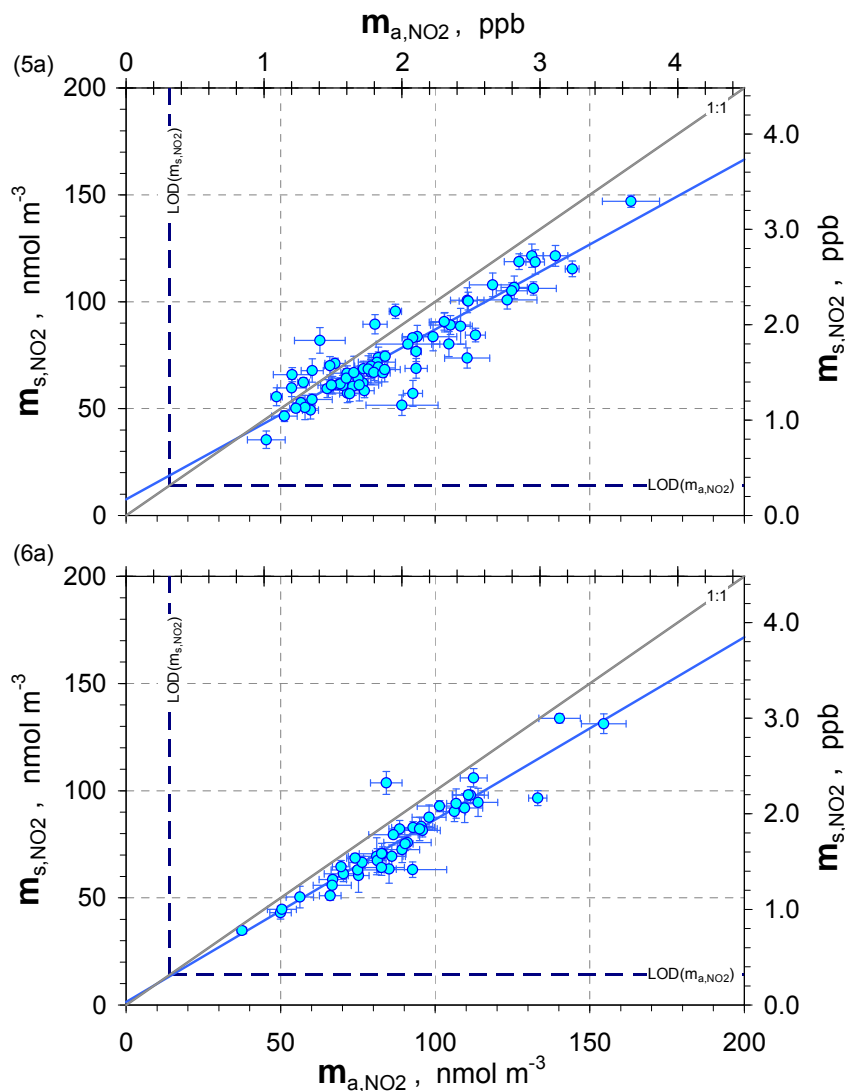


**Figure 33: NO<sub>2</sub> measurements, data class 5 and 6 of sample chamber 2**

(5a), (6a) NO<sub>2</sub> concentration measured at the outlet of the dynamic plant chamber ( $m_{s,NO_2}$ ) vs. NO<sub>2</sub> concentration measured at the inlet of the dynamic plant chamber ( $m_{a,NO_2}$ ). Blue circles identify data pairs for significance of  $\Delta m_{NO_2} = (m_{a,NO_2} - m_{s,NO_2})$ . Blue line is calculated according to bi-variate weighted linear least-squares fitting regression analysis. (5b), (6b) NO<sub>2</sub> exchange flux density ( $F_{ex,NO_2}$ ) vs. NO<sub>2</sub> concentration measured at the outlet of the dynamic plant chamber ( $m_{s,NO_2}$ ). NO<sub>2</sub> compensation point concentration  $m_{comp,NO_2}$  is represented by red filled circle.

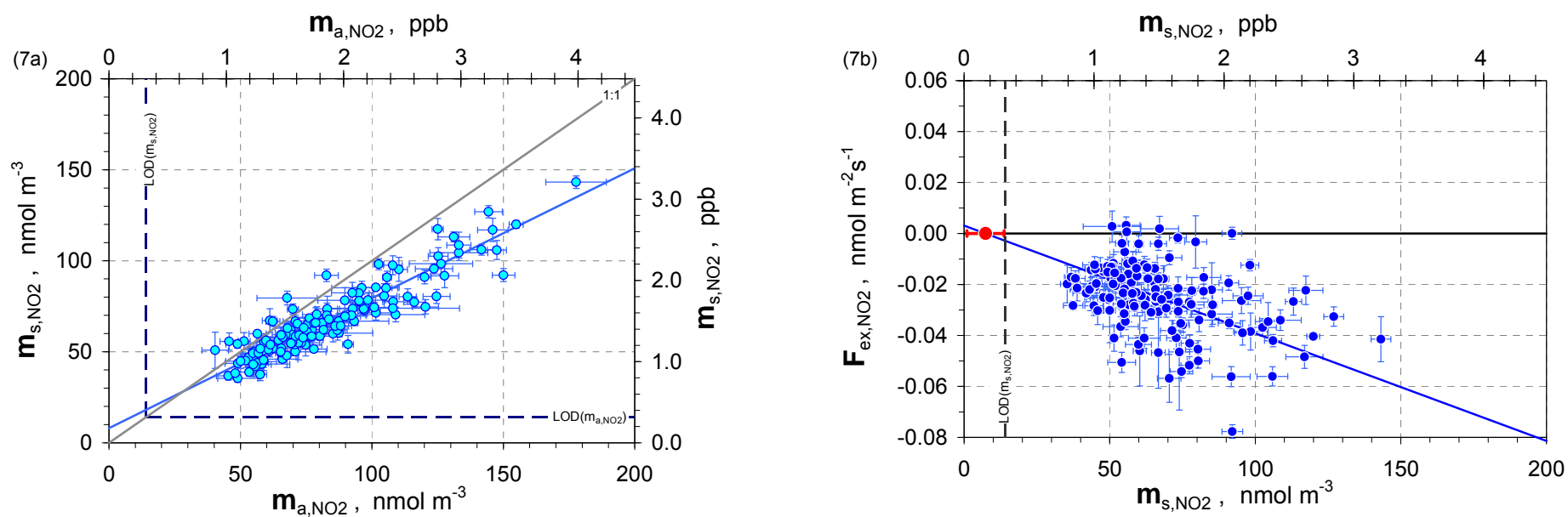


**Figure 34: NO<sub>2</sub> measurements, data class 7 of sample chamber 2**

**(7a)** NO<sub>2</sub> concentration measured at the outlet of the dynamic plant chamber ( $m_{s,NO_2}$ ) vs. NO<sub>2</sub> concentration measured at the inlet of the dynamic plant chamber ( $m_{a,NO_2}$ ). Blue circles identify data pairs for significance of  $\Delta m_{NO_2} = (m_{a,NO_2} - m_{s,NO_2})$ . Blue line is calculated according to bi-variate weighted linear least-squares fitting regression analysis. **(7b)** NO<sub>2</sub> exchange flux density ( $F_{ex,NO_2}$ ) vs. NO<sub>2</sub> concentration measured at the outlet of the dynamic plant chamber ( $m_{s,NO_2}$ ). NO<sub>2</sub> compensation point concentration  $m_{comp,NO_2}$  is represented by red filled circle.

Details of statistical evaluation for NO<sub>2</sub> and O<sub>3</sub> data of sample chamber 1 are listed in Table 21 and for data of sample chamber 2 in Table 22.

**Table 21:** Parameters of bi-variate weighted linear least-squares fitting regression analysis (see Sect. 3.1.6) for data classes 1 -7 of sample chamber 1. Only significant data of  $\Delta m_i = (m_{a,i} - m_{s,i})$  were applied.

| statistical quantity   | unit                 | NO <sub>2</sub> | O <sub>3</sub> | NO <sub>2</sub> | O <sub>3</sub> |
|------------------------|----------------------|-----------------|----------------|-----------------|----------------|
| $N$                    | [1]                  | 91              | 278            | 55              | 226            |
| $R^2(m_{a,i};m_{s,i})$ | [1]                  | 0.8939          | 0.9963         | 0.9248          | 0.9872         |
| $n$                    | nmol m <sup>-3</sup> | 6.5 ±1.75       |                | 8.6 ±2.09       |                |
| $m$                    | [1]                  | 0.91 ±0.025     | 0.95 ±0.002    | 0.79 ±0.021     | 0.82 ±0.003    |
| $m_{comp,i}$           | nmol m <sup>-3</sup> | 14.0 ±33.38     |                | 23.1 ±14.43     |                |
| $m_{comp,i} \neq 0?$   | %                    | 99.98 (HS)      |                | 99.99 (HS)      |                |
| $v_{dep,i}$            | mm s <sup>-1</sup>   | 0.07 ±0.059     | 0.07 ±0.004    | 0.25 ±0.045     | 0.27 ±0.0008   |
| $N$                    | [1]                  | 102             | 377            | 35              | 185            |
| $R^2(m_{a,i};m_{s,i})$ | [1]                  | 0.8886          | 0.9932         | 0.9263          | 0.9910         |
| $n$                    | nmol m <sup>-3</sup> | 6.6 ±1.89       |                | 11.4 ±2.81      |                |
| $m$                    | [1]                  | 0.89 ±0.021     | 0.91 ±0.003    | 0.74 ±0.034     | 0.79 ±0.004    |
| $m_{comp,i}$           | nmol m <sup>-3</sup> | 22.7 ±30.49     |                | 29.0 ±16.30     |                |
| $m_{comp,i} \neq 0?$   | %                    | 99.99 (HS)      |                | 99.99 (HS)      |                |
| $v_{dep,i}$            | mm s <sup>-1</sup>   | 0.09 ±0.062     | 0.12 ±0.004    | 0.30 ±0.079     | 0.32 ±0.017    |
| $N$                    | [1]                  | 47              | 211            | 75              | 306            |
| $R^2(m_{a,i};m_{s,i})$ | [1]                  | 0.8709          | 0.9926         | 0.8861          | 0.9811         |
| $n$                    | nmol m <sup>-3</sup> | 7.1 ±3.19       |                | 6.3 ±1.99       |                |
| $m$                    | [1]                  | 0.86 ±0.041     | 0.87 ±0.004    | 0.74 ±0.025     |                |
| $m_{comp,i}$           | nmol m <sup>-3</sup> | 13.9 ±36.65     |                | 2.4 ±9.63       |                |
| $m_{comp,i} \neq 0?$   | %                    | 98.73 (S)       |                | 96.90 (L)       |                |
| $v_{dep,i}$            | mm s <sup>-1</sup>   | 0.13 ±0.071     | 0.18 ±0.009    | 0.35 ±0.034     | 0.38 ±0.014    |
| $N$                    | [1]                  | 52              | 210            |                 |                |
| $R^2(m_{a,i};m_{s,i})$ | [1]                  | 0.9401          | 0.9932         |                 |                |
| $n$                    | nmol m <sup>-3</sup> | 4.0 ±2.36       |                |                 |                |
| $m$                    | [1]                  | 0.87 ±0.026     | 0.85 ±0.003    |                 |                |
| $m_{comp,i}$           | nmol m <sup>-3</sup> | -24.3 ±35.61    |                |                 |                |
| $m_{comp,i} \neq 0?$   | %                    | 99.99 (HS)      |                |                 |                |
| $v_{dep,i}$            | mm s <sup>-1</sup>   | 0.11 ±0.076     | 0.22 ±0.009    |                 |                |

\* assumption for O<sub>3</sub>:  $m_{comp,O3} = 0$  ( $n_3 = 0$ ).

**Table 22:** Parameters of bi-variate weighted linear least-squares fitting regression analysis (see Sect. 3.1.6) for data classes 1 -7 of sample chamber 2. Only significant data of  $\Delta m_i = (m_{a,i} - m_{s,i})$  were applied.

| statistical quantity    | unit                 |                      | NO <sub>2</sub> | O <sub>3</sub> |              | NO <sub>2</sub> | O <sub>3</sub> |              |  |
|-------------------------|----------------------|----------------------|-----------------|----------------|--------------|-----------------|----------------|--------------|--|
| $R^2(m_{a,i}; m_{s,i})$ | $N$                  | [1]                  | class 1         | 43             | 152          | class 5         | 74             | 274          |  |
|                         | $n$                  | nmol m <sup>-3</sup> |                 | -4.7 ± 3.24    |              |                 |                | 7.5 ± 2.56   |  |
|                         | $m$                  | [1]                  |                 | 1.00 ± 0.031   | 0.95 ± 0.004 |                 | 0.78 ± 0.030   | 0.82 ± 0.004 |  |
|                         | $m_{comp,i}$         | nmol m <sup>-3</sup> |                 | 6860 ± 12428   |              |                 | 14.5 ± 13.20   |              |  |
|                         | $m_{comp,i} \neq 0?$ | %                    |                 | 28.08 (UL)     |              |                 | 99.99 (HS)     |              |  |
|                         | $v_{dep,i}$          | mm s <sup>-1</sup>   |                 | -0.002 ± 0.035 | 0.06 ± 0.004 |                 | 0.29 ± 0.061   | 0.26 ± 0.011 |  |
|                         |                      |                      |                 |                |              |                 |                |              |  |
| $R^2(m_{a,i}; m_{s,i})$ | $N$                  | [1]                  | class 2         | 102            | 443          | class 6         | 43             | 195          |  |
|                         | $n$                  | nmol m <sup>-3</sup> |                 | 3.7 ± 1.40     |              |                 |                | 1.4 ± 2.76   |  |
|                         | $m$                  | [1]                  |                 | 0.89 ± 0.014   | 0.91 ± 0.003 |                 | 0.85 ± 0.033   | 0.80 ± 0.005 |  |
|                         | $m_{comp,i}$         | nmol m <sup>-3</sup> |                 | -16.7 ± 13.94  |              |                 | -34.0 ± 22.60  |              |  |
|                         | $m_{comp,i} \neq 0?$ | %                    |                 | 99.99 (HS)     |              |                 | 99.99 (HS)     |              |  |
|                         | $v_{dep,i}$          | mm s <sup>-1</sup>   |                 | 0.14 ± 0.037   | 0.11 ± 0.004 |                 | 0.19 ± 0.050   | 0.28 ± 0.012 |  |
|                         |                      |                      |                 |                |              |                 |                |              |  |
| $R^2(m_{a,i}; m_{s,i})$ | $N$                  | [1]                  | class 3         | 87             | 283          | class 7         | 140            | 455          |  |
|                         | $n$                  | nmol m <sup>-3</sup> |                 | 4.1 ± 1.99     |              |                 |                | 8.1 ± 1.73   |  |
|                         | $m$                  | [1]                  |                 | 0.88 ± 0.024   | 0.87 ± 0.004 |                 | 0.71 ± 0.021   | 0.77 ± 0.005 |  |
|                         | $m_{comp,i}$         | nmol m <sup>-3</sup> |                 | -13.6 ± 19.45  |              |                 | 7.4 ± 6.40     |              |  |
|                         | $m_{comp,i} \neq 0?$ | %                    |                 | 99.99 (HS)     |              |                 | 99.99 (HS)     |              |  |
|                         | $v_{dep,i}$          | mm s <sup>-1</sup>   |                 | 0.14 ± 0.015   | 0.17 ± 0.007 |                 | 0.42 ± 0.067   | 0.32 ± 0.008 |  |
|                         |                      |                      |                 |                |              |                 |                |              |  |
| $R^2(m_{a,i}; m_{s,i})$ | $N$                  | [1]                  | class 4         | 59             | 208          |                 |                |              |  |
|                         | $n$                  | nmol m <sup>-3</sup> |                 | 8.5 ± 2.61     |              |                 |                |              |  |
|                         | $m$                  | [1]                  |                 | 0.82 ± 0.027   | 0.84 ± 0.004 |                 |                |              |  |
|                         | $m_{comp,i}$         | nmol m <sup>-3</sup> |                 | 16.5 ± 15.25   |              |                 |                |              |  |
|                         | $m_{comp,i} \neq 0?$ | %                    |                 | 99.99 (HS)     |              |                 |                |              |  |
|                         | $v_{dep,i}$          | mm s <sup>-1</sup>   |                 | 0.25 ± 0.047   | 0.22 ± 0.009 |                 |                |              |  |
|                         |                      |                      |                 |                |              |                 |                |              |  |

\* assumption for O<sub>3</sub>:  $m_{comp,O3} = 0$  ( $n_3 = 0$ ).

On closer consideration of the variation of  $F_{ex,NO_2}$  referring to the leaf conductance classes it became apparent that  $F_{ex,NO_2}$  increased with raising classes of  $g_{H_2O}$ . In Figure 35 the median of  $F_{ex,NO_2}$  for each class is presented as well as the interquartile ranges and the minimum and maximum of  $F_{ex,NO_2}$  for data measured at sample chamber 1. The data of sample chamber 2 are displayed in Figure 36. Both enclosed branches showed the same trend. At very low leaf conductance ( $g_{H_2O}$ ) the median of  $F_{ex,NO_2}$  reached values of  $-0.002 \text{ nmol m}^{-2} \text{ s}^{-1}$  (sample chamber 1) and  $-0.015 \text{ nmol m}^{-2} \text{ s}^{-1}$  (sample chamber 2) respectively. With increasing leaf conductance  $F_{ex,NO_2}$  rose up almost linear to  $0.020$  and  $0.024 \text{ nmol m}^{-2} \text{ s}^{-1}$  respectively. The connection between  $NO_2$  exchange rates and stomatal conductance can be identified.

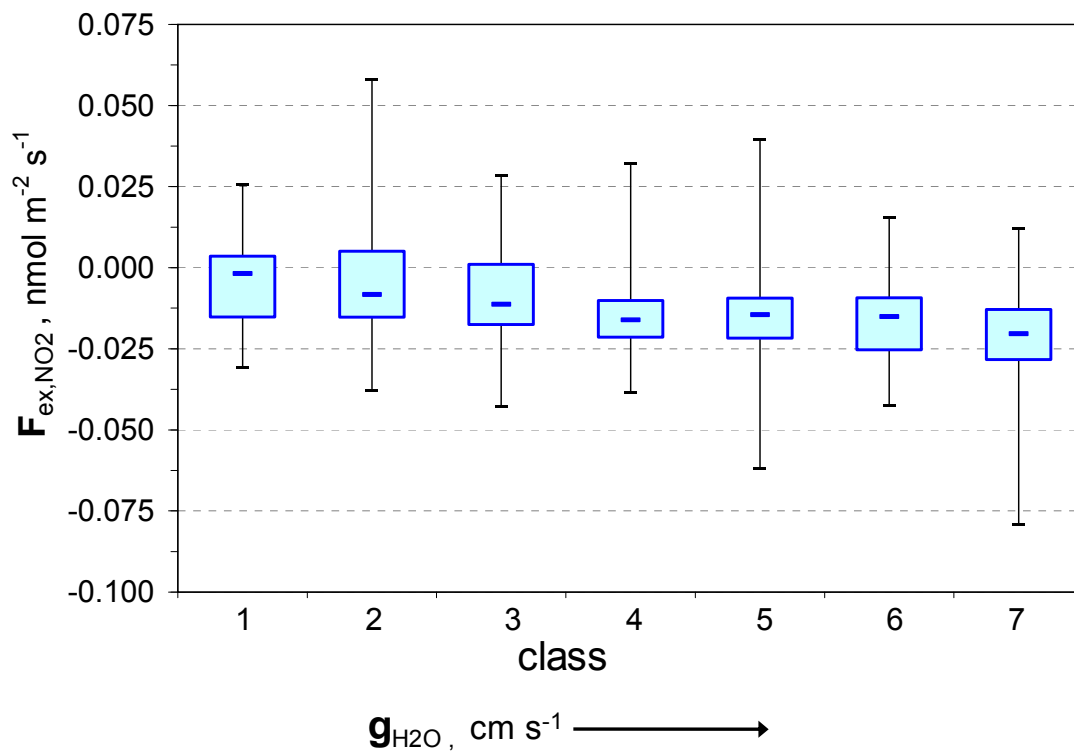


**Figure 35:** Variation of  $NO_2$  exchange flux density ( $F_{ex,NO_2}$ ) of sample chamber 1 for different leaf conductance classes (increasing values of leaf conductance from class 1 to 7). Blue lines denote the median, the boxes the interquartile ranges (0.25 – 0.75), the black lines the minimum and maximum.



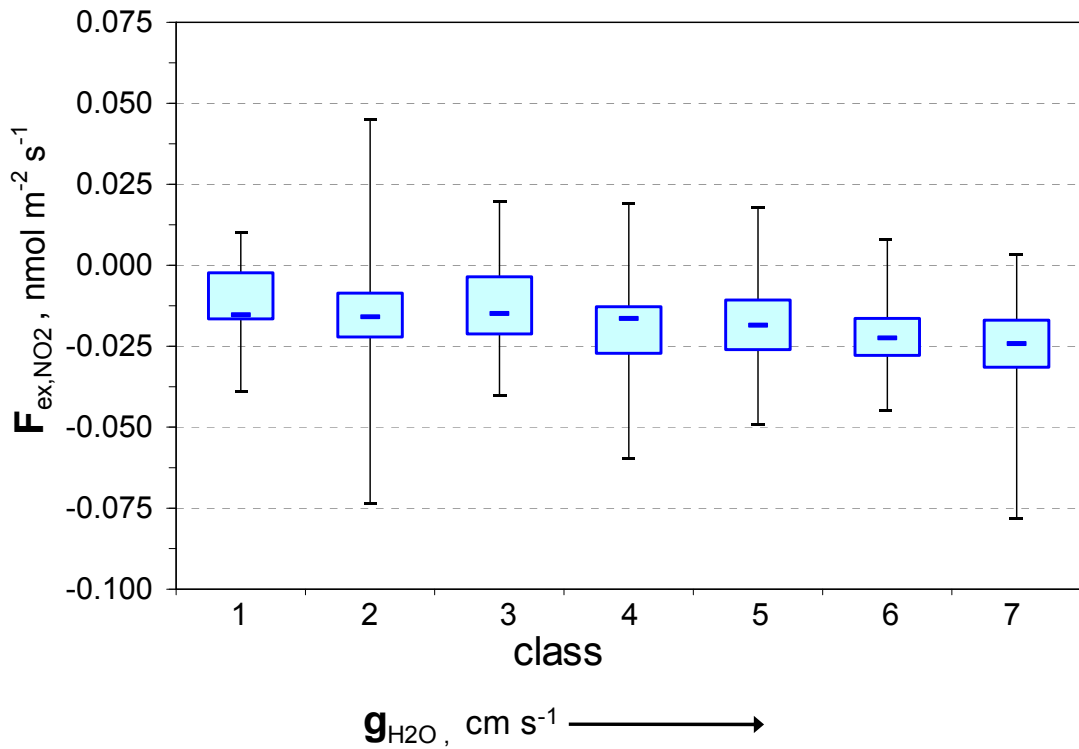


**Figure 36:** Variation of NO<sub>2</sub> exchange flux density ( $F_{ex,NO_2}$ ) of sample chamber 2 for different leaf conductance classes (increasing values of leaf conductance from class 1 to 7). Blue lines denote the median, the boxes the interquartile ranges (0.25 – 0.75), the black lines the minimum and maximum.

#### 4.2.6 O<sub>3</sub> exchange flux density

The analysis of the O<sub>3</sub> data was done in the same way as the analysis of the NO<sub>2</sub> data (see Sects. 2.1.2 and 2.1.3). The results for the evaluation of O<sub>3</sub> exchange flux densities ( $F_{ex,O_3}$ ) and O<sub>3</sub> deposition velocities ( $v_{dep,O_3}$ ) of the classes 1 -7 are presented in Figure 37 to Figure 40 for sample chamber 1 and in Figure 41 to Figure 44 for sample chamber 2. Panels 1a - 7a represent the results of bi-variate weighted linear regression analysis between O<sub>3</sub> concentrations at the plant chamber's inlet ( $m_{a,O_3}$ ) and outlet ( $m_{s,O_3}$ ), while in panels 1b - 7b those of  $F_{ex,O_3}$  versus  $m_{s,O_3}$  are shown. The orange line represents  $v_{dep,O_3}$ . The red circles identify  $F_{ex,O_3}$  data which were significant for  $\Delta m_{O_3} = (m_{a,O_3} - m_{s,O_3})$ . For the analysis of O<sub>3</sub> data an O<sub>3</sub> compensation point concentration  $m_{comp,O_3} = 0$  ( $n_3 = 0$ ) was assumed.

The bi-variate regression analysis for the data from sample chamber 1 resulted in  $R^2(m_{a,O_3}, m_{s,O_3})$  between 0.9811 and 0.9963 and  $v_{dep,O_3}$  ranged between  $0.07 \pm 0.059$  and  $0.38 \pm 0.014 \text{ mm s}^{-1}$ . Values of  $v_{dep,O_3}$  increased with raising class of leaf conductance  $g_{H_2O}$ . The results of sample chambers 1 were comparable with sample chamber 2. Analysis of  $O_3$  data from sample chamber 2 resulted in  $R^2(m_{a,O_3}, m_{s,O_3})$  between 0.9538 and 0.9938. Deposition velocity of  $O_3$  for the seven classes ranged between  $0.06 \pm 0.004$  and  $0.32 \pm 0.008 \text{ mm s}^{-1}$ . In Table 21 and Table 22 the details of the statistical analysis of the  $O_3$  data are listed.

In Figure 45 and Figure 46 the median, the interquartile ranges and the minimum and maximum of  $F_{ex,O_3}$  for each class of  $g_{H_2O}$  are displayed. It is obviously that values of  $F_{ex,O_3}$  increased when  $g_{H_2O}$  became greater. Therefore,  $O_3$  deposition increased with raising leaf conductance. The increasing of  $F_{ex,O_3}$  were more pronounced than the observed increasing of  $F_{ex,NO_2}$ . The median of  $F_{ex,O_3}$  ranged from -0.17 to -0.52  $\text{nmol m}^{-2} \text{ s}^{-1}$  for sample chamber 1 and from -0.16 to -0.49  $\text{nmol m}^{-2} \text{ s}^{-1}$  for sample chamber 2. The rate of increase between the single classes declined with raising class: at high leaf conductances a trend of saturation for the  $O_3$  uptake can be expected. The  $O_3$  exchange rates seem to depend on stomatal conductance like  $NO_2$  to a certain degree. Compared to  $NO_2$  deposition of  $O_3$  were higher at low  $g_{H_2O}$ , this may have been caused by  $O_3$  deposition to leaf, petiole and bark surfaces of the enclosed branches (due to high reactivity of ozone).

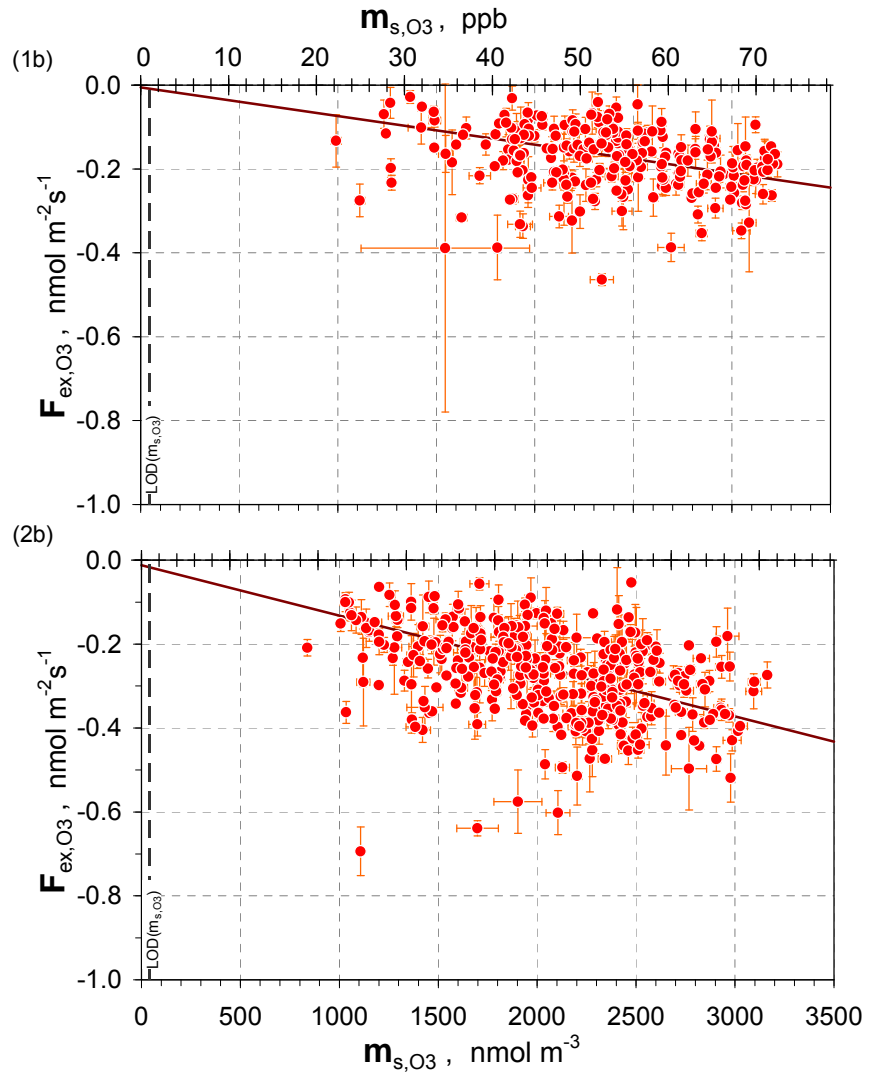
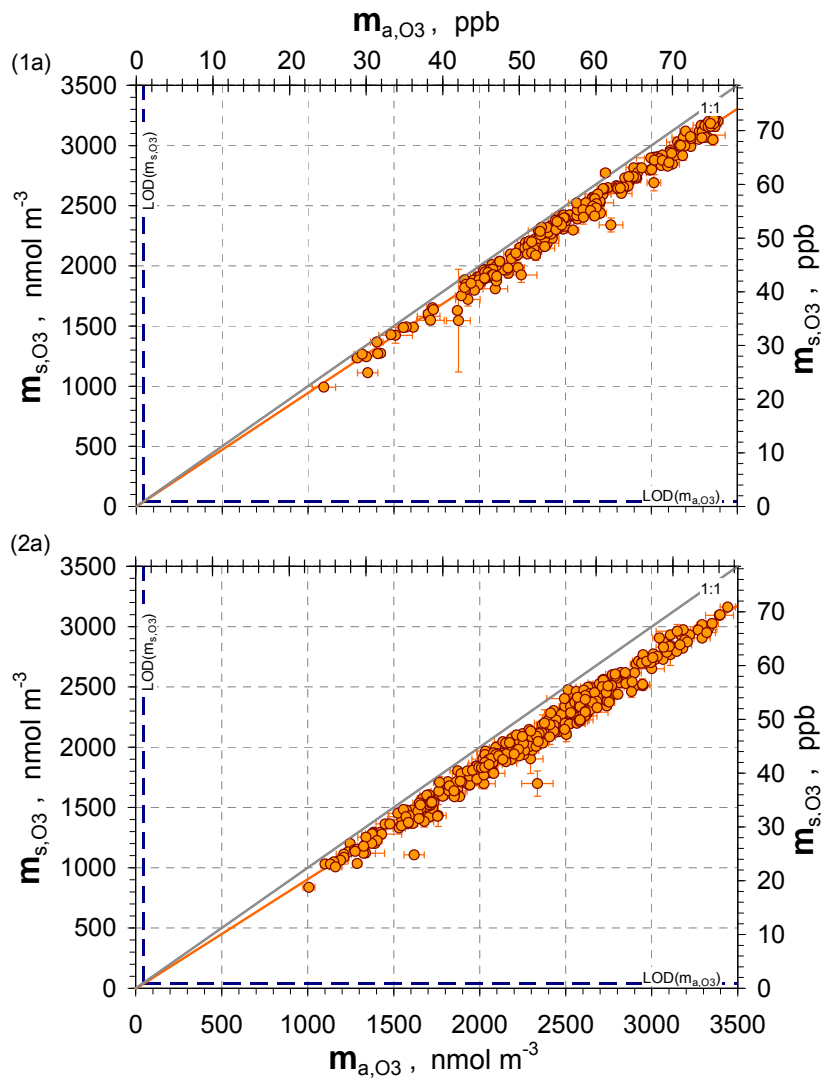


**Figure 37: O<sub>3</sub> measurements, data class 1 and 2 of sample chamber 1**

**(1a), (2a)** O<sub>3</sub> concentration measured at the outlet of the dynamic plant chamber ( $m_{s,O_3}$ ) vs. O<sub>3</sub> concentration measured at the inlet of the dynamic plant chamber ( $m_{a,O_3}$ ). Orange circles identify data pairs for significance of  $\Delta m_{O_3} = (m_{a,O_3} - m_{s,O_3})$ . Orange line is calculated according to bi-variate weighted linear least-squares fitting regression analysis. **(1b), (2b)** O<sub>3</sub> exchange flux density ( $F_{ex,O_3}$ ) vs. O<sub>3</sub> concentration measured at the outlet of the dynamic plant chamber ( $m_{s,O_3}$ ).

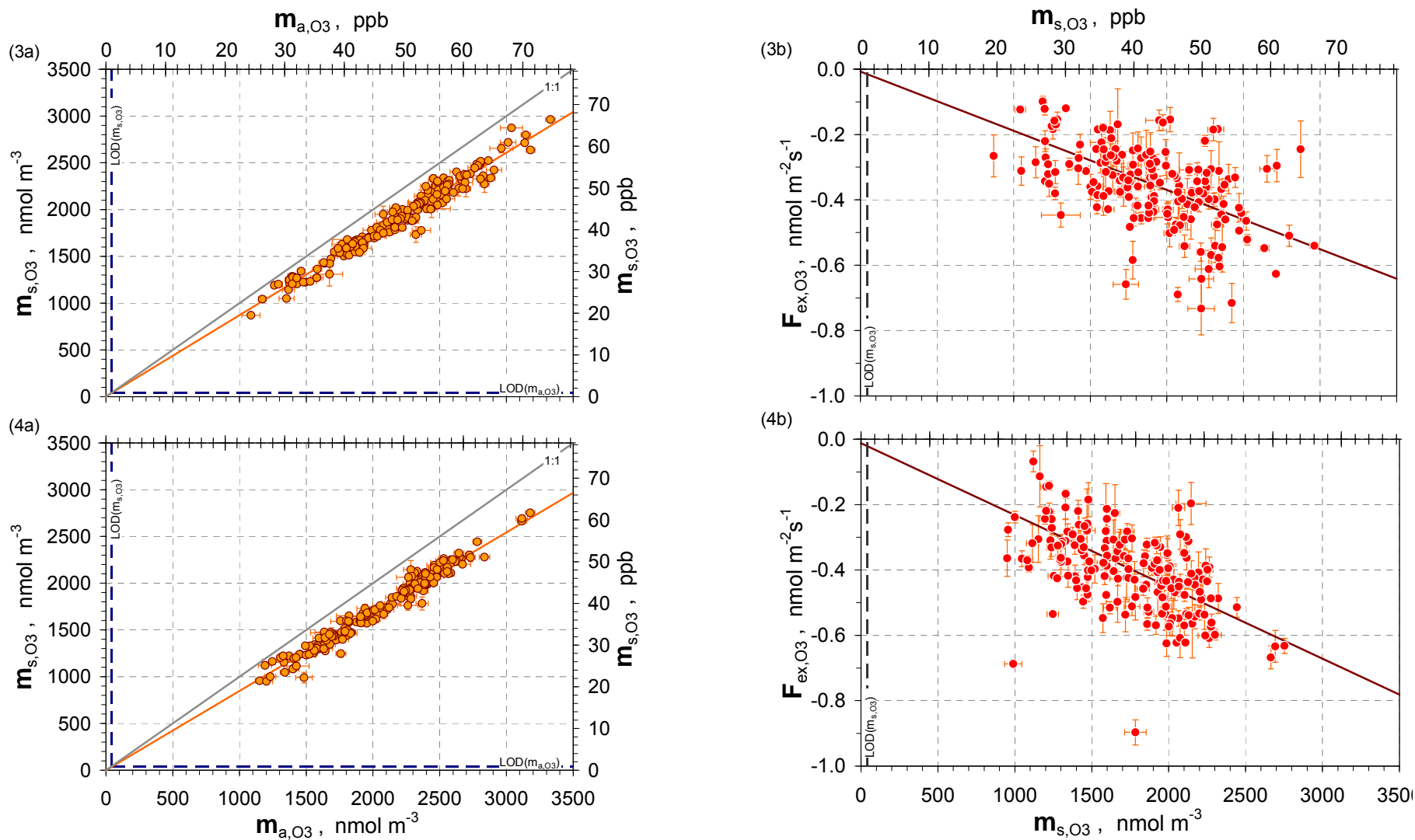


**Figure 38: O<sub>3</sub> measurements, data class 3 and 4 of sample chamber 1**

**(3a), (4a)** O<sub>3</sub> concentration measured at the outlet of the dynamic plant chamber ( $m_{s,O_3}$ ) vs. O<sub>3</sub> concentration measured at the inlet of the dynamic plant chamber ( $m_{a,O_3}$ ). Orange circles identify data pairs for significance of  $\Delta m_{O_3} = (m_{a,O_3} - m_{s,O_3})$ . Orange line is calculated according to bi-variate weighted linear least-squares fitting regression analysis. **(3b), (4b)** O<sub>3</sub> exchange flux density ( $F_{ex,O_3}$ ) vs. O<sub>3</sub> concentration measured at the outlet of the dynamic plant chamber ( $m_{s,O_3}$ ).

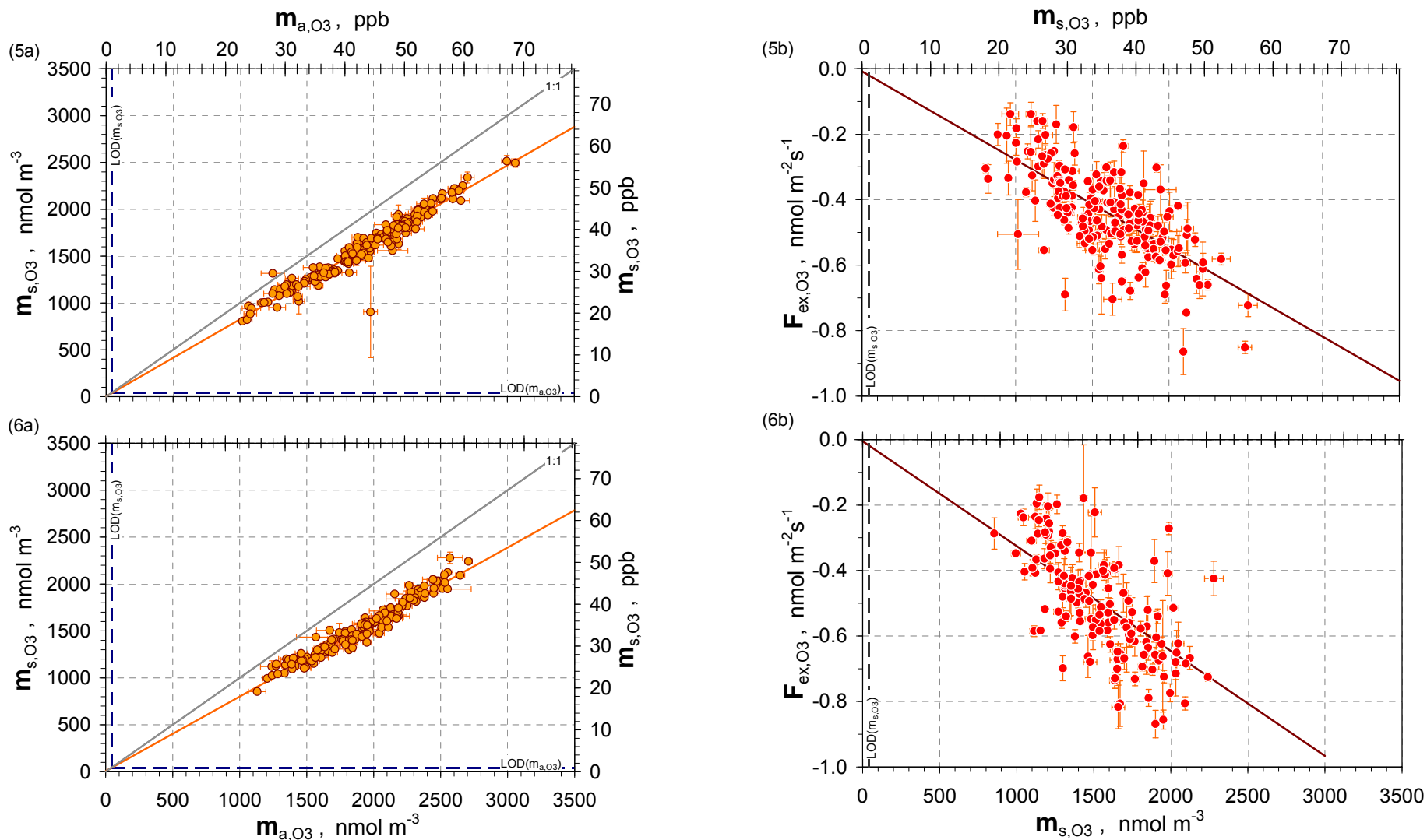


**Figure 39: O<sub>3</sub> measurements, data class 5 and 6 of sample chamber 1**

**(5a), (6a)** O<sub>3</sub> concentration measured at the outlet of the dynamic plant chamber ( $m_{s,O_3}$ ) vs. O<sub>3</sub> concentration measured at the inlet of the dynamic plant chamber ( $m_{a,O_3}$ ). Orange circles identify data pairs for significance of  $\Delta m_{O_3} = (m_{a,O_3} - m_{s,O_3})$ . Orange line is calculated according to bi-variate weighted linear least-squares fitting regression analysis. **(5b), (6b)** O<sub>3</sub> exchange flux density ( $F_{ex,O_3}$ ) vs. O<sub>3</sub> concentration measured at the outlet of the dynamic plant chamber ( $m_{s,O_3}$ ).

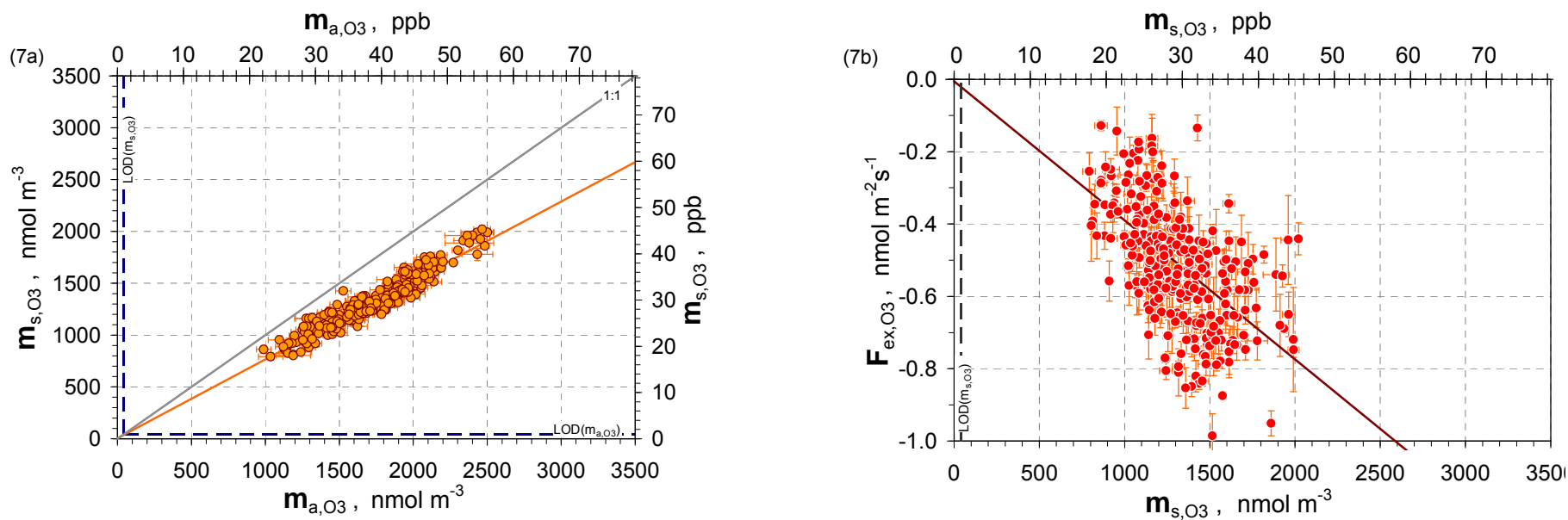


**Figure 40: O<sub>3</sub> measurements, data class 7 of sample chamber 1**

**(7a)** O<sub>3</sub> concentration measured at the outlet of the dynamic plant chamber ( $m_{s,O_3}$ ) vs. O<sub>3</sub> concentration measured at the inlet of the dynamic plant chamber ( $m_{a,O_3}$ ). Orange circles identify data pairs for significance of  $\Delta m_{O_3} = (m_{a,O_3} - m_{s,O_3})$ . Orange line is calculated according to bi-variate weighted linear least-squares fitting regression analysis. **(7b)** O<sub>3</sub> exchange flux density ( $F_{ex,O_3}$ ) vs. O<sub>3</sub> concentration measured at the outlet of the dynamic plant chamber ( $m_{s,O_3}$ ).

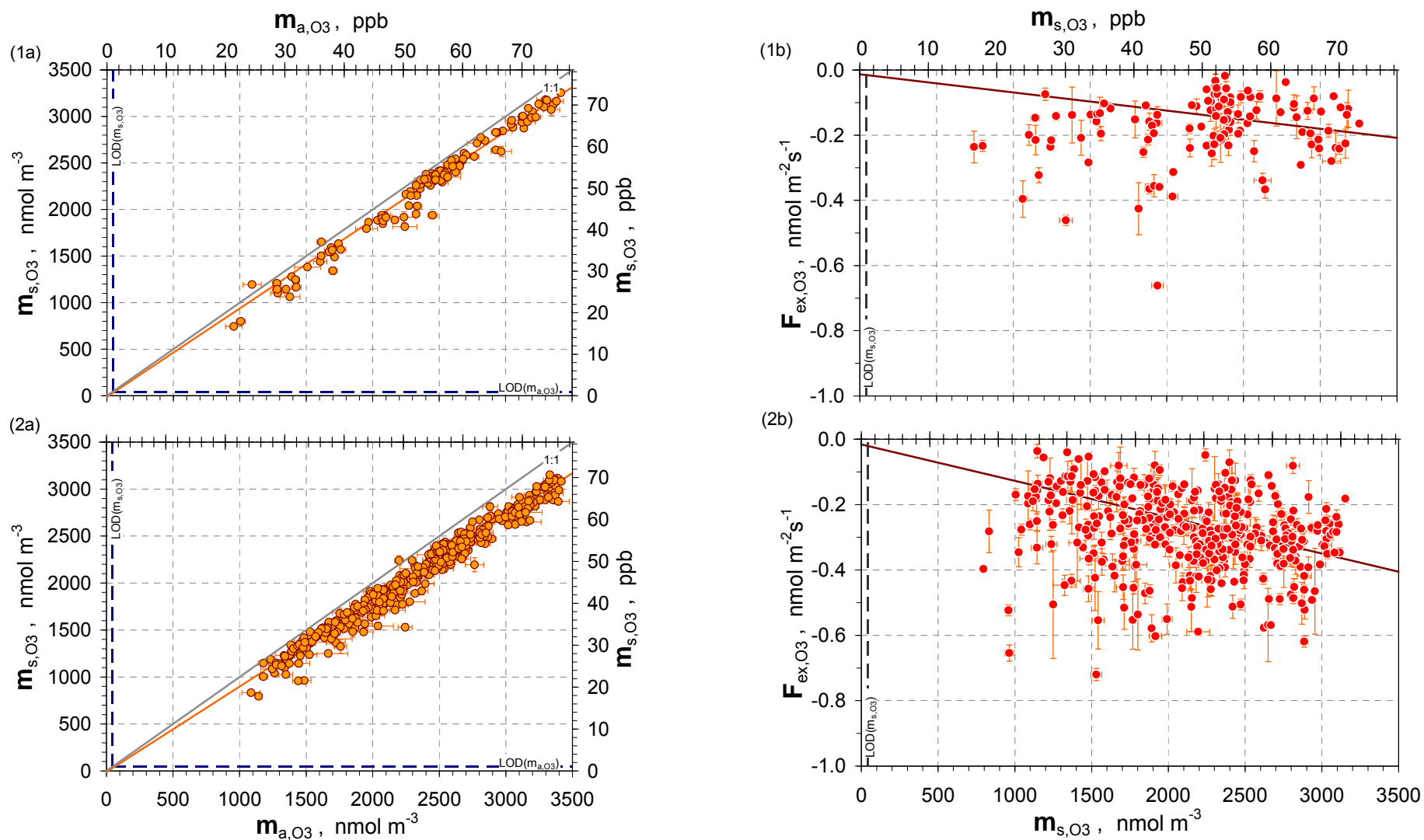


**Figure 41: O<sub>3</sub> measurements, data class 1 and 2 of sample chamber 2**

**(1a), (2a)** O<sub>3</sub> concentration measured at the outlet of the dynamic plant chamber ( $m_{s,O_3}$ ) vs. O<sub>3</sub> concentration measured at the inlet of the dynamic plant chamber ( $m_{a,O_3}$ ). Orange circles identify data pairs for significance of  $\Delta m_{O_3} = (m_{a,O_3} - m_{s,O_3})$ . Orange line is calculated according to bi-variate weighted linear least-squares fitting regression analysis. **(1b), (2b)** O<sub>3</sub> exchange flux density ( $F_{ex,O_3}$ ) vs. O<sub>3</sub> concentration measured at the outlet of the dynamic plant chamber ( $m_{s,O_3}$ ).

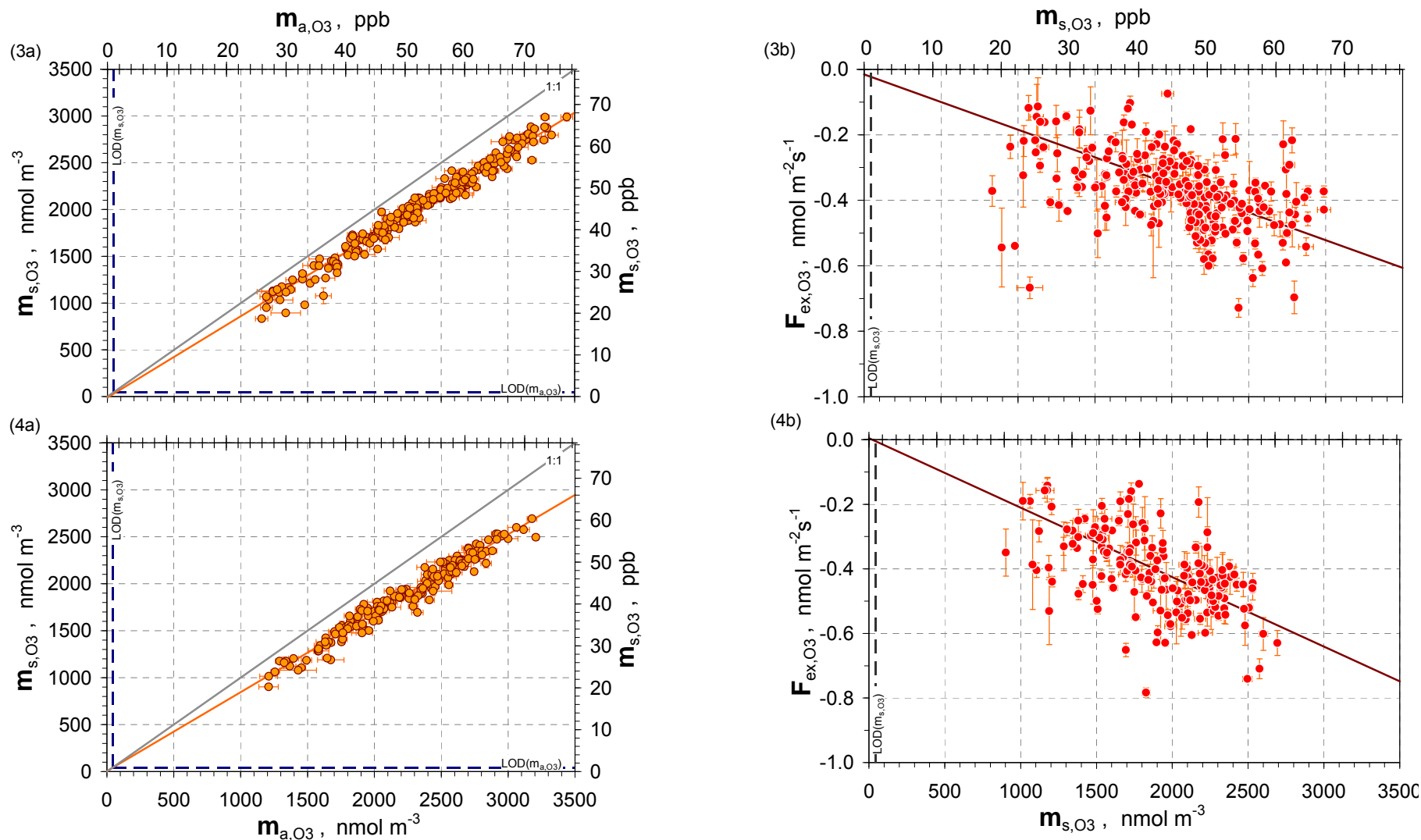
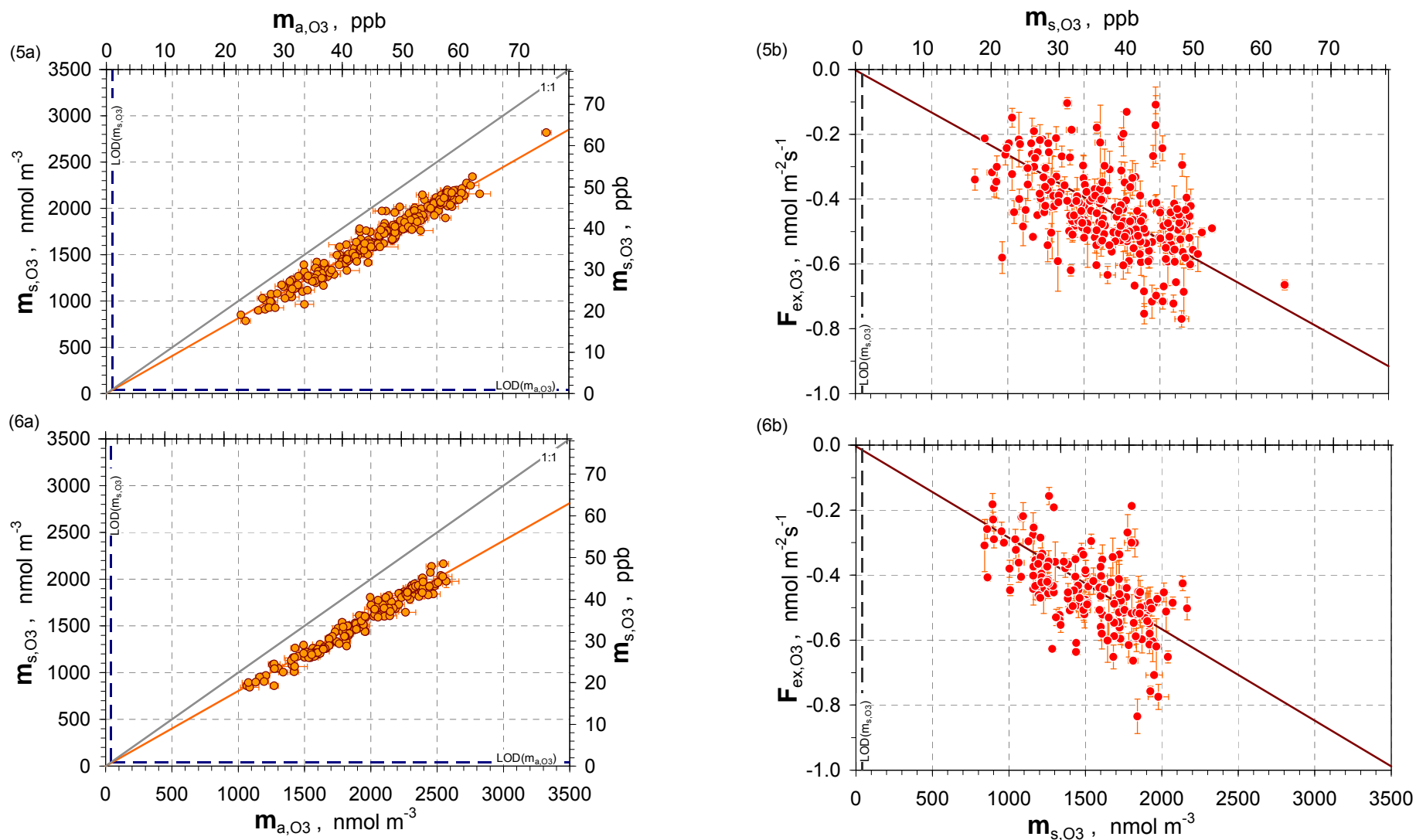


Figure 42: O<sub>3</sub> measurements, data class 3 and 4 of sample chamber 2

(3a), (4a) O<sub>3</sub> concentration measured at the outlet of the dynamic plant chamber ( $m_{s,O_3}$ ) vs. O<sub>3</sub> concentration measured at the inlet of the dynamic plant chamber ( $m_{a,O_3}$ ). Orange circles identify data pairs for significance of  $\Delta m_{O_3} = (m_{a,O_3} - m_{s,O_3})$ . Orange line is calculated according to bi-variate weighted linear least-squares fitting regression analysis. (3b), (4b) O<sub>3</sub> exchange flux density ( $F_{ex,O_3}$ ) vs. O<sub>3</sub> concentration measured at the outlet of the dynamic plant chamber ( $m_{s,O_3}$ ).





**Figure 43: O<sub>3</sub> measurements, data class 5 and 6 of sample chamber 2**

**(5a), (6a)** O<sub>3</sub> concentration measured at the outlet of the dynamic plant chamber ( $m_{s,O_3}$ ) vs. O<sub>3</sub> concentration measured at the inlet of the dynamic plant chamber ( $m_{a,O_3}$ ). Orange circles identify data pairs for significance of  $\Delta m_{O_3} = (m_{a,O_3} - m_{s,O_3})$ . Orange line is calculated according to bi-variate weighted linear least-squares fitting regression analysis. **(5b), (6b)** O<sub>3</sub> exchange flux density ( $F_{ex,O_3}$ ) vs. O<sub>3</sub> concentration measured at the outlet of the dynamic plant chamber ( $m_{s,O_3}$ ).

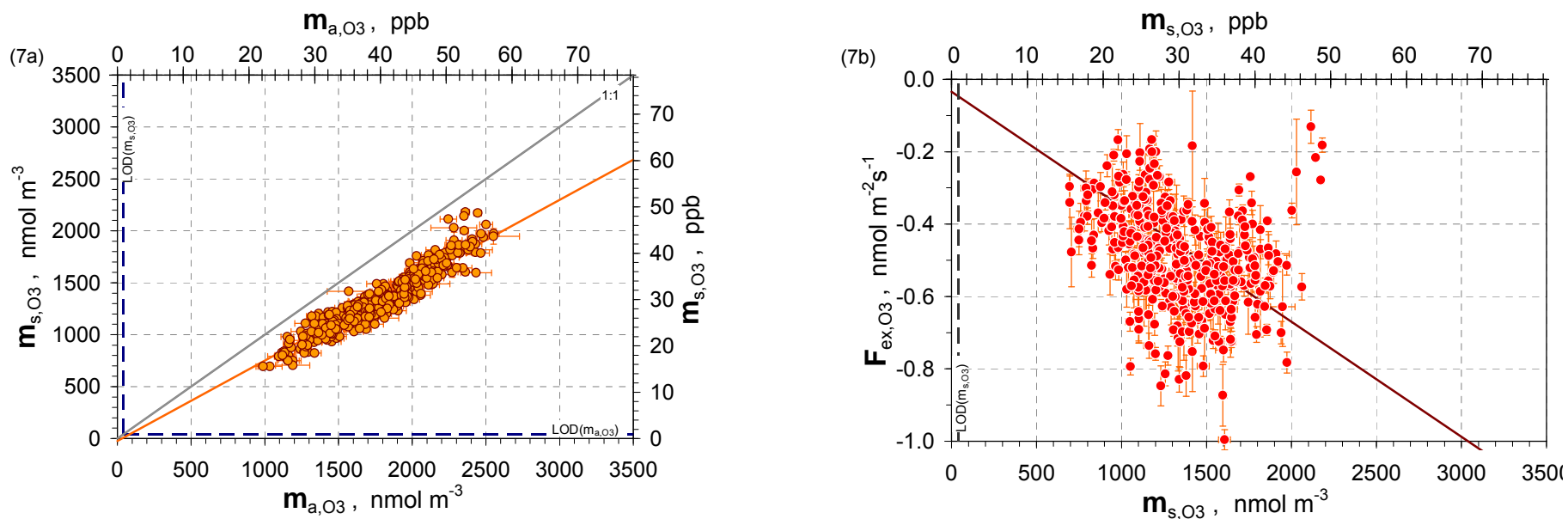


**Figure 44: O<sub>3</sub> measurements, data class 7 of sample chamber 2**

**(7a)** O<sub>3</sub> concentration measured at the outlet of the dynamic plant chamber ( $m_{s,O_3}$ ) vs. O<sub>3</sub> concentration measured at the inlet of the dynamic plant chamber ( $m_{a,O_3}$ ). Orange circles identify data pairs for significance of  $\Delta m_{O_3} = (m_{a,O_3} - m_{s,O_3})$ . Orange line is calculated according to bi-variate weighted linear least-squares fitting regression analysis. **(7b)** O<sub>3</sub> exchange flux density ( $F_{ex,O_3}$ ) vs. O<sub>3</sub> concentration measured at the outlet of the dynamic plant chamber ( $m_{s,O_3}$ ).

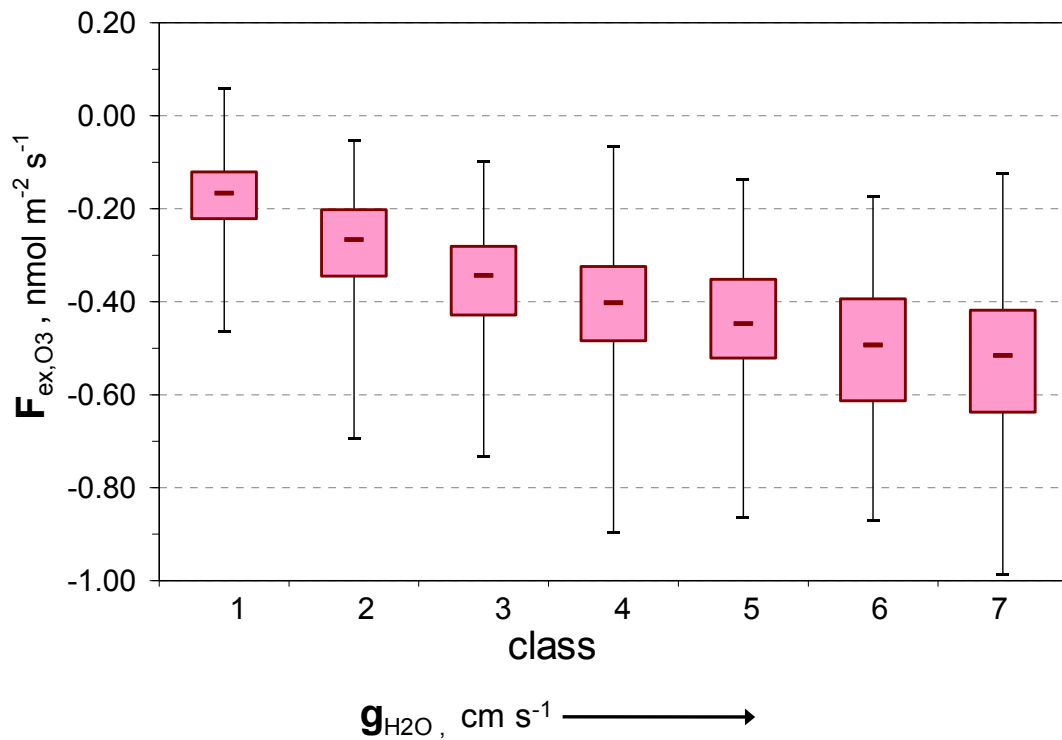


**Figure 45:** Variation of O<sub>3</sub> exchange flux density ( $F_{ex,O_3}$ ) of sample chamber 1 for different leaf conductance classes (increasing values of leaf conductance from class 1 to 7). Red lines denote the median, the boxes the interquartile ranges (0.25 - 0.75), the black lines the minimum and maximum.

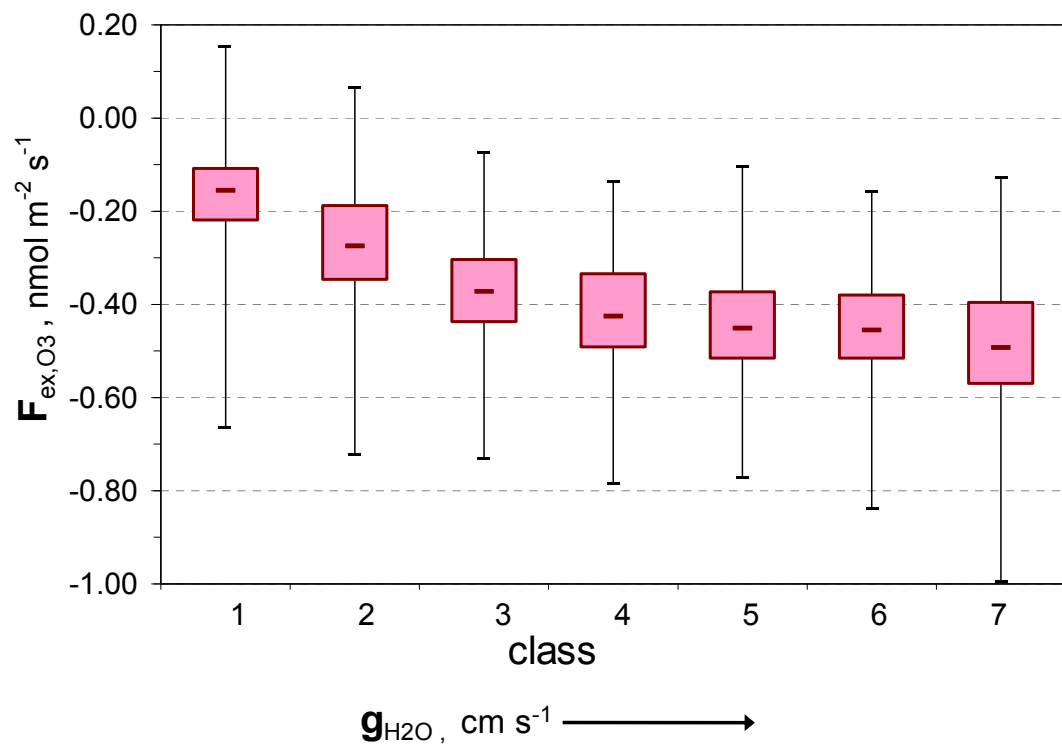


**Figure 46:** Variation of O<sub>3</sub> exchange flux density ( $F_{ex,O_3}$ ) of sample chamber 2 for different leaf conductance classes (increasing values of leaf conductance from class 1 to 7). Red lines denote the median, the boxes the interquartile ranges (0.25 - 0.75), the black lines the minimum and maximum.

## ECHO project

The analysis of the data measured at the ECHO project was performed with the same calculations and criteria as the analysis of the data measured at the EGER project. Here, only exchange flux densities, deposition velocities and compensation point concentrations of  $\text{NO}_2$  were determined. The data were also controlled for the significance criterion for  $\Delta m_{\text{NO}_2} = (m_{a,\text{NO}_2} - m_{s,\text{NO}_2})$  and classified into the same seven classes of  $g_{\text{H}_2\text{O}}$  (see Sect. 4.1.2). Conditions of the classes are displayed in Table 23.

**Table 23:** Conditions of the classes which were used for the classification of the measured data within the ECHO project. All displayed data are mean values.

| class                              |                                      | 1                   | 2                   | 3                   | 4                   | 5                   | 6                   | 7                   |
|------------------------------------|--------------------------------------|---------------------|---------------------|---------------------|---------------------|---------------------|---------------------|---------------------|
| $g_{\text{H}_2\text{O}}$           | $\text{cm s}^{-1}$                   | 0.01                | 0.025               | 0.06                | 0.08                | 0.1                 | 0.13                | 0.16                |
|                                    |                                      | -                   | -                   | -                   | -                   | -                   | -                   | -                   |
|                                    |                                      | 0.025               | 0.06                | 0.08                | 0.1                 | 0.13                | 0.16                | 1.0                 |
| <b>PAR</b>                         | $\mu\text{mol m}^{-2} \text{s}^{-1}$ | 48                  | 110                 | 236                 | 449                 | 397                 | 553                 | 398                 |
| <b>T<sub>air</sub></b>             | $^{\circ}\text{C}$                   | 17.5 $\pm$ 2.0      | 18.5 $\pm$ 2.3      | 19.8 $\pm$ 2.1      | 19.9 $\pm$ 2.8      | 19.0 $\pm$ 3.4      | 18.2 $\pm$ 3.0      | 17.6 $\pm$ 2.4      |
| $F_{\text{ex},\text{CO}_2}$        | $\mu\text{mol m}^{-2} \text{s}^{-1}$ | -0.06<br>$\pm$ 0.78 | -1.30<br>$\pm$ 1.09 | -2.62<br>$\pm$ 1.18 | -3.71<br>$\pm$ 1.07 | -3.81<br>$\pm$ 1.45 | -4.49<br>$\pm$ 1.52 | -4.80<br>$\pm$ 1.48 |
| $F_{\text{ex},\text{H}_2\text{O}}$ | $\text{mmol m}^{-2} \text{s}^{-1}$   | 0.03<br>$\pm$ 0.02  | 0.09<br>$\pm$ 0.05  | 0.18<br>$\pm$ 0.08  | 0.28<br>$\pm$ 0.15  | 0.30<br>$\pm$ 0.14  | 0.37<br>$\pm$ 0.20  | 0.42<br>$\pm$ 0.18  |

### 4.2.7 $\text{NO}_2$ exchange flux densities

During the ECHO measurements 636 data pairs of  $m_{a,\text{NO}_2}$  and  $m_{s,\text{NO}_2}$  have been obtained under daytime conditions. After applying the significance criterion nearly 52 % of the  $\text{NO}_2$  data pairs remained. An additional screening for singular concentration peaks was not done.

The results of the bi-variate weighted linear regression analysis for the classes are presented in Figure 47 to Figure 50. In panels 1a - 7a the bi-variate regression analysis between  $\text{NO}_2$  concentrations at the plant chamber's inlet ( $m_{a,\text{NO}_2}$ ) and outlet ( $m_{s,\text{NO}_2}$ ) are shown, where  $m_{a,\text{NO}_2}$  is represented by the concentration measured at the outlet of the empty reference chamber. Panels 1b - 7b represent  $F_{\text{ex},\text{NO}_2}$  versus  $m_{s,\text{NO}_2}$ . The blue line represents  $v_{\text{dep},\text{NO}_2}$ .

In Table 24 the details of statistical evaluation are listed. The analysis resulted in  $R^2(m_{aNO_2}, m_{s,NO_2})$  between 0.8970 and 0.9951 and  $v_{dep,NO_2}$  between 0.60 and 2.71 mm s<sup>-1</sup>. In these results  $v_{dep,NO_2}$  also increased with raising leaf conductance  $g_{H_2O}$ . The determined  $m_{comp,NO_2}$  always gave negative values. Even if the significance probability of  $m_{comp,NO_2} \neq 0$  is varied from 99.51 % (“significant”) to 99.99 % (“highly significant”) a negative NO<sub>2</sub> compensation point concentration is unrealistic and physically meaningless, but nevertheless indicates the absence of a compensation point.

**Table 24:** Parameters of bi-variate weighted linear least-squares fitting regression analysis for data classes 1 -7. Only significant data of  $\Delta m_{NO_2} = (m_{a,NO_2} - m_{s,NO_2})$  were applied.

| statistical quantity    | unit                 | NO <sub>2</sub> |              |
|-------------------------|----------------------|-----------------|--------------|
| $N$                     | [1]                  | 21              | 25           |
| $R^2(m_{a,i}; m_{s,i})$ | [1]                  | 0.9574          | 0.9951       |
| $n$                     | nmol m <sup>-3</sup> | -6.9 ±2.54      | -4.0 ±1.39   |
| $m$                     | [1]                  | 0.78 ±0.007     | 0.54 ±0.007  |
| $m_{comp,i}$            | nmol m <sup>-3</sup> | -198.0 ±42.22   | -85.8 ±13.42 |
| $m_{comp,i} \neq 0?$    | %                    | 99.99 (HS)      | 99.99 (HS)   |
| $v_{dep,i}$             | mm s <sup>-1</sup>   | 0.60 ±0.026     | 1.81 ±0.047  |
| $N$                     | [1]                  | 38              | 15           |
| $R^2(m_{a,i}; m_{s,i})$ | [1]                  | 0.9434          | 0.9857       |
| $n$                     | nmol m <sup>-3</sup> | -0.4 ±2.46      | -2.9 ±2.23   |
| $m$                     | [1]                  | 0.70 ±0.012     | 0.48 ±0.014  |
| $m_{comp,i}$            | nmol m <sup>-3</sup> | -107.3 ±27.47   | -39.4 ±8.31  |
| $m_{comp,i} \neq 0?$    | %                    | 99.99 (HS)      | 99.99 (HS)   |
| $v_{dep,i}$             | mm s <sup>-1</sup>   | 0.88 ±0.049     | 2.18 ±0.126  |
| $N$                     | [1]                  | 35              | 12           |
| $R^2(m_{a,i}; m_{s,i})$ | [1]                  | 0.8970          | 0.9803       |
| $n$                     | nmol m <sup>-3</sup> | -0.9 ±2.92      | 6.0 ±2.13    |
| $m$                     | [1]                  | 0.61 ±0.012     | 0.43 ±0.026  |
| $m_{comp,i}$            | nmol m <sup>-3</sup> | -50.9 ±10.28    | -5.3 ±5.19   |
| $m_{comp,i} \neq 0?$    | %                    | 99.99 (HS)      | 99.51 (S)    |
| $v_{dep,i}$             | mm s <sup>-1</sup>   | 1.37 ±0.068     | 2.71 ±0.285  |
| $N$                     | [1]                  | 33              |              |
| $R^2(m_{a,i}; m_{s,i})$ | [1]                  | 0.9812          |              |
| $n$                     | nmol m <sup>-3</sup> | -4.9 ±2.27      |              |
| $m$                     | [1]                  | 0.53 ±0.009     |              |
| $m_{comp,i}$            | nmol m <sup>-3</sup> | -89.8 ±22.86    |              |
| $m_{comp,i} \neq 0?$    | %                    | 99.99 (HS)      |              |
| $v_{dep,i}$             | mm s <sup>-1</sup>   | 1.89 ±0.065     |              |

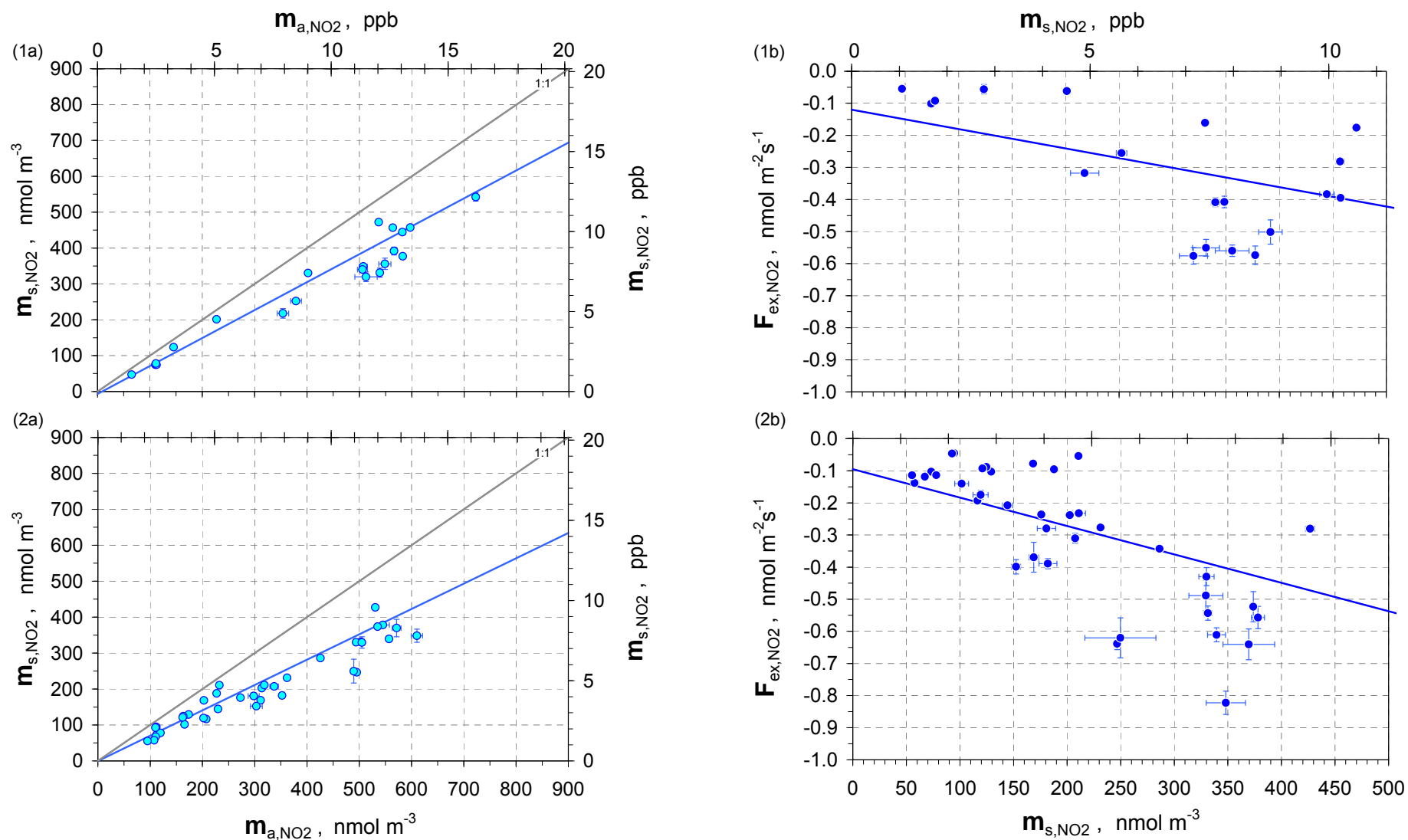


**Figure 47: NO<sub>2</sub> ECHO field measurements, data class 1 and 2**

**(1a), (2a)** NO<sub>2</sub> concentration measured at the outlet of the dynamic plant chamber ( $m_{s,NO_2}$ ) vs. NO<sub>2</sub> concentration measured at the outlet of the reference dynamic plant chamber ( $m_{a,NO_2}$ ). Blue circles identify data pairs for significance of  $\Delta m_{NO_2} = (m_{a,NO_2} - m_{s,NO_2})$ . Blue line is calculated according to bi-variate weighted linear least-squares fitting regression analysis. **(1b), (2b)** NO<sub>2</sub> exchange flux density ( $F_{ex,NO_2}$ ) vs. NO<sub>2</sub> concentration measured at the outlet of the dynamic plant chamber ( $m_{s,NO_2}$ ).

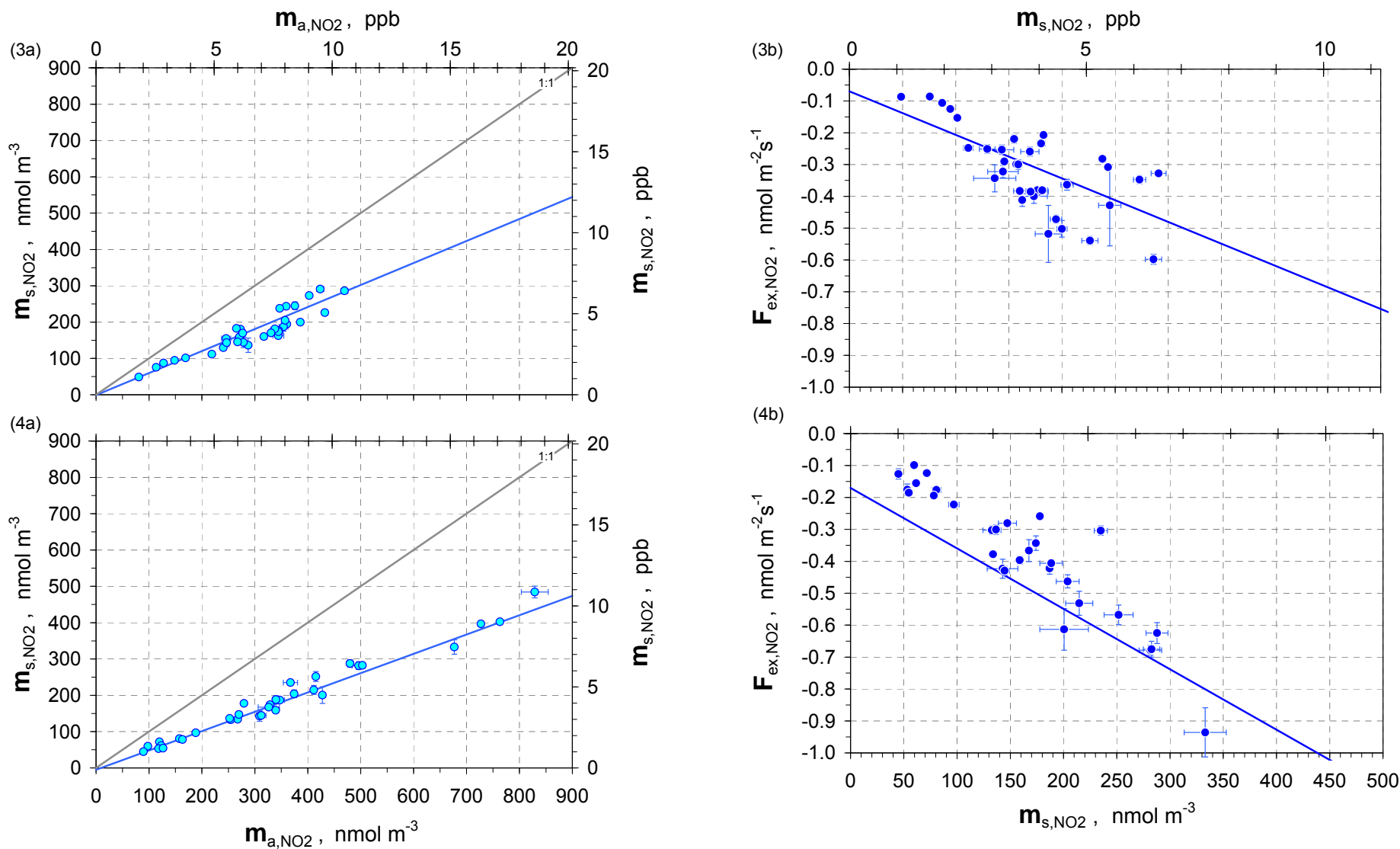


**Figure 48: NO<sub>2</sub> ECHO field measurements, data class 3 and 4**

**(3a), (4a)** NO<sub>2</sub> concentration measured at the outlet of the dynamic plant chamber ( $m_{s,NO_2}$ ) vs. NO<sub>2</sub> concentration measured at the outlet of the reference dynamic plant chamber ( $m_{a,NO_2}$ ). Blue circles identify data pairs for significance of  $\Delta m_{NO_2} = (m_{a,NO_2} - m_{s,NO_2})$ . Blue line is calculated according to bi-variate weighted linear least-squares fitting regression analysis. **(3b), (4b)** NO<sub>2</sub> exchange flux density ( $F_{ex,NO_2}$ ) vs. NO<sub>2</sub> concentration measured at the outlet of the dynamic plant chamber ( $m_{s,NO_2}$ ).

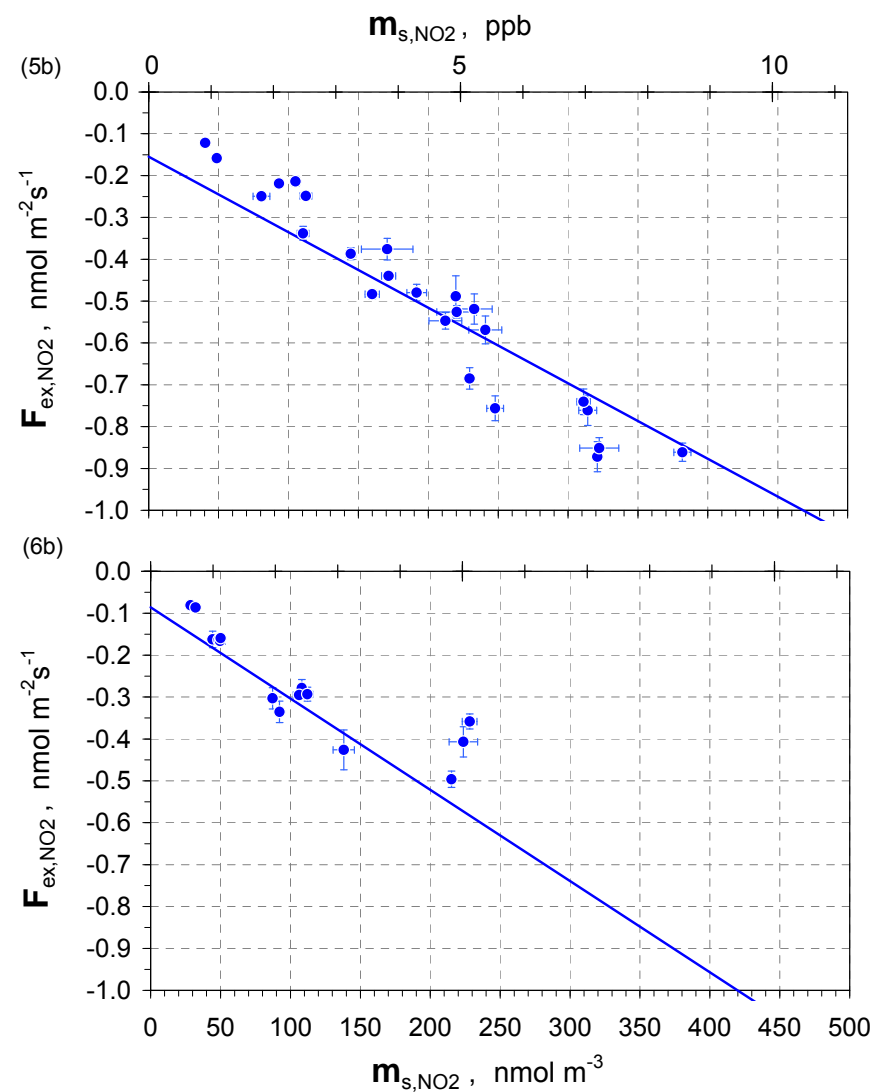
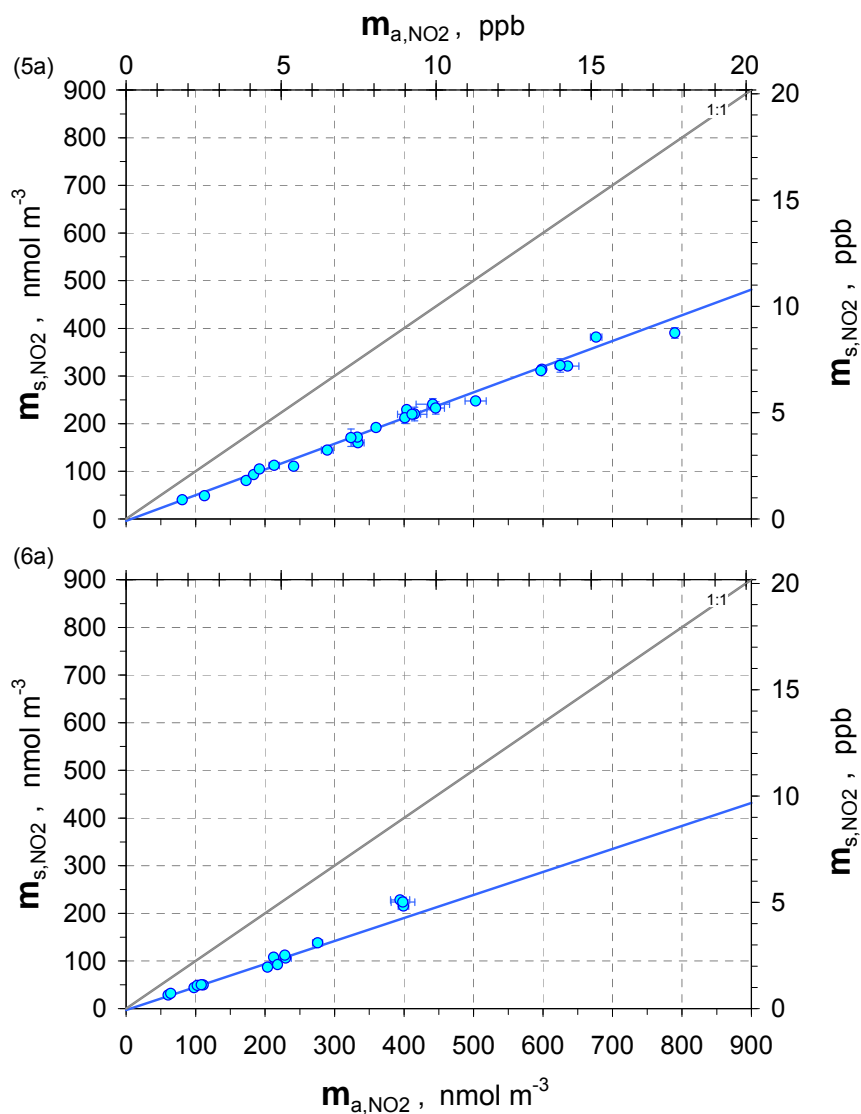


**Figure 49: NO<sub>2</sub> ECHO field measurements, data class 5 and 6**

(5a), (6a) NO<sub>2</sub> concentration measured at the outlet of the dynamic plant chamber ( $m_{s,NO_2}$ ) vs. NO<sub>2</sub> concentration measured at the outlet of the reference dynamic plant chamber ( $m_{a,NO_2}$ ). Blue circles identify data pairs for significance of  $\Delta m_{NO_2} = (m_{a,NO_2} - m_{s,NO_2})$ . Blue line is calculated according to bi-variate weighted linear least-squares fitting regression analysis. (5b), (6b) NO<sub>2</sub> exchange flux density ( $F_{ex,NO_2}$ ) vs. NO<sub>2</sub> concentration measured at the outlet of the dynamic plant chamber ( $m_{s,NO_2}$ ).



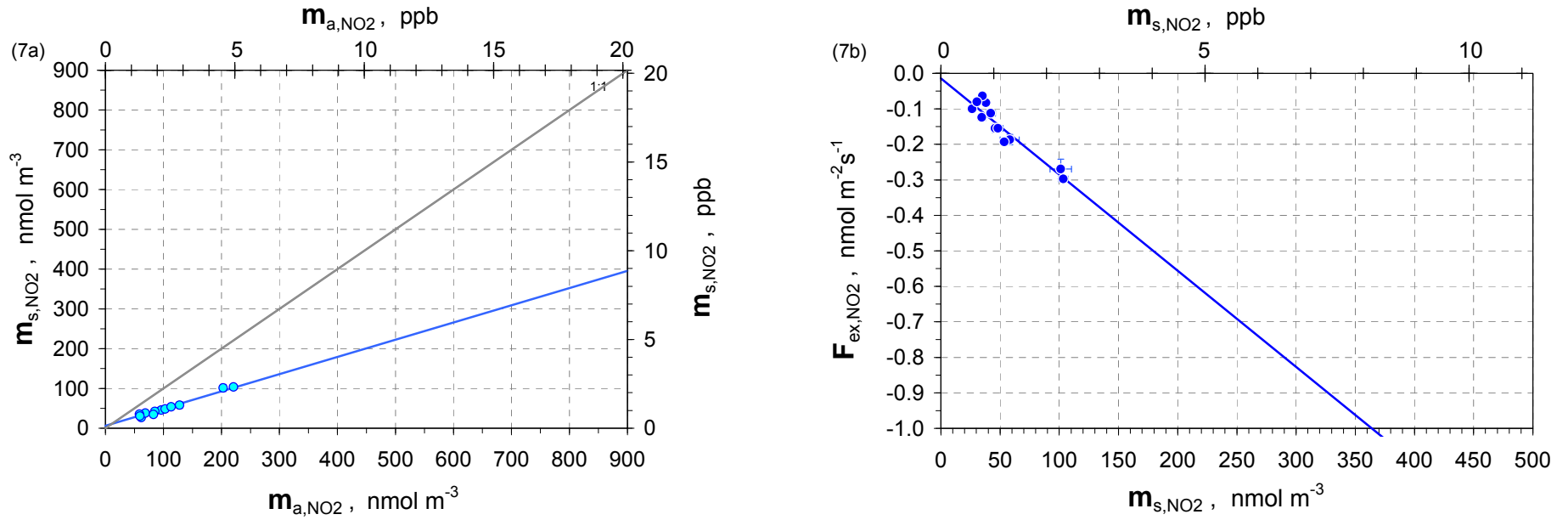


**Figure 50: NO<sub>2</sub> ECHO field measurements, data class 7**

**(7a)** NO<sub>2</sub> concentration measured at the outlet of the dynamic plant chamber ( $m_{s,NO_2}$ ) vs. NO<sub>2</sub> concentration measured at the outlet of the dynamic plant reference chamber ( $m_{a,NO_2}$ ). Blue circles identify data pairs for significance of  $\Delta m_{NO_2} = (m_{a,NO_2} - m_{s,NO_2})$ . Blue line is calculated according to bi-variate weighted linear least-squares fitting regression analysis. **(7b)** NO<sub>2</sub> exchange flux density ( $F_{ex,NO_2}$ ) vs. NO<sub>2</sub> concentration measured at the outlet of the dynamic plant chamber ( $m_{s,NO_2}$ ).

The development of the NO<sub>2</sub> exchange flux densities  $F_{ex,NO_2}$  for the different classes of leaf conductance  $g_{H_2O}$  are displayed in Figure 51.  $F_{ex,NO_2}$  increased with rising  $g_{H_2O}$  and the median reached a maximum value of  $-0.49 \text{ nmol m}^{-2} \text{ s}^{-1}$  at class 5 ( $g_{H_2O} = 0.10 - 0.13$ ). At class 6 and 7  $F_{ex,NO_2}$  declines and become lower than the values of class 1.

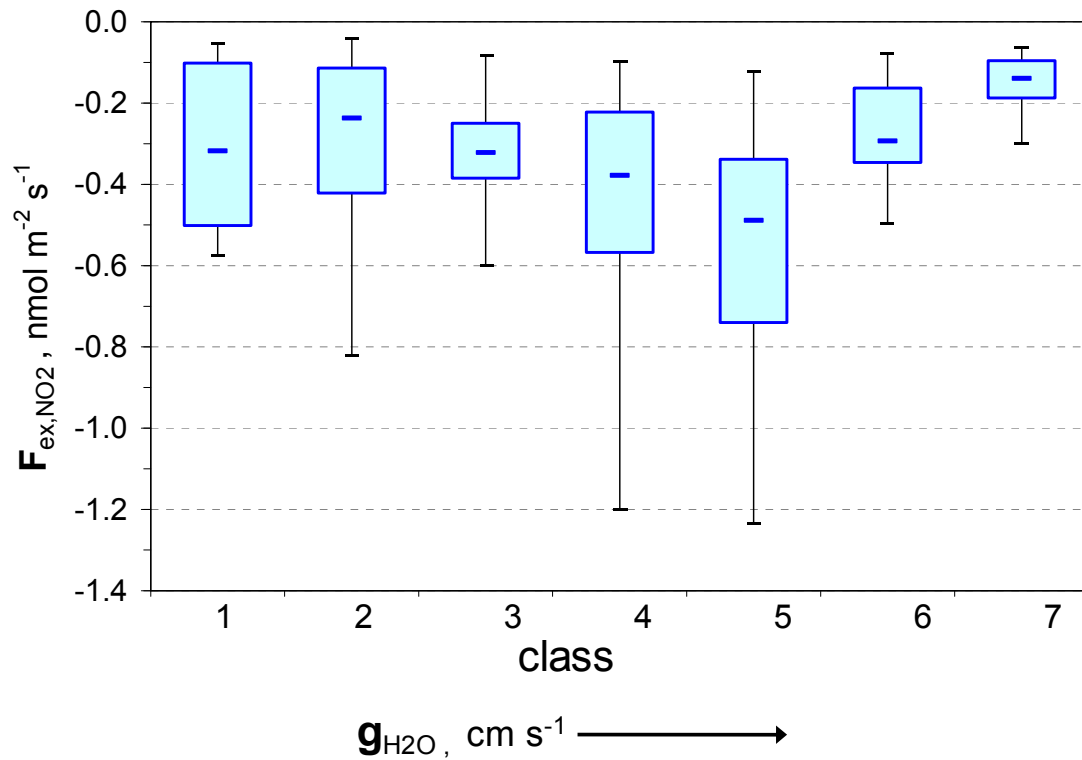


**Figure 51:** Variation of NO<sub>2</sub> exchange flux density ( $F_{ex,NO_2}$ ) of measurements within ECHO for different leaf conductance classes (increasing values of leaf conductance from class 1 to 7). Blue lines denote the median, the boxes the interquartile ranges (0.25 – 0.75), the black lines the minimum and maximum.

## 4.3 Discussion

### 4.3.1 Effects on enclosed plants

Application of a chamber system with enclosed plants or parts of plants requires a control of plant condition to be certain observations and data are transferable and not created under unnatural conditions. To achieve the dynamic chamber requirement that plant physiological processes are not affected by the chamber the chamber walls were made of transparent and almost chemically inert material. The reduction of photosynthetic active radiation (PAR) by the chamber (~10 %) was not a crucial factor because the correlation between CO<sub>2</sub> exchange and PAR intensity indicated that the system is light saturated around 500  $\mu\text{mol photons m}^{-2} \text{s}^{-1}$  (PAR). The PAR transmittance and the high purging air flow rate afford that the physiological processes of the enclosed plant parts are working under natural conditions.

It is important to make sure that the plant is not affected by the chamber, especially for long-term studies. Consequently, we controlled the status of the plants after field experiments. We could not identify visual differences between enclosed and not enclosed plant material. Moreover, no variations in physiological performance were detectable. The photosynthetic capacities of enclosed and control needles were similar. The minor differences were still within a normal spread compared to literature values. The average maximum values for CO<sub>2</sub> uptake of coniferous evergreen trees ranged from 7 to 12  $\mu\text{mol m}^{-2} \text{s}^{-1}$  (LARCHER 2003). In literature light compensation points were specified as 30 to 40  $\mu\text{mol photons m}^{-2} \text{s}^{-1}$  and light saturation points are denoted as 800 to 1000  $\mu\text{mol photons m}^{-2} \text{s}^{-1}$  for sun shoots of coniferous trees under conditions of ambient CO<sub>2</sub> and optimal temperature. For shade shoots of coniferous trees light saturation points were declared between 150 and 200  $\mu\text{mol photons m}^{-2} \text{s}^{-1}$  and light compensation points between 2 and 10  $\mu\text{mol photons m}^{-2} \text{s}^{-1}$  (LARCHER 2003). Our shoots are better classified rather as sun shoots, although because of their position at the bottom of the crown they conform also in some aspects to shade shoots. The value of our calculated light compensation point was between 40 to 70  $\mu\text{mol photons m}^{-2} \text{s}^{-1}$  and our calculated light saturation point was between 500 and 1100  $\mu\text{mol photons m}^{-2} \text{s}^{-1}$ . Our values were higher than literature values but the differences were small between our enclosed and control needles. Hence, these differences were not a sign of a harmful effect of the chamber.

Furthermore, nutrient compositions of needles did not differ. Only for potassium and calcium were differences noticeable. The higher concentration of potassium was found for the young enclosed needles but the concentration was in a normal range, which is specified in literature to be between 5 and 70 mg g<sup>-1</sup>dw (FREY 1998). Potassium is needed during leaf development and it is responsible for the maintenance of the status of plasma swelling. A potassium deficit can be identified by tips of needles drying out and by premature shedding of needles (LARCHER 2003). Such symptoms were not observed. Usual calcium content in plants was 0.4 to 13 mg g<sup>-1</sup>dw. Symptoms of deficiency would be drying of buds, young shoots dying off and chlorosis of the tips of fir trees followed by browning of needles (LARCHER 2003). It can be assumed that the difference between enclosed and controlled needles was not harmful.

Our data sets give good reasons to assume that the enclosed branch behaved normally. Contrasting, in many chamber studies plant conditions were monitored only by measuring CO<sub>2</sub> and H<sub>2</sub>O exchange of the plant and calculating leaf conductance (e.g., THOENE et al. 1996; SPARKS et al. 2001; GEBLER et al. 2002). These measurements allowed the actual plant conditions to be inferred but in contrast to our work no comparison of plants inside and outside the chamber was performed.

#### 4.3.2 NO<sub>2</sub> exchange to leaves

With increasing ambient NO<sub>2</sub> concentrations an increase of NO<sub>2</sub> exchange flux densities could be observed. This agrees with previous studies (RONDÓN et al. 1993; THOENE et al. 1991; WEBER and RENNENBERG 1996; GEBLER et al. 2002) and with the assumption that NO<sub>2</sub> exchange is driven by the NO<sub>2</sub> concentration difference between atmosphere and the gaseous phase of the leaf interior.

Emission fluxes of NO<sub>2</sub> have been measured by several studies. TEKLEMARIAM and SPARKS (2006) reported emissions from four species (wheat, corn, sunflower, Madagascar periwinkle) between 36.8 and 101.0 pmol m<sup>-2</sup> s<sup>-1</sup>. SPARKS et al. (2001) observed NO<sub>2</sub> emissions up to 50 pmol m<sup>-2</sup> s<sup>-1</sup> from several tropical trees and HEREID and MONSON (2001) from field-grown corn. NO<sub>2</sub> emissions from spruce needles were reported by RONDÓN et al. (1993) and GEBLER et al. (2002). In the present study the leaf emission of NO<sub>2</sub> from spruces varied between 0.07 and 58 pmol m<sup>-2</sup> s<sup>-1</sup> measured at

averaged ambient NO<sub>2</sub> concentration of 67.3 nmol m<sup>-3</sup> (1.5 ppb). For oak no emission fluxes have been observed for ambient NO<sub>2</sub> concentrations as low as 0.5 ppb, which is in close accordance with CHAPARRO-SUAREZ et al. (2011) who found no emission from four deciduous trees and a pine species as well.

Our measured deposition fluxes of NO<sub>2</sub> for spruce were on average two or three times higher than the detected emission fluxes. The NO<sub>2</sub> deposition fluxes varied between -0.078 and -0.018 nmol m<sup>-2</sup> s<sup>-1</sup>. NO<sub>2</sub> deposition fluxes reported by THOENE et al. (1996) were in a range between -1.88 and -0.03 nmol m<sup>-2</sup> s<sup>-1</sup> and SPARKS et al. (2001) detected uptake rates on average between -1.55 and -0.15 nmol m<sup>-2</sup> s<sup>-1</sup> for several tropical trees. Thus, NO<sub>2</sub> fluxes of these studies were clearly higher than our measured NO<sub>2</sub> fluxes. For both studies analyzers with NO<sub>2</sub> converters with known interferences due to other oxidized nitrogen compounds were used (see Sect. 2.2). The comparison to the results of these studies could indicate that our performed measuring system, using a blue light converter, is more specific for NO<sub>2</sub> measurements. Similar deposition fluxes up to -0.3 nmol m<sup>-2</sup> s<sup>-1</sup> (at 5 ppb) were reported by CHAPARRO-SUAREZ et al. (2011) using a very similar instrumentation. However, GEBLER et al. (2002) using a photolytic converter reported NO<sub>2</sub> deposition fluxes at a range between -0.12 and -0.02 nmol m<sup>-2</sup> s<sup>-1</sup>, which are obviously like our measured ranges.

Exchange rates of NO<sub>2</sub> depend not only on atmospheric NO<sub>2</sub> concentration but also on stomatal conductance (NEUBERT et al. 1993; HEREID and MONSON 2001; SPARKS et al. 2001; CHAPARRO-SUAREZ et al. 2011). SPARKS et al. (2001) observed for tropical tree species a kind of saturation for NO<sub>2</sub> uptake at higher stomatal conductance. Such observations have not been found in the present study for spruce. However, for oak a decline of the NO<sub>2</sub> exchange flux density, though not a saturation, was recognizable at higher leaf conductance. The NO<sub>2</sub> uptake may be additionally limited by internal resistances (mesophyllic), as reported by several authors (THOENE et al. 1991, 1996; SPARKS et al. 2001). This circumstance is reflected in a smaller measured leaf conductance to NO<sub>2</sub> ( $g_{NO_2,m}$ ) than the predicted NO<sub>2</sub> leaf conductance ( $g_{NO_2,p}$ ), which is calculated from leaf conductance to water vapor (see Eq. (28)). The measured leaf conductance  $g_{NO_2,m}$  was calculated from quotient of  $F_{ex,NO_2}$  and the NO<sub>2</sub> concentration at the outlet of the sample chamber. For oak we found higher measured NO<sub>2</sub> leaf conductance than the predicted conductance. Similar results were found by GEBLER et al. (2002) for spruce. They assumed that the reaction of ascorbate with NO<sub>2</sub> is responsible for maintaining high

fluxes of NO<sub>2</sub> into the leaf and preventing high internal resistances. HANSON et al. (1993) found for broadleaf and conifer species an underestimation of measured leaf conductance by the predicted conductance of between 15 and 30 % as well. Our results for spruce looked different. The measured and predicted NO<sub>2</sub> leaf conductances are listed in Table 25. At higher leaf conductance classes the measured NO<sub>2</sub> conductance was lower than the predicted, however, at the low leaf conductance classes the results were reversed. A common trend for spruce and oak is the decrease in the difference of measured and predicted NO<sub>2</sub> leaf conductance, while initial values are different. Only for spruce predicted NO<sub>2</sub> leaf conductances exceed measured leaf conductances with higher class.

**Table 25:** Measured and predicted leaf conductance to NO<sub>2</sub> deposition. Measured leaf conductance ( $g_{NO_2,m}$ ) was calculated from quotient of  $F_{ex,NO_2}$  and NO<sub>2</sub> concentration at the outlet of the sample chamber, predicted leaf conductance ( $g_{NO_2,p}$ ) was calculated from  $g_{H_2O}$  according to Eq. (28).

| class | Spruce chamber 1                   |                                    |                 | Spruce chamber 2                   |                                    |                 | Oak                                |                                    |                 |
|-------|------------------------------------|------------------------------------|-----------------|------------------------------------|------------------------------------|-----------------|------------------------------------|------------------------------------|-----------------|
|       | $g_{NO_2,m}$<br>mm s <sup>-1</sup> | $g_{NO_2,p}$<br>mm s <sup>-1</sup> | difference<br>% | $g_{NO_2,m}$<br>mm s <sup>-1</sup> | $g_{NO_2,p}$<br>mm s <sup>-1</sup> | difference<br>% | $g_{NO_2,m}$<br>mm s <sup>-1</sup> | $g_{NO_2,p}$<br>mm s <sup>-1</sup> | difference<br>% |
| 1     | 0.054                              | 0.038                              | +41.5           | 0.128                              | 0.062                              | +108.5          | 0.746                              | 0.109                              | +582.2          |
| 2     | 0.053                              | 0.096                              | -45.3           | 0.150                              | 0.096                              | +55.5           | 0.881                              | 0.273                              | +222.2          |
| 3     | 0.102                              | 0.156                              | -34.4           | 0.163                              | 0.157                              | +3.8            | 1.053                              | 0.429                              | +145.4          |
| 4     | 0.136                              | 0.204                              | -33.3           | 0.178                              | 0.204                              | -12.8           | 1.257                              | 0.558                              | +25.4           |
| 5     | 0.143                              | 0.256                              | -44.0           | 0.206                              | 0.256                              | -19.3           | 1.335                              | 0.694                              | +92.3           |
| 6     | 0.144                              | 0.326                              | -55.9           | 0.250                              | 0.323                              | -22.7           | 1.369                              | 0.876                              | +56.3           |
| 7     | 0.269                              | 0.630                              | -57.3           | 0.301                              | 0.0835                             | -64.0           | 1.416                              | 1.409                              | +0.5            |

It seems that at higher leaf conductance the internal resistance becomes more important for the limitation of the NO<sub>2</sub> uptake particularly for spruce. However, we should keep in mind that for dynamic chamber measurements at high leaf conductance, which is equivalent to a low resistance for gas exchange, the impact of the chamber resistances could become a significant factor because the values of the low plant resistances and the chamber resistances can be in the same order of magnitude. In this case both resistances

add a similar rate to the total resistance and cannot be neglected anymore. The deposition of  $\text{NO}_2$  inside the chamber is then not only limited by stomatal and mesophyll resistance. Using predicted  $\text{NO}_2$  leaf conductance calculated from known leaf conductance to water vapor to model  $\text{NO}_2$  exchange fluxes would lead to under- or overestimations of the  $\text{NO}_2$  fluxes.

It was particularly noticeable that at the EGER field site spruces showed a temperature dependence of stomatal conductance and consequently of gas exchange, because stomata close at high leaf temperatures to avoid drought. Hence, very low  $\text{NO}_2$  ( $\text{NO}$ ,  $\text{O}_3$ ) exchange flux densities were detected during daytime if leaf temperature exceeded 23 °C. This plant behavior illustrates the need for following and measuring the plant-physiological processes like photosynthesis ( $\text{CO}_2$  surface exchange flux) and transpiration ( $\text{H}_2\text{O}$  surface exchange flux) and the need to related them to the  $\text{NO}_2$  ( $\text{NO}$ ,  $\text{O}_3$ ) surface exchange. Moreover, it is beneficial to know the plant's optimal conditions in order to interpret the  $\text{NO}_2$  ( $\text{NO}$ ,  $\text{O}_3$ ) exchange measurements without ignorance of the plant's characteristics (e.g. temperature effects on stomatal closure at high temperatures would lead to underestimation of  $\text{NO}_2$  ( $\text{NO}$ ,  $\text{O}_3$ ) exchange behavior if generalized to normal plant behavior).

#### 4.3.3 Deposition velocities of $\text{NO}_2$ and $\text{O}_3$

The measurements on spruce branches were made for two different trees at the same time. Between both enclosed branches no differences in the deposition velocity of  $\text{NO}_2$  and  $\text{O}_3$  were observed.

Until now, reported  $v_{dep,NO_2}$  values were not differentiated into variable classes of leaf conductance. The measured  $v_{dep,NO_2}$  values between 0.07 and 0.42  $\text{mm s}^{-1}$  for spruce were of the same order of magnitude as values described by GEBLER et al. (2002) for field measurements under controlled conditions. GEBLER et al. (2002) described  $\text{NO}_2$  deposition velocities for spruces of 0.09  $\text{mm s}^{-1}$ , which is in the range of our minimal measured value. In contrast THOENE et al. (1991, 1996) described values of 0.4 - 0.9  $\text{mm s}^{-1}$  for laboratory measurements. However, RONDÓN et al. (1993) specified values of 1.8 to 2.1  $\text{mm s}^{-1}$ , which were five times higher than our maximal measured

value. Interestingly, the determined  $v_{dep,NO_2}$  for oak under field conditions were clearly higher than for spruce but in the same range as reported by CHAPARRO-SUAREZ et al. (2011) for oak.

The differences in  $v_{dep,NO_2}$  between our measured values and previous studies may have been caused by unspecific  $NO_2$  analyzers or by neglecting the photolysis of  $NO_2$  for the determination of these previously reported  $v_{dep,NO_2}$ . As mentioned in Sect. 3.3.2.3 we estimated how much the gas-phase reactions will affect  $v_{dep,NO_2}$  under the reported experimental conditions. For the reported values of RONDÓN et al. (1993) a highest expected error of 20 % were calculated according to Eq. (23.1), but the corrected  $v_{dep,NO_2}$  would be still above our measured values. The values of THOENE et al. (1991, 1996) would be in our range if the estimated error would be taken into account. Another reason for different  $v_{dep,NO_2}$  measured on leaf level can be different ages of the enclosed leaflets or needles. GRENNFELT et al. (1983) reported of higher  $v_{dep,NO_2}$  for 1-year-old needles compared to current year needles. Unfortunately, studies about different performance of gas exchange depending on the needle ages are very seldom.

The classification into different leaf conductance classes resulted in increasing  $v_{dep,NO_2}$  values with rising leaf conductance. Consequently  $v_{dep,NO_2}$  is positively correlated to the leaf conductance. This finding agrees with a number of previous studies (NEUBERT et al. 1993; HEREID and MONSON 2001; SPARKS et al. 2001; GEBLER et al. 2002; CHAPARRO-SUAREZ et al. 2011).

The  $O_3$  deposition velocities  $v_{dep,O_3}$  measured for spruce were between 0.06 and 0.38  $mm\ s^{-1}$  depending on the leaf conductance class. These values are in the same magnitude as the deposition velocities determined for  $NO_2$ . However, RONDÓN et al. (1993) reported about  $v_{dep,O_3}$  which were an order of magnitude higher than  $v_{dep,NO_2}$ .

Most of the reported deposition velocities ( $NO_2$  and  $O_3$ ) are based on canopy deposition velocity measurements for both foliar and non-foliar sites using eddy correlation technique. Consequently the gas exchange of the soil, reactions with surfaces and reactions with radicals, for example VOCs emitted from plants, are taken into account. For a deciduous forest  $v_{dep,O_3}$  of 10  $mm\ s^{-1}$  in the summer and 3  $mm\ s^{-1}$  in the winter are reported from PADRO (1991). He also mentioned the values of  $v_{dep,O_3}$  over a vineyard, a cotton field and a senescent grass field the values are 5, 8 and 2  $mm\ s^{-1}$ , respectively (PADRO 1996). For a spruce forest values of 7  $mm\ s^{-1}$  for  $v_{dep,O_3}$  were determined by



PILEGAARD et al. (1995), and the results of a study at a fruit orchard (several varieties of apple) resulted in  $v_{dep,O_3}$  values of 3 to 5 mm s<sup>-1</sup> (WALTON et al. 1997). For NO<sub>2</sub> deposition velocities less values are reported at publications than for O<sub>3</sub>. For wheat fields values of 0.35 mm s<sup>-1</sup> are reported by PILEGAARD et al. (1998) and for the fruit orchard 2 to 6 mm s<sup>-1</sup> by WALTON et al. (1997). Monthly means (Jan to Oct) of  $v_{dep,NO_2}$  for an oak forest were between 0.2 and 6.4 mm s<sup>-1</sup> (PUXBAUM and GREGORI 1998) and for a deciduous forest  $v_{dep,NO_2}$  values of 2 mm s<sup>-1</sup> were reported by HORII et al. (2004). To compare rudimentary deposition velocities determined from canopy or leaf-level measurements the values of the deposition velocity per projected needle area can be converted by multiplying the measured deposition velocity by the leaf area index (LAI). Additionally the existence of a NO<sub>2</sub> compensation point concentration can be considered by a correction of the NO<sub>2</sub> deposition velocity. According to RONDÓN et al. (1993) this correction can be calculated as  $v_{dep,NO_2}^{LAI,cor} = v_{dep,NO_2}^{LAI} \cdot (1 - m_{comp,NO_2}/m_{s,NO_2})$ , where  $m_{comp,NO_2}$  is the NO<sub>2</sub> compensation point concentration and  $m_{s,NO_2}$  is the mean NO<sub>2</sub> concentration during the period. Table 26 presents the NO<sub>2</sub> and O<sub>3</sub> deposition velocities, corrected and not corrected, to the canopy for the different classes of leaf conductance and species.

**Table 26:** Averages of NO<sub>2</sub> and O<sub>3</sub> deposition velocities ( $v_{dep,i}^{LAI}$  in mm s<sup>-1</sup>) per ground area (LAI) and  $v_{dep,NO_2}^{LAI}$  corrected ( $v_{dep,NO_2}^{LAI,cor}$  in mm s<sup>-1</sup>) for NO<sub>2</sub> compensation point concentration when existent. LAI of Spruce forest (EGER) = 5.2, LAI of Oak forest (ECHO) = 4.7.

| class | Spruce chamber 1     |                          |                     | Spruce chamber 2     |                          |                     | Oak                  |
|-------|----------------------|--------------------------|---------------------|----------------------|--------------------------|---------------------|----------------------|
|       | $v_{dep,NO_2}^{LAI}$ | $v_{dep,NO_2}^{LAI,cor}$ | $v_{dep,O_3}^{LAI}$ | $v_{dep,NO_2}^{LAI}$ | $v_{dep,NO_2}^{LAI,cor}$ | $v_{dep,O_3}^{LAI}$ | $v_{dep,NO_2}^{LAI}$ |
| 1     | 0.37                 | 0.30                     | 0.35                | n.a.                 | no $m_{comp,NO_2}$       | 0.29                | 2.84                 |
| 2     | 0.46                 | 0.34                     | 0.62                | 0.71                 | no $m_{comp,NO_2}$       | 0.58                | 4.16                 |
| 3     | 0.68                 | 0.56                     | 0.94                | 0.74                 | no $m_{comp,NO_2}$       | 0.88                | 6.43                 |
| 4     | 0.56                 | 0.73                     | 1.14                | 1.30                 | 1.04                     | 1.12                | 8.90                 |
| 5     | 1.28                 | 0.91                     | 1.40                | 1.50                 | 1.21                     | 1.36                | 8.48                 |
| 6     | 1.58                 | 0.99                     | 1.67                | 1.00                 | no $m_{comp,NO_2}$       | 1.46                | 10.24                |
| 7     | 1.82                 | 1.75                     | 2.00                | 2.20                 | 1.96                     | 1.65                | 12.73                |

The converted NO<sub>2</sub> deposition velocity for the oak stand resulted in values between 2.8 and 17.7 mm s<sup>-1</sup> and an average of 7.7 mm s<sup>-1</sup>. This averaged  $v_{dep,NO_2}^{LAI}$  is in a good agreement with the values reported by PUXBAUM and GREGORI (1998) who found monthly averaged NO<sub>2</sub> deposition velocities of 6.4 mm s<sup>-1</sup> at the month July for an Oak forest.

For the spruce stand  $v_{dep,NO_2}^{LAI}$  values were corrected for the NO<sub>2</sub> compensation point concentration when a compensation point was determined (see Sect. 4.2.5). The average value of  $v_{dep,NO_2}^{LAI,cor}$  was 0.98 mm s<sup>-1</sup>, which is one order of magnitude lower than the reported averaged and corrected NO<sub>2</sub> deposition velocity per ground area for a spruce stand by RONDÓN et al. (1993). The determination of  $v_{dep,O_3}^{LAI}$  resulted in an average value of 1.10 mm s<sup>-1</sup>, which come up to seventh part of the O<sub>3</sub> deposition velocity reported by PILEGAARD et al. (1995) for a Spruce forest.

It should be mentioned that, at least for spruce, the measurements were made at branches in the middle of the canopy. The radiation intensity and thus the stomatal conductance probably differs upwards to the top of canopy and downwards to the ground of forest. Accordingly, values of deposition velocities can differ over the whole tree stand. Therefore RONDÓN et al. (1993) considered their converted deposition velocities to be upper limits as they measured at the tree top.

#### 4.3.4 Compensation point concentration

In literature a wide range of NO<sub>2</sub> compensation point concentrations ( $m_{comp,NO_2}$ ) were reported between 0.1 and 3 ppb (see Table 3). In this study the range of highly significant  $m_{comp,NO_2}$  determined for spruce needles under field conditions was between  $7.4 \pm 6.40$  and  $29.0 \pm 16.30$  nmol m<sup>-3</sup> (0.17 - 0.65 ppb). The bi-variate weighted linear least-square fitting regression analysis of the laboratory measurements resulted in  $m_{comp,NO_2} = 5.9 \pm 9.13$  nmol m<sup>-3</sup> (0.13 ppb) and the significance probability for the existence of  $m_{comp,NO_2}$  was 96.6 % (“likely”) (see Sect. 3.2.4.1). The analysis of the data for oak resulted in negative NO<sub>2</sub> compensation point concentrations, which are unrealistic. Both results, measured under field and laboratory conditions, challenge the existence of a NO<sub>2</sub> compensation point concentration for spruce as well for oak. However, if a compensation point for NO<sub>2</sub> uptake exists the concentration will be less than 1 ppb.

These considerations are in close accordance with laboratory experiments as performed by CHAPARRO-SUAREZ et al. (2011) who also question the existence of a compensation point.

For coniferous trees  $\text{NO}_2$  compensation point concentrations between 0.1 and 0.7 ppb were reported by RONDÓN et al. (1993) and RONDÓN and GRANAT (1994). These values are comparable to the values determined in this study. However, THOENE et al. (1996) determined  $m_{comp,NO_2}$  of 1.64 ppb for spruce and GEBLER et al. (2002) values of 1.7 ppb. Such large values (above 1 ppb) would imply an almost constant  $\text{NO}_2$  emission from the forest at regions with small ambient  $\text{NO}_2$  concentrations, which is not reported so far. These differences in the estimation of an exact compensation point concentration had led to some discussion (LERDAU et al. 2000). The discrepancy between the values determined in this study and those high values reported by previous studies (THOENE et al. 1996; GEBLER et al. 2002) may be explained by using different measurement techniques to detect  $\text{NO}_2$  concentrations. As mentioned above (also see Sect. 2.2) most of the commonly used converters for the conversion of  $\text{NO}_2$  to  $\text{NO}$  are not highly specific for  $\text{NO}_2$ . Converters, which consist of molybdenum, iron sulfate or predicted on liquid phase reaction (luminol), show interferences with other compounds as nitrous acid ( $\text{HNO}_2$ ), nitric acid ( $\text{HNO}_3$ ), peroxyacetyl nitrate (PAN) and other organic nitrates, therefore  $\text{NO}_2$  concentrations will be overestimated. The highly  $\text{NO}_2$  specific blue light converter performed in this study should minimize these source of error. Another reason for different estimations of compensation point concentrations can be the application of different measurement setups and data analysis. For the most results of other authors it is not clear if photochemistry of the  $\text{NO-NO}_2\text{-O}_3$  triad was taken into account or if an experimental setup was used which excluded reactions of  $\text{NO}_2$  photochemistry. The results of this study account for those potential sources of error. For the laboratory measurements a chamber design and an experimental setup were used which excluded photochemistry. During field measurements chemical reactions of the  $\text{NO-NO}_2\text{-O}_3$  triad were part of the natural conditions, therefore the measured values were corrected. The impact of gas-phase reactions on compensation point concentrations is less than on deposition velocity. The overestimation of  $\text{NO}_2$  compensation point concentration would be between 3 and 17 % for the values reported by THOENE et al. (1996) and GEBLER et al. (2002) (see Sect. 3.3.2.3). However, this would not suffice to explain the high values of  $\text{NO}_2$  compensation point concentration.

Furthermore, the determination of deposition velocity and compensation point concentration by applying simple linear regression (no errors considered at all) or bi-variate weighted linear regression (y- and x-errors considered) could be another reason for the discrepancy. In most of the previous studies simple linear regression between exchange flux density  $F_{ex,i}$  and the trace gas concentration at the outlet of the sample chamber  $m_{s,i}$  were applied (RONDÓN et al. 1993; RONDÓN and GRANAT 1994; THOENE et al. 1996; SPARKS et al. 2001; HEREID and MONSON 2001) only GEBLER et al. (2000, 2002) applied a bi-variate algorithm.

Moreover, the observed difference between laboratory and field measurements and between the reported values from literature could have resulted from different plant materials used or different habitat conditions. Previous studies suggest that mesophyllic characteristics like leaf ascorbate concentration may influence  $\text{NO}_2$  exchange rates (RAMGE et al. 1993; TEKLEMARIAM and SPARKS 2006). The apoplastic ascorbate concentration varies with species, environmental conditions (POLLE et al. 1995; SCHWANZ et al. 1996) and stage of development (LUWE 1996). The differences may be due to different ascorbate concentrations. Another reason could be a different colonization of the trees by chemolithoautotrophic nitrifying bacteria. It is known that these bacteria colonize the phyllosphere of trees. HEUSER and ZIMMER (2003) demonstrated autotrophic nitrite oxidizers on leaf surface of English oak (*Quercus robur* L.) and PAPEN et al. (2002) detected them at spruce needles. TEUBER (2003) was able to verify nitrifying bacteria living inside the apoplast of spruce needles. These organisms are able to metabolize  $\text{NH}_4^+$  and  $\text{NO}_2^-$  which is formed when  $\text{NO}_2$  dissolved in water. It is to be assumed that  $\text{NO}_2$  uptake and compensation point concentration will be differing if plants are colonized by nitrifiers or not. From previous studies (PAPEN et al. 2002) it is known that  $\text{NH}_3$  deposition fluxes significantly increased as consequence of metabolic activity of nitrifying bacteria. Possibly, this observation is also valid for  $\text{NO}_2$ .

# Conclusions and Perspectives

In this study a dynamic chamber system for surface exchange flux measurements of reactive and non-reactive trace gases on plants under field and laboratory conditions was presented. I would like to conclude the findings as follows:

1. One of the most important characteristics of the dynamic chamber system is the minimal disturbance of plant physiology and growth. Changes in concentrations of relevant trace gases should be small in order to be comparable to the outer environment. Furthermore, small changes prevent enclosure induced artifacts on plant metabolism and stomata regulation. Reliable investigations should not only focus on a few interesting trace gases but always include CO<sub>2</sub> and water vapor exchange because of plant physiological feedback regulations.
2. According to the “blank” measurements, the wall material of our plant chamber can be considered as chemically inert. I like to emphasize, that mass fluxes to the walls of the chamber can basically not be neglected and must be considered in the mass flux balance of the dynamic plant chamber, if there are any appreciable effects of ad- or desorption.
3. The performance of the dynamic chamber system must be controlled and, if necessary, suitable parameterized correction algorithms have to be applied to maintain/improve the precision of NO<sub>2</sub> concentration and exchange flux density measurements. The sensitivity of the NO/NO<sub>2</sub> analyzer to changes of ambient temperature is one of these parameters. Our analyzer drifted 0.07 ppb/K (NO) and 0.08 ppb/K (NO<sub>2</sub>). The precision of the NO<sub>2</sub> exchange flux densities is almost entirely determined by the precision of the NO<sub>2</sub> concentration measurements, which in turn depends on the sensitivity (limit of detection) of the NO<sub>2</sub> analyzer. Considering best performance of our system, a flux density precision

of  $\leq 10\%$  can be reached, as long as  $\text{NO}_2$  concentrations in the plant chamber differ by 0.1 ppb from the expected  $\text{NO}_2$  compensation point concentration.

4. Determination of  $\text{NO}_2$  concentrations at sub-ppb level and of  $\text{NO}_2$  exchange flux densities at the thousandths (hundredths) of  $\text{nmol m}^{-2} \text{ s}^{-1}$  level definitely require (a) a  $\text{NO}_2$  specific converter (photolytic converter) and (b) a highly sensitive  $\text{NO}/\text{NO}_2$  analyzer (lower detection limit ( $3\sigma$ ) of at least  $13 \text{ nmol m}^{-3}$  (0.3 ppb), better  $4.5 \text{ nmol m}^{-3}$  (0.1 ppb)).
5. The significance of concentration differences  $\Delta m_i$  (between trace gas concentrations measured at the inlet and the outlet of the dynamic chamber) is the fundamental quality criterion for the determination of high quality exchange flux densities and deposition velocities, but particularly for the detection of (highly) significant compensation point concentrations. Especially under field measurements, the percentage of non-significant  $\Delta m_i$  can be rather high due to the temporal variation of ambient concentrations during the measurement interval.
6. Laboratory measurements for the identification of  $\text{NO}_2$  compensation point concentrations under controlled conditions require low, reproducible and verifiable  $\text{NO}_2$  concentration for  $\text{NO}_2$  fumigation experiments. The precision of corresponding  $\text{NO}_2$  concentration measurements is not only limited by the noise of the  $\text{NO}/\text{NO}_2$  analyzer, but also by the noise of the  $\text{NO}_2$  blending procedure. Application of future  $\text{NO}/\text{NO}_2$  analyzers (lower detection limit ( $3\sigma$ )  $< 2.2 \text{ nmol m}^{-3}$  ( $< 0.05$  ppb)) will be useless, unless the uncertainty of the  $\text{NO}_2$  blending for fumigation experiments will be improved significantly.
7. Photo-chemical reactions in the dynamic plant chamber's volume must be considered (or be excluded by corresponding set-ups). Otherwise, particularly the exchange of the  $\text{NO}-\text{NO}_2-\text{O}_3$  triad with the plants could be seriously over- or underestimated. This is particularly important for the determination of the  $\text{NO}_2$  deposition velocity. Under our experimental conditions in the field, the overestimation of the  $\text{NO}_2$  deposition velocity had reached about 80 % if photolysis of  $\text{NO}_2$  has been neglected. Excluding the chemical reaction of  $\text{NO}$  with  $\text{O}_3$  by corresponding experimental design (e.g. using  $\text{NO}$  and  $\text{O}_3$  free purging air), effects of  $\text{NO}_2$  photolysis would still be present, as long as there is appreciable illumination of the plants. This can hardly be avoided because for plant

physiological studies photosynthetically active radiation is essential. The only way out would be to use a chamber wall material where the transmissivity for PAR is high and in the wavelength range of  $j(NO_2)$  negligible. For laboratory studies, the application of light-emitting diodes which do not emit in the wavelength range of  $j(NO_2)$  seems to be very promising.

8. Using an empty (“reference”) chamber for considering (compensating) photochemical reactions would imply that  $NO_2$ -photolysis, as well as the concentrations of  $NO_2$ ,  $NO$  and  $O_3$  in the empty and in the plant chambers are identical; however, this is definitely not the case.
9. For mathematical correctness, deposition velocities and compensation point concentrations should be derived from linear relationships between the originally measured quantities, namely the  $NO$ ,  $NO_2$  and  $O_3$  concentrations at the inlet and the outlet of the dynamic chamber. A straight-forward and thorough statistical treatment of measured data will result in high-quality and reliable data of exchange flux densities, deposition velocities and compensation point concentrations, if solid characterization and quantification of trace gas concentration errors as well as errors of all other quantities (necessary for calculation of the exchange flux densities) is achieved and general Gaussian error propagation as well as bi-variate weighted linear least-squares fitting regression analysis is applied.
10. It is recommended, that results from previous studies on  $NO_2$  exchange flux densities,  $NO_2$  deposition velocities and  $NO_2$  compensation point concentrations which have been obtained by dynamic plant chambers should be handled with care owing to neglecting (at least) the effects of  $NO_2$  photolysis in the plant chamber’s volume and insufficient characterization of the specificity and precision of the  $NO_2$  analyzers. A re-evaluation would be helpful.
11. The control of plant conditions and the plant nutrient composition after field measurements indicated that the enclosed branches were not harmed by the dynamic plant chambers and behaved normally still after six weeks of enclosure.

12. The plant's optimal conditions have to be known to avoid errors in analyzing of the NO<sub>2</sub> (NO, O<sub>3</sub>) exchange measurements. Ignoring temperature effects on stomatal closure, plant gas exchange intensity would be misjudge if interpreting these fluxes as plant behavior without limitation. An underestimation would occur if gas exchange is only measured at high temperatures or an overestimation happens if measuring is performed only at low temperatures.
13. Exchange rates of NO<sub>2</sub> increased with raising NO<sub>2</sub> ambient concentrations and depend also on stomatal conductance. With raising leaf conductance for water vapor the NO<sub>2</sub> uptake increased linearly in case of spruce, whereas oak leaves exhibited a considerable decrease of NO<sub>2</sub> deposition at high leaf conductances at observed NO<sub>2</sub> ambient mixing ratios. Exchange rates of O<sub>3</sub> for spruce were non-linearly related to stomatal conductance and saturated at high leaf conductances.
14. The uptake of NO<sub>2</sub> is also limited by internal resistances. For spruce our results let us assume that the internal resistances add a small percentage to the total resistance of leaf gas exchange at low leaf conductance but increase at higher conductances. For oak the internal resistance seems to play a minor role. But for dynamic chamber measurements the chamber resistances may not be neglected if plant resistances and chamber resistances are in the same order of magnitude. NO<sub>2</sub> fluxes modeled by predicted NO<sub>2</sub> leaf conductances, which were calculated from known leaf conductances to water vapor, resulted in over- or underestimations of NO<sub>2</sub> fluxes.
15. Determination of deposition velocity and compensation point concentration requires a classification of the data, for example by leaf conductance. This is the only way to ensure comparable plant conditions and to assure reliable interpretation.
16. NO<sub>2</sub> deposition velocities ( $v_{dep,NO_2}$ ) are positively correlated to leaf conductance. For spruce  $v_{dep,NO_2}$  ranged between 0.07 and 0.42 mm s<sup>-1</sup> and for oak between 0.06 and 2.71 mm s<sup>-1</sup>. NO<sub>2</sub> deposition velocities of spruce are within the lowest reported range of other reported data. NO<sub>2</sub> and O<sub>3</sub> deposition velocities determined for spruce were of the same magnitude.



17. Estimates of NO<sub>2</sub> deposition velocity per ground area (on a LAI basis) amounted to 7.7 mm s<sup>-1</sup> for oak and to 0.98 mm s<sup>-1</sup> for the spruce stand. Oak data were in a good agreement with reported values, whereas the estimates in case of spruce were lower than reported.
18. Highly significant NO<sub>2</sub> compensation point concentration ( $m_{comp,NO_2}$ ) determined for spruce needles under field conditions ranged between  $7.4 \pm 6.40$  and  $29.0 \pm 16.30$  nmol m<sup>-3</sup> (0.17 - 0.65 ppb). Laboratory measurements resulted in  $m_{comp,NO_2} = 5.9 \pm 9.13$  nmol m<sup>-3</sup> (0.13 ppb) with a significance probability for the existence of  $m_{comp,NO_2}$  of 96.6 % (“likely”). For oak no  $m_{comp,NO_2}$  was found. The results for spruce under field and laboratory conditions challenge the existence of a NO<sub>2</sub> compensation point concentration. There is increasing indication that forests are mainly a sink for NO<sub>2</sub> and potential NO<sub>2</sub> emissions are low. Only when assuming high NO soil emissions, more NO<sub>2</sub> can be formed by reaction with O<sub>3</sub> than plants are able to take up. Under these circumstances forests can be a source for NO<sub>2</sub>.
19. The constant lower values of NO<sub>2</sub> gas exchange flux densities, NO<sub>2</sub> deposition velocities and NO<sub>2</sub> compensation point concentrations in comparison to most previous studies probably based up on usage of more specific NO<sub>2</sub> analyzer with a blue light converter.

This study demonstrated, that the determination of significant NO<sub>2</sub> exchange fluxes, deposition velocities and compensation point concentrations highly depend on the resolution of the NO<sub>2</sub> concentration differences measured at the inlet and outlet of the dynamic chamber. For further research the precision of the NO<sub>2</sub> concentration measurements could be enhanced by using NO<sub>2</sub> analyzers with an improved detection limit, maybe to be better than 10 nmol m<sup>-3</sup> (0.25 ppb). Measurements under laboratory conditions at very low NO<sub>2</sub> concentrations only take advantage of an improved NO<sub>2</sub> analyzer if the blending procedure is improved too. Otherwise the fluctuations due to the blending procedure will affect the precision of the NO<sub>2</sub> concentration measurements.

The field experiment presented in this study illustrated the problems of instationarity of trace gas concentrations during non-simultaneous concentration measurements.

Stationarity can only be achieved if trace gas concentration is constant during measuring period without concentration peaks. To approach this problem another independent measuring system can be used to determine the ambient trace gas concentration constantly. However, according to the available technique the use of one single instrument is preferable to guarantee precise simultaneous concentration measurements at the inlet and outlet of the dynamic chamber. Operation of two trace gas analyzers with an absolute accuracy and precision much better than the expected difference between inlet and outlet concentration is currently not available. Another option would be a two channel analyzer, which could measure directly the concentration difference between the inlet and outlet of the dynamic chamber. A different option would be the reduction of the switching time between measurements of chamber inlet and outlet. However, as a consequence tubing lengths would have to be reduced, which is hard to handle for field measurements, especially when analyzers are affected by temperature fluctuations and therefore should be operated under constant temperature conditions.

A main conclusion of this study is that photo-chemical reactions in the dynamic plant chamber's volume must be considered. So all reactions inside the chamber have to be known for an accurate chemical correction. For detailed understanding it would be necessary to verify if the reactions of the NO-NO<sub>2</sub>-O<sub>3</sub> triad cover the main production and destruction processes inside the chambers. Additional processes include reactions of the reactive trace gases with plant surfaces and water films on the surface and reactions with volatile organic compounds (VOC's) emitted by the plant itself. In this context another interesting point is the formation of nitrous acid (HONO) by disproportionation of NO<sub>2</sub> and the rapidly decomposing of HONO into NO. This reaction would provide a NO source inside the chamber. This possibility is indicated by changing signs of NO fluxes from negative to positive (equivalent to emission) just by chemical gas phase correction.

This study exhibits some interesting findings about the specific gas exchange behavior of spruce and oak. Issues like different leaf types (sun and shade leaves), plant and leaf age or the impact of stem and bark deserve closer attention. For further investigations another question will be if NO<sub>2</sub> exchange behavior would change if the nitrogen supply via soil changes. A higher nitrogen fertilization of soil could cause a lower nitrogen uptake by leaves and vice versa.

On the other hand the bottom up way of analysis of the nitrogen metabolism raises the question of nitrogen uptake limitation. One reason maybe changes in plant metabolism affecting nitrate reductase activity or apoplastic ascorbate concentration. Further investigations of this issue is needed especially for forest forming species like spruce, beech and oak as well as plants at the subcanopy level.

More process related gas exchange measurements at leaf level are required to compare results with flux measurements above canopy performed as eddy covariance measurements. This could help to discover misunderstandings in the biosphere-atmosphere exchange model of the ecosystem forest. A further method linking leaf and canopy level can be the use of open-top chambers. This method is well known for exposing plant mesocosms to elevated  $\text{CO}_2$  and could be used as well for  $\text{NO}_2$  fumigation of a whole plant.



# References

- Alsheimer, M.: Charakterisierung räumlicher und zeitlicher Heterogenität der Transpiration unterschiedlicher montaner Fichtenbestände durch Xylemflussmessungen, *Bayreuther Forum Ökologie* **49**, 1-143, 1997.
- Amman, M., Stalder, M., Sutter, M., Brunold, C., Baltensperger, U., Jost, D.T., Turler, A. and Gaggeler, H.W.: Tracing uptake and assimilation of NO<sub>2</sub> in spruce needles with <sup>13</sup>N, *Journal of Experimental Botany* **46**, 1685-1691, 1995.
- Atkinson, R., Baulch, D.L., Cox, R.A., Crowley, J.N., Hampson, R.F., Hynes, R.G., Jenkin, M.E., Rossi, M.J. and Troe, J.: Evaluated kinetic and photochemical data for atmospheric chemistry: Volume I – gas phase reactions of O<sub>x</sub>, HO<sub>x</sub>, NO<sub>x</sub> and SO<sub>x</sub> species, *Atmospheric Chemistry and Physics* **4**, 1461-1738, 2004, <http://www.atmos-chem-phys.net/4/1461/2004/>.
- Beier, N. and Schneewind, R.: Chemical reactions of gases in tubes of probing systems and their influence on measured concentrations, *Ann. Geophysicae* **9**, 703-707, 1991.
- Bollmann, A. and Conrad, R.: Influence of O<sub>2</sub> availability on NO and N<sub>2</sub>O release by nitrification and denitrification in soils, *Global Change Biology* **4**, 387-396, 1998.
- Burkhard, J. and Eiden, R.: Thin water films on coniferous needles, *Atmospheric Environment* **28**, 2001-2017, 1994.
- von Caemmerer, S. and Farquhar, G.D.: Some relationships between the biochemistry of photosynthesis and the gas exchange of leaves, *Planta* **153**, 376-387, 1981.
- Cantrell, C.A.: Technical note: Review of methods for linear least-squares fitting of data and application to atmospheric chemistry problems, *Atmospheric Chemistry and Physics* **8**, 5477-5487, 2008.
- Chaparro-Suarez, I.G.: Untersuchungen zum Austausch von Stickstoffdioxid (NO<sub>2</sub>) zwischen Pflanzen und Atmosphäre, Phd Thesis, Johannes Gutenberg University Mainz, Mainz, Germany 110 p, 2008.
- Chaparro-Suarez, I.G., Meixner, F.X., Kesselmeier, J.: Nitrogen dioxide (NO<sub>2</sub>) uptake by vegetation controlled by atmospheric concentrations and plant stomatal aperture, *Atmospheric Environment*, 2011, doi: 10.1016/j.atmosenv.2011.07.021 (in press).
- Coe, H., Gallagher, M.W. and Choularton, T.W.: NO<sub>x</sub> and O<sub>3</sub> exchange above a forest canopy in southern Scotland. In: Slanina, J., Angeletti, G. and Beilke, S. (Eds.), *General assessment of biogenic emissions and deposition of nitrogen compounds*,

- sulphur compounds and oxidants in Europe, Air Pollution Research Report 47, Commission of the European Communities, Directorate-General for Science, Research and Development, Brussels, Belgium, pp. 189-200, 1993.
- Conrad, R.: Compensation concentration as critical variable for regulating the flux of trace gases between soil and atmosphere, *Biogeochemistry* **27**, 155-170, 1994.
- Cox, R.A., Jones, B.M.J., Penkett, S.A. and Sheppard, D.A.: Mechanism of photochemical and free radical oxidation of sulfur compounds in the gas phase, paper presented at the 5th International Conference of the Commission on Atmospheric Chemistry and Global Pollution, Oxford, England, Aug. 28 to Sept. 3, 1983
- Crutzen, P.J.: The role of NO and NO<sub>2</sub> in the chemistry of the troposphere and stratosphere, *Annual Reviews Earth Planet, Science* **7**, 443-472, 1979.
- Crutzen, P.J.: Role of the tropics in atmospheric chemistry. In: *The geophysiology of Amazonia*, edited by R.E. Dickinson, 107-132, John Wiley & Sons, New York, 1987.
- Dean, J.V. and Harper, J.E.: Nitric oxide and nitrous oxide production by soybean and winged bean during in vivo nitrate reductase assay, *Plant Physiology* **82**, 718-732, 1986.
- Denman, K.L., G. Brasseur, G., A. Chidthaisong, P. Ciais, P.M. Cox, R.E. Dickinson, D. Hauglustaine, C. Heinze, E. Holland, D. Jacob, U. Lohmann, S Ramachandran, P.L. da Silva Dias, S.C. Wofsy and X. Zhang, 2007: Couplings Between Changes in the Climate System and Biogeochemistry. In: *Climate Change 2007: The Physical Science Basis. Contribution of Working Group I to the Fourth Assessment Report of the Intergovernmental Panel on Climate Change* [Solomon, S., D. Qin, M. Manning, Z. Chen, M. Marquis, K.B. Averyt, M.Tignor and H.L. Miller (eds.)]. Cambridge University Press, Cambridge, United Kingdom and New York, NY, USA.
- Dindorf T., Kuhn, U., Ganzeveld, L., Schebeske, G., Ciccioli, P., Holzke, C., Köble, R., Seufert, G. and Kesselmeier, J.: Significant light and temperature dependent monoterpene emissions from European beech (*Fagus sylvatica* L.) and their potential impact on the European volatile organic compound budget, *Journal of Geophysical Research* **111**, D16305, 2006, doi:10.1029/2005JD006751.
- Drummond, J.W., Castledine, C., Green, J., Denno, R., Mackay, G.I. and Schiff, H.I.: New technologies for use in acid deposition networks. In *Monitoring Methods for Toxics in the Atmosphere*. ASTM Special Technical Publication No. 1052, Philadelphia, 1989.
- Erisman, J.W., Sutton, M.A., Galloway, J., Klimont, Z. and Winiwarter, W.: How a century of ammonia synthesis changed the world, *Nature Geoscience* **1**, 636-639, 2008.
- Fangmeier A., Hadwiger-Fangmeier A., Van der Eerden L. and Jäger H.-J.: Effects of atmospheric ammonia on vegetation - A review, *Environmental Pollution* **86**, 43-82, 1994.

- Fehsenfeld, F.C., Dickerson, R.R., Hübler, G., Luke, W.T., Nunnermacker, L.J., Williams, E.J., Roberts, J.M., Calvert, J.G., Curran, C.M., Delany, A.C., Eubank, C.S., Fahey, D.W., Fried, A., Gandrud, B.W., Langford, A.O., Murphy, P.C., Norton, R.B., Pickering, K.E. and Ridley, B.A.: A Ground-Based Intercomparison of NO, NO<sub>x</sub> and NO<sub>y</sub> Measurement Techniques, *Journal of Geophysical Research* **92**(D12), 14,710-14,722, 1987.
- Fehsenfeld, F.C., Drummond, J.W., Roychowdhury, U.K., Galvin, P.J., Williams, E.J., Buhr, M.P., Parrish, D.D., Hübler, G., Langford, A.O., Calvert, J.G., Ridley, B.A., Grahek, F., Heikes, B.G., Kok, G.L., Shetter, J.D., Walega, J.G., Elsworth, C.M., Norton, R.B., Fahey, D.W., Murphy, P.C., Hovermale, C., Mohnen, V.A., Demerjian, K.L., Mackay, G.I. and Schiff, H.I.: Intercomparison of NO<sub>2</sub> measurement techniques, *Journal of Geophysical. Research* **95**, 3579-3597, 1990.
- Foken, T.: Lufthygenisch-bioklimatische Kennzeichnung des oberen Egertales (Fichtelgebirge bis Karlovy Vary), *Bayreuther Forum Ökologie* **100**, 1-70, 2003.
- Frey W., Lösch R.: *Lehrbuch der Geobotanik. Pflanze und Vegetation in Raum und Zeit.* Spektrum Akademischer Verlag, München. 528 p., 2004.
- Fuhrer, J. and Erismann, K.H.: Uptake of NO<sub>2</sub> by plants grown at different salinity levels, *Experientia* **36**, 409-410, 1980.
- Galloway, J.N., Dentener, F.J., Capone, D.G., Boyer, E.W., Howarth, R.W., Seitzinger, S.P., Asner, G.P., Cleveland, C.C., Green, P.A., Holland, E.A., Karl, D.M., Michaels, A.F., Porter, J.H., Townsend, A.R. and Vorosmarty, C.J.: Nitrogen cycles: past, present and future, *Biogeochemistry* **70**, 153-226, 2004.
- Gehrig, R. and Baumann, R.: Comparison of 4 different types of commercially available monitors for nitrogen oxides with test gas mixtures of NH<sub>3</sub>, HNO<sub>3</sub>, PAN and VOC and in ambient air, paper presented at EMEP Workshop on Measurements of Nitrogen-Containing Compounds, EMEP/CCC Report 1/93, Les Diablerets, Switzerland, 1993.
- Gerstberger, P., Foken, T. and Kalbitz, K.: Biogeochemistry of forested catchments in a changing environment: A German case study, *Ecological studies*, Springer, chapter The Lehstenbach and Steinkreuz catchments in NE Bavaria, Germany, 15-41, 2004.
- Geßler, A., Rienks, M. and Rennenberg, H.: NH<sub>3</sub> and NO<sub>2</sub> fluxes between beech trees and the atmosphere - correlation with climatic and physiological parameters, *New Phytologist* **147**, 539-560, 2000.
- Geßler, A., Rienks, M. and Rennenberg, H.: Stomatal uptake and cuticular adsorption contribute to dry deposition of NH<sub>3</sub> and NO<sub>2</sub> to needles of adult spruce (*Picea abies*) trees, *New Phytologist* **156**, 179-194, 2002.
- Grennfelt, P., Bengtson, C. and Skärby, L.: Dry deposition of nitrogen dioxide to scots pine needles. In: *Precipitation, scavenging, dry deposition and resuspension*, edited by R. Pruppacher, H.R.G. Semonin and W.G.N. Slinn, Elsevier, New York 1983.

- Grosjean, D. and Harrison, J.: Response of chemiluminescence NO<sub>x</sub> analyzers and ultraviolet ozone analyzers to organic air pollutants, *Environmental Science & Technology* **19**, 862-865, 1985.
- Gut, A., Scheibe, M., Rottenberger, S., Rummel, U., Welling, M., Ammann, C., Kirkman, G.A., Kuhn, U., Meixner, F.X., Kesselmeier, J., Lehmann, B.E., Schmidt, W., Müller, E. and Piedade, M.T.F.: Exchange fluxes of NO<sub>2</sub> and O<sub>3</sub> at soil and leaf surfaces in an Amazonian rain forest, *Journal of Geophysical Research* **107**(D20), 8060, doi: 10.1029/2001JD000654, 2002.
- Hanson, P.J., Rott, K., Taylor, G.E.Jr., Gunderson, C.A., Lindberg, S.E. and Ross-Todd, B.M.: NO<sub>2</sub> deposition to elements representative of a forest landscape, *Atmospheric Environment* **23**, 1783-1794, 1989.
- Hanson, P.J. and Lindberg, S.E.: Dry deposition of reactive nitrogen compounds: A review of leaf, canopy and non-foliar measurements, *Atmospheric Environment* **25A**, 8, 1615-1634, 1991.
- Hereid, D.P. and Monson, R.K.: Nitrogen oxide fluxes between corn (*Zea mays* L.) leaves and the atmosphere, *Atmospheric Environment* **35**, 975-983, 2001.
- Heuser, T. and Zimmer, W.: Genus- and Isolate-Specific Real-Time PCR Quantification of *Erwinia* on Leaf Surfaces of English Oaks (*Quercus robur* L.), *Current Microbiology* **47**, 214-219, 2003.
- Hicks, B. B., Baldocchi, D.D., Meyers, T.P., Hosker, R.P., Matt, D.R.: A preliminary multiple resistance routine for deriving dry deposition velocities from measured quantities, *Water, Air, & Soil Pollution* **36**, 311, 1987.
- Hill, C.: Vegetation: a sink for atmospheric pollutants, *Journal of the Air Pollution Control Association* **21**, 341-346, 1971.
- Horii, C.V., Munger, J.W., Wofsy, C., Zahniser, M., Nelson, D. and McManus, J.B.: Fluxes of nitrogen oxides over a temperate deciduous forest, *Journal of Geophysical Research* **109**, D08305, 2004, doi:10.1029/2003JD004326.
- Hosaynali Beygi, Z., Fischer, H., Harder, H.D., Martinez, M., Sander, R., Williams, J., Brookes, D.M., Monks, P.S. and Lelieveld, J.: Oxidation photochemistry in the Southern Atlantic boundary layer: Unexpected deviations of photochemical steady state, *Atmospheric Chemistry and Physics Discuss.* **11**, 7045-7093, 2011, doi:10.5194/acpd-11-7045-2011.
- Jacob, D.J. and Wofsy, S.C.: Budgets of Reactive Nitrogen, Hydrocarbons, and Ozone over the Amazon Forest during the Wet Season, *Journal of Geophysical Research* **95**(D10), 16737-16754, 1990.
- Jensen, E.S. and Pilegaard, K.: Absorption of nitrogen dioxide by barley in open-top chambers, *New Phytologist* **123**, 359-364, 1993



- Johansson, C.: Pine forest: a negligible sink for atmospheric NO<sub>x</sub> in rural Sweden, *Tellus* **39B**, 426-438, 1987.
- Jones, H.G.: *Plants and microclimate*, 2nd ed., Cambridge (Cambr. Univ. Pr.), 1992.
- Kelly, T.J., Stedman, D.H., Ritter, J.A. and Harvey, R.B.: Measurements of Oxides of Nitrogen and Nitric Acid in Clean Air, *J. Geophys. Res.*, **85**, C12, 7417-7425, 1980.
- Kelly, J., Spicer, C.W. and Ward, G.F.: An assessment of the luminol chemiluminescence technique for measurement of NO<sub>2</sub> in ambient air, *Atmospheric Environment* **24A**, 2397-2403, 1990.
- Kesselmeier J., Merk L., Bliefernicht M., and Helas G.: Trace gas exchange between terrestrial plants and atmosphere: carbon dioxide, carbonyl sulfide and ammonia under the rule of compensation points. In: *General Assessment of Biogenic Emissions and Deposition of Nitrogen Compounds, Sulphur Compounds and Oxidants in Europe*, CEC Air Pollution Research Report 47 (edited by Slanina J., Angeletti G. and Beilke S.), pp. 71-80, 1993.
- Kesselmeier, J., Meixner, F.X., Hofmann, U., Ajavon, A., Leimbach, S. and Andreae, M.O.: Reduced sulfur compound exchange between the atmosphere and tropical tree species in southern Cameroon, *Biogeochemistry* **23**, 23-45, 1993.
- Kesselmeier, J., Schäfer, L., Ciccioli, P., Brancaleoni, E., Cecinato, A., Frattoni, M., Foster, P., Jacob, V., Denis, J., Fugit, J.L., Dutaur, L. and Torres, L.: Emission of monoterpenes and isoprene from a Mediterranean oak species *Quercus ilex* L. measured within the BEMA (Biogenic Emissions in the Mediterranean Area) project, *Atmospheric Environment* **30**, 1841-1850, 1996.
- Kesselmeier, J., Bode, K., Hofmann, U., Mueller, H., Schaefer, L., Wolf, A., Ciccioli, P., Brancaleoni, E., Cecinato, A., Frattoni, M., Foster, P., Ferrari, C., Jacob, V., Fugit, J.L., Dutaur, L., Simon, V. and Torres, L.: Emission of short chained organic acids, aldehydes and monoterpenes from *Quercus ilex* L. and *Pinus pinea* L. in relation to physiological activities, carbon budget and emission algorithms, *Atmospheric Environment* **31** (SI), 119-134, 1997.
- Kesselmeier, J., Bode, K., Gerlach, C. and Jork, E.M.: Exchange of atmospheric formic and acetic acids with trees and crop plants under controlled chamber and purified air conditions, *Atmospheric Environment* **32**, 1765-1775, 1998.
- Kisser-Priesack, G.M., Scheunert, I. and Gnatz, G.: Uptake of <sup>15</sup>NO<sub>2</sub> and <sup>15</sup>NO by plant cuticles, *Naturwissenschaften* **74**, 550-551, 1987.
- Kisser-Priesack, G.M., Bienek, D. and Ziegler, H.: NO<sub>2</sub> binding to defined phenolics in the plant cuticle, *Naturwissenschaften* **77**, 492-493, 1990.
- Klepper, L.: Nitric oxide (NO) and nitrogen dioxide (NO<sub>2</sub>) emissions from herbicide-treated soybean plants, *Atmospheric Environment* **13**, 537-542, 1979.

- Kuhn, U., Wolf, A., Gries, C., Nash, T.H. and Kesselmeier, J.: Field measurements on the exchange of carbonyl sulfide between lichens and the atmosphere, *Atmospheric Environment* **34**, 4867-4878, 2000.
- Kuhn, U., Rottenberger, S., Biesenthal, T., Wolf, A., Schebeske, G., Ciccioli, P., Brancaleoni, E., Frattoni, M., Tavares, T.M. and Kesselmeier, J.: Isoprene and monoterpene emissions of Amazonian tree species during the wet season: Direct and indirect investigations on controlling environmental functions, *Journal of Geophysical Research* **107**(D20), 8071, doi: 10.1029/2001JD000978, 2002.
- Kurtenbach, R., Becker, K.H., Gomes, J.A.G., Kleffmann, J., Lörzer, J.C., Sittler, M., Wiesen, P., Ackermann, R., Geyer, A., Platt, U.: Investigations of emissions and heterogeneous formation of HONO in a road traffic tunnel, *Atmospheric Environment* **35**, 3385-3394, 2001.
- Larcher, W.: *Physiological Plant Ecology*, 4th ed., Springer-Verlag, Berlin Heidelberg New York, 2003.
- Lea, P.J. and Mifflin, B.J.: Alternative route for nitrogen assimilation in higher plants, *Nature* **251**, 614-616, 1974.
- Lea, P.J., Wolfenden, J., Wellburn, A.R.: Influence of air pollutants upon nitrogen metabolism, In: Alscher, R., Wellburn, A.R., eds. *Plant Responses to the Gaseous Environment*. London: Chapman & Hall, 279-299, 1994.
- Lee, Y.N. and Schwartz, S.E.: Evaluation of the rate of uptake of nitrogen dioxide by atmospheric and surface liquid waters, *Journal of Geophysical Research* **86**, 11971-11973, 1981.
- Lendzian, K.J. and Kerstiens, G.: Interactions between plant cuticles and gaseous air pollutants, *Aspects of Applied Biology* **17**, 97-104, 1988.
- Lerdau, M.T., Munger, J.W. and Jacob, D.J.: The NO<sub>2</sub> Flux Conundrum, *Science* **289**(5488), 2291-2293, 2000.
- Logan, J.A.: Nitrogen oxides in the troposphere: Global and regional budgets, *Journal of Geophysical Research Atmospheres* **88**, 10785-10807, 1983.
- Ludwig, J.: *Untersuchungen zum Austausch von NO und NO<sub>2</sub> zwischen Atmosphäre und Biosphäre*, PhD Thesis, University of Bayreuth, Bayreuth, Germany, 251 pp, 1994.
- Ludwig, J., Meixner, F.X., Vogel, B. and Forstner, J.: Soil-air exchange of nitric oxide: An overview of processes, environmental factors and modeling studies, *Biogeochemistry* **52**, 225-257, 2001.
- Luwe, M.: Antioxidants in the apoplast and symplast of beech (*Fagus sylvatica* L.) leaves: seasonal variations and responses to changing ozone concentrations in air, *Plant Cell and Environment* **19**(3), 321-328, 1996.

- MacDougall, D. and Crummett, W.B.: Guidelines for Data Acquisition and Data Quality Evaluation in environmental chemistry, *Analytical Chemistry* **52**, 2242-2249, doi: 10.1021/ac5064a004, 1980.
- Massman, W.J.: A review on the molecular diffusivities of H<sub>2</sub>O, CO<sub>2</sub>, CH<sub>4</sub>, CO, O<sub>3</sub>, SO<sub>2</sub>, NH<sub>3</sub>, N<sub>2</sub>O, NO and NO<sub>2</sub> in air, O<sub>2</sub> and N<sub>2</sub> near STP, *Atmospheric Environment* **32**, 1111-1127, 1998.
- Matthews, R.D., Sawyer R.F. and Schefer R.W. Interferences in Chemiluminescent Measurement of NO and NO<sub>2</sub> Emissions from Combustion Systems, *Environmental Science & Technology* **11**, 1092-1096, 1977.
- Maeck, G.: Organ-specific changes in the activity and subunit composition of glutamine-synthetase isoforms of barley (*Hordeum vulgare* L.) after growth on different levels of NH<sub>4</sub><sup>+</sup>, *Planta* **196**, 231-238, 1995.
- Maeda, Y.K., Aoki, K. and Munemori, M.: Chemiluminescence method for the determination of nitrogen dioxide, *Analytical Chemistry* **52**, 307-311, 1980.
- Meixner, F.X.: Surface Exchange of Odd Nitrogen Oxides, *Nova Acta Leopoldina* **70**(288), 299-348, 1994.
- Meixner, F.X., Fickinger, Th., Marufu, L., Serca, D. Nathaus, F.J., Makina, E., Mukurumbira, L., Andreae, M.O.: Preliminary results on nitric oxide emission from a southern African savanna ecosystem, *Nutrient Cycling in Agroecosystems* **48**, 123-138, 1997.
- Neubert, A., Kley, D. and Wildt, J.: Uptake of NO, NO<sub>2</sub> and O<sub>3</sub> by sunflower (*Helianthus annuus* L.) and Tobacco plants (*Nicotiana tabacum* L.): dependence on stomatal conductivity, *Atmospheric Environment* **27A**(14), 2137-2145, 1993.
- Nussbaum, S., Von Ballmoos, P., Gfeller, H., Schlunegger, U.P., Fuhrer, J., Rhodes, D. and Brunold, C.: Incorporation of atmospheric <sup>15</sup>NO<sub>2</sub>-nitrogen into free amino acids by Norway spruce *Picea abies* (L.) Karst, *Oecologia* **94**, 408-414, 1993.
- Padro, J.: Seasonal contrast in modeled and observed dry deposition velocities of O<sub>3</sub>, SO<sub>2</sub> and NO<sub>2</sub> over three surfaces, *Atmospheric Environment* **27A**(6), 807-814, 1993.
- Padro, J.: Summary of ozone dry deposition velocity measurements and model estimates over vineyard, cotton, grass and deciduous forest in summer, *Atmospheric Environment* **30**(13), 2363-2369, 1996.
- Pape, L., Ammann, C., Nyfeler-Brunner, A., Spirig, C., Hens, K. and Meixner, F.X.: An automated dynamic chamber system for surface exchange measurement of non-reactive and reactive trace gases of grassland ecosystems, *Biogeosciences* **6**, 405-429, <http://www.biogeosciences.net/6/405/2009/>, 2009.

- Papen, H., Geßler, A., Zumbusch, E., Rennenberg, H.: Chemolithoautotrophic Nitrifiers in the Phyllosphere of a Spruce Ecosystem Receiving High Atmospheric Nitrogen Input, *Current Microbiology* **44**, 56-60, 2002.
- Park, J.Y. and Lee, Y.N.: Solubility and decomposition kinetics of nitrous acid in aqueous solution, *Journal of Physical Chemistry* **92**, 6294-6302, 1988.
- Pflüger, R. and Mengel, K.: Die photochemische Aktivität von Chloroplasten aus unterschiedlich mit Kalium ernährten Pflanzen, *Plant and Soil* **36**, 417-425; 1972.
- Phillips, N., Bond, B.J., McDowell, N.G., Ryan, M.G.: Canopy and hydraulic conductance in young, mature and old Douglas-fir trees, *Tree Physiology* **22**, 205-211, 2002.
- Pilegaard, K., Jensen, N.O. and Hummelshøj, P.: Seasonal and diurnal variation in the deposition velocity of ozone over a spruce forest in Denmark, *Water, Air and Soil Pollution* **85**, 2223-2228, 1995.
- Pilegaard, J., Hummelshøj, P., Jensen, N.O.: Fluxes of ozone and nitrogen dioxide measured by eddy correlation over a harvested wheat field, *Atmospheric Environment* **32**(7), 1167-1177, 1998.
- Plake, D.: Vertikale Konzentrationsprofile und Flüsse von reaktiven und nicht reaktiven Spurengasen im Fichtelgebirge, Diplomarbeit Thesis, Universität Münster, Münster, 144 pp, 2009.
- Polle, A., Wieser, G. and Havranek, W.M.: Quantification of ozone influx and apoplastic ascorbate content in needles of Norway spruce trees (*Picea abies* L., Karst) at high altitude, *Plant, Cell and Environment* **18**(6), 681-688, 1995.
- Puxbaum, H. and Gregori, M.: Seasonal and annual deposition rates of sulphur, nitrogen and chloride species to an oak forest in north-eastern Austria (Wolkersdorf, 240 m A.S.L.), *Atmospheric Environment* **32**(20), 3557-3568, 1998.
- Raivonen, M., Vesala, T., Pirjola, L., Altimir, N., Keronen, P., Kulmala, M. and Hari, P., Compensation point of NO<sub>x</sub> exchange: Net result of NO<sub>x</sub> consumption and production, *Agricultural and Forest Meteorology* **149**, 1073-1081, 2009.
- Ramge, P., Badeck, F.W., Plöchl, M. and Kohlmaier, G.H.: Apoplastic antioxidants as decisive elimination factors within the uptake process of nitrogen dioxide into leaf tissues, *New Phytologist* **125**, 771-785, 1993.
- Rennenberg, H. and Geßler, A.: Consequences of N deposition to forest ecosystems - Recent results and future research needs, *Water, Air and Soil Pollution* **116**, 47-64, 1999.
- Ridley, B.A., Carroll, M.A., Torres, A.L., Condon, E.P., Sachse, G.W., Hill, G.F. and Gregory, G.L. An intercomparison of results from ferrous sulphate and photolytic converter techniques for measurements of NO<sub>x</sub> made during the NASA GTE/CITE 1 aircraft program, *Journal of Geophysical Research* **93**(D12), 15,803-15,811, 1988.

- Riederer, M., Kurbasik, K., Steinbrecher, R. and Voss, A.: Surface areas, lengths and volumes of *Picea abies* (L.) Karst. Needles: determination, biological variability and effect of environmental factors, *Trees* **2**, 165-172, 1988.
- Robertson, G.P. and Groffman, P.M.: Nitrogen transformation, in: *Soil microbiology, ecology, and biochemistry*, edited by: Paul, E.A., Elsevier, Heidelberg, 2007.
- Rondón, A. and Granat, L.: Studies on the dry deposition of NO<sub>x</sub> to coniferous species at low NO<sub>2</sub> concentrations, *Tellus* **46B**, 339-352, 1994.
- Rondón, A., Johansson, C. and Granat, L.: Dry deposition of nitrogen dioxide and ozone to coniferous forest, *Journal of Geophysical Research* **98**, 5159-5172, 1993.
- Ryerson, T.B., Williams, E.J. and Fehsenfeld, F.C.: An efficient photolysis system for fast-response NO<sub>2</sub> measurements, *Journal of Geophysical Research* **105**(D21), 26,447-26,461, 2000.
- Sakakibara, H., Shimizu, H., Hase, T., Yamazaki, Y., Takao T., Shimonishi, Y., Sugiyama, T.: Molecular Identification and Characterization of Cytosolic Isoforms of Glutamine Synthetase in Maize Roots, *Journal of Biological Chemistry* **271**(47), 29561-29568, 1996.
- Saxe, H.: Stomatal-dependent and stomatal-independent uptake of NO<sub>x</sub>, *New Phytologist* **103**, 199-205, 1986.
- Schäfer, L., Kesselmeier, J. and Helas, G.: Formic and Acetic acid emission from conifers measured with a "cuvette" technique, in *CeC Air Pollution Research 39: Field Measurements and Interpretation of Species Related to Photooxidants and Acid Deposition*, edited by G. Angeletti, S. Beilke, and J. Slanina, 319-323, Eur. Comm., Brussels, 1992.
- Schiff, H.I., Mackay, G.I., Castledine, C., Harris, G.W. and Tran, Q.: Atmospheric measurements of nitrogen dioxide with a sensitive luminol instrument, *Water, Air and Soil Pollution* **30**, 105-114, 1986.
- Schjoerring, J.K., Husted, S., Mack, G., Nielsen, K.H., Finnemann, J., Mattsson, M.: Physiological regulation of plant-atmosphere ammonia exchange, *Plant and Soil* **221**, 95-102, 2000.
- Schjoerring, J.K., Husted, S., Mattsson, M.: Physiological parameters controlling plant-atmosphere ammonia exchanges, *Atmospheric Environment* **32**, 491-498, 1998.
- Schulze, E.-D.: Air pollution and forest decline in a spruce (*Picea abies*) forest, *Science* **244** (4906), 776-783, 1989, doi:10.1126/science.244.4906.776.
- Schwanz, P., Picon, C., Vivien, P., Dreyer, E., Guehl, J.-M. and Polle, A.: Responses of antioxidative systems to drought stress in pendunculate oak and maritime pine as modulated by elevated CO<sub>2</sub>, *Plant Physiology* **110**, 393-402, 1996.

- Seinfeld, J.H. and Pandis, S.N.: Atmospheric Chemistry and Physics: From Air Pollution to Climate Change, 2nd ed., John Wiley & Sons, Inc., Hoboken, New Jersey, 2006.
- Serafimovich, A, Siebicke, L, Staudt, K, et al.: ExchanGE processes in mountainous Regions (EGER) - Documentation of the Intensive Observation Period (IOP2) June, 1st to July, 15th 2008, Arbeitsergebnisse. 37, Universität Bayreuth, Abteilung Mikrometeorologie ISSN 1614-8916, Bayreuth. 147pp, 2008.
- Sieghardt, H.: Schwermetall- und Nährelementgehalte von Pflanzen und Bodenproben schwermetallhaltiger Halden im Raum Bleiberg in Kärnten (Österreich). II. Holzpflanzen, Zeitschrift für Pflanzenernährung und Bodenkunde **151**, 21-26, 1988.
- Skärby, L., Bengtson, C., Boström, C.A., Grennfelt, P. and Troeng, E.: Uptake of NO<sub>x</sub> in Scots pine, *Silva Fennica* **15**, 396-398, 1981.
- Sparks, J.P., Monson, R.K., Sparks, K.L. and Lerdau, M.: Leaf uptake of nitrogen dioxide (NO<sub>2</sub>) in a tropical wet forest: implications for tropospheric chemistry, *Oecologia* **127**, 214-221, 2001.
- Steinbacher, M., Zellweger, C., Schwarzenbacher, B., Bugmann, S., Buchmann, B., Ordóñez, C., Prevot, A.S.H. and Hueglin C.: Nitrogen oxide measurements at rural sites in Switzerland: Bias of conventional measurement techniques, *Journal of Geophysical Research* **112**, D11307, doi:10.1029/2006JD007971, 2007.
- Stulen, I., Perez-Soba, M., De Kok, L.J., Van der Eerden, L.: Impact of gaseous nitrogen deposition on plant functioning, *New Phytologist* **139**, 61-70, 1998.
- Taylor, J.R.: An introduction to error analysis: The study of uncertainties in physical measurements, Oxford University Press, Mill Valley, CA, 270 p, 1982.
- Teklemariam, T.A. and Sparks, J.P.: Leaf fluxes of NO and NO<sub>2</sub> in four herbaceous plant species: The role of ascorbic acid, *Atmospheric Environment* **40**, 2235-2244, 2006.
- Teuber, M.: Nachweis, Lokalisation und Quantifizierung von autotrophen Nitrifizierern im Kronenraum der Fichte (*Picea abies* (L.) Karst.), Phd Thesis, Research Centre Karlsruhe, Albert-Ludwigs University Freiburg i. Brsg., Freiburg im Breisgau, Germany 253 p, 2003.
- Thoene, B., Schröder, P., Papen, H., Egger, A. and Rennenberg, H.: Absorption of atmospheric NO<sub>2</sub> by spruce (*Picea abies* L. Karst.) trees: I. NO<sub>2</sub> influx and its correlation with nitrate reduction, *New Phytologist* **117**, 575-585, 1991.
- Thoene, B., Rennenberg, H. and Weber, P.: Absorption of atmospheric NO<sub>2</sub> by spruce (*Picea abies*) trees: II. Parameterization of NO<sub>2</sub> fluxes by controlled dynamic chamber experiments, *New Phytologist* **134**, 257-266, 1996.

- Thomas, C. and Foken, T.: Flux contribution of coherent structures and its implications for the exchange of energy and matter in a tall spruce canopy, *Boundary-Layer Meteorology* **123**, 317-337, 2007.
- Tischner, R.: Nitrate uptake and reduction in higher and lower plants, *Plant, Cell and Environment* **23**, 1005-1024, 2000.
- Trebs, I., Bohn, B., Ammann, C., Rummel, U., Blumthaler, M., Koenigstedt, R., Meixner, F.X., Fan, S. and Andreae, M.O.: Relationship between the NO<sub>2</sub> photolysis frequency and the solar global irradiance, *Atmospheric Measurement Techniques* **2**, 725-739, <http://www.atmos-meas-tech.net/2/725/2009/>, 2009.
- Vallano, D.M. and Sparks, J.P.: Quantifying foliar uptake of gaseous nitrogen dioxide using enriched foliar  $\delta^{15}\text{N}$  values, *New Phytologist* **177**, 946-955, 2008.
- Walton, S., Gallagher, M.W., Choularton, T.W. and Duyzer, J.: Ozone and NO<sub>2</sub> exchange to fruit orchards, *Atmospheric Environment* **31**(17), 2767-2776, 1997.
- Wang, Y., Jacob, D.J. and Logan, A.: Global simulation of tropospheric O<sub>3</sub>-NO<sub>x</sub>-hydrocarbon chemistry 1. Model formulation, *Journal of Geophysical Research* **103**(D9), 10713-10725, 1998.
- Warneck, P.: *Chemistry of the Natural Atmosphere*, San Diego, New York, Boston, Academic Press Inc, 1988.
- Weber, P., Nussbaum, S., Fuhrer, J., Gfeller, H., Schlunegger, U.P., Brunold, C. and Rennenberg, H.: Uptake of atmospheric <sup>15</sup>NO<sub>2</sub> and its incorporation into free amino acids in wheat (*Triticum aestivum*), *Physiologia Plantaru* **94**, 71-77, 1995.
- Weber, P. and Rennenberg, H.: Dependency of nitrogen dioxide (NO<sub>2</sub>) fluxes to wheat (*Triticum aestivum* L.) leaves from NO<sub>2</sub> concentration, light intensity, temperature and relative humidity determined from controlled dynamic chamber experiments, *Atmospheric Environment* **30**(17), 3001-3009, 1996a.
- Weber, P. and Rennenberg, H.: Exchange of NO and NO<sub>2</sub> between wheat canopy monoliths and the atmosphere, *Plant and Soil* **180**, 197-208, 1996b.
- Wellburn, A.R.: Why are atmospheric oxides of nitrogen usually phytotoxic and not alternative fertilizers, *New Phytologist* **115**, 395-429, 1990.
- Wendel, A., Stedman, D.H., Cantrell, C.A. and Damrauer, L.D.: Luminol-based nitrogen oxide detector. *Analytical Chemistry* **55**, 937-940, 1983.
- Wildt, J., Kley, D., Rockel, A., Rockel, P., Segschneider, H.J.: Emission of NO from several higher plant species, *Journal of Geophysical Research* **102**(D5), 5919-5927, 1997.
- Williams, E.J., Hutchinson, G.L. and Fehsenfeld, F.C.: NO<sub>x</sub> and N<sub>2</sub>O emissions from soil, *Global Biogeochemical Cycles* **6**, 351-388, 10.1029/92gb02124, 1992.

- Winer, A.M., Peters, J.W., Smith, J.P. and Pitts, J.N.: Response of Commercial Chemiluminescent NO-NO<sub>2</sub> Analyzers to other Nitrogen-Containing Compounds, *Environmental Science & Technology* **8**, 1118-1121, 1974.
- Yienger, J.J. and Levy II, H.: Empirical model of global soil-biogenic NO<sub>x</sub> emissions, *Journal of Geophysical Research* **100**(D6), 11, 447–11, 464, 1995.
- Yoneyama, T., Ito, O., Engelaar, W.M.H.G.: Uptake, metabolism and distribution of nitrogen in crop plants traced by enriched and natural <sup>15</sup>N: Progress over the last 30 years, *Phytochemistry Reviews* **2**, 121-132, 2003.
- York, D., Evensen, M., Lopez Martinez, M., De Basabe Delgado, J., Unified equations for the slope, intercept, and standard errors of the best straight line, *American Journal of Physics* **72**(3), 367-375, 2004.



